The Structural Evolution of Thin Shale Detached Deepwater Fold and Thrust Belts

Tobias James Scott Dalton

Submitted in accordance with the requirements for the degree of Doctor of Philosophy

The University of Leeds

School of Earth and Environment

May 2017

The candidate confirms that the work submitted is his own, except where work which has formed part of jointly authored publications has been included. The contribution of the candidate and the other authors to this work has been explicitly indicated below. The candidate confirms that appropriate credit has been given within the thesis where reference has been made to the work of others.

Chapter 4 comprises a jointly authored paper published by the Geological Society of London, in the "Petroleum Geoscience of the West Africa Margin", special publications 438, in May 2016, doi/10.1144/SP438.4. The title of the paper is "Influence of mechanical stratigraphy on multi-layer gravity collapse structures: insights from the Orange Basin, South Africa" the authors are T. J. S. Dalton, D. A. Paton, and D. T. Needham. The work in this paper is directly attributable to T. J. S. Dalton. D.A. Paton and D.T. Needham's contributions were to assist in improving and editing the text.

Chapter 5 comprises a jointly authored paper published by the AAPG in *Interpretation*, Volume 3, No. 4 in November 2015, doi:10.1190/INT-2015-0034.1. The title of the paper is "Temporal and spatial evolution of deepwater fold thrust belts: Implications for quantifying strain imbalance" the authors are T. J. S. Dalton, D. A. Paton, D. T. Needham and N. Hodgson. The work contained within the paper is directly attributable to T. J. S. Dalton. D. A. Paton, D. T. Needham and N. Hodgson's contributions were to assist in improving and editing the text and in providing the data for the study.

Chapter 6 comprises a jointly authored paper published In Marine and Petroleum Geology, Volume 82, in January 2017, doi:10.1016/j.marpetgeo.2017.10.013. The paper is titled "The importance of missing strain in Deep water Fold and Thrust Belts" the authors are T. J. S. Dalton, D. A. Paton, S. J. Oldfield, D. T. Needham and A. M. Wood. The work contained within the paper is directly attributable to T. J. S. Dalton. D. A. Paton, S. J. Oldfield, D. T. Needham and A. M. Wood's contributions were to assist in improving and editing the text and in collecting data in the field locations used for the study.

Acknowledgements

I am eternally indebted to the supreme contributions of Dr Douglas Paton without whom the project would not have been possible in particular I would like to thank him for his support, advice, funding, assistance and friendship. I would also like to thank my other supervisor Dr Tim Needham whose supreme advice and editing skills have been superb. I would also like to thank Dr Estelle Mortimer for reading through and suggesting improvements to my work.

I would also like to recognize the contributions of my friends and colleagues over the years at the School of Earth and Environment, especially Dr Jon Mound, Dr Chris Davies, Dr Andrew Walker, Dr Rob Thomas, Dr David Thompson, Dr Dan Morgan, Dr Geoff Lloyd, Dr Andy Nowacki, Dr Dave Cornwall all of whom have both provided friendship and acted as a scientific sounding board. I would like to give huge thanks to my office friends for making the whole PhD experience an entertaining and enjoyable one especially Jamie Lakin, Edine Pape, Andrew Parsons, Simon Oldfield, Ben Allen, Ben Craven, James Norcliffe, Dr Mohamed Gouiza, Dr Diego Constantino, Holly Rowlands, Alan Wood, and a huge number of others.

I would like to acknowledge PASA, Spectrum and NAMCOR for the provision of and rights to the data for this project. I would also like to recognize and thank Midland Valley and Schlumberger for the provision of their data analysis tools without which the project would have been impossible

I would also like to thank my parents for their inestimable emotional and financial support throughout my education.

Abstract

Deepwater fold and thrust belts (DWFTBs) have been recognized on most the world's passive margins. They play a key role in the redistribution of gravitationally induced strain from the continental margin into the abyssal plain. Commonly they form tripartite systems linked by a detachment or detachments, containing: an updip extensional domain dominated by normal faulting, a downdip contractional domain dominated by folding and thrusts, and a transitional domain between. Typically they are commonly classified based upon their driving forces, geometry and detachment lithology. Systems concentrated on active margins and those detaching onto salt detachments are well described and modelled, but do not provide models applicable to other margin types.

The geometry of thin shale detached DWFTBs on passive margins are poorly constrained. A wide variety of geometric arrangements are observable that do not conform to our current understanding of their formation. Through observation, interpretation and restoration of interpreted seismic profiles this study proposes new models for their formation and growth in both two and three dimensions.

A consistent deficit of extensional versus compressional displacement in favour of extension has been observed in DWFTB systems. This study reveals this to be a consistent feature across DWFTBs and relates it to an early compactional phase of deformation in their development. This study then further investigates this phenomenon through field studies, seismic interpretation and the restoration of DWFTB structures at a range of scales. This study proposes this missing strain component is compensated for by the internal deformation, through folding and thrusting, of sediments within the DWFTB itself.

Finally this thesis draws on the understanding gained from the entire margin to discuss what DWFTB development reveals about wider margin and tectonic scale processes.

1.1 Table of Contents

List of Figures

List of Tables

Introduction

In this section I intend to give a brief outline of the rationale, aims, objectives and layout of the thesis, as well as describe why the Orange Basin of South Africa and Namibia is an appropriate location for the study.

1.1 Rationale

Deep water fold and thrust belts (DWFTBs) are common features on many of the world's passive margins. They play a key role in the distribution of gravitationally induced strain on continental margins. They form significant structures for hydrocarbon exploration in Angola, Nigeria, the Gulf of Mexico (Brognon and Verrier, 1966; Brooks et al., 2000; Ambrose et al., 2005; Morley et al., 2011) acting as trapping structures, controlling fluid flow and creating drilling hazards.

Many studies have categorized and described DWFTBs on the basis of their geometry, detachment lithology and driving mechanism (Rowan et al., 2004; Krueger and Gilbert, 2009; Morley et al., 2011). Detachment lithology and thickness plays a key role in the style of the deformation structures that form, it can be separated into salt, thick shale and thin shale décollements. Salt and thick shale detached systems are well documented in the literature (Duval et al., 1992; Diegel et al., 1995; Peel et al., 1995; Rowan et al. 1999; Hudec and Jackson, 2004). Thin shale detached systems (Type 1a, Morley et al., 2011) are less well described. DWFTBs floored by thick shale and salt have fundamentally different mechanical behaviours due to the nature of their mobile thick decollements (Homza & Wallace, 1995; Sapin et al., 2012; Mahanjane & Franke, 2014). The application of these models is inappropriate for understanding thin shale detached systems. To address this issue this study focusses on observing and interpreting thin detachment systems to identify, catalogue and understand how they initiate and behave. The overarching aim is to produce a model of their behaviour.

1.2 Aims and Objectives

This study aims to observe, quantify and discuss the initiation and formation of thin shale detached DWFTBs. I investigate this through the interpretation of multiple 2D seismic reflection surveys across the extent of the Orange Basin, South Africa and Namibia. I also undertake restorations to understand the process of their formation and to quantify their effects on the margin. I have supplemented these interpretations with field studies in the Spanish Pyrenees to observe the inner working of DWFTBs beyond seismic resolution.

- I aim to quantify the effects of sub-seismic deformation on seismic scale restorations. I look at the structures that form in the sediments in-between seismic scale faults to understand their impact on the development of the margin and on hydrocarbon systems.
- I aim to look at variations in the geometry of collapse structures across the margin and throughout DWFTB systems to understand their 3D development. I consider what the geological controls on these variations are and their relative importance. Through this I intend to describe the post rift development of the Orange Basin with respect to the development of DWFTBs.
- Based upon the understanding I gain from these aims, I further aim to create a model for the initiation and development of DWFTBs above thin shale detachments in two and 3 dimensions.

These aims are achieved by considering the following research questions:

1.2.1 What role does stratigraphy play on DWFTBs?

The role of detachment lithology is well documented in the literature (Davis et al., 1983; Davis & Engelder, 1985; Morley & Guerin, 1996; Rowan et al., 2004; Morley et al., 2011) as is the role of the lithology of the deforming wedge relating to its cohesiveness (Ramberg, 1981; Dahlen et al., 1984; Weijermars et al., 1993; Maltman & Bolton, 2003;

Peel, 2014). However, the complex and changeable depositional history along continental margins means the optimal conditions for a style of collapse may only persist over a geographically limited area, despite the driving mechanisms being persistent over a wider region. The tendency for studies to limit their analysis to geographically limited areas, commonly a function of data availability, prevents the wider observation of the effects of stratigraphy on the development of DWFTBs. The provision of data along 1400 km of the South African and Namibian margin makes such an analysis possible in this study.

1.2.2 What are the range of geometric structures possible in thin shale detached DWFTBs?

The geometry of thin shale detached systems is defined in the literature as tripartite linked systems with an updip extensional domain, a transitional domain and a downdip compressional domain (Rowan et al., 2004; Krueger & Gilbert, 2009; King & Backe, 2010; Morley et al, 2011). Many studies reflect this model in their interpretations (e.g. Cobbold et al., 2004; Shaw et al., 2005; Paton et al., 2008; Scarselli et al., 2016). Some studies present interpretations that are exceptions to this model such as multiple detachments (Corredor et al., 2005), counter region extensional faults in the contractional domain (Sapin et al., 2012), no transitional domain and multiple detachments (Mahanjane & Franke, 2014). However, there is a lack of studies that present multiple sections across a single structure that allow us to observe whether exceptions are truly exceptional or are common features of DWFTB development in a dynamic environment. The availability of a closely spaced grid of seismic profiles allows the construction of accurate 3D models through entire DWFTBs that helps resolve this question.

1.2.3 Where is the strain taken up in DWFTB systems and what are we missing from seismic examples of DWFTBs?

An imbalance between updip extension and downdip contraction has been well documented in the literature (Granado et al., 2009; Butler & Paton, 2010; de Vera et al., 2010) and several authors have proposed explanations for this observed imbalance for example ; lateral deformation (Gonzalez-Mieres & Suppe, 2006; Butler & Paton, 2010); out-of-plane structures (Granado et al., 2009, de Vera et al., 2010)); or internal compaction (Granado et al., 2009). These hypotheses are testable through the observation and interpretation of 3D structures, restorations and via field studies of DWFTBs. There are no known examples of outcropping large, intact, gravity driven-linked systems equivalent in scale to those seen on passive margins. Within the limited number of field scale publications of smaller DWFTBs (McClay et al., 2004; Lopez-Mir et al., 2014, 2015) the broad structures have been well categorized. However, the effects of deformation on the internal characteristics of sediments within the DWFTB are not the focus of these studies. By observing in detail two examples of DWFTBs in the field (Laspuña and Armeña, Spain) and comparing them to seismic examples I am able to tackle these questions.

1.3 Location of the study areas and data

This study is broadly focussed on the Orange Basin offshore South Africa and Namibia and uses a combination of 2D seismic reflection surveys (Figure 1.1). The study also incorporates the southern portion of the Luderitz Basin to the north of the Orange Basin (Figure 1.1). The data (whilst from a wide range of vintages with varying data quality) is broadly excellent particularly in regions of the margin dominated by DWFTBs (Figure 1.2). This quality and volume of seismic data allows an in depth analysis of thin shale detached DWFTBs across the entire margin, allowing the investigation of the effects of changes in shelf geometry, lithology and sedimentation on these features.

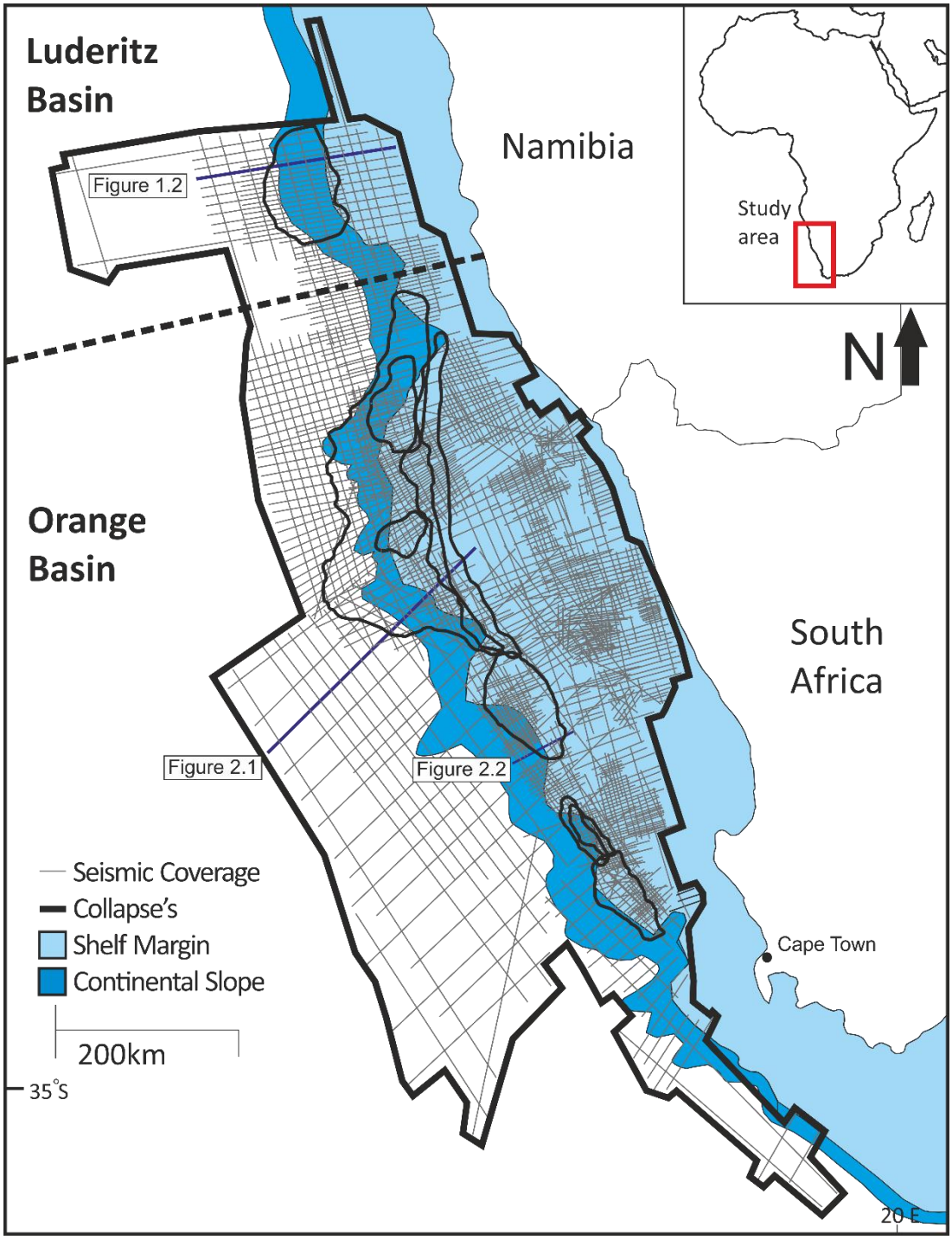

Figure 1.1. Location of the study area including a map of the seismic data coverage used in this study, the locations of the DWFTBs identified and described in this study, and the locations of Figures, 1.2, 2.1 and 2.2.

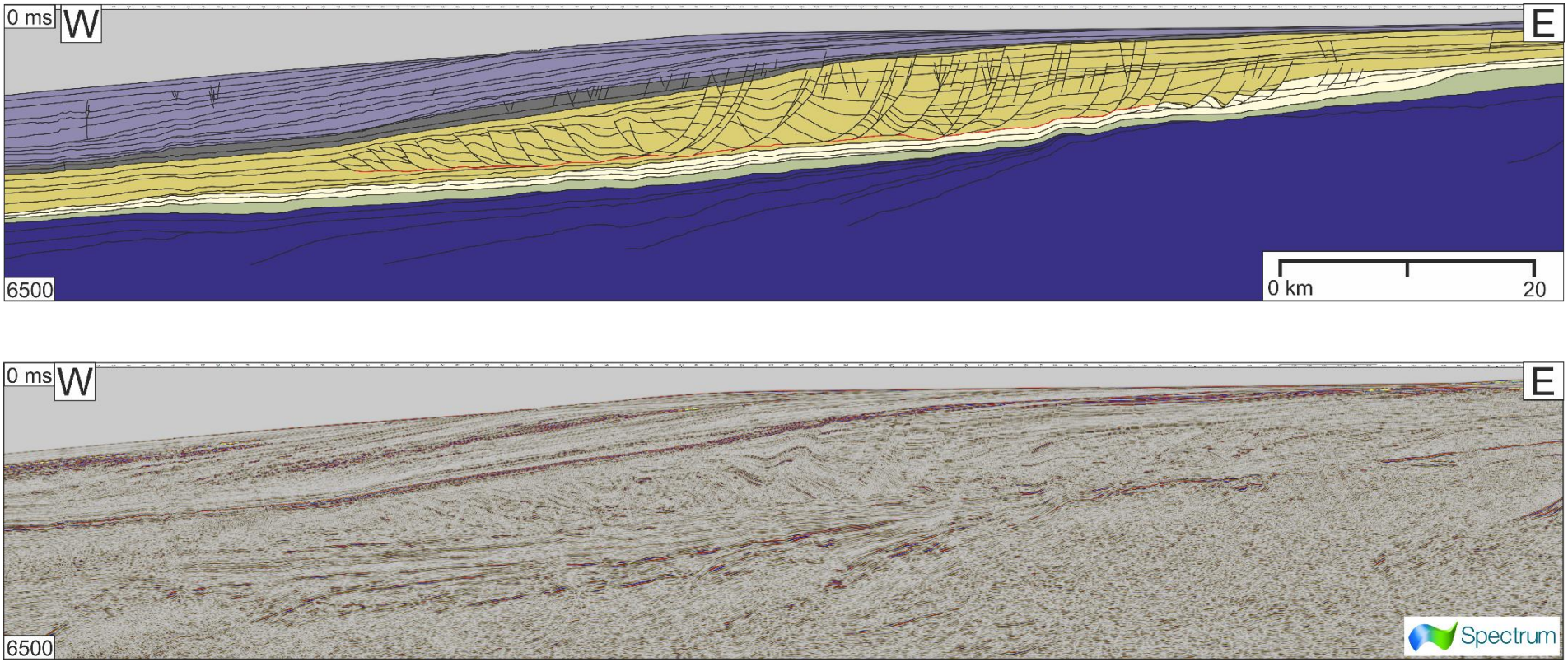

Figure 1.2. Interpreted and uninterpreted seismic lines taken from the north of the study area (Figure 1.1 for location) displaying the data quality and a DWFTB system in the Luderitz basin.

To supplement the seismic reflection studies I also undertook field studies in the Spanish Pyrenees as discussed in Chapter 6 (Figure 1.3). The inclusion of field studies allows regions of seismic uncertainty to be populated with data and to understand what processes the sediments undergo within active gravity-driven DWFTBs.

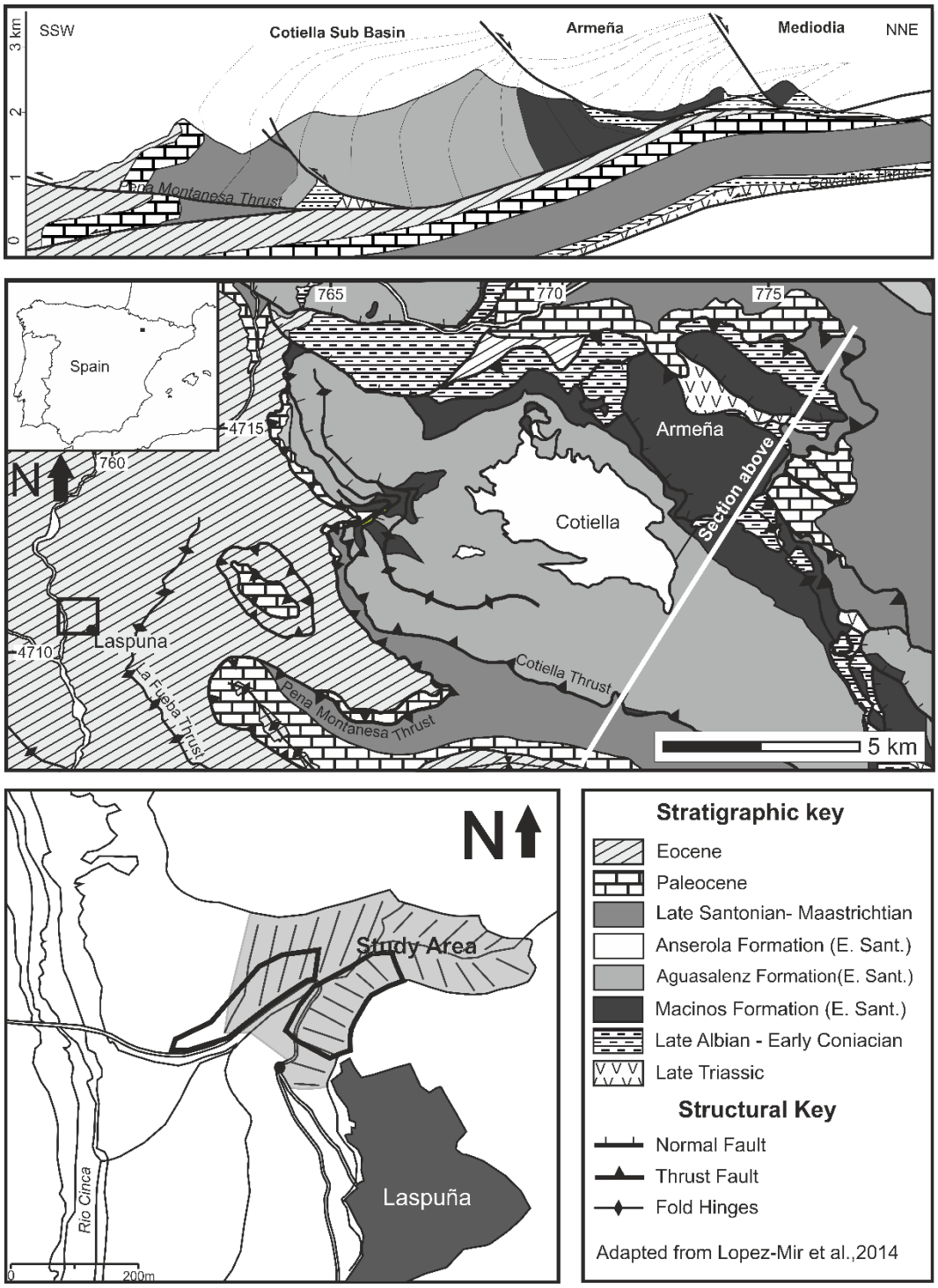

Figure 1.3. Map of the field locations included in this study from the Spanish Pyrenees including major structural features of the area.

1.4 Layout of Thesis

The thesis is composed of seven chapters; three introductory chapters, three data chapters and a discussion chapter. The introductory chapters outline the literature for the study area and for DWFTBs; the data used; and the methods applied. The data chapters are each presented as self-contained papers with their own introductions, backgrounds and discussions. As such Chapter 2 on the background literature has been kept brief so as to limit repetition. Chapter 3 discusses the data and methodologies used in the thesis as well as providing a brief introduction to some of the interpretations used to develop models of the basin.

Chapter 4 contains the final accepted version of a manuscript published online by the Geological Society of London and due for full publication in the "Petroleum Geoscience of the West Africa Margin" in vol. 438 in January 2017. It presents a range of gravity collapse structures across the Orange Basin. It then discusses their variations in geometry before proposing models to explain why different gravity collapse structures form.

Chapter 5 contains the final accepted version of a manuscript published by AAPG in *Interpretation*, Vol. 3., No. 4 in November 2015. The chapter looks more closely at a single deep water fold and thrust belt in the Southern portion of the Orange Basin. This chapter proposes a model to explain how these collapses systems initiate and then grow over time.

Chapter 6 contains a final version of a manuscript submitted to Marine and Petroleum Geology in September 2016. The chapter compares and restores field and seismic examples of DWFTBs. It finds a scalar relationship between DWFTBs of different sizes. It also identifies sub-seismic compressional features within the field examples.

I then use this to explain missing strain components described previously in restorations of seismic scale systems. In the final discussion chapter I discuss the structure of the basin and the DWFTBs within it. I then discuss the implications of this research on our understanding of DWFTB systems. Finally I propose a model for the initiation and growth of DWFTBs in the context of the basin and in 3-D.

2 Geological Setting

This chapter outlines the geological setting of the Orange Basin before presenting a summary of our current understanding of Deepwater Fold and Thrust belts (DWFTBs). Each of the data chapters are presented in the format of individual manuscripts incorporating the relevant geological settings, rationales, literature reviews and methods: this chapter provides the reader with a generalized overview. Each subsequent data chapter provides a more detailed and relevant review of our current understanding of each aspect of the DWFTB system being investigated.

2.1 Geology of the Orange Basin

The Orange Basin is located offshore South Africa and Namibia on the south western margin of the African continent (Figure 1.1). Its name derives from the Orange River, which is the main source of sediment supply for the basin (Austin & Uchupt, 1982). To the north it is bounded by the smaller Luderitz Basin, the southern portion of which is included in this study, and to the south by the Agulhas-Falkland fracture zone (Maslanyi et al., 1992).

The basin initiated with the break-up of Gondwana during the Late Jurassic (Nürnberg & Müller, 1991), this rifting formed a set of graben and half grabens infilled by synrift sediments during the Late Jurassic to the Early Cretaceous (Jungslager et al., 1999; Mohammed et al., 2016). Maslanyi et al. (1992) divides the synrift into two phases: the first comprising lacustrine sediments filling deeper portions of the rift coarsening up to fluvial systems on the basinal highs; the second phase is associated with continued siliciclastic and lacustrine deposition along with widespread volcanism and the emplacement of Seaward Dipping Reflectors (SDRs), possibly associated with the onshore Parana-Etendeka flood basalts (Clemson et al, 1997). Post rifting, a transitional phase of siliciclastic sequences of fluvial red beds to sand prone deltaics were deposited (Figure 2.3) in elongated, margin parallel, basins up to 2 km thick (Gerrard & Smith, 1982; Paton et al., 2008). The onset of full marine conditions occurred at the end of the

Barremian and into the Aptian (Brown et al., 1995) during which time sequences of black shales up to 300 m thick were deposited, with TOCs (Total Organic Carbon) of up to 25% (Herbin et al., 1987; Paton et al., 2007). Overlying this sequence is a thick, up to 5.5 km (Brown et al., 1995), deposit of Aptian to Campanian aged clay-rich marine sediments with some infrequent interbedded silts which coarsen upward into medium sands. There are some geographically restricted massive sandstones developed locally (Hirsch et al., 2009) during this period. This depositional phase is dominated by the formation and rapid growth of multiple DWFTB systems across the length of the margin associated with significant increases in the rate of deposition (Light et al., 1992; Muntingh & Brown, 1993; Butler & Paton, 2010; de Vera et al. 2010; Scarselli et al., 2016). During the mid-Campanian substantial uplift of the margin, of up to 750 m on the inner shelf (Paton et al., 2008), shifting sedimentation distally and eroding the middle Aptian to Campanian sediments off the shelf (McMillan, 2003). A thin succession of Maastrichtian chalks were latterly deposited onto the paleo-slope across the entire basin (McMillan, 2003). Sedimentation during the Cenozoic occurred outboard of the previous slope break, prograding out from the shelf (Hirsch et al., 2009), and depositing up to 1.5 km of clays off the margin (Paton et al., 2008), but as little as 50 m onto the shelf (McMillan, 2003), (Figure 2.1). DWFTBs are common features within the southern portion of the Cenozoic megasequence (Hirsch et al., 2009). A number of studies recognize DWFTBs in the basin but do not discuss their impact on the depositional and structural development of the margin.

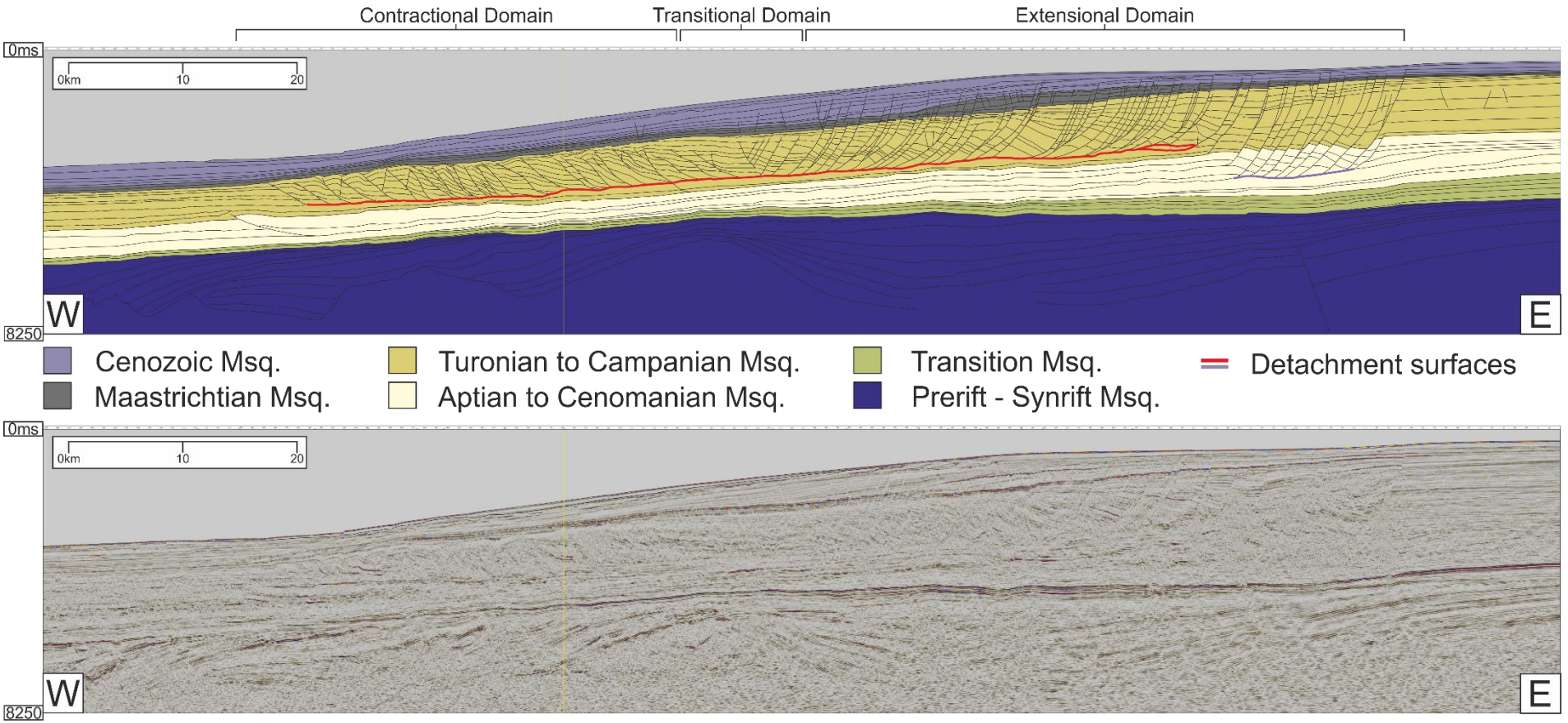

Figure 2.1. Interpreted and un-interpreted 132 km long PSTM section SPOB12-05, vertically exaggerated 3:1. The section is representative of a typical seismic line from the Orange basin. The interpreted image shows the megasequences associated with significant changes in depositional history in the Basin. See Figure 1.1 for location of seismic profile and colour coded detachments

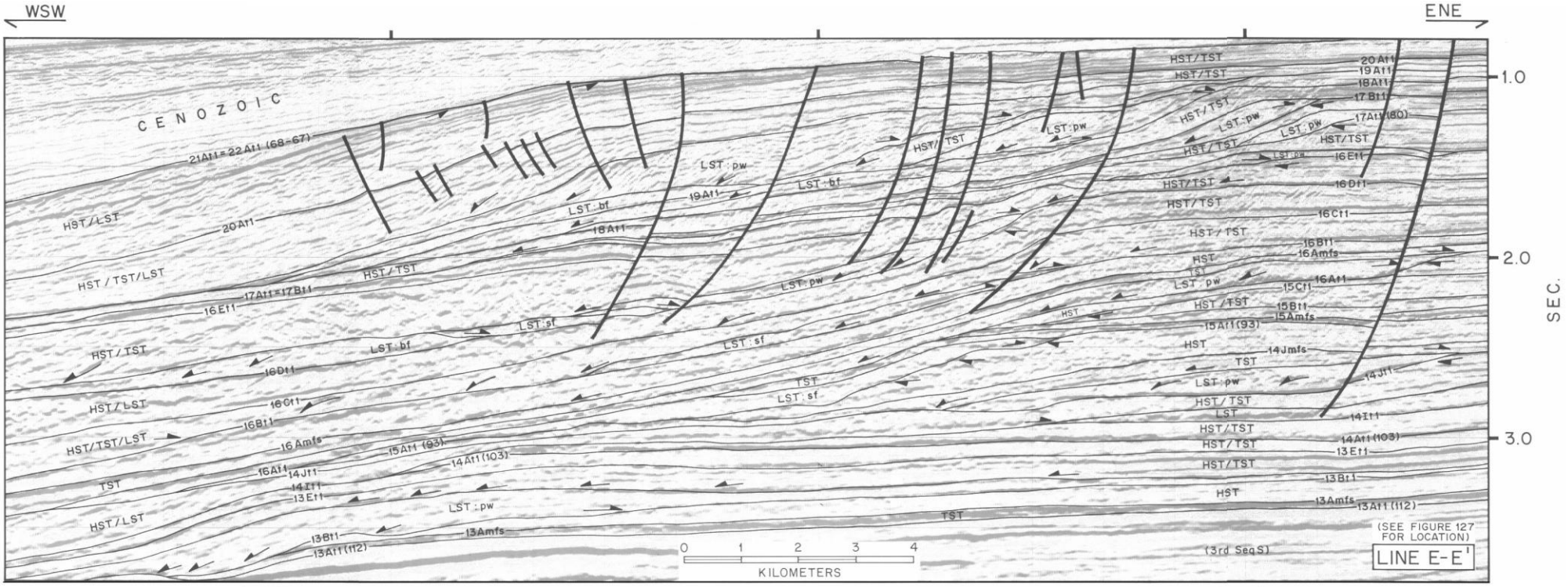

Figure 2.2. Interpreted cross-section from Brown et al. (1995) showing significant tectonostratigraphic packages in the Orange Basin. Location is shown on Figure 1.1.

2.1.1 Tectonostratigraphic megasequences

Brown et al. (1995) uses a combination of well logs from the continental shelf with sequence stratigraphic analysis of seismic profiles to identify a number of basin wide unconformities to sub-divide the basin into depositional sequences (Figure 2.2). This classification system defines a number of significant horizons that I use to date tectonostratigraphic megasequences used in this study (Figure 2.3), namely; 6At1 (117.5 Ma) which marks the end of the synrift and the beginning of the transitional phase; 13At1 (112 Ma) at the end of the Barremian marking the end of the transitional phase and the beginning of the passive phase which I further subdivide into three 13At1 forming the base of the Aptian to Cenomanian megasequence; 15At1 (93 Ma) forms the top of the Aptian to Cenomanian and the base of the Turonian to Campanian megasequence; 18At1 (75 Ma) marks the top of the Turonian to Campanian and the base of the Maastrichtian megasequence); finally the 22At1 (67 Ma) reflection marks the top of the Maastrichtian and the base of the Cenozoic megasequences (Figure 2.1).

Significant horizons used in this study from Brown et al. (1995) have been included in the chronostratigraphy in Figure 2.3. Additionally the chronostratigraphy in Figure 2.3 contains all of the sequences used in Chapters 3-6 as each study divides up the margin differently for their specific purpose.

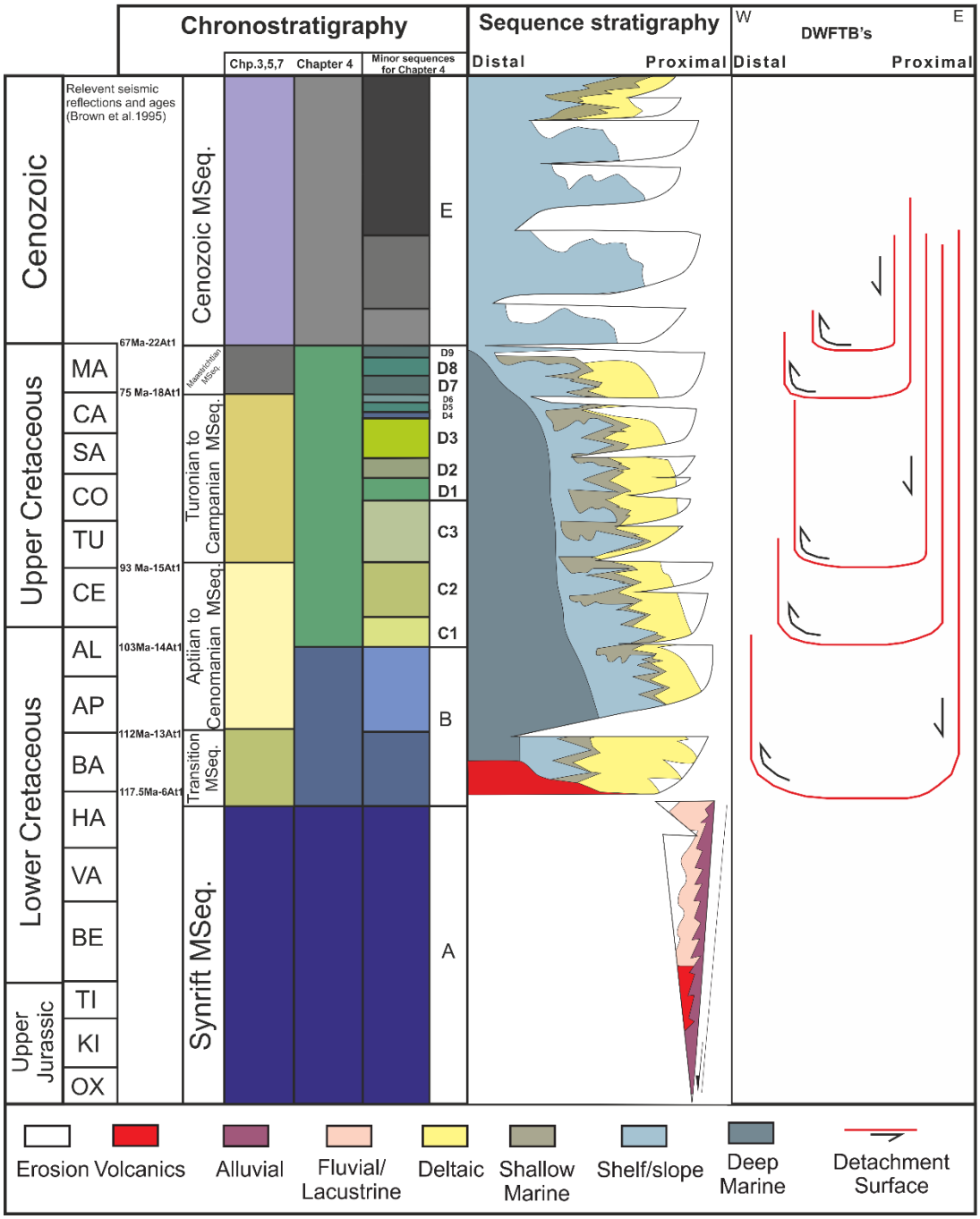

Figure 2.3. Chronostratigraphy of the Orange basin showing the significant picks from Brown et al. (1995) and the megasequences applied in Chapters 4-6 to allow comparison. OX-Oxfordian, KI- Kimmeridgian, TI- Tithonian, BE Berriasian, VA – Valanginian, HA – Hauterivian, BA, Barremian, AP – Aptian, AL – Albian, CE – Cenomanian, TU – Turonian, CO – Coniacian, SA – Santonian, CA – Campanian, MA – Maastrichtian.

2.2 Gravity-driven collapse systems

Deepwater fold thrust belts (DWFTBs) are prevalent structures on many of the world's passive margins. The best description of them may be considered to be that of Peel (2014) who states "*Gravity-driven deformation of thin skinned linked systems in which a body of sediments is translated basinwards, accommodated by extension in its updip portion, and contraction in its downdip region*". The system is linked by a thick or thin detachment or detachments (Rowan et al., 2004; Briggs et al., 2006; Morley et al., 2011) that releases gravitational potential energy via the sliding of, or internal spreading of, sediments (De Jong and Scholten, 1973; Ramberg, 1981). The updip portion is referred to as the extensional domain and is dominated by normal faults and extensional tectonics. The downdip portion of the system is referred to as the contractional or compressional domain and is dominated by folding, thrusting and contractional tectonics. The region in between these two domains is sometimes referred to as the transitional or translational domain. This zone is considered to be a region that undergoes neither net extension nor contraction as it moves basinward. This region can be broad and maybe chaotic in its character, where extensional and contractional tectonics coexist and interfere. Or the region can be slight, merely expressing as a rotated fault block bounded updip by a normal fault and downdip by a thrust. Figure 2.1 shows the division of a line in the study area into these three domains.

2.2.1 Driving mechanisms

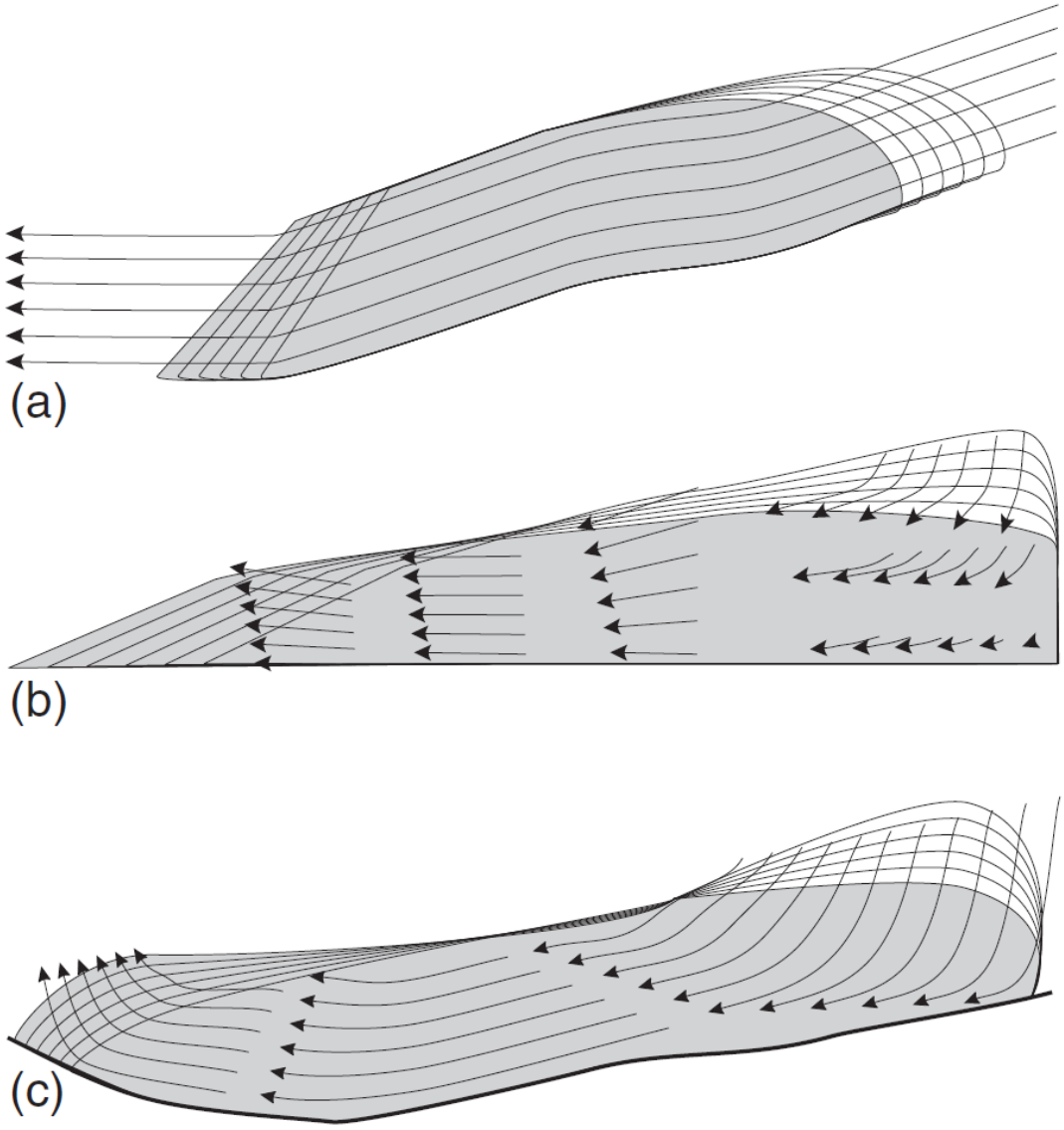

Figure 2.4. Schematic describing the difference between; a) gravity sliding and b) gravity spreading; and c) mixture of both, from Rowan et al. (2004).

All continental margins have gravitational potential due to their slope. They may become unstable and fail downslope, if the slope is built up or steepened, this may occur due to regional tilting or deposition. The redistribution of this overburden can be achieved through gravity sliding or gravity spreading (Figure 2.4). In gravity sliding the material that makes up the wedge acts as a block and slides along the detachment, whose dip angle forms the main control (De Jong and Scholten, 1973; Ramberg, 1981; Rowan et al., 2004). In pure gravity spreading the material that makes up the wedge deforms under its own weight and spreads along the

detachment surface, it is controlled by the surface slope angle, the strength of the sediments in the wedge and the coefficient of friction of the detachment (De Jong and Scholten, 1973; Ramberg, 1981; Rowan et al., 2004). Whilst these models exist as the two end member scenarios most DWFTBs are a blend of the two processes. This means that often, as the wedge begins to slide basinward it internally deforms, spreading as it does so. Peel (2014) sets out a simple geometric method of separating the relative contributions of these two mechanisms. Establishing their relative contributions allows us to recognize the main driving mechanisms for failure; with spreading systems requiring a constant influx of sediment to create an overburden at the top of the system; whilst sliding may only require increase in updip uplift (Peel, 2014).

The driving mechanisms of DWFTBs are controlled by a number of factors including: sedimentation, which increases surface slope angle and increases updip overburden (Davis et al., 1983; Shaw et al., 2004; Rowan et al., 2004); tectonic uplift, which increase the dip of the detachment and the surface slope angle (Dahlen et al., 1983; Morley et al., 2011). The behaviour of the DWFTB is also controlled by: fluid pressure, which reduces the coefficient of friction along the detachment making slip easier whilst loss of fluid pressure would lock systems (Moore and Vrolijik, 1992; Saffer and Bekins, 1998); detachment lithology, salt and mobile shales form diapirs that rise and deform overlying sediments or form welds stopping continued sliding (Morley & Guerin, 1996; Rowan et al. 1999); and the strength of the sediments (Peel, 2014). The movement of the sediments downslope will alter the controlling factors, e.g., sliding will reduce the overall surface slope angle (Rowan et al., 2004), and so periods of quiescence may occur in the development of a DWFTB as slopes re-establish through continued sedimentation or continued uplift and tilting. However, the process is generally a gradual one rather than one of rapid punctuated movements such as in landslides. In the Orange basin, there is evidence of catastrophic gravity failure in the form of MTCs particularly during later phases of DWFTB development though these represent a different mechanism of gravitational strain redistribution. This means that a syn-kinematic evolution of faulting, erosion and sedimentation over long time periods is frequently observed (Shaw et al., 2004; Scarselli et al., 2016). We use these controlling factors to classify different DWFTB systems as outlined below.

2.2.2 Classification

DWFTBs have been divided into different classifications based upon their geometry, driving mechanism and detachment lithology (Krueger and Gilbert, 2009; Morley et al., 2011). Krueger and Gilbert (2009) classify DWFTBs into four types based upon these three factors (Figure 2.5) namely; accretionary prisms formed by subduction at active margins; regional salt décollement fold thrust belt (FTB) formed above thick mobile salt deposits; regional shale décollement FTB formed above a thin shale along a single slip surface; and finally non-discrete décollement FTB where the detachment cuts up and down sequence to multiple slip horizons. This creates a set of geometrically different end members, but does not allow for settings where multiple end member geometries may be present.

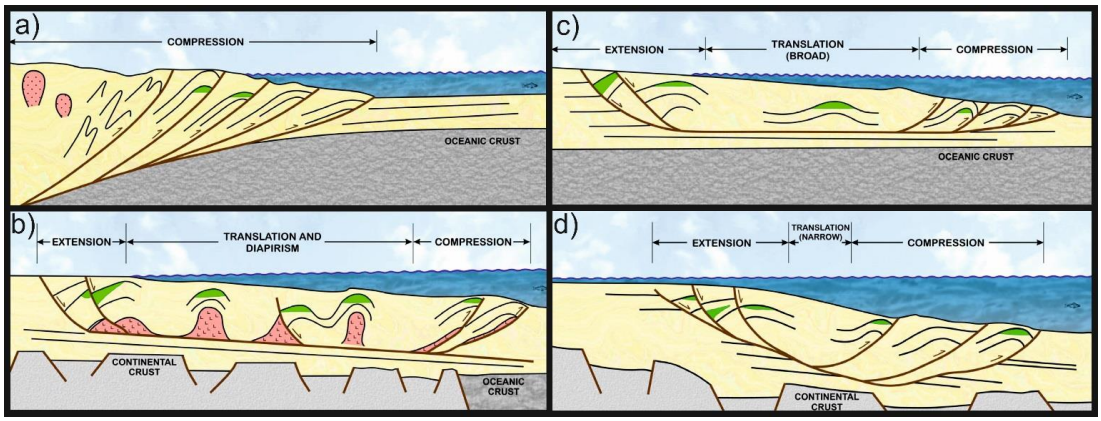

Figure 2.5. Image from Krueger and Gilbert (2009) showing the four classifications of DWFTBs. a) Accretionary Prism; b) Regional Salt décollement; c) Regional Shale décollement; d) Non-discrete Décollement.

Morley et al. (2011) sub-divide them more subtly using the same factors (Table 2.1). Initially into two: near and far field stress systems, where the DWFTB is either driven by a nearby stress (Type 1), such as gravitational instability on passive margins or by a distant system (Type 2) such as an accretionary prism formed by a subducting plate. These are further subdivided into; Type 1a, DWFTBs décolling onto a seaward dipping overpressured shale detachment such as in the Orange Basin or the Niger Delta; Type 1b, DWFTBs décolling onto a seaward dipping salt detachment such as in Angola; Type 2ai linked systems within a single or between opposing converging continents such as in NW Borneo; Type 2aii weakly or unlinked systems in the early phases of continental convergence such as in the Banda Arc; Type 2b weakly or unlinked

systems on active margins such as in the Barbados accretionary prism or the South Caspian Sea. By not describing the geometry present this system is more useful for classifying DWFTBs.

Stress type	Type 1			Type 2		
	Predominantly/ exclusively near field stress			Mixed near field and far field stress Type 2a	Predominantly/ exclusively far field stress Type 2b	
Tectonic setting	Potentially any type of setting with a slope to deepwater. In practice predominantly passive margins			Continental convergence zones	Continental convergence zones Type 2bi	Accretionary prisms Type 2bii
Detachment type	Type 1a Shale		Type 1b Salt	Shale	Shale	Shale
Detachment dip	O	L	O	L	L	L

Landward = L, Oceanward = O

Table 2-1. Classification of DWFTBs from Morley et al. (2011).

This study focusses on thin shale detached DWFTBs (Type 1a, Morley et al, 2011) which express elements along their length akin to both non-discrete and regional shale décollement FTBs (Krueger & Gilbert, 2009). The behaviour of thick shale and salt systems are fundamentally different in their dynamics from the behaviour of thin shale detached systems (Morley & Guerin, 1996). Thick detachment intervals shale and salt detached systems is itself dynamic and prone to diapirize, in contrast to thin detachment systems in which the slip horizon is relatively passive, although changes in overpressure can exert a control on activity (Morley & Guerin, 1996). For this reason models applicable to the thicker detachments are not necessarily applicable to thin systems.

2.2.3 Restoration of DWFTBs

Sequential structural restoration of cross-sections has long been a recognized and important technique for the validation and quantification of interpretations, as well as for improving our understanding of the development of complex structures (Dahlstrom, 1969; Rowan and Kligfield, 1989; Rowan, 1993). Many studies have

undertaken restorations on DWFTBs globally, in order to quantify their movement and ascertain how they form, develop and distribute strain over time (Duval et al., 1991; Morgan & Karig, 1995; Peel et al., 1995; Rowan et al., 2004; Corredor et al., 2005; Hudec et al., 2005). Most of these studies have concentrated on restorations of salt and thick shale detached systems, which behave in a very different fashion to thin shale detached systems. Several restorations have been undertaken specifically within the Orange Basin (Granado et al., 2007; de Vera et al., 2010; Butler & Paton, 2010; Peel, 2014). Butler & Paton (2010) and de Vera et al (2010) both identify an imbalance between the measured strain in the extensional and compressional domains, in favour of extension. This missing strain component is estimated to be 10 - 25 % of total extension, implying that a considerable amount of strain is distributed elsewhere, either within the DWFTB itself or out of section. The restoration in Peel (2014) measures the relative contributions of gravity spreading (32%) vs gravity gliding (68%) establishing the system is dominated by gravity gliding.

2.2.4 Our understanding of the 3D geometry of DWFTBs

Discussion of the 3D geometry of thin shale detached systems is limited in the literature. This is likely to be a result of data limitations either because data do not cover entire systems, or the gridding of 2D profiles is too widely spaced creating too much uncertainty between lines. However, 3D models have been proposed by Hesthammer and Fossen (1999), de Vera et al (2010) and Scarselli et al. (2016) (Figure 2.6). The model of Hesthammer and Fossen (1999) was intended to relate more to gravity slides or underwater landslides than to DWFTBs although the model does show some parallels with DWFTBs. The similarities being: the existence of three distinct domains of updip extension, downdip contraction and a complex domain of translation in between; slip concentrating along a mechanically weak layer. However, the rapid rate of collapse and the exposed toe is not comparable to the DWFTBs of the study area. Despite this, this model could be regarded as part of a suite of features related to DWFTBs, specifically where basins are underfilled allowing free air slope collapse (Imber et al., 2003; Khani and Back, 2012, 2015). The broad bowl

shaped fault scarp of the extensional domain and the equally wide toe domain are frequently inferred as the shape of the collapses.

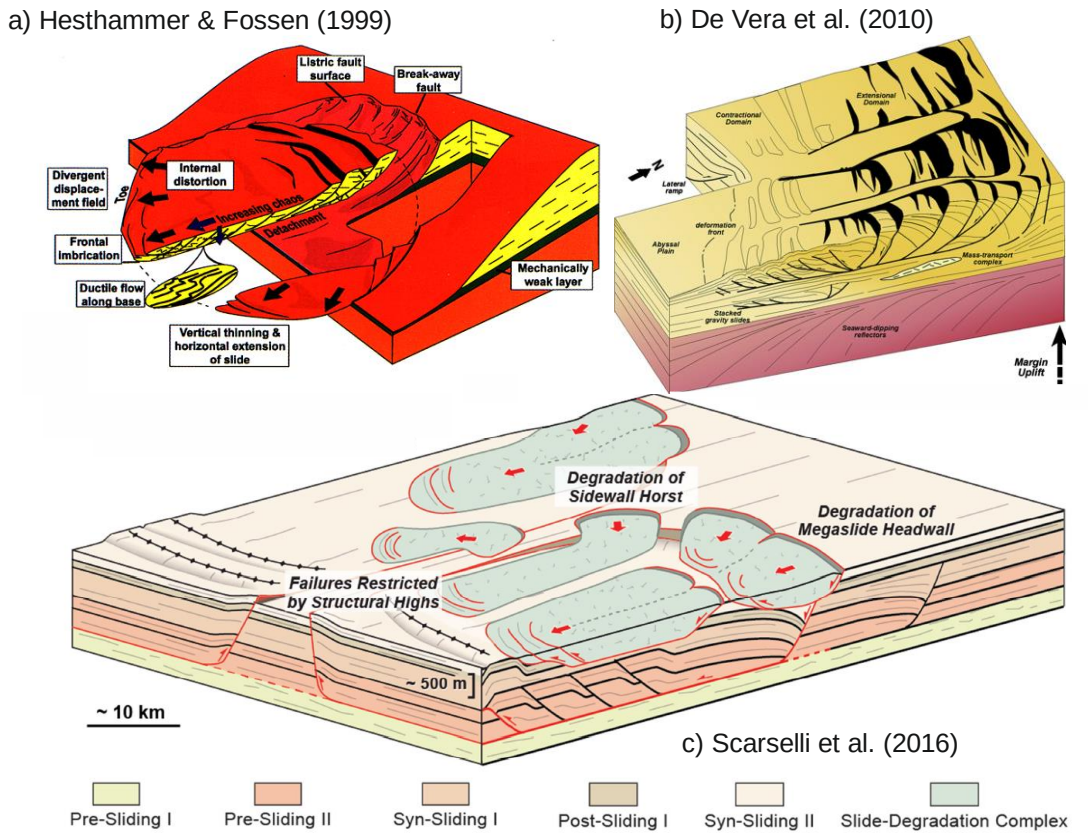

Figure 2.6. A set 3D models from papers of collapse structures above thin shale detachments; a) model from Hesthammer & Fossen (1999); b) Model from de Vera et al. (2010); c) model from Scarselli et al. (2016).

The model proposed by de Vera et al. (2010 (Figure 2.6 b)) describes the overall system consisting of a set of parallel linked systems, bounded ridges of undeformed material. De Vera et al. (2010) further infer a bulbous extensional domain that translates to a narrow contractional domain that preserves the sediments on both of the flanks. The model of Scarselli et al. (2016) shares similar features with that of de Vera et al. (2010) but concentrates on how DWFTBs relate to overlying megaslides that form on exposed footwalls. In neither model do they infer interaction between separate margin parallel collapse systems. All of these models propose that collapses are relatively uniform in their width with contractional and extensional domains present in all parallel sections. Overall there are no current 3D models of the growth and development of DWFTBs above thin shale detachments. Furthermore there is no consideration of sub-seismic deformation.

An additional review of the background literature is provided in individual data chapters. The next chapter looks at the data and methodologies used in this study.

3 Data and Methods

In this chapter I present and discuss the data used in this study, I then describe the methods applied to process, interpret and quantify these data, I characterize the large scale structure of the margin that forms the framework for the data analysis and finally, I address some of the uncertainties present in the interpretation.

3.1 Seismic Data

The data in this study comprise: 1306 2-D pre-stack time migrated (PSTM) seismic reflection profiles from 55 surveys with a 2D line length of 79313 km, released by the Petroleum Agency of South Africa and Spectrum; 122 pre-stack depth migrated (PSDM) seismic profiles from 3 surveys, 2D line length of 24722 km released from Spectrum (Figure 3.1, Table 3.1). The data range in vintage from 1976 – 2012, and have a maximum recording depth from 4000-10000 milliseconds (ms) in PSTM and from 14.5 km to 22.5 km for PSDM (see Table 3.1 for more detail). The 3 PSDM surveys form three unconnected surveys with line spacing of up to 35 km, which lacks sufficient coverage to capture the effects of deformation along the entire margin, and so I have preferentially used the PSTM data for maps and interpretation. Of the 55 PSTM surveys, 42 contain significant mis-ties both internally and with other surveys and are thus not suitable to use to create thickness maps and have been excluded. The data present a broad range in seismic reflective quality, as described in Table 3.1, the best quality data sets are also the tied surveys. These surveys are also located along the shelf margin where the DWFTB systems are concentrated. For these reasons the mis-tied data concentrated on the continental shelf have been broadly disregarded in this study, though some individual lines are presented where they display interesting features or structures not observed in other sections. The location and topology of the key surveys used for this study are presented in Figure 3.1. A review of the data is presented in Table 3.1 which summarises each individual survey.

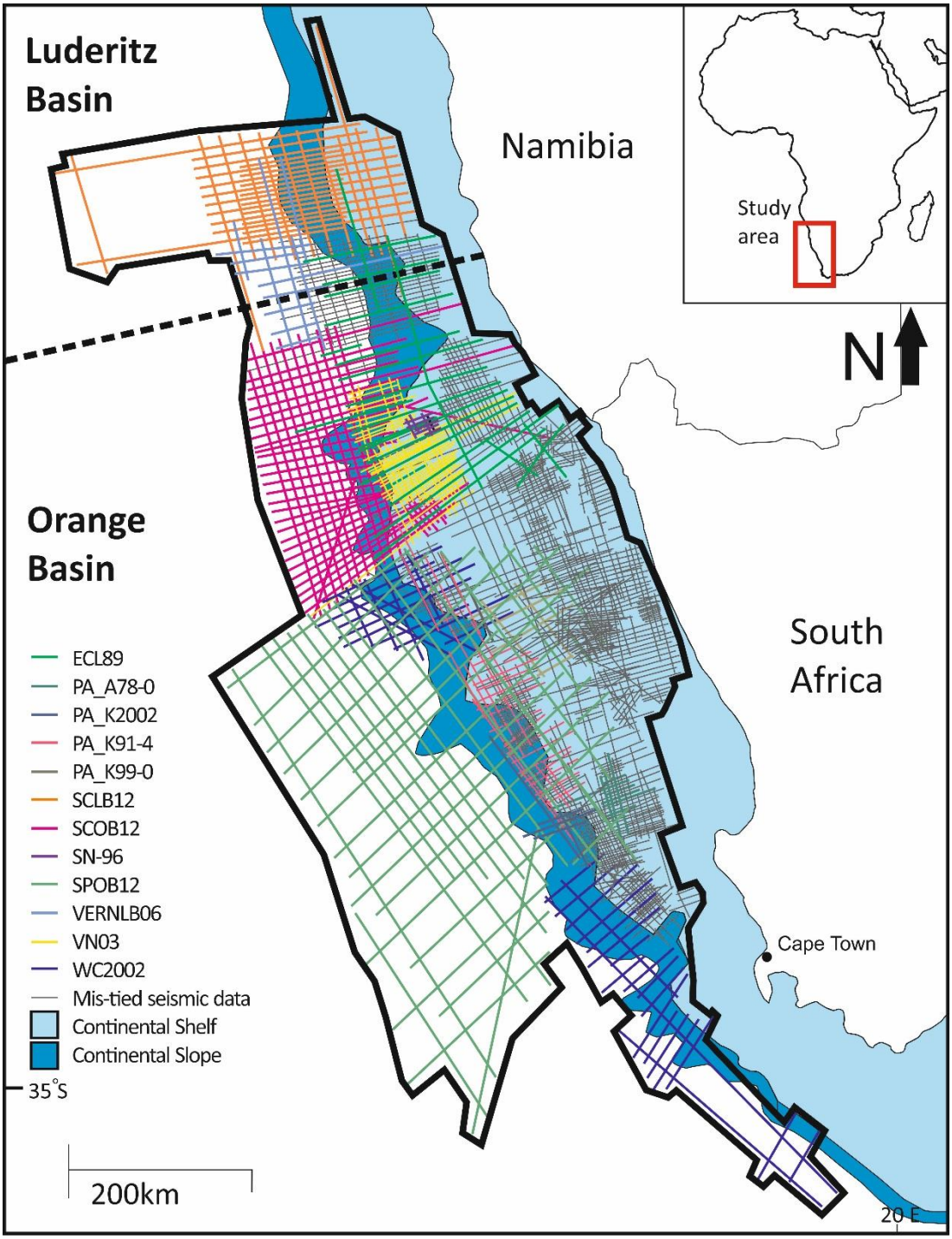

Figure 3.1. Map presenting the seismic data used to produce isochrons and surface maps in this study.

	Lines	Depth	Length	DM/TM	Tied	Quality			Vintage	Source
		ms	km			Ceno.	Cret.	Rift		
ECL89	27	6000-8000	3528	PSTM	y	5	4	3	1989	Spectrum
GNA-97	7	8000	639	PSTM	n	5	4	2	1997	Spectrum
NAM92	36	7000	2643	PSTM	n	3	3	1	1992	Spectrum
PA_A76-0	21	5750-6000	1459	PSTM	n	3	3	3	1976	PASA
PA_A78-0	29	5000	1665	PSTM	y	4	4	2	1978	PASA

PA_A79-0	8	4500-6000	289	PSTM	n	3	3	2	1979	PASA
PA_A80-0	17	4500	286	PSTM	n	3	3	2	1980	PASA
PA_A81-0	70	4800-6000	1286	PSTM	n	2	2	1	1981	PASA
PA_A82-0	31	5000-6000	1039	PSTM	n	3	2	1	1982	PASA
PA_A83-0	78	5000-6200	620	PSTM	n	2	2	2	1983	PASA
PA_A84-0	31	5050	823	PSTM	n	3	3	2	1984	PASA
PA_A86-0	35	5000	979	PSTM	n	3	3	2	1986	PASA
PA_A87-0	41	5000	1318	PSTM	n	3	4	2	1987	PASA
PA_A88-0/1	136	4000-5000	5344	PSTM	n	3	3	3	1988	PASA
PA_A89-0	6	4800	130	PSTM	n	2	2	1	1989	PASA
PA_A91-0	18	4800	1123	PSTM	n	4	3	3	1991	PASA
PA_A91-3	12	6800	485	PSTM	n	4	4	3	1991	PASA
PA_A92-2	12	6800	582	PSTM	n	4	4	3	1992	PASA
PA_A93-2	6	4000-6800	182	PSTM	n	3	3	2	1993	PASA
PA_AA99-0	14	6150	571	PSTM	n	2	1	1	1999	PASA
PA_AB99-0	7	6150	121	PSTM	n	2	2	2	1999	PASA
PA_AK76-0	30	5000-5800	1439	PSTM	n	3	3	2	1976	PASA
PA_BA82-0	4	5000	208	PSTM	n	2	2	1	1982	PASA
PA_BA87-0	8	5000	220	PSTM	n	3	3	2	1987	PASA
PA_K2002	28	7000	484	PSTM	y	5	5	3	2002	PASA
PA_K79-0/1	17	6000	524	PSTM	n	3	3	3	1979	PASA
PA_K80-0	23	5000-5800	1430	PSTM	n	4	4	3	1980	PASA
PA_K82	3	4000-5000	23	PSTM	n	3	3	2	1982	PASA
PA_K86-0	3	5000	110	PSTM	n	3	3	3	1986	PASA
PA_K88-0	4	4800	94	PSTM	n	3	3	2	1988	PASA
PA_K89-0	26	4800	510	PSTM	n	4	3	3	1989	PASA
PA_K91-0	4	5000	76	PSTM	n	3	2	2	1991	PASA
PA_K91-4	28	6800	2116	PSTM	y	4	4	3	1991	PASA
PA_K92-1	50	6800-7000	1986	PSTM	n	3	3	2	1992	PASA
PA_K93-1	34	6800	1537	PSTM	n	2	2	1	1993	PASA
PA_K99-0	12	6150	518	PSTM	y	4	3	3	1999	PASA
PA_O76-0	6	5750-6750	321	PSTM	n	4	3	3	1976	PASA
PA_O89-0	6	5800	138	PSTM	n	4	3	3	1989	PASA
PA_O91-0/2	5	4800-6800	154	PSTM	n	4	3	2	1991	PASA
PA_O92-3	3	6800	75	PSTM	n	4	3	2	1992	PASA
PA_P81	8	4800-5000	386	PSTM	n	3	3	2	1981	PASA
PA_P82	3	4050-6050	117	PSTM	y	3	3	2	1982	PASA
PA_P84-0	4	5050	108	PSTM	n	3	3	1	1984	PASA
PA_P91-0/1	24	4800/7000	952	PSTM	n	4	4	2	1991	PASA
PA_P92-4	8	6800	210	PSTM	n	4	3	2	1992	PASA
PA_P93-4	13	6800	221	PSTM	n	3	3	1	1993	PASA
PA_SA92	50	7000	3236	PSTM	n	2	1	1	1992	PASA
RON97	24	8000	3002	PSTM	n	5	4	3	1997	Spectrum
SCLB12	33	16km	5602	PSDM	y	5	4	4	2012	Spectrum
SCLB12	33	9600	5602	PSTM	y	5	4	4	2012	Spectrum
SCOB12	54	14.5-16km	8446	PSDM	y	5	5	3	2012	Spectrum
SCOB12	54	9600	8446	PSTM	y	5	5	3	2012	Spectrum
SN-96	14	8100	537	PSTM	y	4	5	3	1996	Spectrum
SPOB12	35	14.5-22.5km	10674	PSDM	y	5	5	3	2012	Spectrum
SPOB12	35	9600	10674	PSTM	y	5	5	3	2012	Spectrum
VERNLB06	13	9000	1314	PSTM	y	5	5	3	2006	Spectrum
VN03	51	9000-10000	3755	PSTM	y	4	4	3	2003	Spectrum

WC2002	36	9000	3678	PSTM	y	5	4	3	2002	Spectrum

Table 3-1. Table of data used in the study containing: the name of the survey, how many lines are contained within it, its horizontal coverage and vertical coverage, whether it is in time or depth: whether the survey is tied or not (yes (y) or no (n)); an overview of the quality of the data out of 5 (1 being poor, 5 being excellent) at three intervals; the Cenozoic, the Cretaceous and the Synrift; the vintage; and the data provider.

Well data for this study are sparse and of low quality and is, concentrated on the continental shelf and is associated with the mis-tied data. The nature of DWFTB systems commonly produces significant disruption of sedimentary packages depositing off the slope e.g., growth faults produce geographically limited mini basins; faulting causes slumping of the margin eroding out packages distally (Ortiz-Karpf et al., 2016; Scarselli et al., 2016). This precludes confident picking of significant reflectors off the shelf and into the abyssal plain, thus further reducing the efficacy of using well data. For these reasons, I have not used well data directly for dating and picking, but have instead correlated sections to tied and dated sections from published studies (Brown et al., 1995; Figure 2.2); Paton et al., (2007, 2008) (Figure 5.3); Mello et al. (2012); Mohammed (2013), and Serica Energy, (2014) (Figure 3.4).

3.1.1 Field data

To observe and consider sub-seismic deformation, I undertook fieldwork at two outcrops of DWFTBs in the Spanish Pyrenees; Laspuña and Armeña. The outcrop at Laspuña (Figure 1.3) is expressed in the opposing cliff faces that make up a small valley below Laspuña. Several days were spent in the valley photographing and collecting structural data to produce profiles of the cliffs appropriate for restoration. The evolution and development of the growth faults at Armeña have been well described (McClay et al, 2004; Lopez-Mir et al., 2014, 2015). The intention at Armeña was to observe and measure any syn-kinematic compressive features contemporaneous with the development of growth faulting. With the aim of producing a restorable section to compare with those made at Laspuña.

3.2 Methodologies

This section presents an overview of the methods applied to collect and interpret the data used in this study.

3.2.1 Seismic picking and dating

The study has primarily been interpreted using PSTM due to greater data coverage, though some individual sections are presented in the depth domain. Seismic interpretation was undertaken within the Schlumberger's Petrel 2012 and 2014 framework utilising the Guided Autotracking and Seeded 2D Autotracking tools. A system of loop tying was used to ensure the interpretation of consistent horizons across the basin. This is particularly pertinent when picking through faulted sections in DWFTB's as horizons are commonly eroded or alter seismic character. As such I have employed sequence stratigraphic methods to identify and interpret consistent horizons that share a characteristic geometry, as discussed in Williams (1993) and Muntingh & Brown (1993) (Figure 3.2).

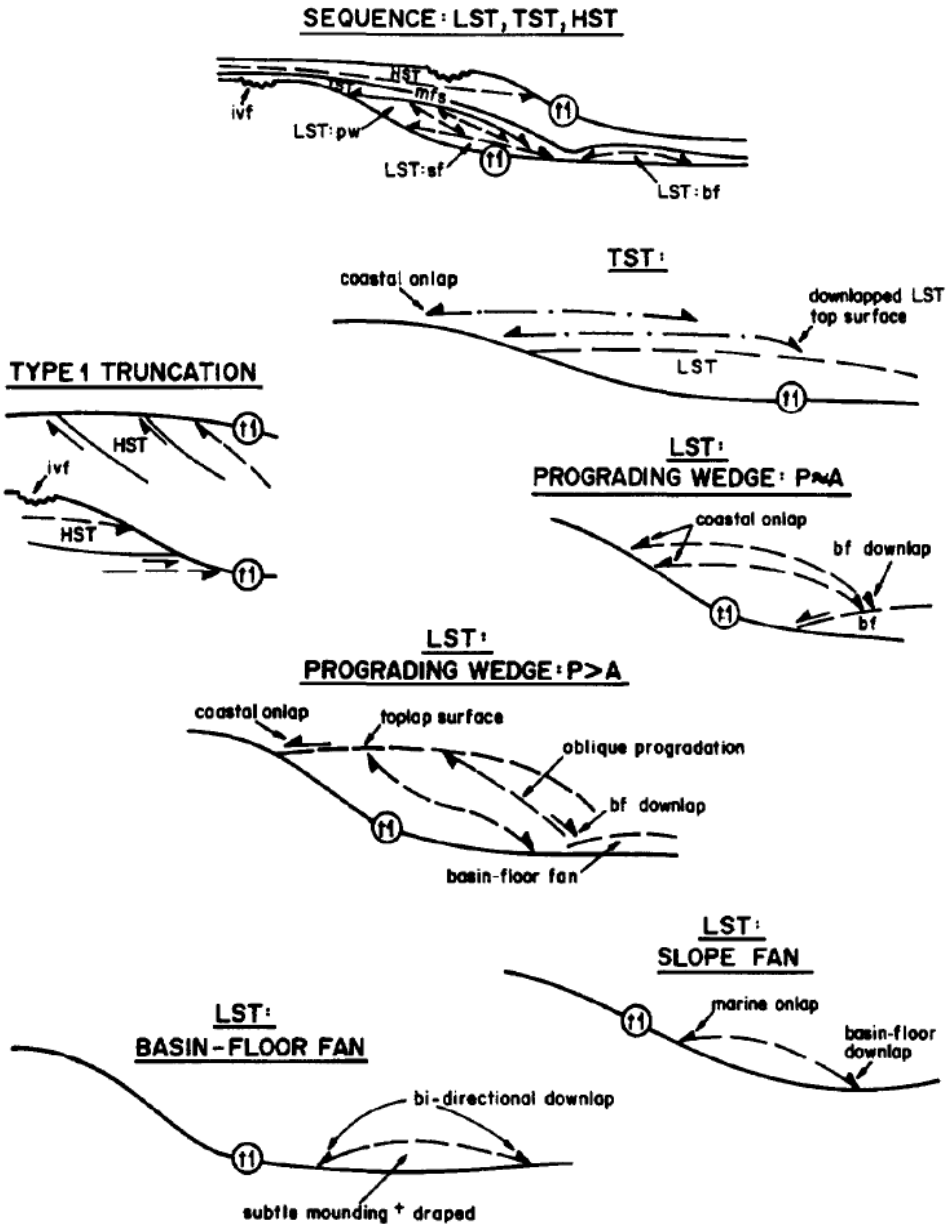

Figure 3.2. Schematic used for picking seismic facies from Muntingh & Brown (1993).

This study focusses mainly on the processes on the continental slope, for which I have no well control. The active nature of DWFTBs during deposition makes precise dating of sediment/reflector packages imprecise. Given these limitations well-tying is not the best mechanism for the identification and dating of sediments and structures within the basin, and so has not been applied in this study.

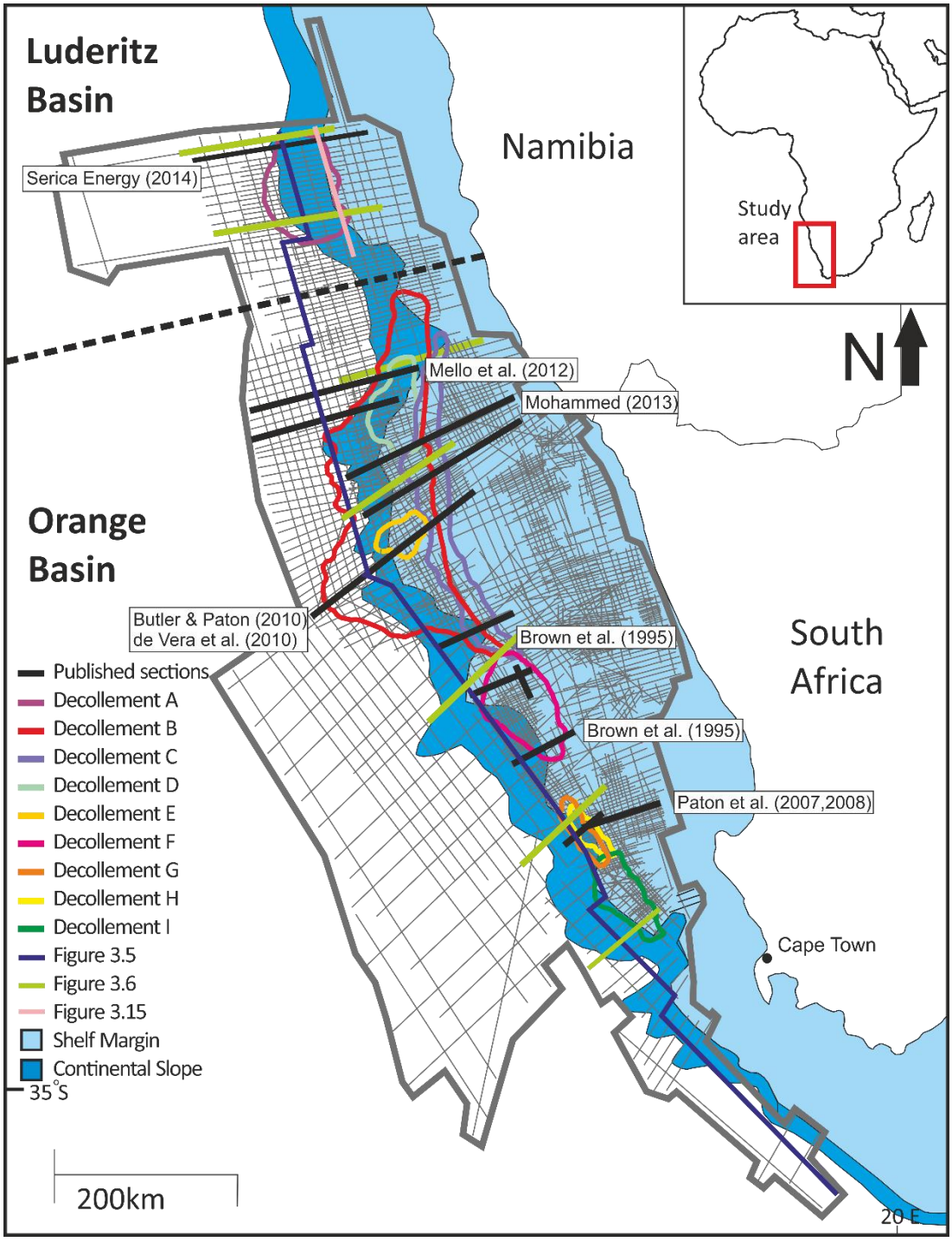

Figure 3.3. Map showing the locations of published studies in the Orange and Luderitz Basin used to date this study. Additionally the location of identified décollements and the geometry of them are shown.

The lack of reliable and applicable well data forced me to identify alternative methods of determining the timing of structures and packages within the basin. The

tectonostratigraphic history of the basin allows the identification of several megasequence-scale packages such as the Synrift and Cenozoic that are delineated by significant basin-wide regional unconformities, as described in 3.3.1. In order to sub-divide the basin into smaller sequences, I have combined detailed seismic interpretation with a 6 published studies that use well data from the various parts of the basin to date the sequences (Figure 3.3). The published studies and interpreted sections from the basin used are: Brown et al. (1995; Figure 2.2); Paton et al. (2007, 2008; Figure 5.3); Mello et al. (2012); Mohammed (2013), and Serica Energy (2014) (Figure 3.4). I have correlated the interpreted horizons from these published profiles with the seismic data available in this study, often using the same seismic reflection profiles, then progressively loop-tying out from these lines to produce a consistent framework for the entire basin. This provides reasonable relative timing for depositional and structural activity. Using these sections I have produced a section along the length of the basin that correlates all of the published interpretations and shows variations in the thicknesses of packages and the location and depths of DWFTBs along the margin (Figure 3.5).

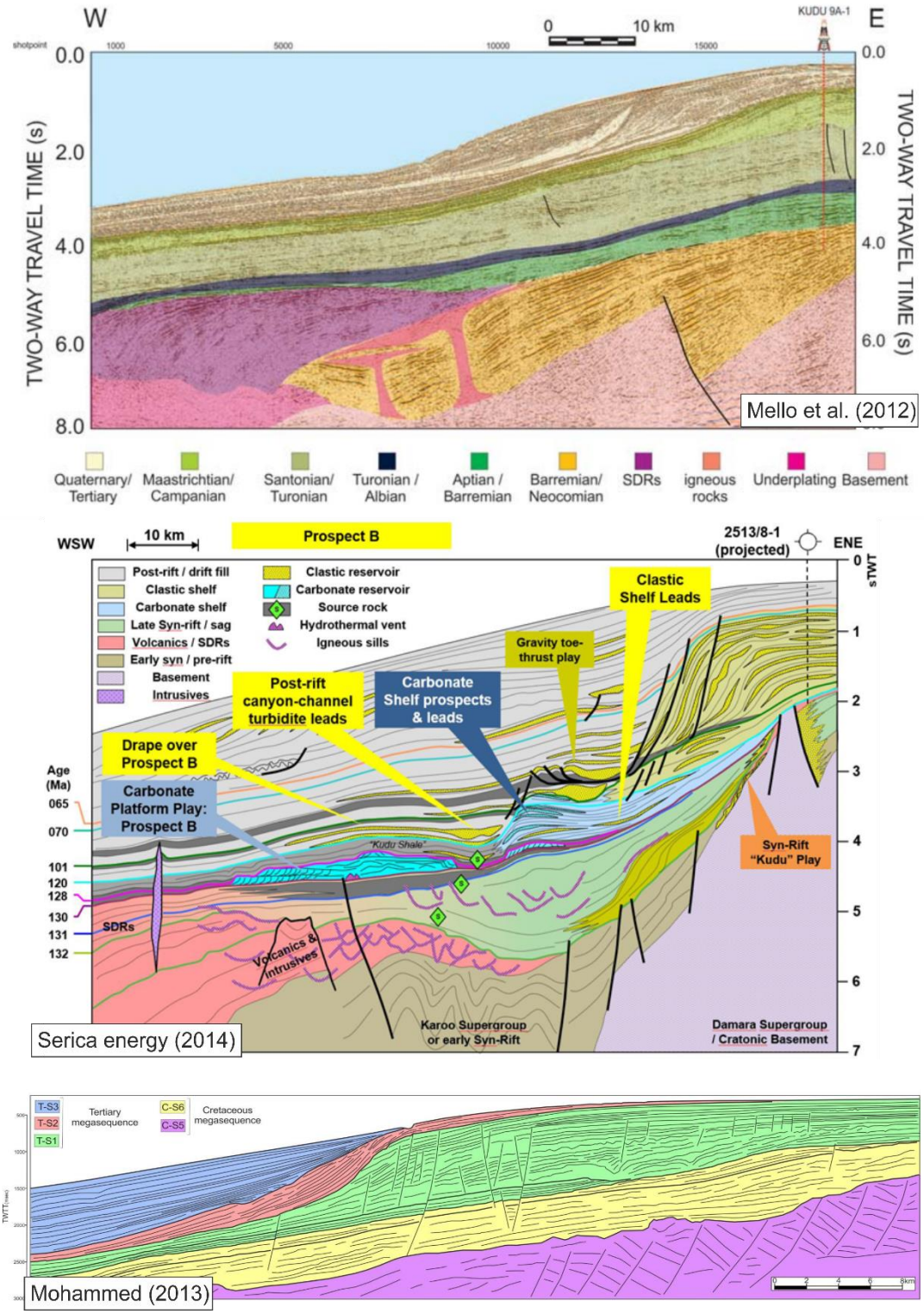

Figure 3.4. Seismic sections from Mello et al. (2012), Serica Energy (2014) and Mohammed (2013), used to correlate dating in this study. See Figure 3.3 for locations

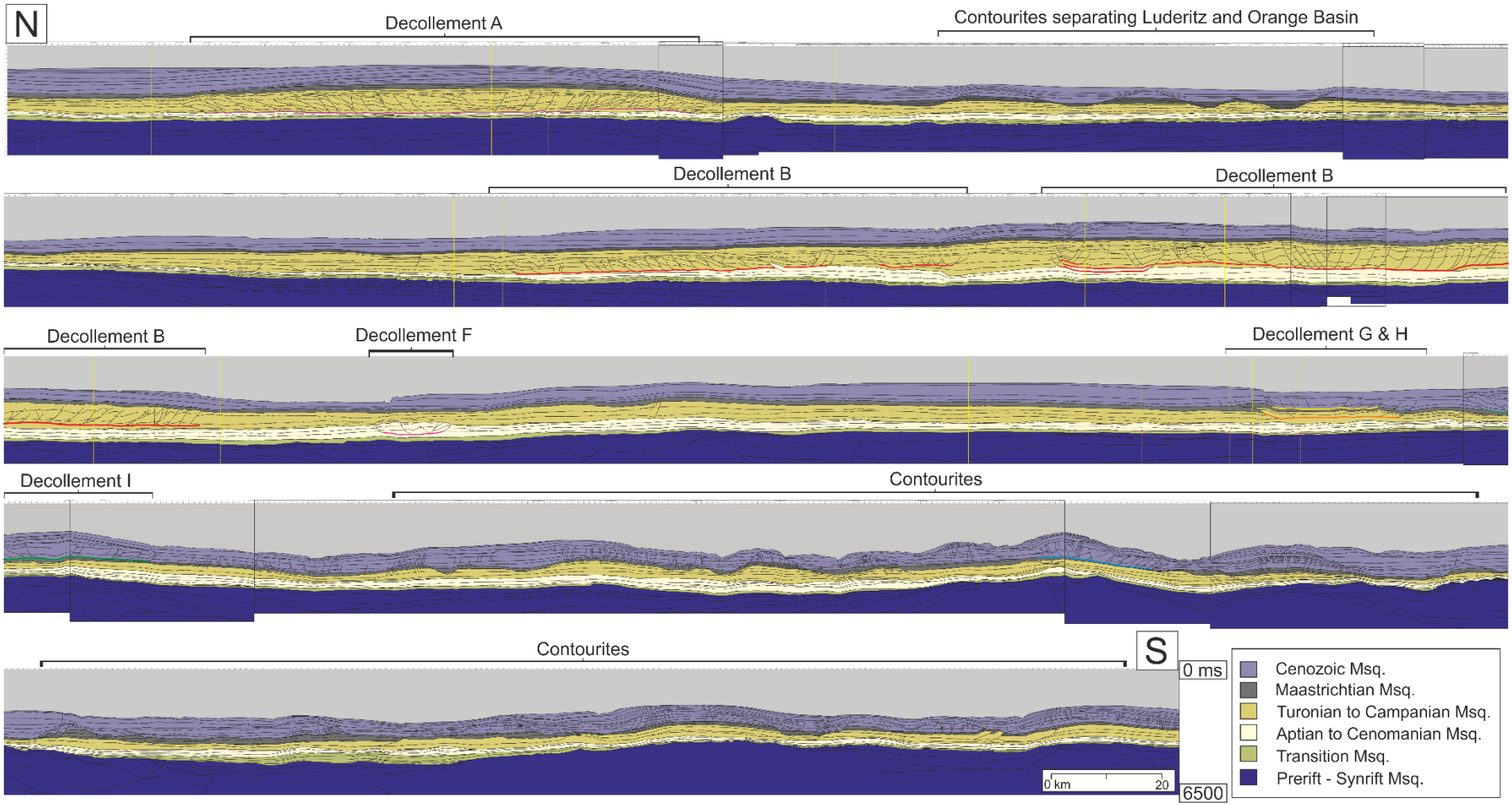

Figure 3.5. 1300 km long section transecting the length of the study area (Figure 3.3 for location) showing changes in thickness of major megasequences and the location of decollements (larger version included in Appendix).

3.2.2 The Basin

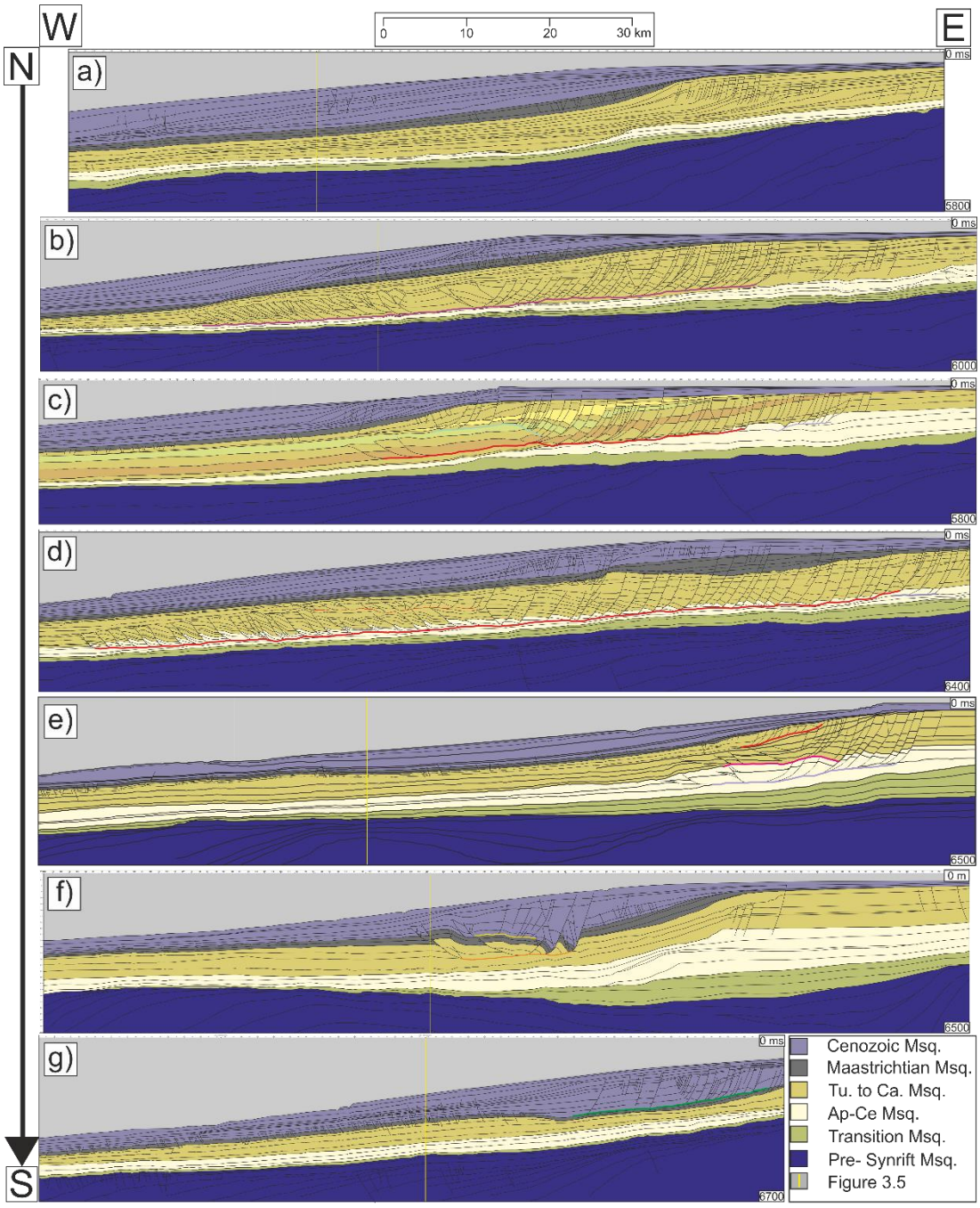

Figure 3.6. Seven parallel interpreted sections perpendicular to the margin (Figure 3.3) showing changes in thickness and deposition of megasequences and variable geometry of DWFTBs across the margin. a) SCLB12-53 most northerly section from the Luderitz Basin showing normal faulting to the east with no defined detachment. b) SCLB12-17, section through décollement A with a classical geometry. c) ECL89-14, highly unusual section showing far greater extension than compression spread over three décollements (B, C & D). d) SCOB12-103, typical section from the centre of the basin with unusual thickness of Maastrichtian. e) SPOB12-011, bizarre section showing three

stacked décollements (B, C & F) each with separate extensional and compressional domains. f) SPOB12-23a (PSDM) section shows increasing thickness of Cenozoic sediments and the occurrence of later Cenozoic aged DWFTB developments above décollements G & H. g) WC2002-21, Southern section showing Cenozoic aged DWFTB associated with thicker deposition, also showing contourite development in the Cretaceous. All sections, except f), are presented in PSTM and all are vertically exaggerated 3:1 (larger version included in Appendix).

Here I describe elements of the basin and elucidate in more detail observations from the initial interpretation phase of this study. Figure 3.6 shows a set of margin perpendicular interpreted seismic profiles made along the basin from north to south. These interpretations along with Figure 3.5, show some of the features discussed in this section as well as displaying the variation in package thickness and DWFTB expression across the basin. Larger interpreted and uninterpreted versions of the seismic profiles plus a number of additional sections not featured in this thesis have been included in the appendix.

3.2.2.1 Megasequences

The margin has been divided into six megasequences (Figure 2.1 & 2.3) following the scheme defined by Paton et al. (2008). These megasequences are delineated by a set of horizons described by Brown et al. (1995; Figure 2.2) identified through the picking of stratal relationships of onlaps, offlaps, downlaps and truncations (Figure 3.7). The megasequences from oldest to youngest are: the Synrift, the Transition, the Aptian to Cenomanian, the Turonian to Campanian, the Maastrichtian and the Cenozoic.

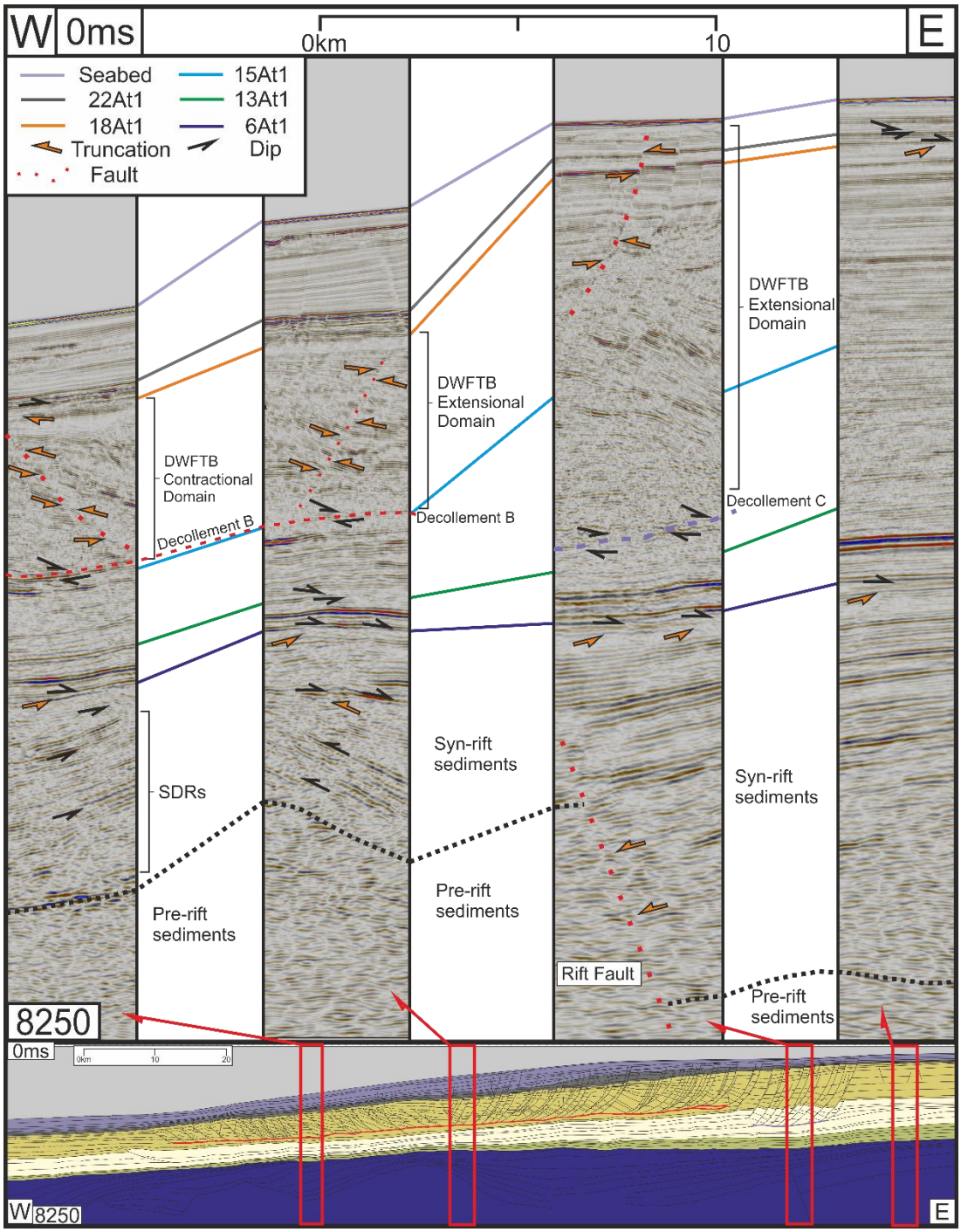

Figure 3.7. Four portions of the seismic profile seen in Figure 2.1, indicating the 5 key horizons described by Brown et al. (1995) used in this study to delineate the basin into 6 megasequences. Arrows on the profiles indicate the stratal relationships used to pick these horizons.

3.2.2.1.1 The Synrift Megasequence;

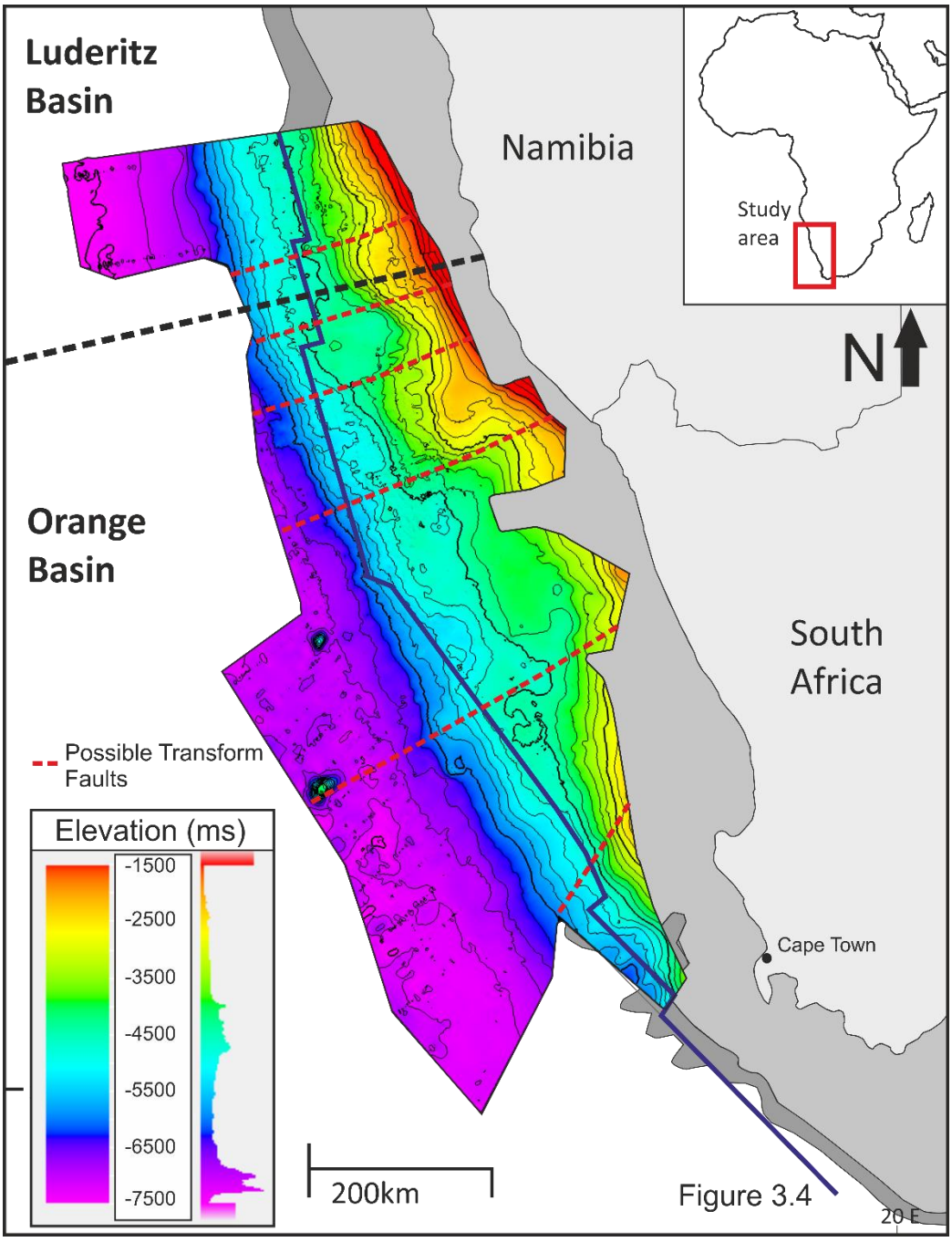

Figure 3.8. Surface map of the top of the Synrift Megasequence including the location of possible transform faults that provide structural controls on later deposition. Location of the profile in Figure 3.5 is also projected onto the surface.

The Synrift Megasequence is the oldest megasequence considered in this study and encompasses the syn-rift and pre-rift sediments. Up-dip (inboard) portions of sections

show rift-scale normal faults onto which syn-rift sediments have been deposited in growth packages that fill and overtop the graben and half-graben basins (Figures 3.4 & 3.6). Down-dip (outboard) of these rifts fanning packages of seaward dipping reflectors (SDRs) can be seen that transition outboard to oceanic crust (Koopman et al., 2013; Figure 3.7). Reflectivity at the base of this megasequence is poor and discontinuous and generally representative of the pre-rift. Further up sequence syn-rift sediments and SDRs are identified by higher amplitude fanning sequences of continuous reflections. Cut-offs and truncations highlight and identify the fault planes of the rifted fault blocks (Figure 3.7). The uppermost reflections of the synrift megasequence are of very high amplitude and are continuous across the basin. This final package of very high amplitude reflections within the syn-rift megasequence is concomitant with the 6At1 reflector identified in Brown et al. (1995) and represents a depositional hiatus that forms an unconformity at the base of the subsequent megasequence forming an unconformity. Figure 3.8 is a surface map of the top of the Synrift Megasequence prior to the deposition of the Transition megasequence sediments. In it some, ENE-WSW orientated lineaments are identifiable based on distinctive changes in the elevation of the megasequence along the margin, these relate to transform faults that segment the basin. This is evidence of structural inheritance which provides a control on later sedimentation (Paton et al., 2008; Mohammed, 2013).

3.2.2.1.2 The Transition Megasequence

This Transition Megasequence represents the transitional phase from active rifting to post-rift thermal subsidence. It is formed during the continent/continent break-up and initiation of plate separation by oceanic spreading of Gondwana. It has broadly the same thickness across the basin (up to 500 ms, Figure 3.9). The earliest phase of deposition is restricted in its extent and fills pre-existing structural lows in the top of the Synrift Megasequence. As accommodation filled and rates of sedimentation increased a period of progradation ensued that extends across the entire shelf. The earliest phase of deposition is defined by onlapping of reflections onto the upper surface of the Synrift Megasequence in restricted highs and lows on the surface of 6At1.

Moving up through the sequence, broad parallel reflections that extend across the margin downlap progressively more distally as the packages prograde out into the basin are observed. The top of this sequence forms a subtle unconformity with the subsequent megasequence, defined by truncation. This unconformity correlates to the same reflector as 13At1 as described by Brown et al. (1995).

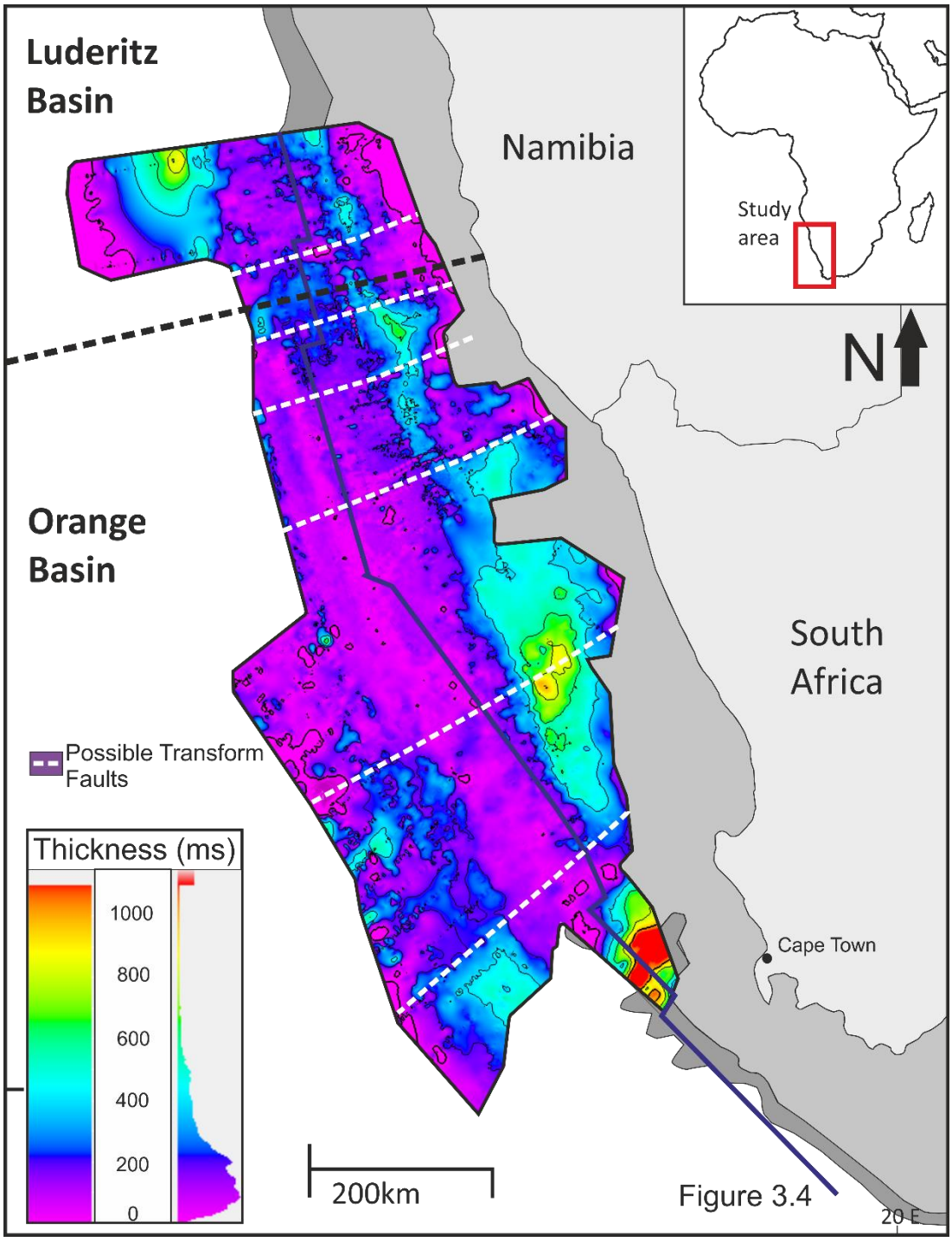

Figure 3.9. Isochron map of transition megasequence.

Figure 3.9 shows an isochron of the Transition megasequence with the transform lineaments projected onto the surface. From this it is evident that some faults still exert a control on sedimentation at this time while others have ceased activity.

3.2.2.1.3 The Aptian to Cenomanian Megasequence;

The Aptian to Cenomanian Megasequence initiated as a phase of progradation that build out onto the underlying transitional megasequence. This progradation latterly develops into an aggradational phase creating significant relief between the shelf and abyssal plane. A number of slip horizons pervade this megasequence reflecting the deposition of thick muds (Paton et al., 2007, Figures 3.5 & 3.6). These slip horizons have been used by both early and contemporaneous DWFTBs, and by late phase Maastrichtian DWFTBs that fold overlying older DWFTB systems in the Turonian - Campanian (décollement C & E). Reflectivity is strong within this megasequence (Figure 3.7). The Aptian to Cenomanian Megasequence is defined by a set of parallel reflections that initially downlap onto 13At1 before eventually aggrading to form a significant slope (Figure 3.6). The top of this package forms an unconformable surface concomitant with the 15At1 horizon in Brown et al. (1995).

3.2.2.1.4 Turonian – Campanian Megasequence;

This Turonian to Campanian megasequence corresponds to a period of high rates of sedimentation (Light et al., 1992; Muntingh & Brown, 1993; Paton et al., 2007) producing distinctive aggradational and progradational packages. It is dominated by DWFTB systems at the shelf margin and contains multiple detachment surfaces. Reflectivity is strong forming delineable packages of reflections that aggrade or prograde out into the basin. Approaching the paleo shelf break, vertically aligned discontinuities in horizontal reflectivity define normal faults within the extensional domain of DWFTBs (Figure 3.7). These offsets become progressively larger seaward as the faults increase in displacement. Further into the basin geographically isolated

packages of reflections form on top of these fault blocks representative of syn-kinematic growth sediments.

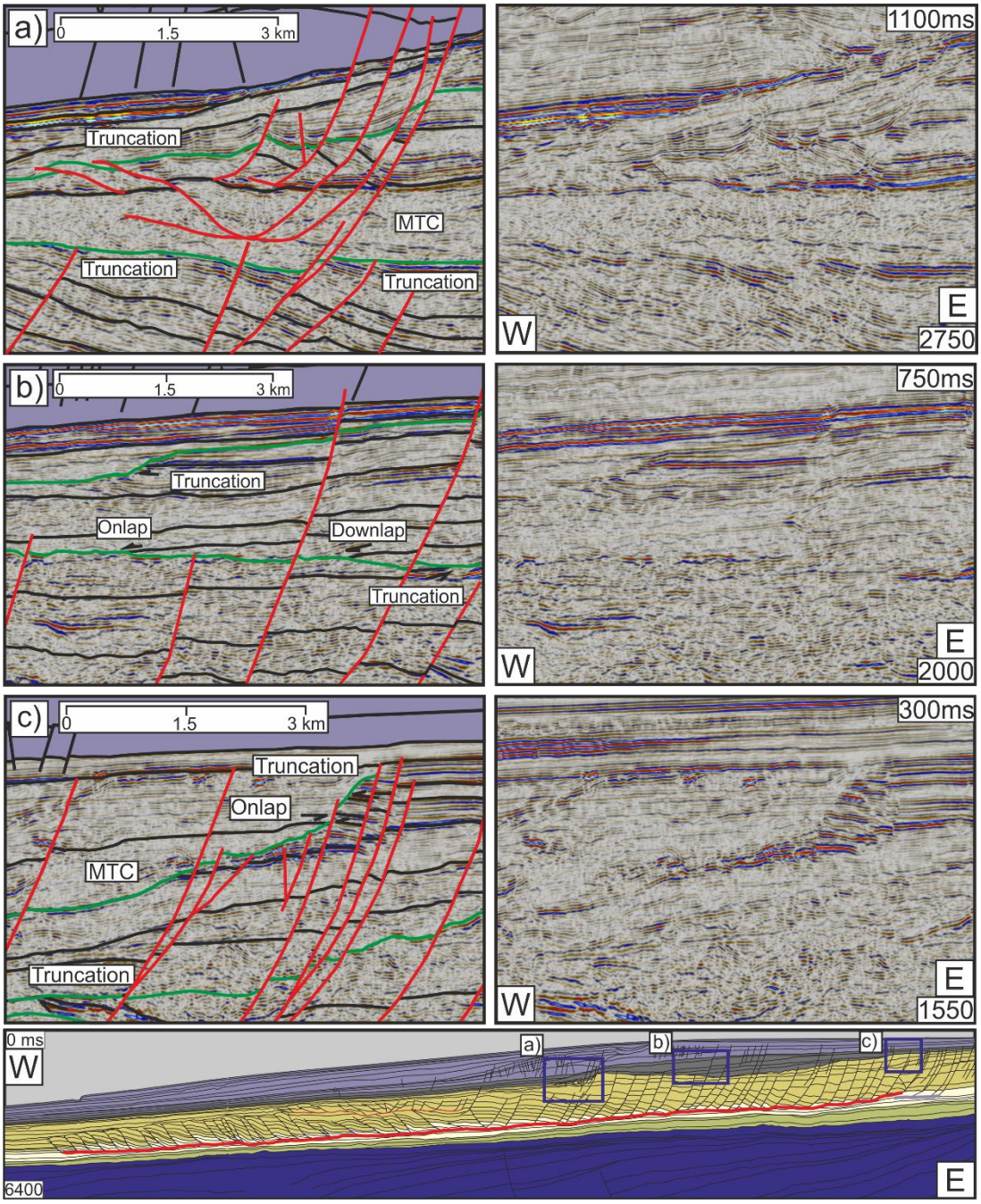

Figure 3.10. A set of interpreted and uninterpreted seismic sections from the top of the extensional domain in Figure 3.6 d), showing a range of seismically resolvable structures formed by slope margin processes. a) Smaller DWFTB systems forming above an older/concurrent extensional domain, note the multiple detachments and erosional unconformities. b) Erosion of upper portions of an active extensional domain forming a mini basin that is then infilled. c) Two erosional surfaces picked out by truncations showing the collapse of the top of the paleo-shelf and the formation of a MTC.

There are a variety of different arrangements of syn-kinematic sediments deposited above the fault blocks representing a range of geological processes (Figure 3.10). For example, the truncation of some reflections by younger reflections is representative of the erosion of the footwall of normal faults, sometimes indicating multiple phases of erosion; a loss of reflectivity and formation of discontinuous reflections is indicative of Mass Transport Complexes (MTC's); onlap and overstepping of reflections indicative of the formation of restricted basin on top of the extensional domain.

The isochron thickness map in Figure 3.11 shows the location of deposition for sediments in the Aptian to Cenomanian and Turonian to Campanian megasequences. Projected onto the section are outlines for the location of décollement surfaces. A strong correlation can be seen between areas of thickest sedimentation and the location of DWFTB systems. Deposition is concentrated around the mouth of the Orange River, with fewer sediments being deposited in the far south and between the Orange and Luderitz Basins, areas which are dominated by contourites (Figure 3.5). This relationship will be revisited and discussed in Chapter 7.

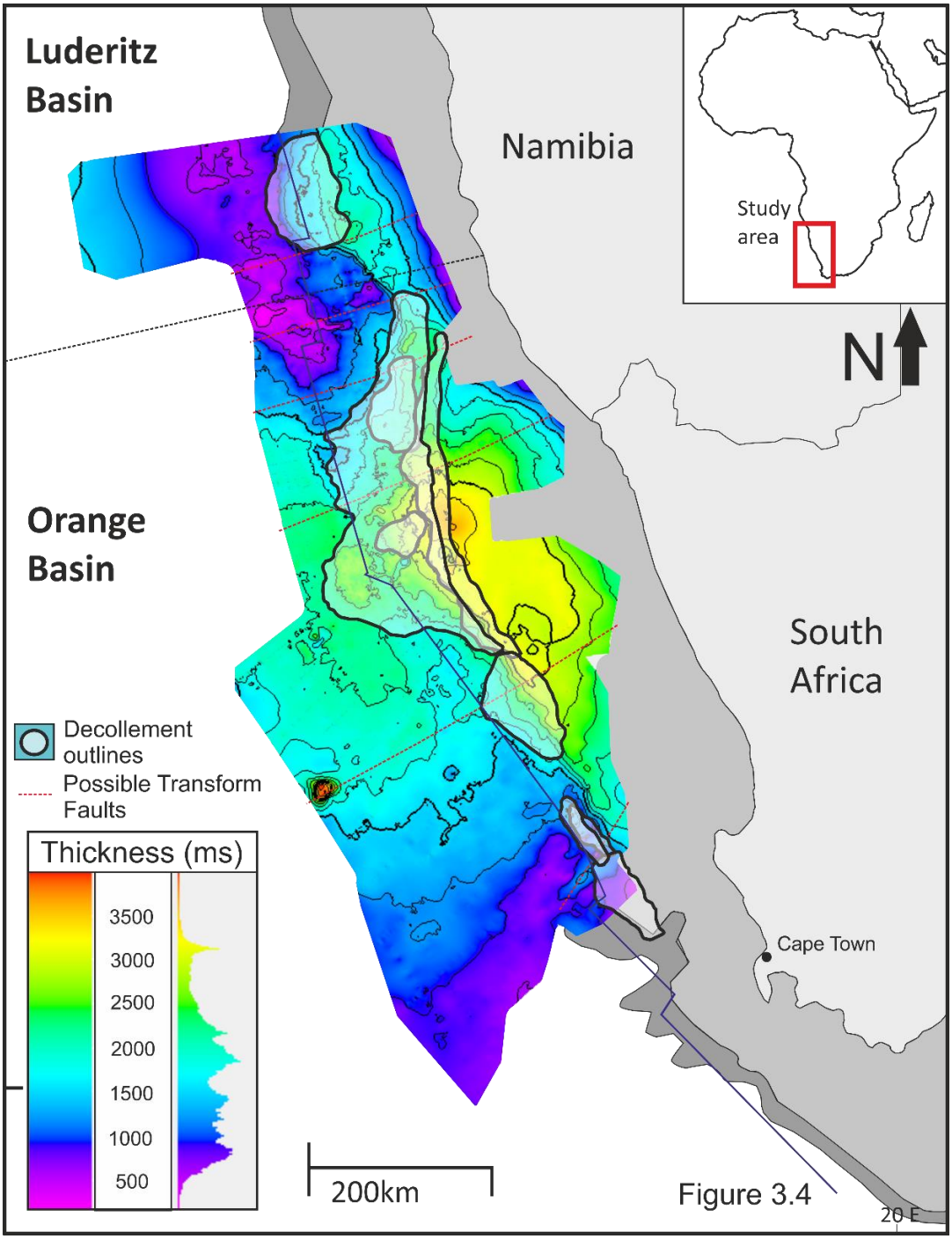

Figure 3.11. Isochron map of the Aptian to Cenomanian and Turonian to Campanian megasequences. The location of décollements are projected onto the map.

3.2.2.1.5 Maastrichtian Megasequence;

The Maastrichtian Megasequence is the latest depositional phase of the Cretaceous before a depositional hiatus and the formation of a considerable regional unconformity. Whilst the megasequence is relatively thin it is useful for dating activity in DWFTB systems across the margin. It is characterized by a distinctive set of parallel, high-

amplitude reflections that extend across the abyssal plane and continental slope throughout the basin (Figure 3.7). It is entirely eroded out on the continental margin but where present in the basin it can reach thicknesses up to 800 ms thick, (in the top of active extensional faults) though it is generally ~150 ms thick (Figure 3.12).

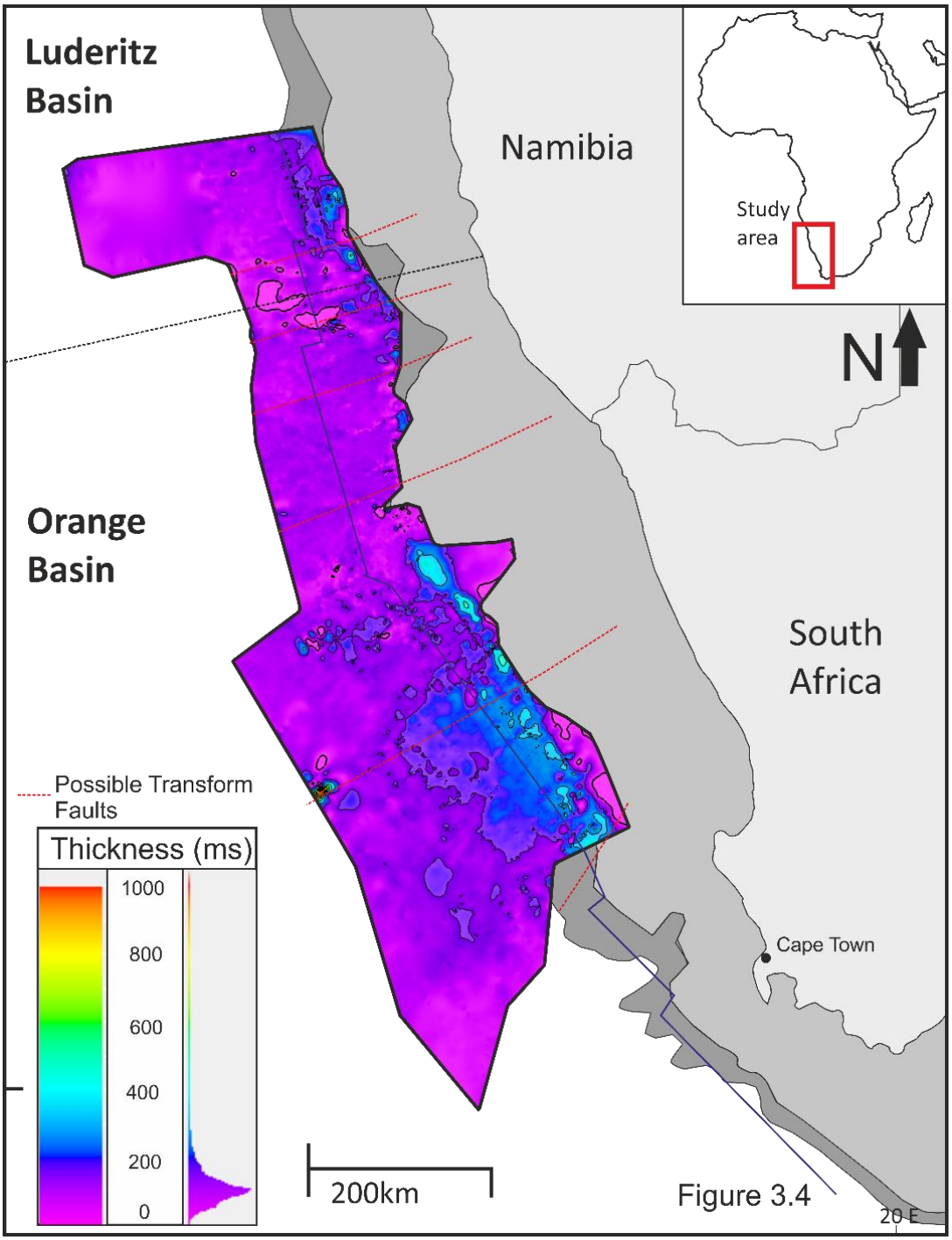

Figure 3.12. Isochron map of the Maastrichtian Megasequence.

3.2.2.1.6 Cenozoic Megasequence;

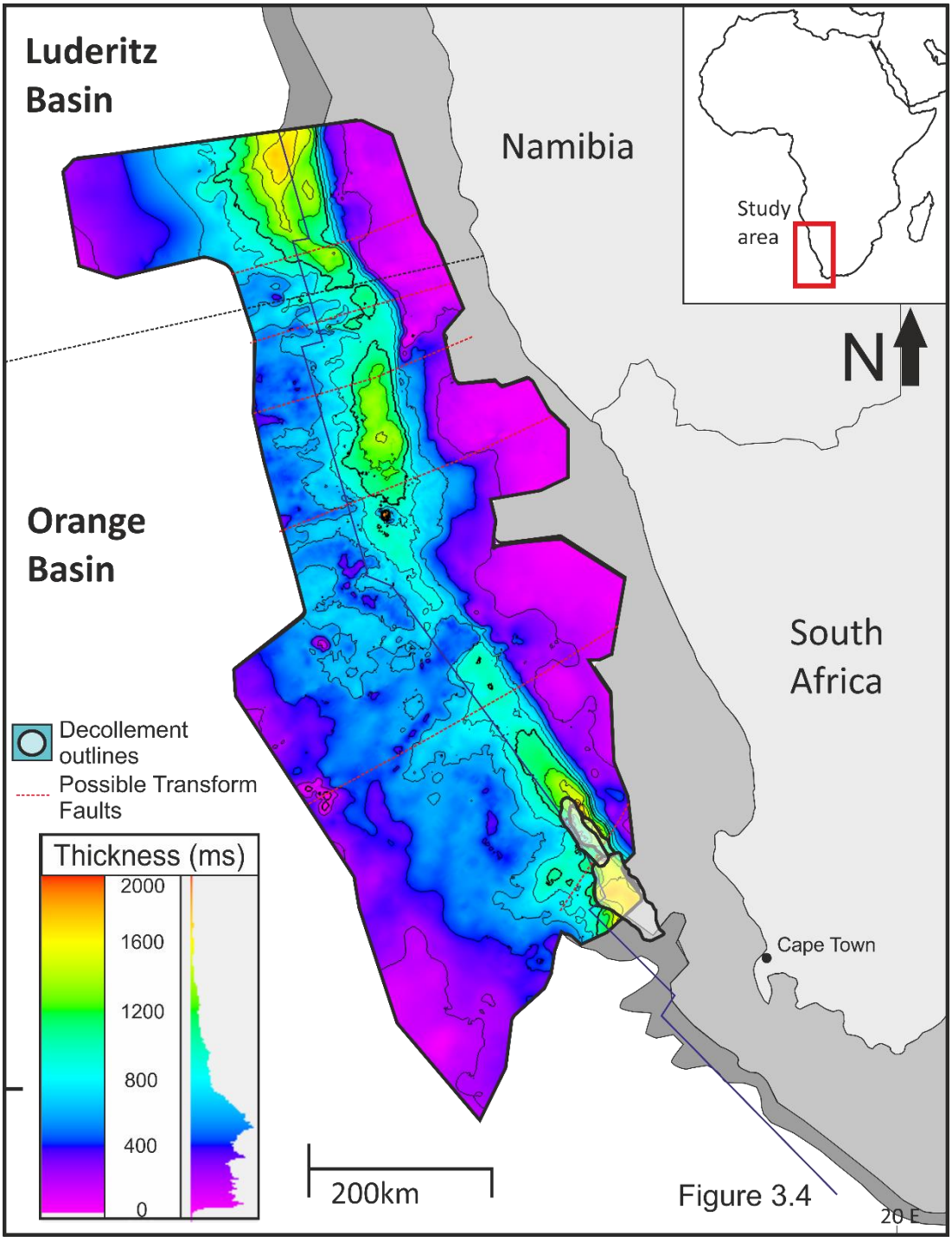

Figure 3.13. Isochron map of the Cenozoic megasequence. The outline of décollements G, H & I which were active during the Cenozoic have been projected onto the map.

During the Cenozoic there was a considerable reduction in the rate of sedimentation (McMillan, 2003) compared to the Middle and Late Cretaceous. Sedimentation shifted outboard of the paleo-shelf break and formed prograding clinoform geometries that

extended out into the basin. A wide variety of other structures are present across the margin including contourites, slides, MTCs and DWFTBs. Reflectivity within the Cenozoic is strong and of high amplitude. The megasequence is bounded by the seabed at the top and a marked regional unconformity at its base (22AT1, Brown et al., 1995; Figure 3.7). The unconformity is characterised by a high amplitude reflection off the shelf break and as a boundary of changing reflectance on the paleo-shelf margin. It is up to 2000 ms thick in places basinward of the shelf margin (Figure 3.13) and reduces to one or two wavelets inboard on the shelf margin. Laterally, it is thickest in the periphery of the study area, in the far north and south of the study area. This is away from the main sediment input at the mouth of the Orange River. In the far south, multiple DWFTBs persist (Figure 3.3) that are correlative with the location of thicker sedimentation, however DWFTBs have not reactivated in the north despite having a similar sedimentary thickness (Figure 3.13).

3.2.3 Detachments

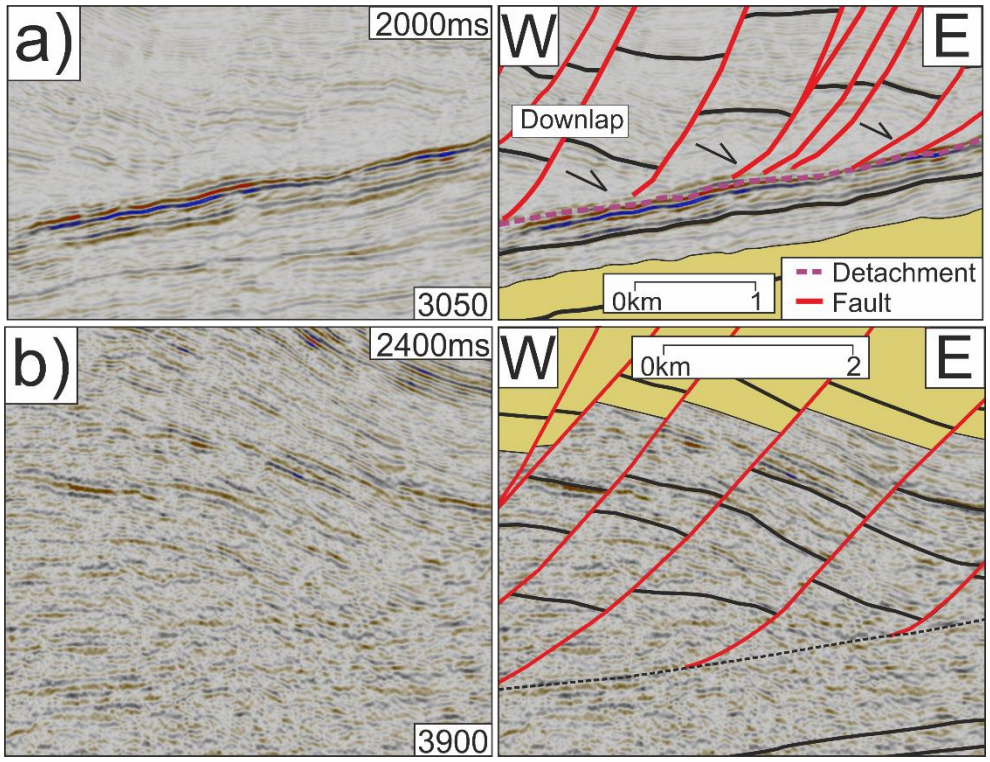

Figure 3.14. Image showing the difficulties associated with picking décollement horizons. a) From section g) in Figure 3.6; detachment is picked by downlapping reflections onto a high amplitude reflection dipping in the opposite sense. b) A more typical view from Figure 2.1; the décollement is indistinct due to attenuation of the signal by overlying beds.

Most of the gravity collapse structures exist within the Turonian to Campanian Megasequence. Though some smaller isolated systems are also present in the Aptian to Cenomanian Megasequence and within the Cenozoic Megasequence. The seismic reflection data for these megasequences is mostly of excellent quality, though the complex geometries produced by DWFTB's do exert a considerable control on the reflectivity present, particularly towards the base of faults and within the transitional portions of collapse structures (Figure 3.14).

I have identified nine décollement surfaces in the study area (Figure 3.3). These are discrete shared detachments that persist over large areas of the basin (over 100 km). The faults and décollements have been picked using the "Interpret Fault" tool on Schlumberger's Petrel 2012.1/2014.2. The interpretation of the detachments are based upon identifying downlapped reflections onto slope parallel continuous reflections (Figure 3.14). The amplitude of these reflections tends to be exceptionally low. In some areas, reflections are apparently conformable above and below the décollement. Single décollement surfaces may follow a single horizon for significant distances but can also cut up and down section, particularly at the periphery of the collapse.

The DWFTBs persist across the extent of the margin and are linked to periods and regions of the basin experiencing high rates of sedimentation (Figures 3.11 & 3.13). Figures 3.11 & 3.13 show this relationship particularly well, where unusually thick accumulations of sediments are deposited DWFTBs have developed, shifting sediment from the shelf to the abyssal plain. The main slip surfaces appear to be organically rich mud deposits associated with maximum flooding surfaces and base of slope systems during periods of low sedimentation (Paton et al., 2007).

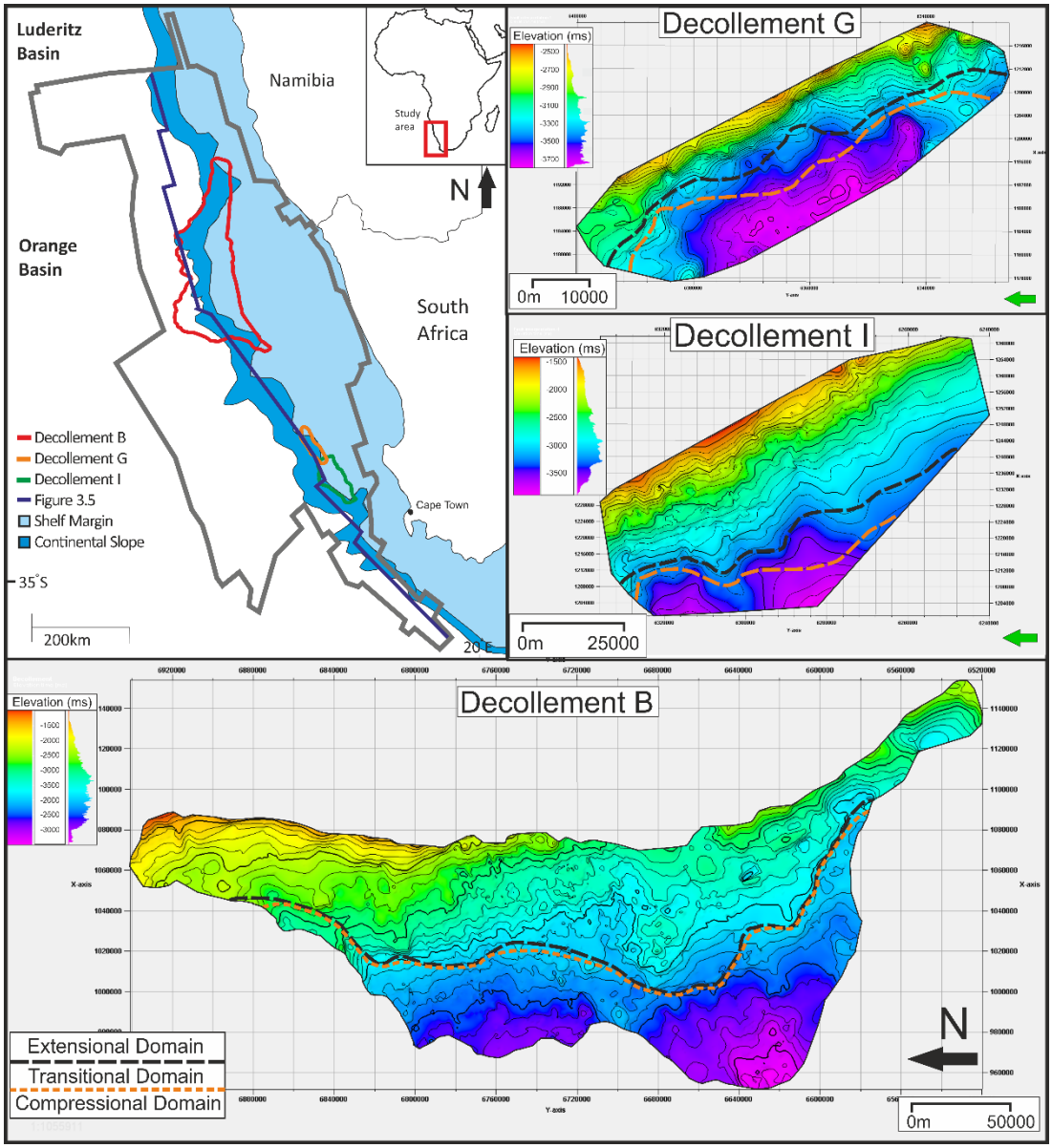

Figure 3.15. Three surface maps of decollements B, G and I. Two lines have been projected onto the maps to delineate the extensional, transitional and compressional domains (additional surface décollement maps are provided in the appendix).

The geometry of the collapses themselves is highly variable, as seen in Figure 3.3. They are mostly elongate with their longest axis being parallel to the shelf, though Décollement B, which is considerably larger and with a longer collapse history, has produced a more unusual geometry.

Detailed interpretation of the décollement surfaces in 3D shows they are internally complex (Figure 3.15). The décollement surfaces all dip generally basinward. Although the base surface has some rugosity it is overall reasonably consistent along strike. In the

down dip part of the system, some of the mapped decollements are clearly deeper in the middle of their strike length especially décollement G (Figure 3.15). The lowest areas are clustered towards the middle of the contractional domains. These detachments commonly switch between horizons both laterally and distally as proposed in the non-discrete shale detached DWFTBs model described by Krueger and Gilbert (2009). The décollements exhibit an arcuate geometry. Whilst this could be an effect of the projection of surfaces between widely spread seismic lines and thus an artefact of the modelling software, these may represent the remnants of previous discrete collapses. In terms of the 3D models proposed by de Vera et al (2010) and Scarselli et al. (2016) these could be the lateral ramps of discrete collapse systems. By observing crosslines through these structures it is clear these are geological structures (Figure 3.16 & 3.17). The normal faults in the crossline in Figure 3.16 show frequent changes in orientation across the section, and also migrate between different detachment surfaces. These observations are reflected in the detachment surface map in Figure 3.17 where arcuate forms relate to changes in dip orientation. So perhaps these features should be considered as separate discrete DWFTBs split by lateral ramps. However, looking at the most northerly section in Figure 3.5, which is parallel and down-dip of Figure 3.16, no changes in fault orientation are present. Instead, they are of consistent orientations, split about the centre of the collapse with faults in the north dipping south and faults in the south dipping north, all faults detaching onto a single horizon. From this its seems likely that discrete DWFTBs form separated by lateral ramps as described by de Vera et al (2010) and Scarselli et al. (2016) but they do eventually amalgamate to form a single collapse structure over time. This will be discussed further in Chapter 7.

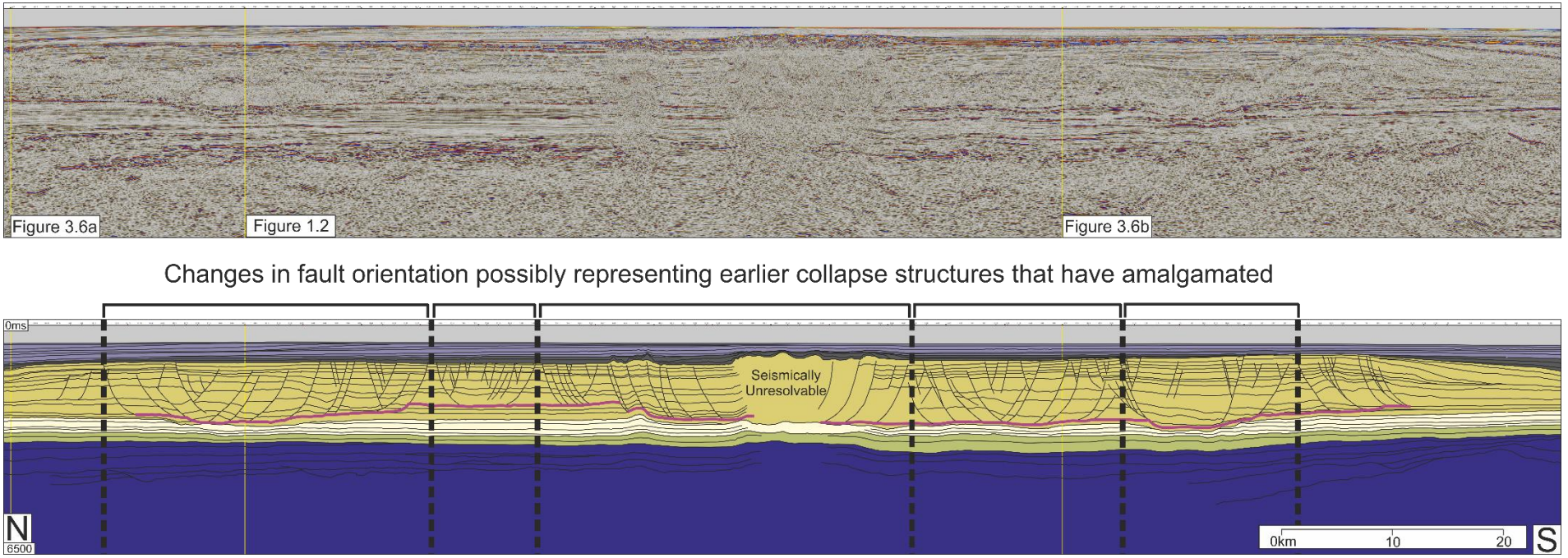

Figure 3.16. Interpreted and uninterpreted seismic section (SCLB12-14) from the Luderitz basin (Figure 3.3 for location) indicating the presence of changes in fault orientation along the length of a DWFTB detached onto Décollement A (larger version included in Appendix).

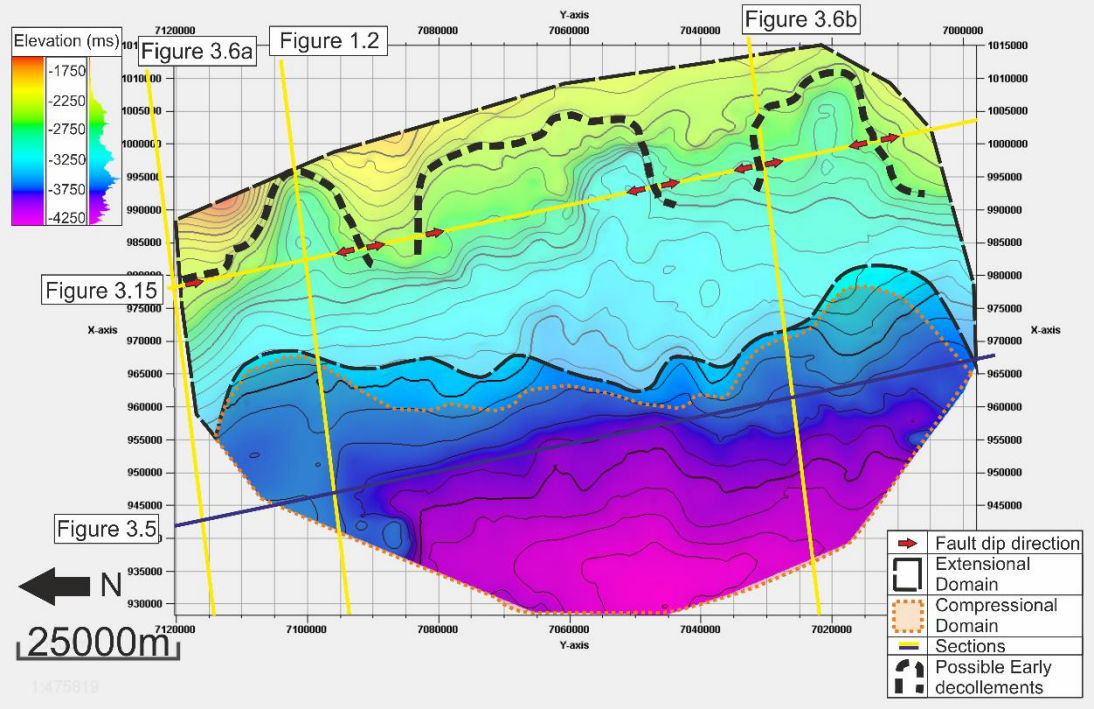

Figure 3.17. Map in time of the Décollement A with the location of the contractional, transitional and extensional domains marked. Also marked are changes in fault orientation of potential discrete DWFTBs observed in Figure 3.16 as well as the potential outline of these discrete bodies.

3.2.4 Restorations

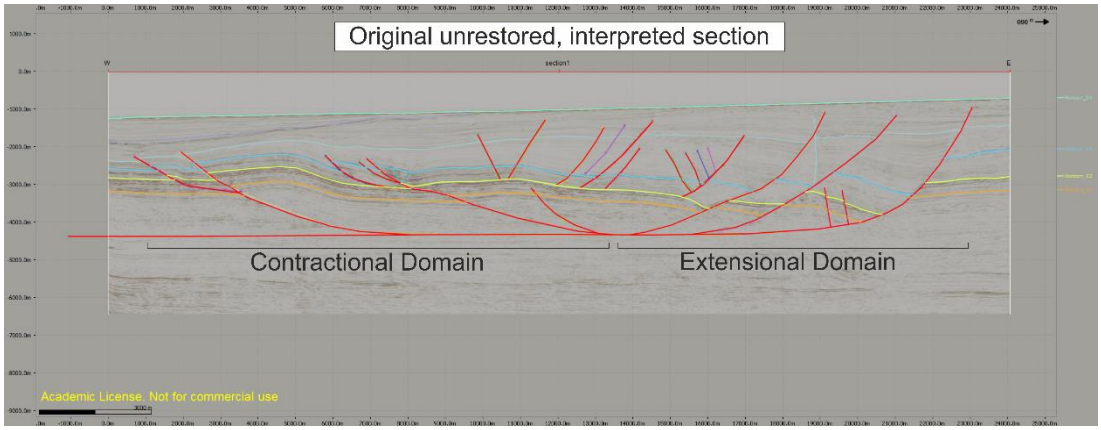

Figure 3.18. Example of a depth converted seismic section interpreted in Midland Valley's Move 2014.2 software (Line 3 featured in Chapter 5).

All of the restorations presented in this study have been undertaken using Midland Valley's Move 2011, 2012.1 and 2014.1 software. Restorations have been performed sequentially starting with the latest fault to form and proceeding backwards to the first fault to deform, akin to the methods applied by Lickorish & Ford (1998) and

Bland et al. (2006). These same methods have been applied to DWFTBs in the Orange Basin by de Vera et al. (2010) and the contractional domain in Butler & Paton (2010). A stepped example of this method is presented below.

3.2.4.1 Restoration Method

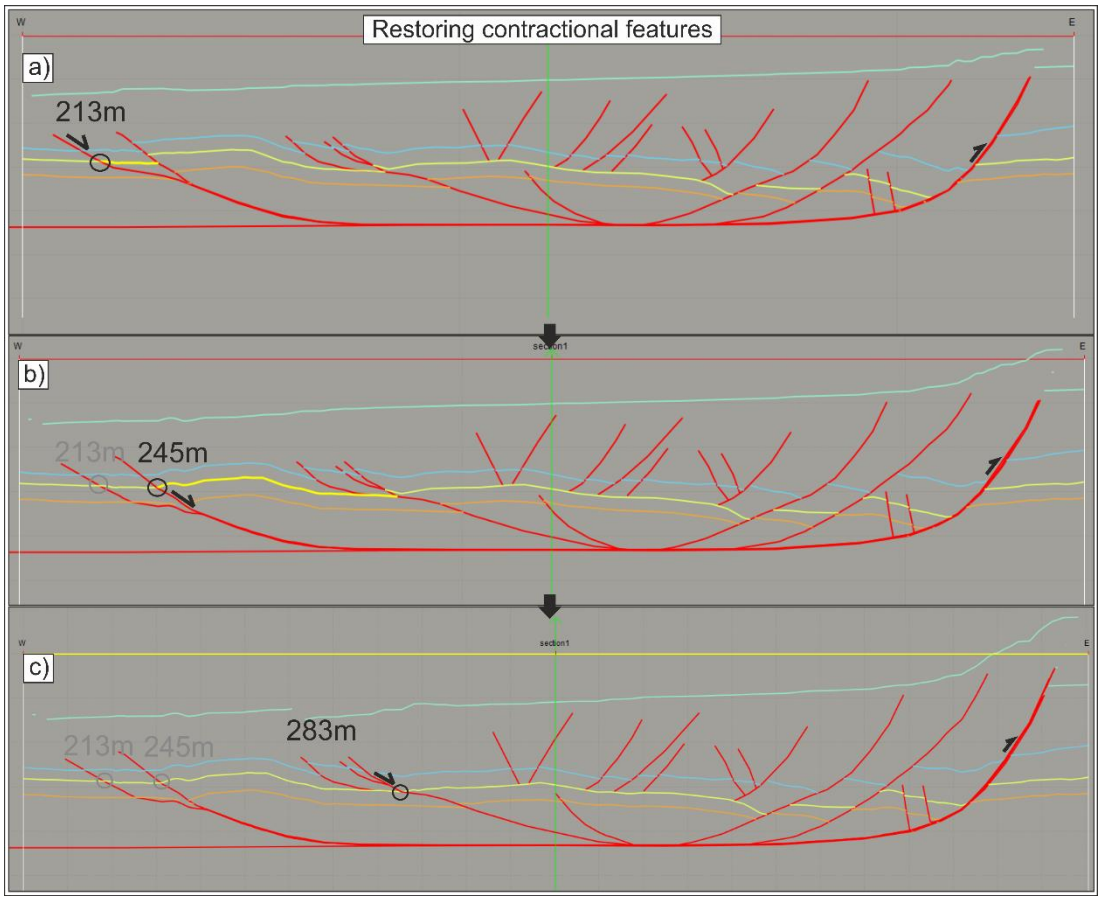

Figure 3.19. Stepped restorations of contractional thrust faults from west to east (a-c) restoring the DWFTB in Figure 3.18. Values for fault heave are labelled in black above the restored fault.

The first step in producing a restoration is to import a true scale, depth converted (for depth conversions please see Appendix), seismic image into the Move software package (Figure 3.18). The faults are interpreted on the image followed by a number of distinctive pre-, syn- and post-kinematic horizons. Restorations are generally undertaken using pre-kinematic beds (Orange and Yellow horizons on Figure 3.18) to extrapolate values of the maximum displacement on a fault, rather than representing punctuated phases of movement. Faults are tackled sequentially starting with the contractional domain (Figure 3.19), with the most proximal thrust fault being restored first (Figure 3.19a). The horizons are shifted down the fault plane, counter

to their initial transit, until the horizon in the hangingwall meets with the same horizon in the footwall. During this movement the entire structure is shifted along the décollement and up the most proximal normal fault, as all deformation is assumed to take place between these two faults. Measurements of the displacement are recorded during this shift and totalled to produce a figure for the total displacement accommodated through thrusting. In the example in Figure 3.19 this is 741 m.

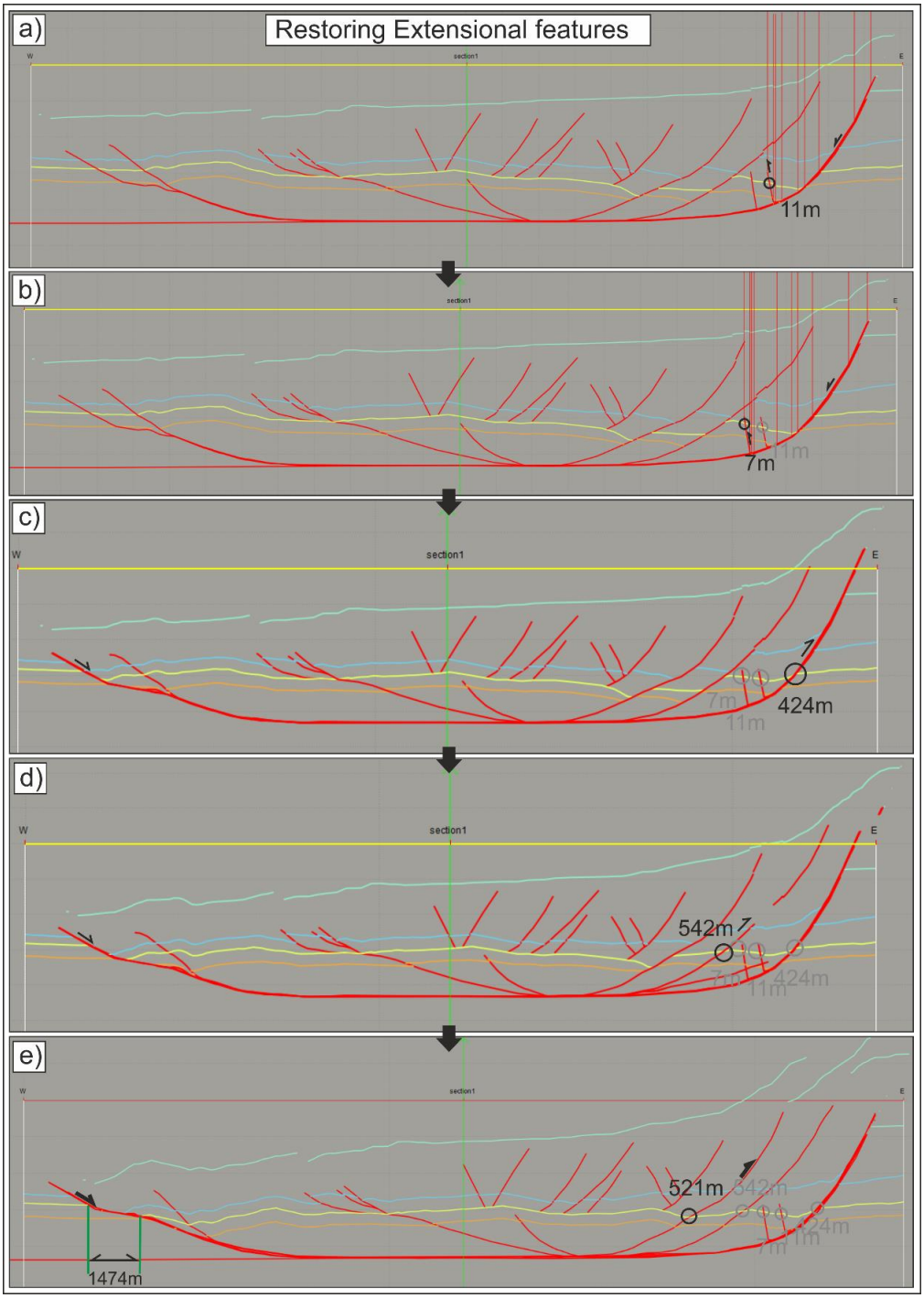

Figure 3.20. Stepped restorations of the extensional domain for Figure 3.18

This process is now repeated for the extensional domain (Figure 3.20) with the most proximal extensional fault now being restored and the most distal compressional fault being inverted. The extensional faulting totals 1505 m, this number has already compensated for the contractional displacement along the thrusts and thus records an imbalance between contraction and extension in favour of extension. When restored as two separate systems the total contraction is still 741 m and the extension is 2246 m, thus 1505 m of excess extension is not compensated for by thrusting. This shortfall is also measurable directly from the section (Figure 3.20e) as the distance between the green lines at the thrust tip (1474 m). However, it is clear the section is not restored to a realistic starting geometry, as folding has not been compensated for.

In order to compensate for folding it is necessary to perform a line length restoration (Figure 3.21). This is done by flattening the horizons and comparing their lengths. In order to observe any shortfall in contraction the restored and flattened horizon needs to be compared to an original pre-deformed length. In Figure 3.21a an assumed initial slope geometry is shown in blue, which represents our original pre-deformed length. The pre-kinematic restored horizons and the initial slope geometry are then flattened to create line-length restorations. These restored line lengths are compared to establish if there has been any shortening.

In the example presented in Figure 3.21 the deformation assumed to be concentrated between the most distal normal fault and the most proximal thrust. For the yellow horizon a current length of 18874 m is recorded (22939-1795-2270, line length less the lengths of the horizons external to the DWFTB e.g. proximal of the most proximal normal fault and distal of the most distal thrust). The line length of the blue horizon between these faults is 20048 m (24113-1795-2270), thus the difference between these lengths is 1174 m (20048-18874). That is to say compensating for folding there is 1174 m more extension than there are compressional features to compensate for. A missing strain component is calculated of 6.2% (1174/20048x100). In chapter 5 this additional contractional component caused by folding has been added to the compression.

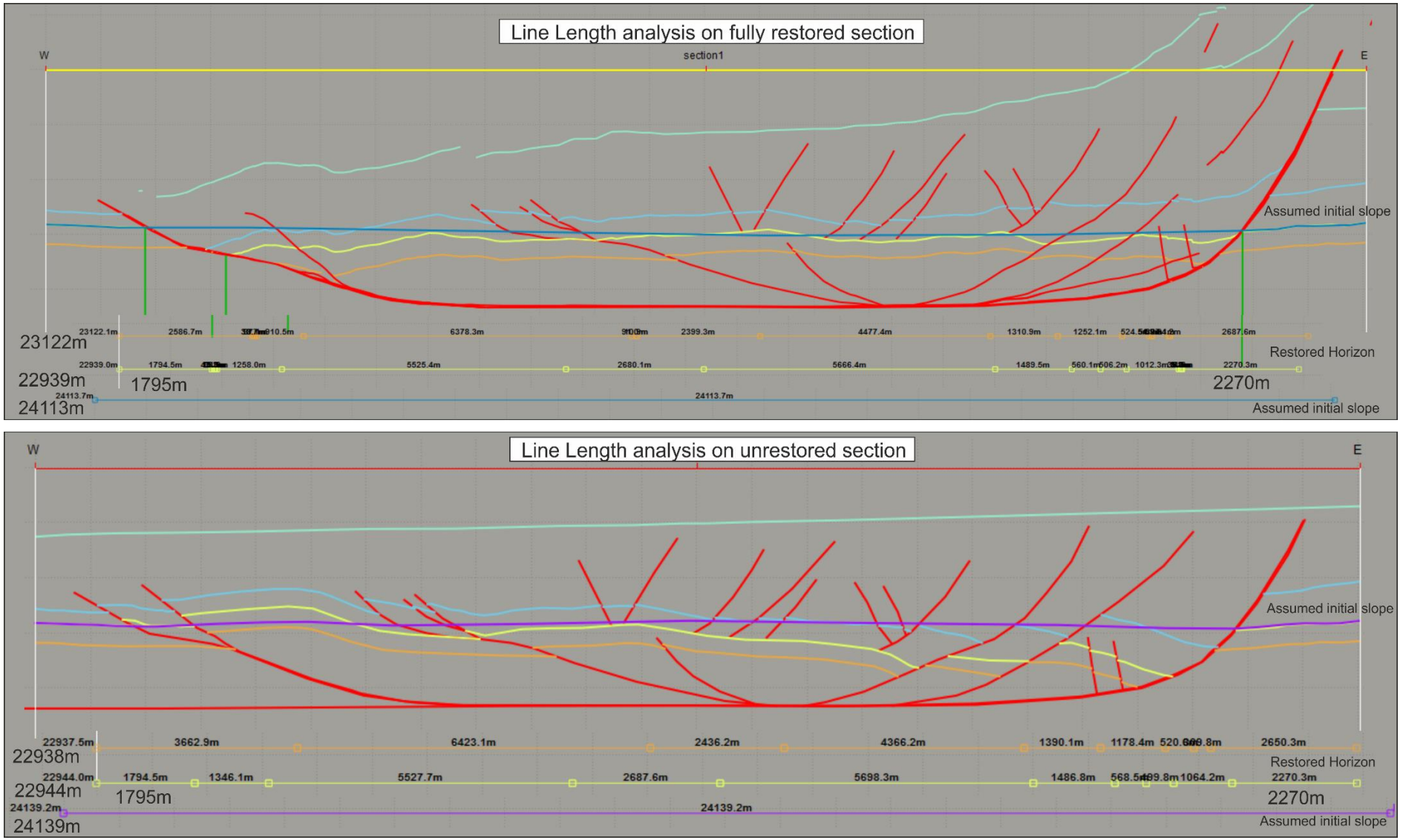

Figure 3.21. Two line length analyses of the interpreted section line in Figure 3.18.

It is worth comparing these totals to line length restorations undertaken on an un-sequentially restored section (3.21b). This produces only a 5 m difference in total length. This difference seems to be an artefact of the software applying a mild stretch to beds during the restoration process. This process can also be repeated on alternative horizons such as the orange horizon and produces similar results (7%). Additional reconstructions used in this thesis are included in the appendices.

3.3 Uncertainties

In a project that is heavily reliant on seismic interpretation, the competence and biases of the interpreter are significant factors. The interpretation of seismic data is by its nature exposed to human error and open to multiple interpretations (Bond et al., 2007, 2012). The imaging is are also challenging in regions of structural complexity and especially at depth (Figure 3.14 and 3.16). To address this issue, I attempt to work from areas of confidence and extrapolate into areas of complexity. A good example of the problem of uncertainty can be seen in Figure 3.22, which presents four interpretations of the same seismic line (VN03-063ab) by different authors (Butler and Paton (2010), de Vera et al (2010); Mohammed (2013) and this study). These interpretations match in areas where reflectivity is good, for example the proximal portions of extensional domain and the distal toe thrusts. However, towards the transitional domain and below the main detachment sizable differences in interpretation persist e.g. two authors indicate a lower detachment systems while two do not; and different fault interpretations are present in the transitional domains. Failure to recognize the lower décollement (Décollement E) misattributes extensional strain to the upper system, whilst also failing to recognize the additional contractional strain being absorbed by the underlying thrusts. Despite this, three of the studies undertook restorations of this seismic line and found comparable missing strain components, so perhaps the quantitative effects of mis-interpretation are limited. But the understanding of the mechanical behaviour of the slope and the wider system is clearly incorrect.

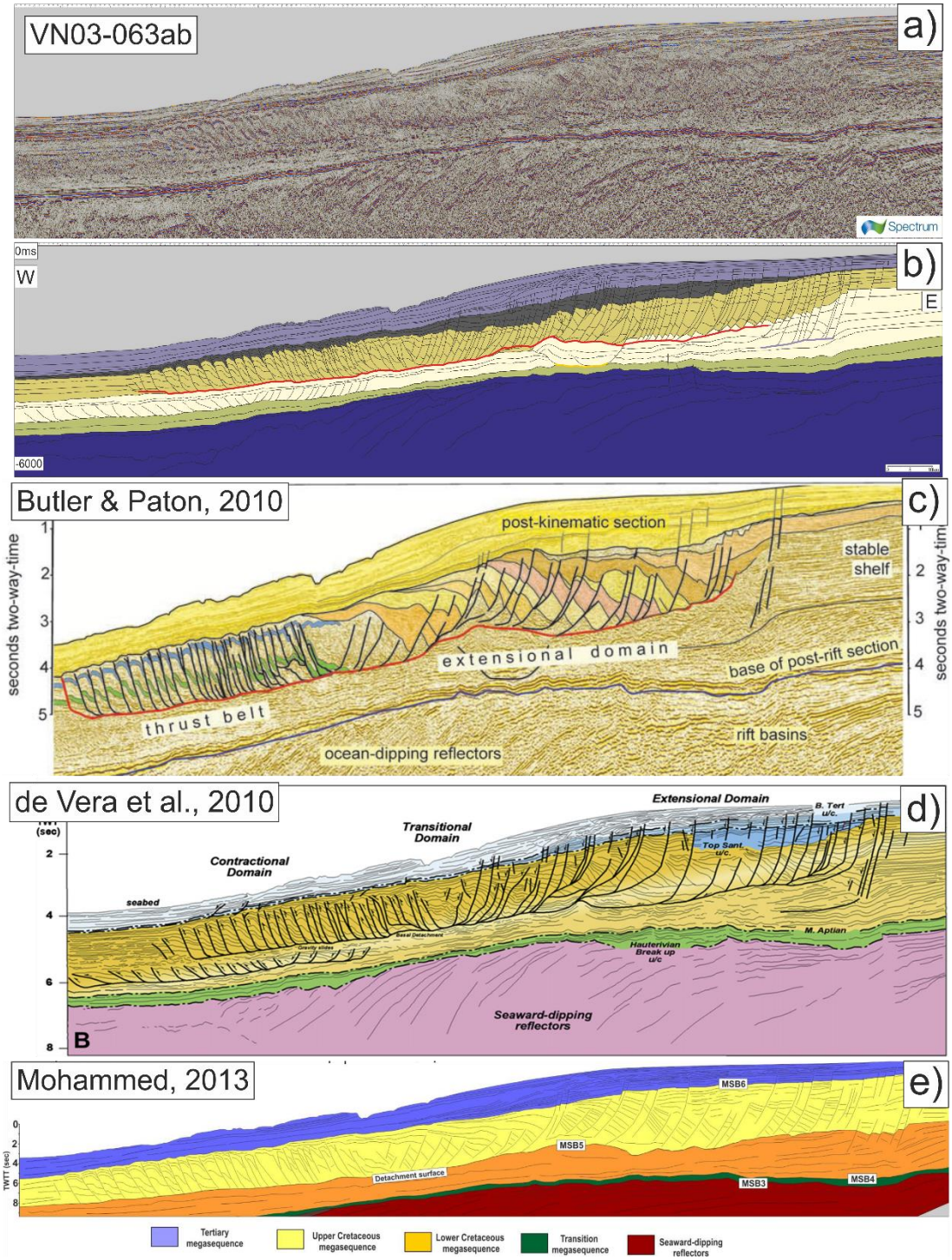

Figure 3.22. An uninterpreted seismic section of line VN03-063ab and four interpreted sections of the same line. a) Uninterpreted seismic section vertically exaggerated 5:1. b) Interpreted seismic line using data from surrounding sections to inform areas of uncertainty. c) Interpreted section from Butler and Paton (2010). d) Interpreted section from de Vera et al. (2010). e) Interpreted section from Mohammed (2013).

The uncertainties produced by regions of poor data can be partially overcome by iterative interpretation based on the addition of complementary parallel and cross-

cutting seismic, where the imaging is better or the features are more pronounced. By undertaking this study in the context of holistic interpretation of an entire margin (Figure 3.5) I am able to considerably limit the effects of uncertainty though recognize it cannot be entirely eliminated.

This chapter has set out to provide an overview of the techniques and interpretations that have been undertaken and form the framework for this study. More detailed discussions of the data and methods applied to each individual study are presented in each data chapter. Some of the interpretations and structures introduced in this chapter will be returned to in the final discussion chapter.

4 Chapter 4; Influence of mechanical stratigraphy on multi-layer gravity collapse structures: insights from the Orange Basin, South Africa

[*This chapter is composed of a paper published by the Geological Society of London, in the "Petroleum Geoscience of the West Africa Margin", special publications 438, published online in May 2016, doi/10.1144/SP438.4. A published version is included in the Appendices.*]

Abstract: Gravity collapse structures are common features on passive margins and typically have a tripartite configuration including an up-dip extensional domain, a transitional domain and a down-dip compressional domain with a common detachment underlying the system. A number of studies have classified these systems, yet few document the wide variations in geometry. This study documents the gravity collapse structures of the Namibian and South African Orange Basin; these structures represent some of the best imaged examples of this important process. We first demonstrate the geometry and kinematic evolution of these systems, focusing on examples of the tripartite configuration from a typical collapse. We then highlight the significant variability in the structures of the system and describe features such as cross-cutting in margin-parallel sections, portions of the system with multiple detachments, systems with stacked synchronous detachments and the temporal evolution of faults within the system. By integrating our observations from a number of sections, we present a model explaining the spatial and temporal evolution of the system. This enables us to discuss likely causes of collapse structures and also, by placing the system into a well constrained stratigraphic context, how the presence of both maximum flooding surfaces and early margin deltaic sequences have a fundamental control on the resulting collapse geometry.

4.1 Introduction

Deep water fold–thrust belts (DWFTBs) and their associated extensional systems occur in many passive margin systems throughout the world and provide an excellent opportunity to study the formation and development of both extensional and

compressional faults. A considerable variation in the structural style of collapse systems is seen across different margins and this is generally accepted to result from differences in both the driving mechanisms for collapse and the geometry and nature of the detachment surface (Rowan et al. 2004; Krueger & Gilbert 2009; Morley et al. 2011).

Morley et al. (2011) classified DWFTBs into two broad categories: those controlled by near-field stress systems created by sediment loading and differential uplift/subsidence at passive margins (Type I) and those controlled by far-field stress regimes associated with active margins (Type II). Type I DWFTBs are further divided into Type Ia (shale detachment), such as those in the Orange Basin, and Type Ib (salt detachment), such as in Angola. Krueger & Gilbert (2009) proposed that DWFTBs should be divided into those found on active margins (caused by subduction) and those found on passive margins in a similar manner to the far- and near-field stress systems. Krueger & Gilbert (2009) then subdivided the passive margin systems into three categories based on the nature of their décollement: regional salt, regional shale and local non-discrete, where the local detachments are discontinuous and lead to a regional décollement crossing stratigraphic levels (Figure 4.1).

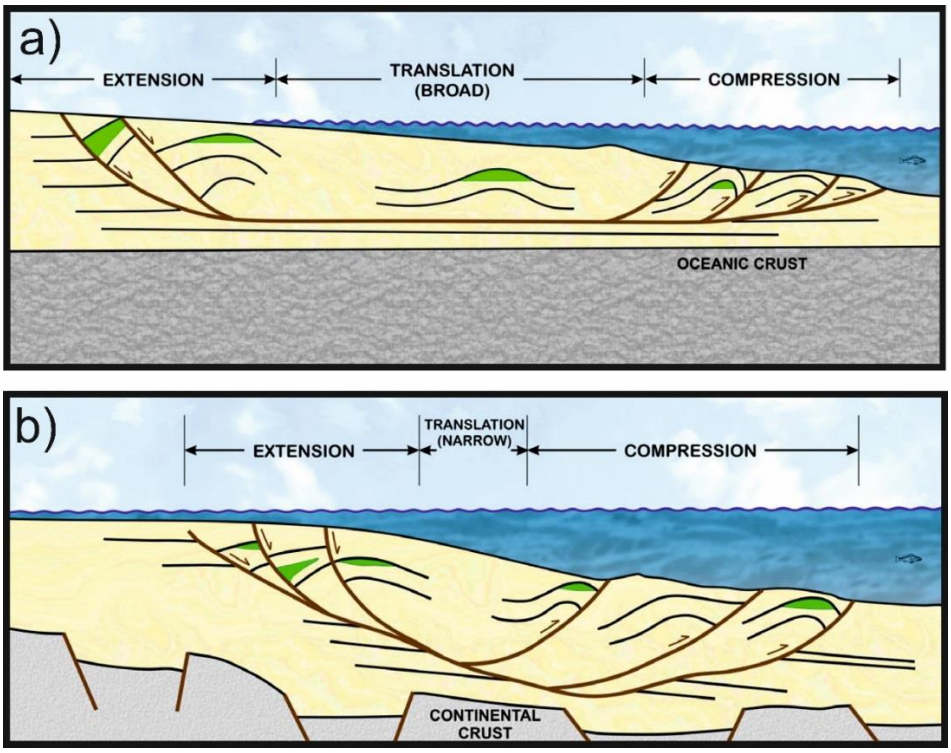

Figure 4.1. Model of gravitational collapse (Krueger & Gilbert 2009). (a) Typical features and geometry of gravity system controlled by a regional detachment. (b) Geometry where no regional décollement is present.

In this study we focused on shale detachment systems that, regardless of the driving mechanism, commonly consist of three domains (Figure 4.1): an up-dip extensional domain dominated by normal faulting; a down-dip compressional domain composed of imbricate thrusts and folds; and a transitional domain. The transitional domain (sometimes referred to as the translational domain) is not referred to by all researchers, but is defined as an area between the extensional and compressional domains that is either a package of largely undeformed sediments (Corredor et al. 2005; Krueger & Gilbert 2009) or an area in which both compressional and extensional features overprint (Butler & Paton 2010; de Vera et al. 2010). This overprint arises from a shift in the location of the point of contact between the compressional and extensional domains. It is often difficult to resolve the internal geometry of the transitional domain because of limited seismic imaging. The basic premise of area balancing during deformation is expected to apply to these coupled systems; however, the work of de Vera et al. (2010) and Butler & Paton (2010) in the Orange Basin established an imbalance between the extension and compression domains of up to 25% in favour of extension, leaving a considerable missing component of contractional strain to be explained.

In this study, we looked in detail at the three domains along a typical section from the Orange Basin system and compared them with other portions of the same collapse structure to observe variations along-strike. From these observations we constructed a model to explain the temporal evolution of this important margin process. Finally, we considered how the margin stratigraphy played a critical role in the nature of the deformation and propose that this had a significant and, until now, unrecognized control on this process, which occurs on many passive margins.

4.2 Regional setting

The Orange Basin is the southernmost basin on the West African passive margin. It formed during the break-up of Gondwana and subsequent spreading of the South Atlantic Ocean (Muntingh & Brown 1993; Brown et al. 1995; Paton et al. 2008; Koopmann et al. 2014).

It underwent significant rifting during the Late Jurassic to Early Cretaceous, forming graben and half-graben infilled with synrift siliciclastic and lacustrine sediments (Jungslager et al. 1999; Mohammed et al. 2015, this volume). This was followed by continental break-up in the Barremian and the establishment of a passive continental margin, onto which a thick post-rift sedimentary sequence was deposited (Gerrard & Smith 1982). The thickness of the post-rift sediments ranges from 3 km in the south and north to up to 5.6 km in the centre of the basin. This sediment was largely sourced from the Orange River (Paton et al. 2008) and is broadly separated into two phases: black shales and claystones were deposited during an early drift phase and then a later drift phase deposited a thick succession of interbedded heterolithic sediments composed of shales and claystones (Figure 4.2). It is within the latter phase that we observed the greatest number of gravity collapse structures. Although much of the margin stratigraphy is claystone, we defined the system as dominated by a shale detachment because the décollement surfaces are shale intervals. These correspond to maximum flooding surfaces, with some identified as proved source rocks (van der Spuy et al. 2003). This Cretaceous succession underwent considerable tilting, up to 750 m in the inner margin (Paton et al. 2008), at the end of the Maastrichtian to produce a considerable proximal unconformity with the overlying Cenozoic sequence. Most of the Cenozoic sequence was deposited outboard into the basin and varies in thickness from 250 to 450 m on the margin and from 500 to 1400 m on the continental slope and beyond. The hydrocarbon system sequence stratigraphy and deeper structures of the Orange Basin are well established (Light et al. 1993; Muntingh & Brown 1993; Paton et al. 2007, 2008; Hirsch et al. 2010).

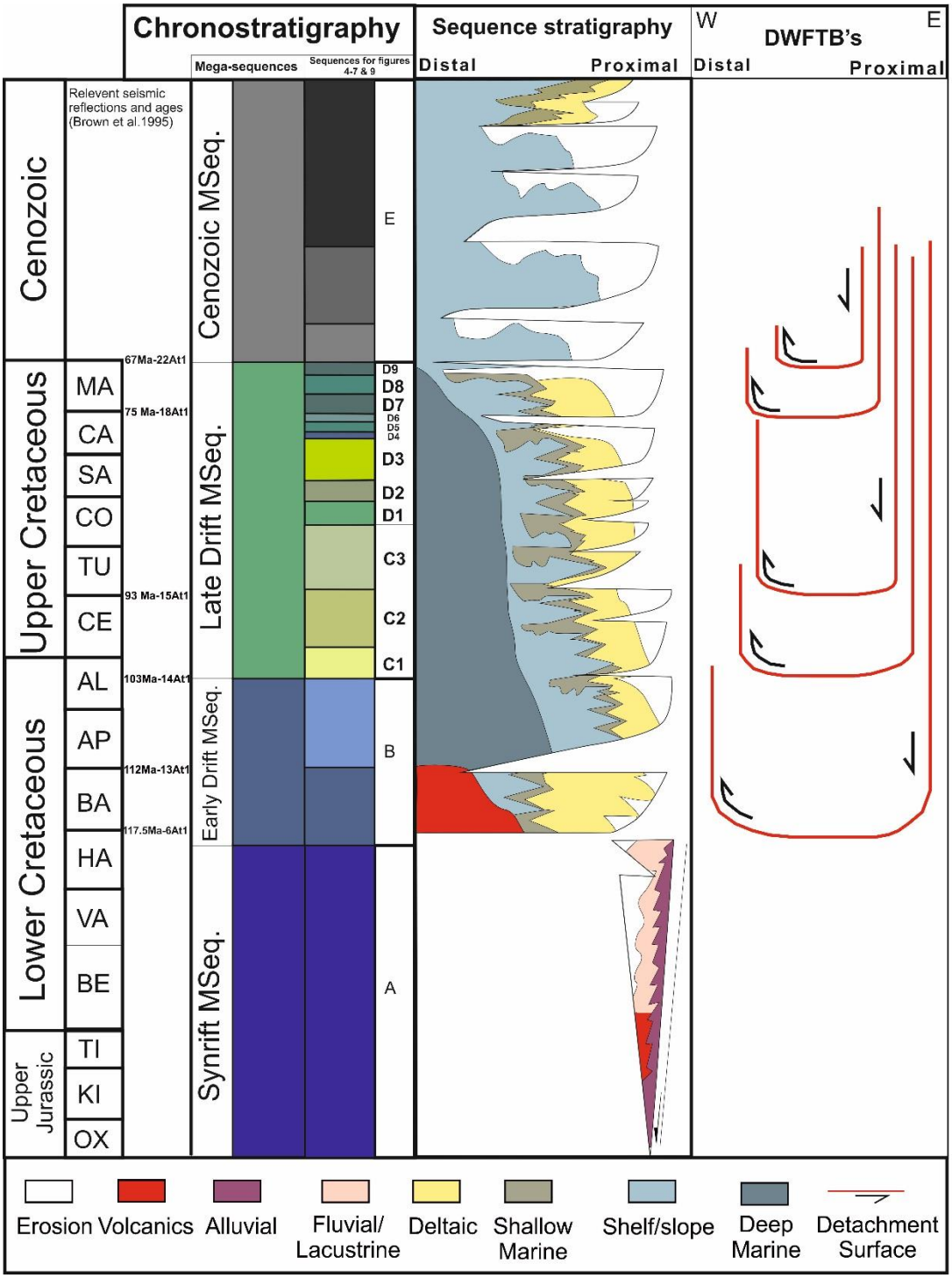

Figure 4.2. Chronostratigraphy of Orange Basin adapted from Paton et al. (2008) showing the depths to which the deep water fold–thrust belts penetrate across the entire basin.

4.3 Data and methods

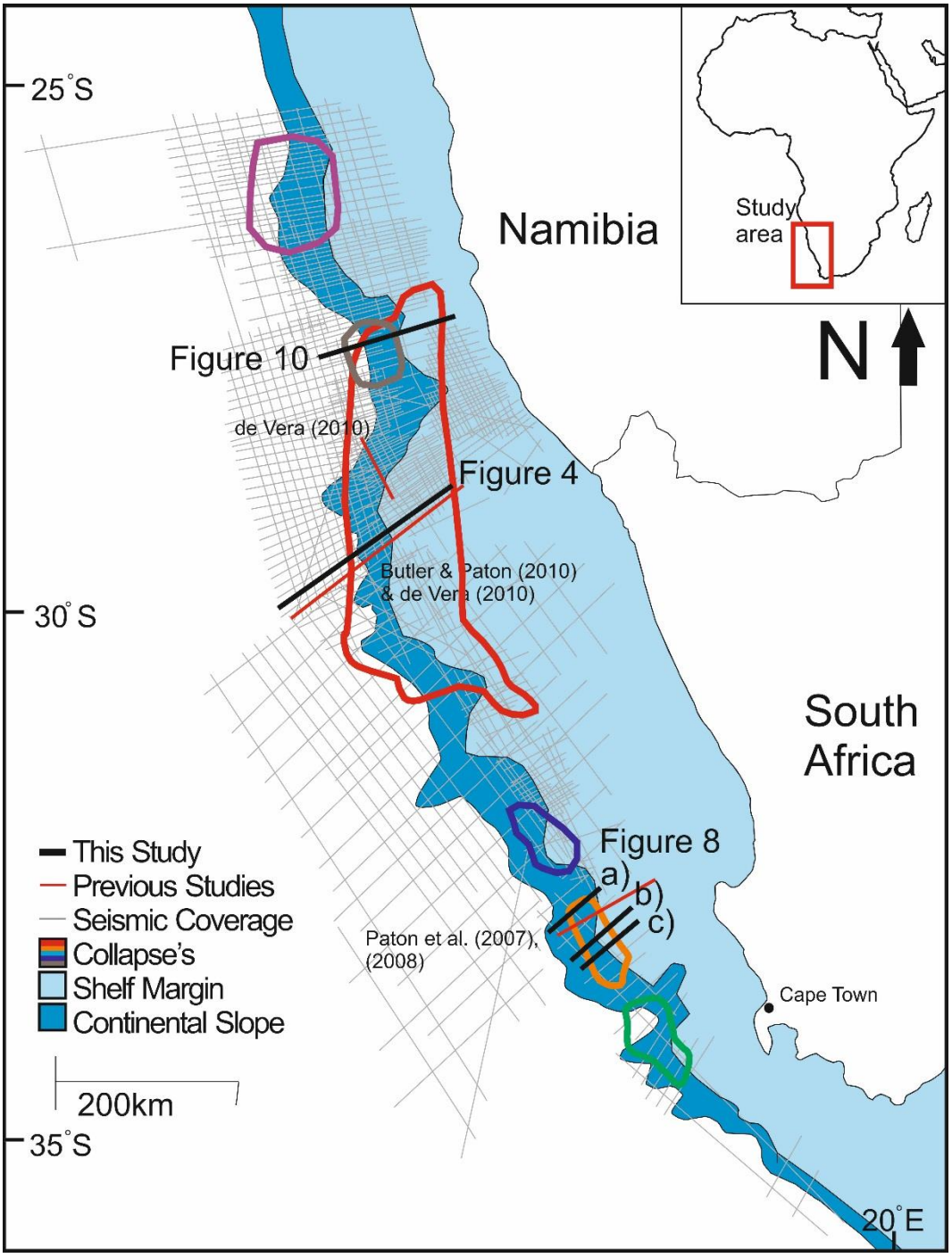

Figure 4.3. Map of Orange Basin indicating the location of lines used in this study, the location of lines used in previous studies (Paton et al. 2007, 2008; Butler et al. 2010; de Vera et al. 2010) and an outline representing the total data coverage used in this study.

This study combined 38 480 km of vintage two dimensional pre-stack time migration seismic data released by the Petroleum Agency of South Africa with 45 386 km of two-dimensional seismic data from Spectrum (Figure 4.3) of which 24 042 km was pre-stack

depth migration (PSDM) data obtained using fast-track Kirchoff migration. The maximum recording lengths were in the range 7–10 s two way travel time; the vintage data were acquired between 1976 and 2012 and the Spectrum data were acquired in 2012. The line spacing of this deep seismic coverage was between 8 and 15 km and it provided unprecedented data coverage of the basin and allowed us to review the entire margin (Paton et al. 2015). We present here our interpretations of the Spectrum PSDM seismic lines because these provided better images. Well data for the basin are extensive, although limited to the shelf margin, and have been used in previous studies (e.g. Muntingh & Brown 1993; Paton et al. 2008) to define the margin stratigraphy and to define stratigraphic ages for our seismic intervals (Figure 4.2). Stratigraphic megasequences and associated regional and local unconformities have been identified using reflection termination, cut-offs and onlap relationships with the sequence stratigraphic system based on the work of Muntingh & Brown (1993). As we focused on the detailed architecture of the syn-kinematic packages, we subdivided the megasequences into sequences based on variations in the seismic character that indicated changes over time in the depositional or structural environment and rates of deposition. We used a unified stratigraphic system to define these sequences across the margin (Figure 4.2). We defined the packages regionally across the section as megasequences A–E and further subdivided megasequences C and D numerically in a temporal succession. However, because the packages were often isolated, any one section may not show a complete sequence.

4.4 Regional sections

We present here a 160 km long east–west-oriented regional seismic profile (Figure 4.4) that illustrates both the main structural elements of the margin and one of the simpler collapse structures in the centre of the basin (Figure 4.3). This is shown down to a depth of 6.4 km. Based on the previous regional interpretations of Paton et al. (2008), we divided the stratigraphy into four megasequences: Synrift, Late Jurassic to Hauterivian (A); Early Drift, Barremian to Aptian (B); Late Drift, Aptian to

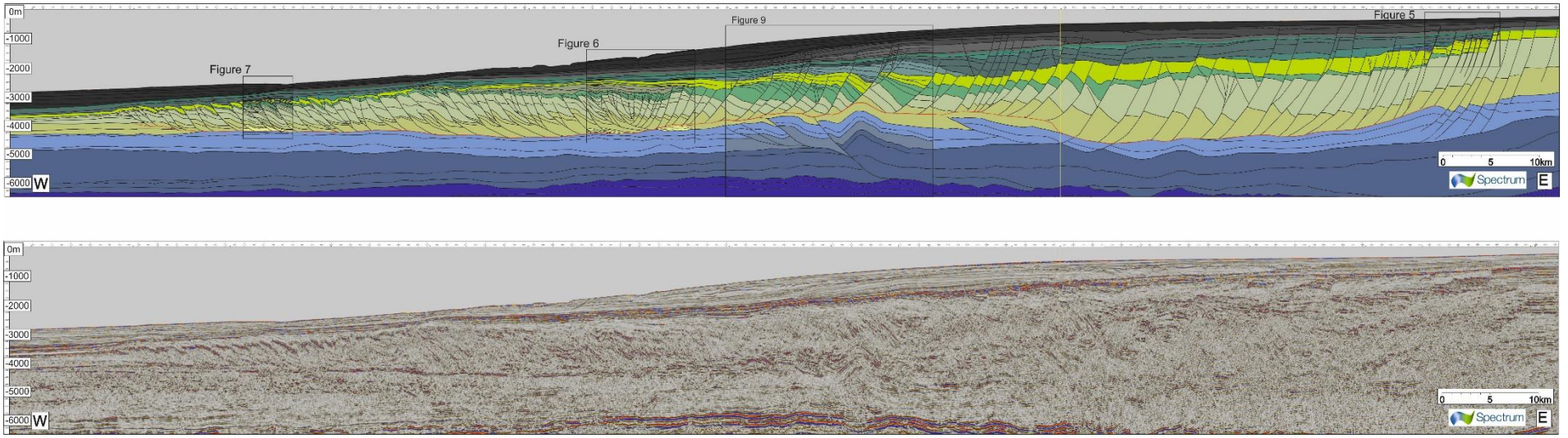

Figure 4.4. Pre-stack depth migrated un-interpreted and interpreted sections of Line 1 (see Figure 4.3 for location) shown with a vertical exaggeration of 3:1. The colours correspond to each megasequence (Figure 4.2). The Synrift megasequence is purple, the Early Drift megasequence is blue, the Late Drift megasequence is green and the Cenozoic megasequence is grey; different shades correspond to discrete packages within each megasequence. The detachments are picked out in red (larger version included in Appendix).

Maastrichtian (C and D); and Cenozoic (E). To aid the interpretation across the margin, including the structural features and local unconformities, we divided the megasequences into seismic sequences based on the character of internal seismic reflections. Although the synrift packages were imaged in the dataset (Paton et al. 2015), we focused on the sequences stratigraphically above the top synrift reflection. The top of the synrift package was delineated by a package of high-amplitude parallel reflections, present across the basin, onto which Barremian-age stratigraphy was deposited. In this section, the nature of the contact was represented by an aggradational sequence of reflections conformable with the top of the synrift package. It is important to note that elsewhere in the basin this boundary has a progradational relationship marked by downlapping reflections onto the synrift sediments prior to an aggradational phase. The Late Drift megasequence is deposited conformably on the Early Drift package and is defined by its higher reflectivity.

Evident within this Late Drift megasequence are numerous unconformities represented by the truncation and onlapping of reflections. These unconformities only occur off the palaeo-slope margin and are often restricted to fault blocks; they are therefore not regional in extent. Reflections within the centre of this package are both folded and faulted. In the proximal portion of the basin, westwards-dipping normal faults are identified by dislocated packages shifting down-dip of one another (eastern end of Figure 4.4); this is the extensional portion of the gravity collapse structure. Continuing westwards and down-dip, the seismic character becomes increasingly chaotic and complex and we define this as the transition domain.
The most distal part of the system, the compressional domain, is characterized by a series of east dipping thrust faults identifiable by high-amplitude, steeply dipping reflections that appear to be stacking packages on top of one another.

These structural features will be discussed in more detail later; however, it is important to note at this point that although the main décollement for this collapse (red reflection in Figure 4.4) is broadly coincident with the top of the Early Drift megasequence, it does not have a constant slope and shows significant changes in the direction and angle of dip. The décollements are picked based on where the faults terminate, as identified through cut-offs and changes in the dip of the reflections.

The Late Drift megasequence is capped by a regional truncation at the top of the palaeo-shelf picked out by the green line (Figure 4.4), whereas these sequences are conformable at the base of the palaeo-slope. The unconformity is, however, still interpretable by a change from a low- to a high-amplitude reflection along this boundary. The Cenozoic package is defined by a change in the location of deposition from proximal to a more distal position on the continental slope. The package is considerably thinner than the Cretaceous sequence on the central margin and thickens significantly to the west. Each of the structural elements is considered in more detail in the following sections.

4.4.1 Extensional domain

To define the structures in more detail, we subdivided the megasequence into a number of sequences (A–E, Figure 4.2). Figure 4.5 shows a typical interpreted section from the upper portions of the extensional system, where the latest faults formed prior to detaching onto a regional décollement. This interpretation focuses on the upper part of the extensional portion of the structure and shows a more detailed breakdown of the Late Drift megasequence (sequences C and D). These packages are defined based on the internal seismic facies and reflection termination and reveal relative changes in sediment supply and fault-controlled accommodation space (Brown et al. 1995).

Internally, sequence C3 has an absence of seismic impedance contrast, resulting in only limited internal geometry being imaged, but it is conformable with the high-amplitude reflections at the base of sequence D1 and is truncated by sequence D3.

This suggests that D1 was being deposited as the upper portions of C3 were being eroded and that the discontinuity was a direct result of faulting. D3 has a thick package of high-amplitude reflections that allow several horizons to be tracked internally. When restored, sequence D3 forms a westwards-thickening wedge. Changes in spacing between traceable horizons in D3 show slight changes in thickness along its length, indicating that different faults were active at different points.

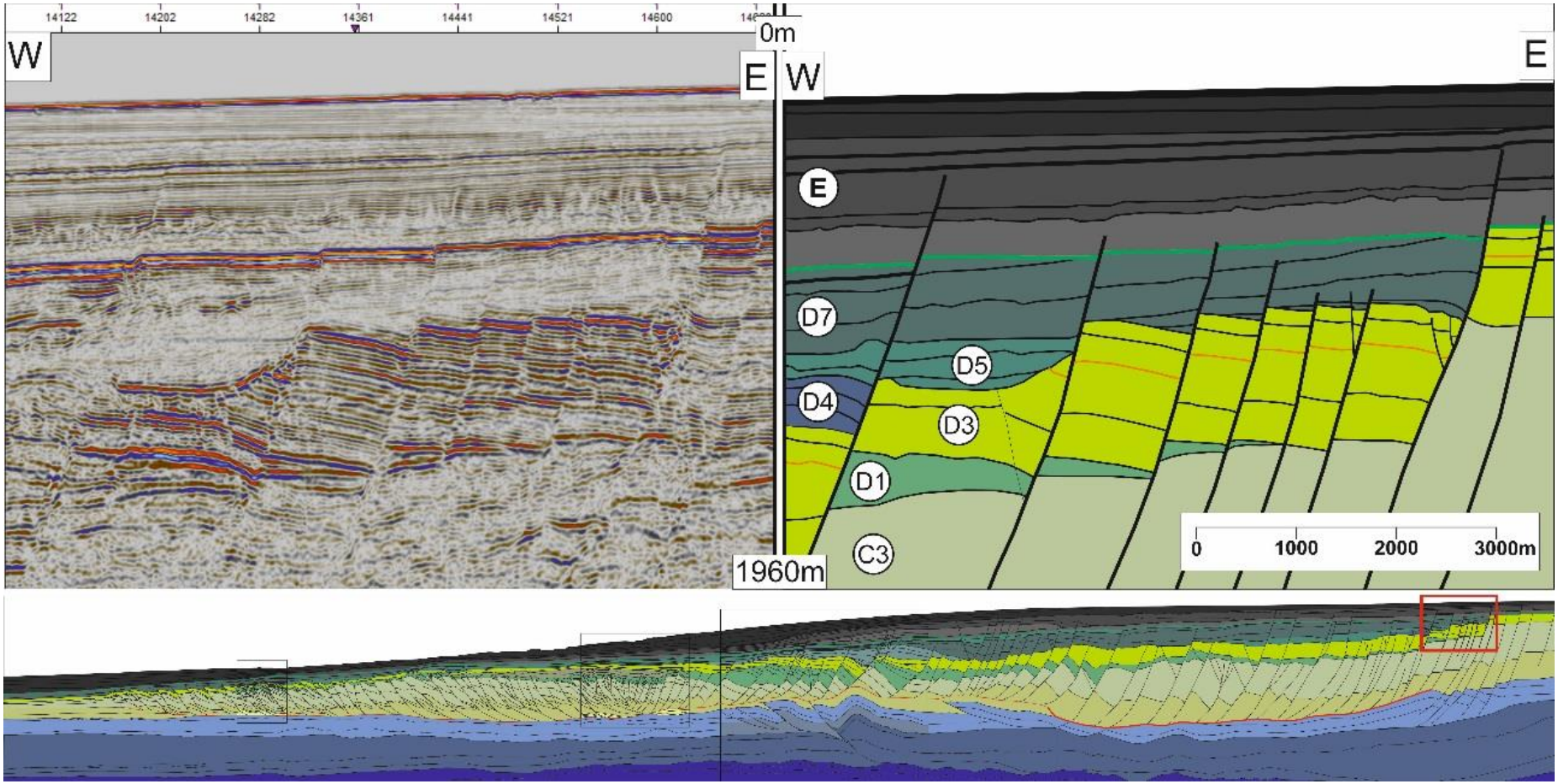

Figure 4.5. Detailed interpreted and uninterpreted sections of the extensional domain from Figure 4.4 the section is vertically exaggerated 3:1.

Of particular note are the small changes in thickness in the packages above and below the orange horizon (Figure 4.5), which indicate the movement of small faults in the package between two faults with far larger throws. As the largest thickness changes occur on the faults on which D4 and D7 truncate, this implies that the deformation tends to concentrate onto a few larger, more widely spaced faults – that is, large faults become large and stay large, thus stopping smaller faults from growing. Sequence D4, defined by a package of low-amplitude reflections, reinforces this point. Its presence in only the west of the section abutting a large fault plane implies that it grew more rapidly at this point than faults to the east.

This created a larger accommodation space that was rapidly infilled, as indicated by folding of the reflections into the fault. D3 is clearly truncated by the base of sequence D5 with a rugose contact that appears to represent the collapse of the top of the fault block. D5 has chaotic and poorly imaged reflectance that infills the eroded section truncated at the top of D4. As shown in Figure 4.4, D5 extends for 16 km west of Figure 4.5 and continues to erode earlier fault blocks. Its chaotic seismic character and erosive base suggest that it is a mass transport complex (MTC). Several similar MTCs can be seen throughout the extensional portion of the collapse features (e.g. Posamentier & Kolla 2003; McGilvery et al. 2004).

Sequence D7 is defined by a series of reflections that onlap onto the top of D4 and D5 and are clearly imaged on the tops of the fault blocks. This implies that fault movement outstripped sediment supply at this point. It also appears that several of the faults had switched off by this time. As the sediment supply increased and the faults switched off, the sediments began to bury the fault blocks and deformation was again concentrated into the larger faults, where we observed some limited sediment growth into the fault plane. The truncation of D7 by megasequence E – that is, the boundary between the Late Drift and Cenozoic megasequences – can be seen throughout the palaeo-continental margin and the upper palaeo-slope. It is unclear how much sediment has been eroded, although Paton et al. (2008) suggested it may have been as much as 750 m. Only the two largest faults were active after this unconformity formed, although they offset it with only small throws

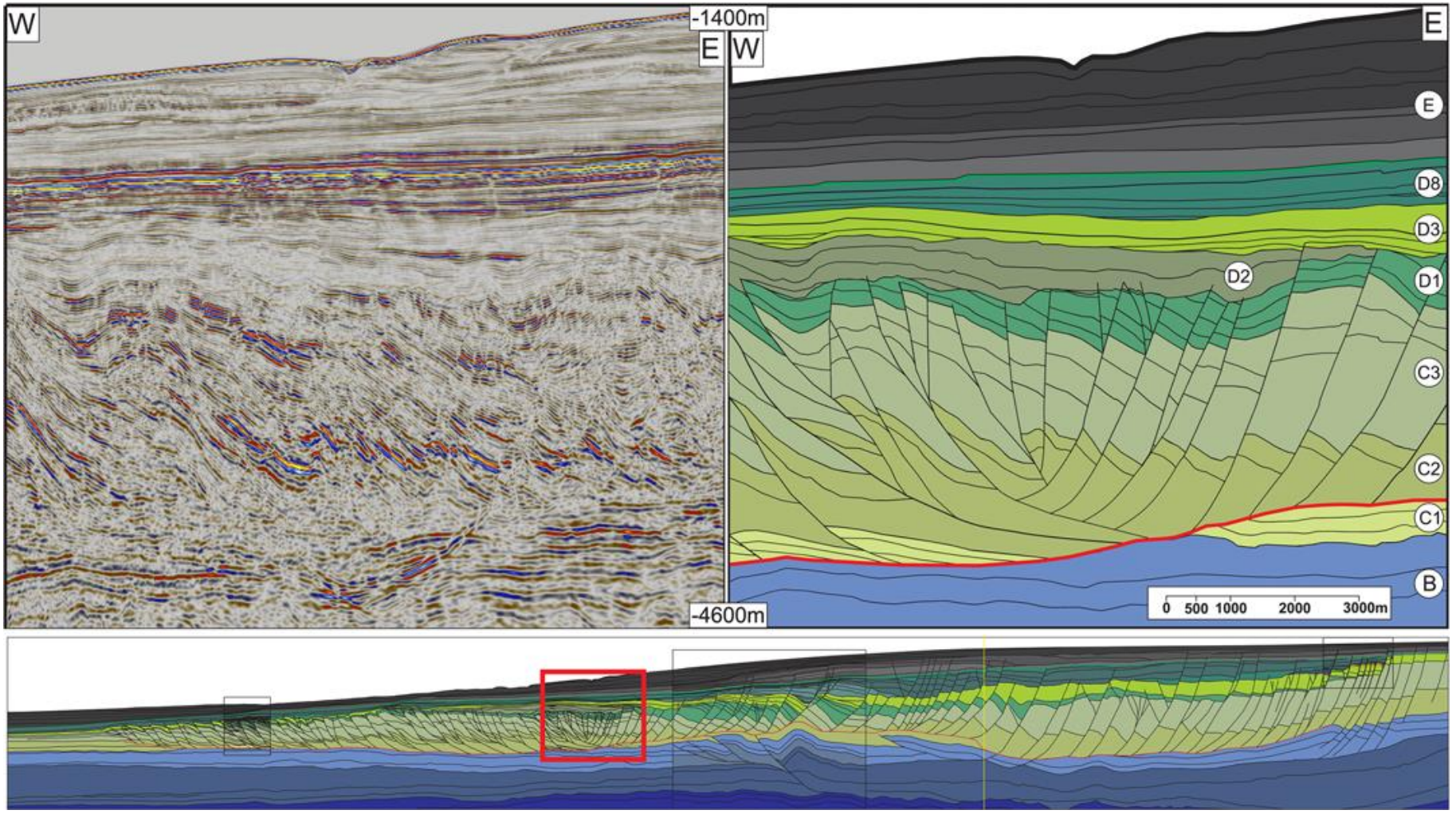

Figure 4.6. Detailed interpreted and uninterpreted sections of the transitional domain from Figure 4.4 the section is vertically exaggerated 3:1.

4.4.2 Transitional domain

The section in Figure 4.6 shows the point at which the extensional domain changed into the compressional domain and indicates that this occurred predominantly within megasequences C and D.

Megasequence B contains the high-amplitude parallel reflections that denote the top of the Early Drift megasequence, although these reflections become less distinct immediately beneath the most deformed section of the transition zone, probably due to signal attenuation. These reflections are composed of coarsening upwards silt–medium sandstone packages (Paton et al. 2007) that represent the progradation of the Aptian deltaic margin and are capped by a maximum flooding surface that forms the detachment. Sequence C1 is defined as a set of lower amplitude parallel reflections that have a variable relationship across the section with the surrounding sequences. In the east of the section they are conformable with megasequence B; the reflections become truncated towards the west by the base of sequence C2. They reappear in the west as a set of reflections conformable with C2 and downlap onto megasequence B. We interpret this as a shift in the depth of the main décollement that is immediately above B in the east and cuts down to an inter-megasequence B layer with the consequence of translating the C1 package downslope by c. 2300 m towards the west.

C2 is defined by low-amplitude, largely discontinuous reflections and is conformable with C3, which consists of higher amplitude, more continuous reflections. The lowest reflections in C2 to the east and centre downlap onto B and C1 and are directly above the detachment at this point; they are conformable with C1 in the west as the detachment cuts down-sequence, as described earlier. The division between the C2 and C3 intervals is identifiable by an easily correlated, high-amplitude reflection package. This allows us to define fault cut-offs with confidence. In the east, these faults dip steeply landwards with normal offsets and detach onto the main basal décollement. Progressing west they become more closely spaced and detach onto a shallow basinwards-dipping thrust fault located above the regional décollement. A shift from extensional to compressional tectonics occurs on top of this thrust fault. The low amplitudes at the base of C2 are probably a result of the coalescing of

multiple faults at this level, causing increased stress at this depth. The thickness of C2/C3 is largely maintained throughout the margin, including the area of intense faulting, which suggests that it I largely a pre-kinematic sequence deposited prior to collapse, although some reflections in the top of C3 show limited thickening into fault planes, suggesting some degree of syn-kinesis.

Sequence D1 is defined here by a set of low amplitude reflections that are largely conformable with C3; as in the previous sequence, cut-offs are used to define the location of faults. Many packages have wedge-like geometries that thicken into fault planes, implying fault growth during deposition and making this a syn-kinematic succession. From the position of cut-offs in the region in which normal faulting gives way to thrusting, it can be seen that several faults stopped moving. The upper boundary is truncated by sequence D2. This sequence is defined upwards by a series of low-amplitude continuous reflections that onlap onto the erosional truncation defining the top of D1. They form a tapering wedge to the east, where the formation onlaps onto significant faults with throws of 120 and 250 m. There appear to be numerous minor truncations of horizons against one another within the formation, possibly due to limited deposition in what are effectively mini-basins. Some faults do persist into the base of D2, but most are truncated by it, implying an erosional episode followed by progressive infill during which limited reactivation occurred, causing minor folding as opposed to faulting in the overlying sequence. At this point of the section, sequence D3 is defined by low-amplitude continuous reflections that downlap onto D2, infilling its uneven upper surface, before latterly adopting a more aggradational geometry. Minor folding of some reflections at the western end of the section imply limited localized reactivation on some thrusts. Sequence D8 is composed of high-amplitude reflections conformable with D3. The contact between these two horizons can be traced into the compressional domain down-dip. The top of D8 appears conformable with megasequence E (Cenozoic).

The transitional domain in the centre of Figure 4.6 generally picks out a large fold structure detaching onto a thrust above the regional décollement. The back-limb of the fold is cut by normal faults, which progressively become thrust faults towards the crest, some of which are likely to be inverted normal faults. The precise contact between the compressional and extensional domains (e.g. the transitional zone) is

narrow, similar to the modes proposed by Corredor et al. (2005) and Krueger & Gilbert (2009); however, the possible inversion may imply a more complex structural style, as suggested by de Vera et al. (2010) and Butler & Paton (2010).

4.4.3 Compressional domain

Figure 4.7 is a typical section from the distal end of the compressional domain and we have divided it into nine packages. Megasequence B, which is correlated from the transitional domain, is defined by several near-horizontal reflections that show a consistent increase in amplitude from east to west, probably reflecting a progressive change in its petrophysical properties. Sequences C1–C3, despite being of varying amplitudes, have the same geometry of stacked, steeply east-dipping reflections (35^{o} using PSDM data) that shallow and flatten with depth to become parallel with the top reflection of megasequence B. Definable packages of reflections stack with discrete cut-offs that pick out a set of imbricate thrusts. Sequence D1 is defined by a set of discontinuous low-amplitude reflections that onlap the thrust planes and downlap onto C3. The reflections are folded and have been truncated by both sequence D3 and by one another. The variation in thickness and the associated onlap onto anticlines of D1 suggest that thrusting was active during the deposition of D3 and was frequently emergent, leading to folding and erosion of the depositing sediments in a syn-kinematic fashion. This onlap implies that the deformation rates were greater than the sedimentation rates during this interval. D3 truncates D1 with a set of low-amplitude, but continuous, reflections. These reflections are folded above the underlying thrust planes, but are only cut by two of the thrusts with far smaller throws. Although it is clear that the faults remained active during this period, the rate of deformation relative to sedimentation had slowed significantly.

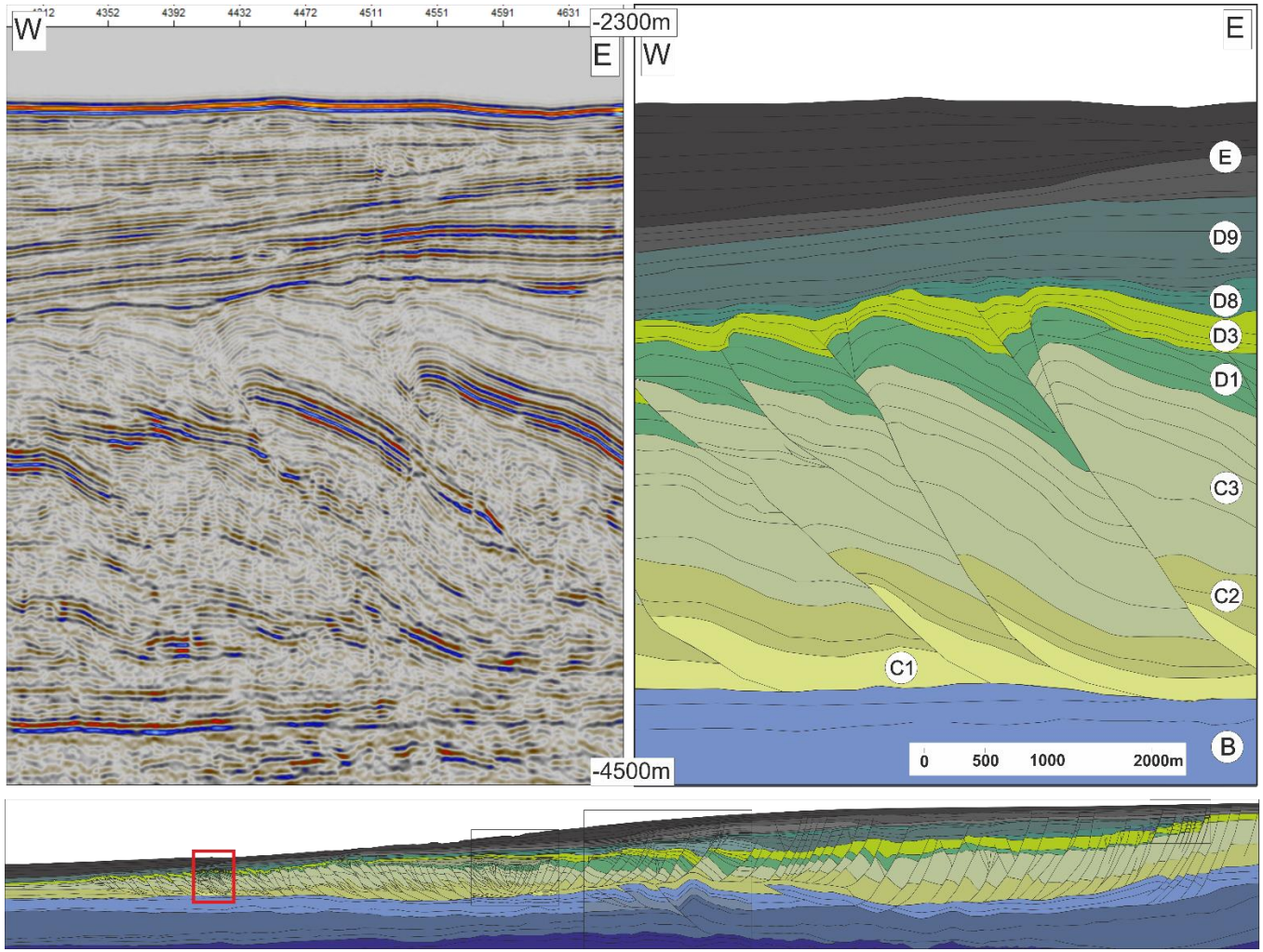

Figure 4.7. Detailed interpreted and uninterpreted sections of the compressional domain from Figure 4.4 the image is vertically exaggerated 3:1.

Sequence D8 truncates the crests of the folded reflections in D3 and onlaps in the synclines formed by the dipping reflections on the back-limb of the thrust faults. This suggests the end of deformation in this part of the compressional domain, with sediment infilling the remnant topography, although the sediment supply is insufficient to entirely fill the bathymetric lows. The last of these lows were filled by small onlapping packages at the base of sequence D9, which is otherwise conformable with D8. As with the transitional domain, the contact between the Late Drift (D) and the Cenozoic megasequences (E) is conformable. In a broader context, when viewing the compressional domain Figure 4.4, the imbricates have a relatively equal spacing and become progressively less deformed away from the transition zone, while also deforming ever-younger sequences. The dips of the faults shallow from 40–50^{o} at the transitional domain to 15–25^{o} at the frontal thrusts. They progressively deform younger sequences, implying that once the dip of the thrusts becomes too high, it is preferential to deform more distal sediments.

4.5 Variations in DWFTB geometry

Having summarized the structural elements that comprise a typical section for gravity collapse, we now outline how the styles of deformation deviate from this typical section by looking at variations along the margin, as illustrated by a number of additional sections.

4.5.1 Lateral variation

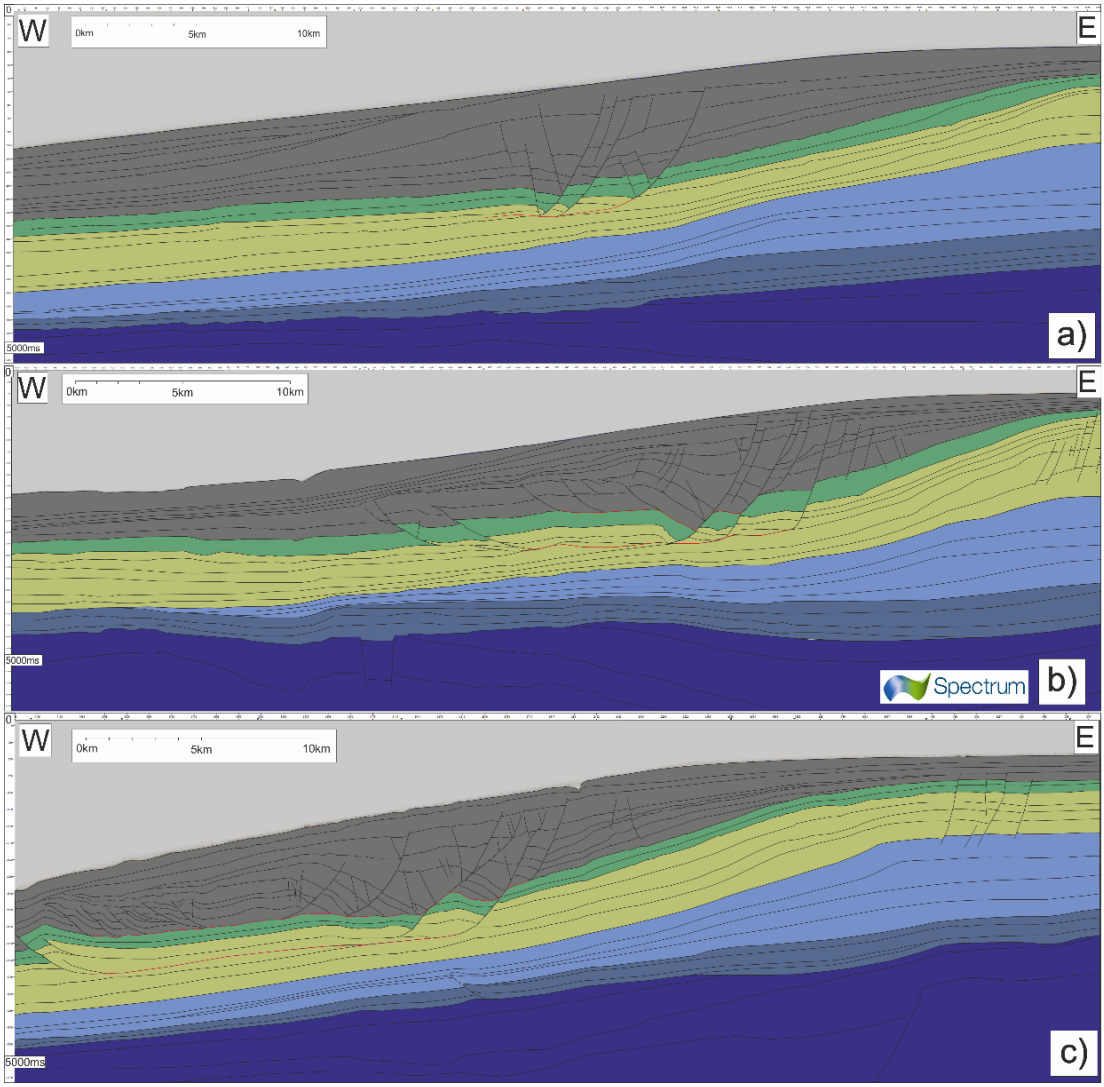

Figure 4.8. Three interpreted sections (a–c) from the south of the Orange Basin (Figure 4.3) adapted from Dalton et al. (2015). All sections are 35 km long and are presented as pre-stack time-migrated with vertical exaggerations of 3:1.

The three sections in Figure 4.8 are modified from Dalton et al. (2015) and show three slip-parallel 35 km long sections running north–south (see Figure 4.3 for locations) through a DWFTB in the southern portion of the Orange Basin. Growth strata indicate that collapse initiated during the deposition of the Cenozoic megasequence, which detaches onto a maximum flooding surface at the top of the Campanian in the Late Drift megasequence (Paton et al. 2008). Section (a) consists of an extensional domain with no corresponding compressional domain. Section (b) has a more classical geometry with both extensional and compressional domains detached onto the Campanian décollement; however, an additional set of thrusts detach onto the

contact between the Cenozoic and Late Drift megasequences. Section (c) indicates that this upper detachment is far more developed with a separate set of normal faults detaching onto the base of the Cenozoic megasequence. The geometries of reflections in the extensional domain indicate slip occurring along both detachments synchronously, suggesting that gravitationally driven strain is distributed between both systems. The Campanian detachment has larger throws, suggesting that it has taken more of the strain, although the folding of the Cenozoic reflections in the far west appears to restrict its westerly development. The imbalance between the two detachments in section (c) suggests that the Cenozoic detachment is more efficient; however, as the system grows northwards the Campanian detachment becomes more important. This may relate to local variations in the slip potential of the detachment surfaces, such as changes in thickness, overpressure or lithology.

4.5.2 Multiple detachments

The presence of multiple detachment horizons in gravity collapse systems has been recognized previously (e.g. Totterdell & Krassay 2003; Rowan et al. 2004; Corredor et al. 2005; Briggs et al. 2006), but few studies have documented how the position and interaction of different slip horizons creates a range of complex geometries indicating changes in the timing and location of deformation.

Sub-Aptian failure. The focus of previous studies of the Orange Basin collapse structures (Butler and Paton 2010; de Vera et al. 2010) has been on the system contained within the Late Drift megasequence. Figure 4.9 presents a more detailed interpretation of a portion of the extensional domain of the collapse (see Figure 4.4 for location). We see here that the main detachment in the Late Drift megasequence is underlain by a set of thrusts detaching onto the top of the Synrift megasequence. This lower detachment is formed along a maximum flooding surface between the top of the Synrift megasequence (Hauterivian) and the base of the Early Drift megasequence (Barremian) identified by Brown et al. (1995). Folding of the upper detachment and overlying horizons by the developing underlying thrusts imply that they formed later.

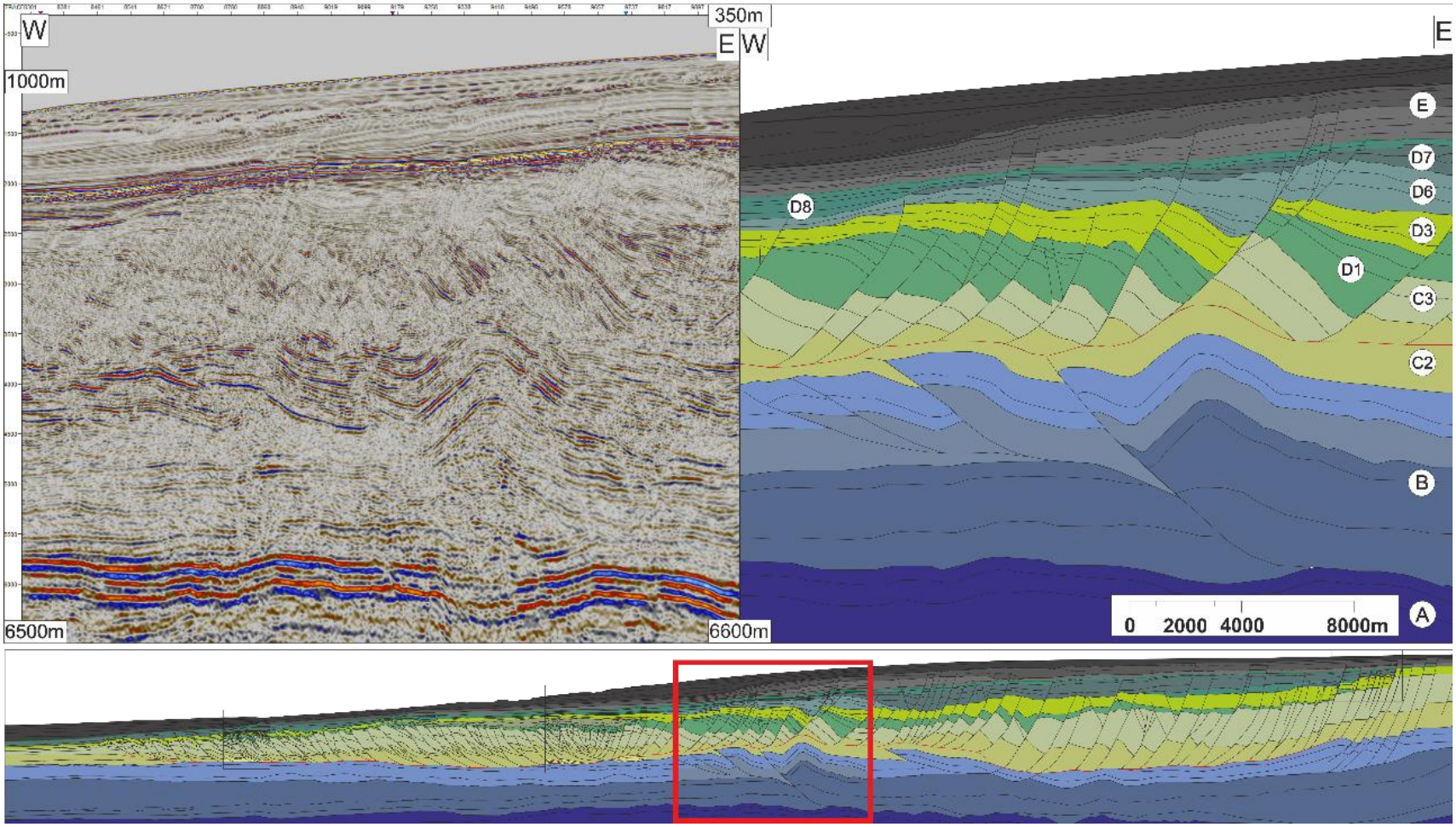

Figure 4.9. Detailed interpreted and uninterpreted section from Figure 4.4 showing folding of the upper detachment by and lower detachment system. Section is vertically exaggerated 3:1.

In addition, thickening in sequence D6 into the fault immediately above the fold suggests that its inception led to reactivation of this fault. The lack of significant thickening of sequence D7 suggests that thrusting had largely ceased by the time of its deposition. This suggests that although the upper system was initiated first, both systems existed coevally. The vergence of these lower thrusts is consistent with the same basinwards translation as the upper system. The most proximal normal faults present in the east of the section clearly penetrate into the Early Drift megasequence and are likely to link directly to these thrusts, although the seismic resolution prevents clear confirmation. D6 is not present above these faults (Figure 4.5) and may have either been eroded out or not been deposited; however, the infilling of the subsequent D7 into the fault planes suggests that these faults were most active prior to its deposition.

4.5.3 Stacked detachments.

Sections through the far north of the largest collapse structure provide further insights into the multi-layer detachment systems (Figs 4.3 & 4.10). In Figure 4.10, an 83 km long section shows several different detachment surfaces at a number of stratigraphic intervals, picked by the identification of mutual fault terminations. In the east of the section, a 30 km long package of normal faults extends up to 2.5 km from a detachment layer within the Early Drift megasequence to the Cenozoic horizon. A second smaller extensional domain, 12 km long with faults extending vertically 600 m up from the detachment, is seen down-dip and is contained entirely within the Early Drift megasequence, representative of an early phase of collapse. Two compressional domains also exist: a lower detachment in the Early Drift megasequence, along the Aptian–Barremian maximum flooding surface (Muntingh & Brown 1993), contains thrusts penetrating up to 1.1 km into the overlying Late Drift megasequence, whereas an upper 45 km long detachment, along the Cenomanian–Turonian maximum flooding surface (Paton et al. 2007), consists of widely spaced thrusts extending 700 m up from the detachment and is entirely within the Late Drift megasequence. Reflections in the lower compressional domain demonstrate two

periods of activity; one period is synchronous with the lower extensional system, with which it shares a detachment and a later phase of reactivation leading to thrusting and folding of the Late Drift megasequence. The upper detachment may have been active synchronously with the lower compressional domain, but remained active for longer, as indicated by thrusting and folding of the dark green sequence. It is interesting to note that the upper system terminates at the location at which the first thrust of the lower system emerges. Altering the slope angle of the upper detachment at this point may have made further slip along it non-viable. The upper extensional system remained active throughout the Late Drift megasequence and clearly transferred considerable strain down-dip. However, the upper compressional domain remained active during this period, although this domain does not appear to be genetically linked at this point, so the process of transmission of strain between the upper and lower compressive domains is not clear. No genetic link emerged in reviewing parallel sections; in fact, the lower system disappeared relatively rapidly. The transition from extensional to compressional domains along the upper detachment in this section was of a very different character to that seen in Figure 4.6 and appeared as a zone of largely deformed sediments, as described by Corredor et al. (2005) and Krueger & Gilbert (2009).

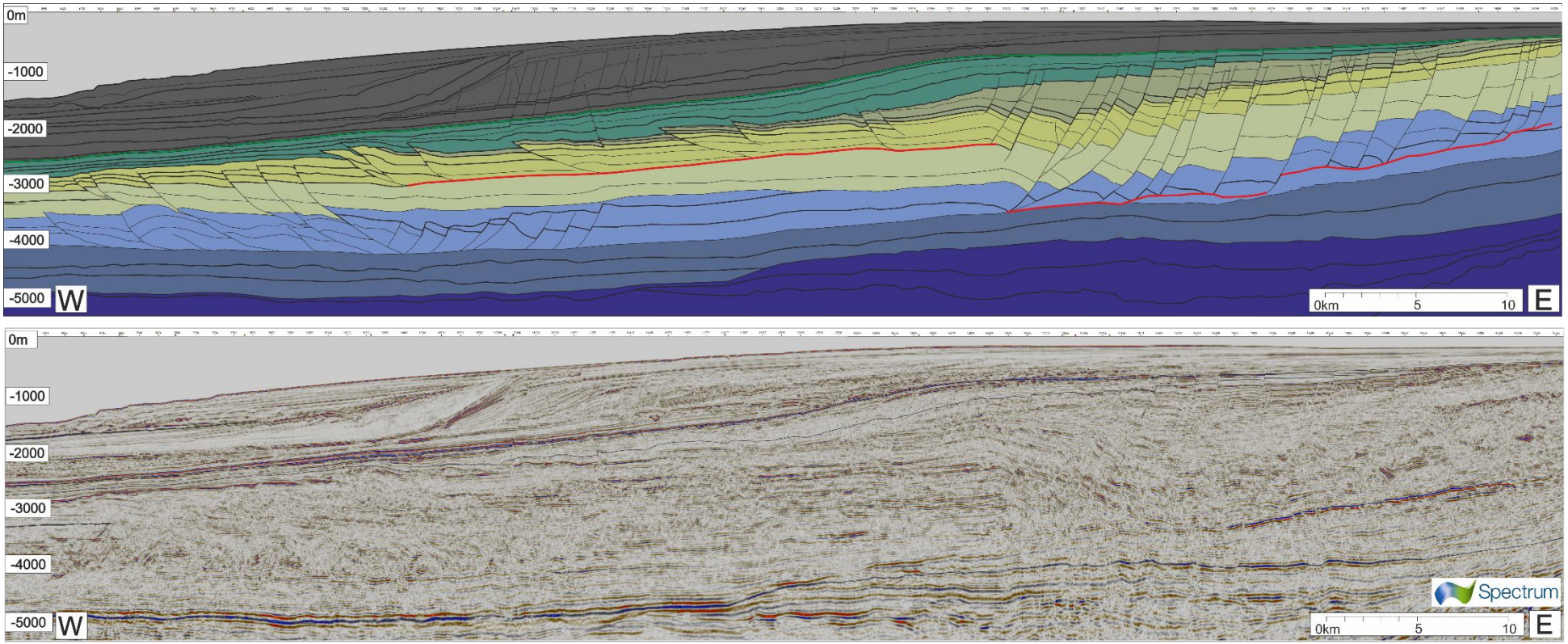

Figure 4.10. Interpreted section taken from northern portion of the same collapse structure as featured in Figure 4.4. Section is vertically exaggerated 3:1.

4.6 Discussion

The presence of gravity collapse structures has been documented on many margins and some of the inherent variability has been discussed in detail elsewhere (Morley et al. 1996; Rowan et al. 2004; Krueger & Gilbert 2009; Morley et al. 2011). Studies that have focused on systems driven by thin shale detachments generally propose that they are relatively coherent bodies presenting little variation within a single system. We discuss here how the observed lateral variability in geometries observed in this study has influenced our understanding of thin shale detachment systems. We also consider the greater complexity observed in these features to synthesize a new temporal model of collapse development in the Orange Basin.

4.6.1 Model for the temporal evolution of a collapse structure

Variations in the style and character of deformation appear consistently across the width of the Orange Basin, including the spacing between thrusts, the depth and location of slip detachment surfaces, and the nature of the transition zone. Although there is also considerable variation in the thickness of the Upper Cretaceous sediments across the basin, the same regional detachment is present throughout. This means that the changes in the styles of deformation observed are present within a single DWFTB so that any single end-member model is not applicable. Dalton et al. (2015) have demonstrated that the extensional domain was initiated prior to the formation of a later compressional phase. In this study, we have shown through growth packages that the earliest phase of collapse was located in the centre around the transition zone. For example, D8 in Figure 4.6 is a post-kinematic horizon, but in Figure 4.7 it is clearly a syn-kinematic package and is entirely eroded out to the west, where the overlying D9 package, here post-kinematic, becomes syn-kinematic, showing that later phases of movement occur progressively more distally than earlier phases. Few sequences can be tracked throughout the entire structure as they are either truncated by later sequences or are only locally present. However, analyses on the megasequence scale and of larger traceable sequences reinforce this finding. New faults formed and grew at the outer extents of the collapse, although older faults were still active with a reduction in offset. Successive younger faults formed

out from the transition zone, down-dip to the west in the case of the compressional domain and up-dip to the east in the case of the extensional domain. The high fidelity of the seismic imaging of our data showed that the transition domain represents a short-wavelength change from extensional to compressional tectonics as opposed to being a zone of overprinted regimes and, more importantly, that it appears to remain fixed. In general, the position of maximum strain migrates away from the transition domain, although we do observe fault reactivation occurring (Figure 4.9).

It is similarly clear that if we can relate later, more proximal, movements to ever more distal thrusts, then this would reinforce the concept that these regimes preserve the original contact between them as a block of material that ceases to deform, allowing the translation of strain downslope. Observations of the underlying thrust systems, and the timing of structures above and beneath in Figure 4.9, indicate a synchronous relationship between the systems – that is, the overlying detachment was folded by the underlying system, which remained active throughout. This suggests that they are both part of a single system as opposed to being two stacked systems of different ages.

Although many studies make reference to multiple detachment horizons (Rowan et al. 2004; Krueger & Gilbert 2006; Morley et al. 2011; Peel 2014), their presence is generally not included in models of gravity collapse systems. Growth strata indicate that these alternative detachments are often not merely spatially and temporally separate collapse events, but are linked integral portions of the same system. They thus have an important role in terms of strain distribution. They preferentially appear on more mature systems and link to the youngest, most proximal, normal faults. This implies that they form after a point at which continued deformation along the extant distal compressional regime is no longer as efficient as linking to a lower detachment. Sequence-scale observations show that these structures take a long time to form and experience multiple reactivations, which control deposition and erosion along the margin. With this in mind, we have produced a model for the formation and growth of these systems in thin shale detachment systems (Figure 4.11).

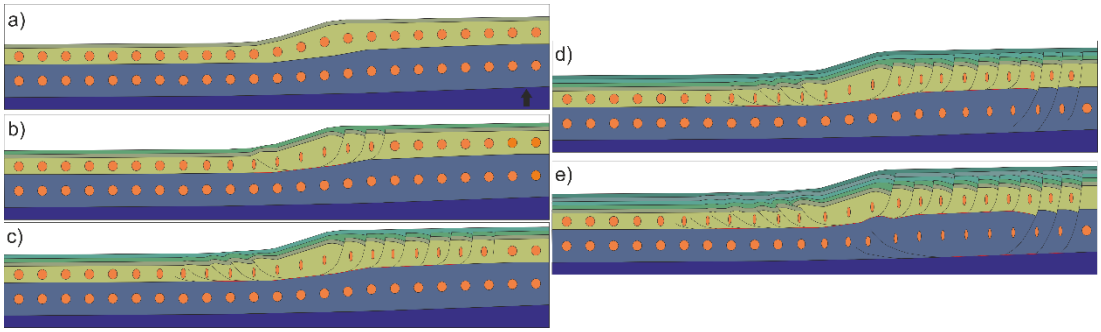

Figure 4.11. Multistage model of gravity collapse culminating in the formation of a lower detachment. Orange ellipses represent the distribution of strain within the DWFTB and reflect the findings of Dalton et al. (2015) that considerable compaction of the margin is required prior to the formation of the compressional domain.

Our model assumes that continued lateral compaction and deformation of the sediments above and ahead of the original detachment reaches a point at which it is no longer the most efficient way of accommodating the gravitationally induced stress. Assuming that the underlying sediments are comparatively under-compacted and in the presence of an appropriate alternative slip horizon, strain is now accommodated along a lower décollement. However, it is not clear how the strain is transferred from normal faults connected to a lower system. The strain recorded in the upper compressional domain is shown in Figure 4.9, where both the upper compressional regime and the most proximal normal faults deform age-equivalent sediments and thus must be linked. The extensional domain in Figure 4.8c shows two slip surfaces that have been exploited by the same faults at different times and it is possible that the same relationships exist in the more mature system in Figure 4.10, although continued deformation has made this relationships difficult to ascertain.

Brown et al. (1995) indicated that our detachment horizons are maximum flooding surfaces, presumably composed of low basal friction shales, which, as long as they are sufficiently thick and continuous, will continue to allow slip (Rowan et al. 2004). If the shale thins or is absent from a section, then the system will lock up. This locking up of the system while the overburden builds up sufficiently to lead to the re-initiation of failure by overcoming frictional cohesion results in the development of isolated sediment imbalances at the head of fault scarps (de Vera et al. 2010). This, in turn, leads to the formation of MTCs, which rework the sediments of the upper

portion of the extensional domain. This explains why we tend to see the large-scale development of MTCs only on mature systems prone to more lock ups. They become more prevalent stepping back towards the coast, where fewer shale intervals were deposited, and provide potential slip surfaces on what were palaeo-continental margins.

The initial geometries are controlled by the original local accumulations of sediments. The most amenable slip horizons – for example, the shale with the lowest frictional cohesion – will be used in preference to other slip horizons. This cohesion may, however, vary across the basin depending on the original depositional conditions and better slip horizons may be used elsewhere (Dalton et al. 2015). The collapse systems in this study were commonly associated with maximum flooding surfaces or the base of slope systems.

4.6.2 Stratigraphic controls on margin collapse

Although the majority of the passive margin stratigraphy on the Orange Basin is claystone, our observations imply that there is a strong control on the location and evolution of the collapse structures from variations in stratigraphy. The principle slip surfaces have been well documented as being relatively thin (c. 100 m), organic-rich shale horizons (e.g. Muntingh & Brown 1993; Paton et al. 2008) that act as low friction surfaces. This depositionally controlled variation in the basin can be related to the two end-member model for gravity collapse structures on shale detachments (Krueger & Gilbert, 2009). One end-member suggests slip along a single detachment horizon, whereas in the second endmember the detachment switches between local over-pressured shale horizons as variations in depositional occurrence and slip potential allow. In the Orange Basin, examples of both end-members are observed with the upper compressional domain in Figure 4.10 There is clearly slipping along a single regional plane, while the easterly extensional domain has a highly undulating character suggestive of smaller localized slip horizons.

The model presented by Morley et al. (2011) characterizes the collapse systems within the Niger Delta and Orange Basin as being of equivalent types (Type 1a). Both are detached on shale and, although there is much discussion as to the existence of

shale diapirism, there appears to be distinct differences in the style of deformation between the two basins. The implications of a thick shale interval versus a thin horizon, as commented on by Rowan et al. (2004), alters the nature of the failure. Critical wedge concepts (Bilotti & Shaw 2005; Briggs et al. 2006) assume the oceanwards propagation of the system. As long as there is low basal friction, then the system will continue to propagate. If there is a thick detachment layer, then it will localize all of the deformation on to the basal system. For example, where the Akata shale in the Niger delta is thick, it internally deforms and the whole overburden can behave as a mechanically strong unit (Corredor et al. 2005). This could cause long wavelength folding with some localized faulting (Costa & Vendeville 2002) and would not require significant intra-stratigraphic deformation. In the Orange Basin, in contrast, and in other basins dominated by interbedded heterolithic sediments with thin detachments, the mechanically strong unit above the detachment will need to undergo considerable intrastratigraphic deformation, such as folding and intralayer thrusting, to allow it to transfer strain down-dip (Dalton et al. 2015).

Our observations also show that the collapse is controlled not just by the detachment thickness, but also by variations in the margin stratigraphy. Existing stratigraphic studies of the Orange Basin (Brown et al. 1995; Paton et al. 2007, 2008) show that there are two key stratigraphic variations in the evolution of the basin. During the Aptian (megasequence B in this study), the stratigraphy facies consists of a landwards-stepping clastic front. This results in the landward migration of the delta foreset to marine shale transition. Overlying the delta system is the main shelf margin sequence with interbedded organic-rich shale horizons. This results in a complex distribution of the décollement horizons and corresponding multiphase development, which is described in the following parts of Figure 4.12:

(a) Stratigraphic distribution of the stable passive margin.

(b) Extensional faulting initiates on the continental slope, detaching onto an advantageous shale horizon and subsequently leading to thrusting down-dip on the abyssal plain.

(c) Continued gravitational imbalance on the margin leads to additional faults forming proximal and distal to the original collapse, which continues itself to deform.

(d) The ability of the upper detachment to redistribute strain down-dip becomes less efficient and so new extensional faults penetrate down to a lower shale horizon to compact lower, relatively under-compacted, sediments.

(e) This process continues to exploit lower shale horizons to redistribute strain; the original systems may also continue to deform, although lower systems may alter the structural development of the overlying systems. The propagation of the faults to the lower packages is, in part, controlled by the stratigraphy of the margin and the location of the delta front.

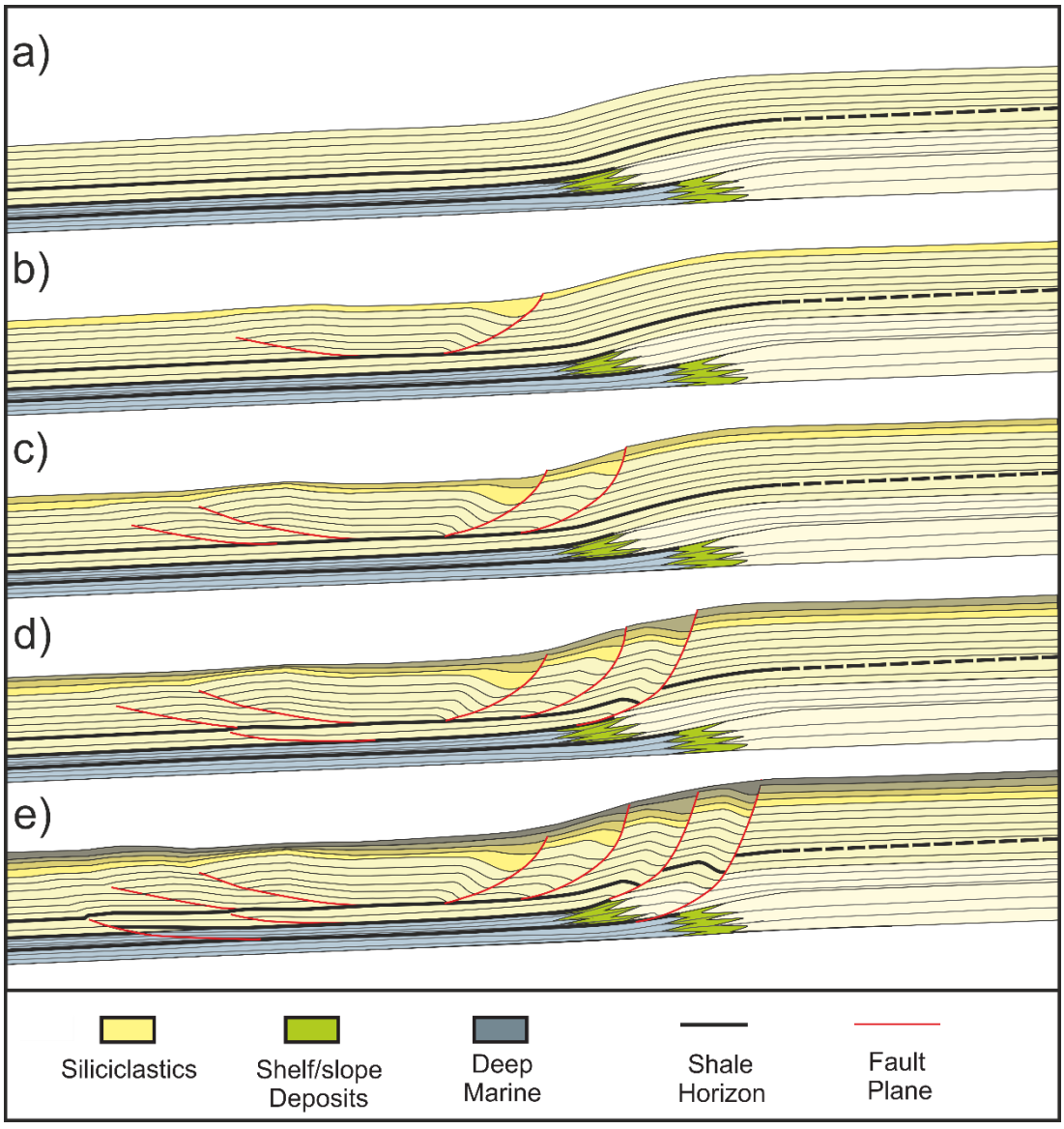

Figure 4.12. Model explaining the role of deposition on the location and development of detachment horizons. (a) Section through a typical margin showing three stacked sequences, two with shale horizons at the base of slope and the upper shale horizon representing a maximum flooding surface. (b) Development of a simple single detachment system slipping along the maximum flooding surface. (c) System matures with the development of additional faults and eventually locks up. (d) In

response to system locking up, alternative slip horizons along the lower base of slope shale are used instead. (e) Even lower detachment horizons are sought as the shale in (d) is restricted depositionally.

4.7 Conclusions

Using very well imaged examples of gravity collapse structures from the Namibian and South African Atlantic passive margin, we have illustrated the significant variation in the structures present in these tripartitie systems. This variation includes the typical up-dip extensional faults and down-dip thrust faults, but also multi-detachment faulting and folding, stacked detachments, cross-cutting and the complex progressive evolution of the system.

As this system is dominated by a series of relatively thin detachments, we suggest that the role of stratigraphy, especially the distribution of maximum flooding organic-rich units, plays a fundamental role in both the style and spatial distribution of the deformation. We propose that such a model helps to explain the differences that occur in thick shale systems, salt systems and thinly bedded heterolithic systems.

4.8 References

Bilotti, F. and Shaw, J. H., (2005). Deep-water Niger Delta fold and thrust belt modelled as a critical-taper wedge: the influence of elevated basal fluid pressure on structural styles. AAPG Bulletin, 89, 1475–1491.

Briggs, S. E., Davies, R. J., Cartwright, J. A., Morgan, R., (2006). Multiple detachment levels and their control on fold styles in the compressional domain of the deepwater west Niger Delta. Basin Research, 18, 435–450.

Brown, L. F., Jr., Benson, J. M., Brink, G. J., Doherty, S., Jollands, E. H., Jungslager, A., Keenen, A., Muntingh, A., van Wyk, N. J. S., (1995). Sequence stratigraphy in offshore South African divergent basins - An atlas on exploration for Cretaceous lowstand traps Soekor (Pty) Ltd: AAPG, Studies in Geology 41.

Butler, R. W. H. and Paton, D. A., (2010). Evaluating lateral compaction in deepwater fold and thrust belts: how much are we missing from 'nature's sandbox'? GSA Today, 20, 4–10.

Corredor, F., Shaw, J. H., Bilotti, F., (2005). Structural styles in the deep-water fold and thrust belts of the Niger Delta. AAPG Bulletin, 89, 735–780.

Costa, E. & Vendeville, B. C., (2002). Experimental insights on the geometry and kinematics of fold-and thrust belts above weak, viscous evaporitic décollement. Journal of Structural Geology, 24, 1729–1739.

de Vera, J., Granado, P., McClay, K., (2010). Structural evolution of the Orange basin gravity-driven system, offshore Namibia. Marine and Petroleum Geology, 27, 233–237.

Dalton, T. J. S., Paton, D. A., Needham, D. T., Hodgson, N., (2015). Temporal and spatial evolution of deepwater fold thrust belts: implications for quantifying strain imbalance. Interpretation, 3, SAA71–SAA87.

Gerrard, T. and Smith, G. C., (1982). Post-Palaeozoic succession and structure of the south-western African continental margin. In: Watkins, J. S. & Drake, C. L. (eds) Studies in Continental Margin Geology. AAPG Memoir, 34, 49–74.

Hirsch, K. K., Scheck-Wenderoth, M., van Wees, J. D., Kuhlmann, G., Paton, D. A. (2010). Tectonic subsidence history and thermal evolution of the Orange Basin. Marine and Petroleum Geology, 27, 565–584.

Jungslager, E. H. A. (1999). Petroleum habitats of the Atlantic margin of South Africa. In: Cameron, N. R., Bate, R. H. & Clure, V. S. (eds) The Oil and Gas Habitats of the South Atlantic. Geological Society, London, Special Publications, 153, 153–168, http://doi.org/10.1144/GSL.SP.1999.153.01.10.

Koopmann, H., Schreckenberger, B., Franke, D., Becker, K. & Schnabel, M., (2014). The late rifting phase and continental break-up of southern South Atlantic: the mode and timing of volcanic rifting and formation of earliest oceanic crust. In: Wright, T.J., Ayele, A., Ferguson, D. J., Kidane, T. & Vye-Brown, C. (eds) Magmatic Rifting and Active Volcanism. Geological Society, London, Special Publications, 420. First published online December 18, 2014, http://doi.org/10.1144/SP420.2.

Krueger, A. and Gilbert, E., (2006). Mechanics and kinematics of back thrusting in deep water fold-thrust belts – observations from the Niger Delta (abstract). 2006 AAPG Annual Meeting, Houston, TX, USA, Abstracts Volume, 15, 58.

Krueger, A. and Gilbert, E., (2009). Deepwater fold-thrust belts: not all the beasts are equal. AAPG Datapages, Search and Discovery, Article #30085. http://www.searchanddiscovery.com/documents/2009/30085krueger/index.html.

Light, M. P. R., Maslanyj, M. P., Greenwood, R. J., Banks, N. L., (1993). Seismic sequence stratigraphy and tectonics offshore Namibia. In: Williams, G. D. & Dobb, A. (eds) Tectonics and Seismic Sequence Stratigraphy. Geological Society, London, Special Publications, 71, 163–191, http://doi.org/10.1144/GSL.SP.1993.071.01.08.

McGilvery, T. A. and Cook, D. L., (2004). Depositional elements of the slope/basin depositional system offshore Brunei. Proceedings of the Indonesia Petroleum Association Meeting, 7–8 December, Jakarta, Indonesia, 407–420.

Mohammed, M., Paton, D. A., Collier, R. E. L. I., Hodgson, N., Negonga, M., (2016). Interaction of crustal heterogeneity and lithospheric process in determining passive margin architecture on the Namibian margin. In: Sabato Ceraldi, T., Hodgkinson, R. A. & Backe, G. (eds) Petroleum Geoscience of the West Africa Margin. Geological Society, London, Special Publications, 438, http://doi.org/10.1144/SP438.9.

Morley, C. K. and Guerin, G., (1996). Comparison of gravity-deformation styles and behaviour associated with mobiles shales and salt. Tectonics, 15, 1154–1170.

Morley, C. K., King, R., Hillis, R., Tingay, M., Backe, G., (2011). Deepwater fold and thrust belt classification, tectonics, structure and hydrocarbon prospectivity: a review. Earth Science Reviews, 104, 41–91.

Muntingh, A. and Brown, L. F. J., (1993). Sequence stratigraphy of petroleum plays, post-rift Cretaceous rocks (Lower Aptian to Upper Maastrichtian), Orange Basin, South Africa. In: Masterson, A. R. (ed.) Siliciclastic Sequence Stratigraphy. Recent Developments and Applications. AAPG Memoir, 58, 71–98.

Paton, D. A., di Primio, R., Kuhlmann, G., van der Spuy, D., Horsfield, B., (2007). Insights into the petroleum system evolution of the southern Orange Basin, South Africa. South African Journal of Geology, 110, 261–274.

Paton, D. A., van der Spuy, D., di Primio, R., Horsfield, B., (2008). Tectonically induced adjustment of passive-margin accommodation space; influence on hydrocarbon potential of the Orange Basin, South Africa. AAPG Bulletin, 92, 589–609.

Peel, F. J. (2014). The engines of gravity-driven movement on passive margins: quantifying the relative contributions of spreading v. gravity sliding mechanisms. Tectonophysics, 633, 126–142, http://doi.org/10.1016/j.tecto.2014.06.023.

Posamentier, H. W. and Kolla, V. (2003). Seismic geomorphology and stratigraphy of depositional elements in deep-water settings. Journal of Sedimentary Research, 73, 367–388.

Rowan, M. G., Peel, F. J., Vendeville, B. C., (2004). Gravity-driven fold belts on passive margins. In: McClay, K. R. (ed.) Thrust Tectonics and Hydrocarbon Systems. AAPG Memoir, 82, 157–182.

Totterdell, J. M. and Krassay, A. A., (2003). The role of shale deformation and growth faulting in the Late Cretaceous evolution of the Bight Basin, offshore southern Australia. In: Van Rensbergen, P., Hillis, R. R., Maltman, A. J. & Morley, C. K. (eds) Subsurface Sediment Mobilization. Geological Society, London, Special Publications, 216, 429–442, http://doi.org/10.1144/GSL.SP.2003.216.01.28.

van der Spuy, D., Ziegler, T., Bowyer, M., (2003). Deepwater 2D data reveal Orange Basin objectives off western South Africa. Oil & Gas Journal, 101, 44–49.

Welbon, A. I. F., Brockbank, P. J., Brunsden, D., Olsen, T.S. (2007). Characterising and producing from reservoirs in landslides: challenges and opportunities. In: Jolley, S. J., Barr, D., Walsh, J. J. & Knipe, R. J. (eds) Structurally Complex Reservoirs. Geological Society, London, Special Publications, 292, 49–74, http://doi.org/10.1144/SP292.3

5 Chapter 5; Temporal and spatial evolution of deepwater fold thrust belts: Implications for quantifying strain imbalance

[*This chapter is composed of a paper published by the AAPG in Interpretation, Volume 3, No. 4 in November 2015, doi:10.1190/INT-2015-0034.1. A published version is included in the Appendices, along with restorations for lines 1, 2, 4 & 5. A restoration of Line 3 is presented in Chapter 3 section 3.2.4.*]

Abstract; Deepwater fold and thrust belts (DWFTBs) occur in a large number of active and passive continental margins, and their occurrence play an important role in controlling the structural configuration and stratigraphic evolution of margins. Although DWFTBs that are located on passive margins are a coupled system, in which up-dip extension is linked to down-dip contraction, many studies have established a significant imbalance between these two domains in favour of net extensional strain. We have sequentially restored a series of parallel sections from the Orange Basin, South Africa, to quantify the amount of extension and contraction along a single collapse system. We found there to be a constant shortfall in the amount of contraction relative to extension in these features, which allowed us to quantify the lateral compaction of the margin as 5%. We also established a temporal model for the development and growth of thin shale detachment gravity collapse structures on passive margins. This model had implications not only for the kinematic and geometric evolution of these systems but also on the geomechanical process involved, in particular the accommodation of strain through compactional processes rather than discrete faulting.

5.1 Introduction

The development of deepwater fold and thrust belts (DWFTBs) on passive continental margins is an important process that has been recognized on margins globally, including the Gulf of Mexico, the Scotia Basin, the Bight Basin (e.g., Totterdell and Krassay, 2003; Ambrose et al., 2005; Deptuck et al., 2009), and many South Atlantic margins, in particular, Brazil, Angola, Niger Delta, Congo, and the Orange Basin (e.g., Hudec and

Jackson, 2004; Bilotti and Shaw, 2005; Corredor et al., 2005; Jackson et al., 2008). DWFTBs are linked fault systems of up-dip extension and down-dip contraction that often share a common detachment and result from gravitationally induced margin instability. As proposed by Morley et al. (2011), DWFTBs can be classified in a number of ways, including driving mechanism, sediment thickness, and basal detachment characteristics. This in part explains the significant structural variety that has been previously identified within DWFTBs

(e.g., Rowan et al., 2004; Krueger and Gilbert, 2009; Morley et al., 2011). This variety is caused by differences in lithology, failure mechanisms, detachment geometries, and detachment lithologies. Most studies (e.g., Rowan et al., 2004; Morley et al., 2011) separate margin collapses into two broad categories based on detachment lithologies: salt-detached and shale-detached systems. Shale systems are further subdivided into thin shale detachment and thick or mobile shale detachments (Morley et al., 2011).

The Orange Basin, located on the Namibian and South African sector of the West African passive margin, is an excellent environment to study the formation and growth of thin shale DWFTBs and their associated extensional fault systems. Gravity collapse structures can be broadly divided into three tectonic regions: (1) an up-dip extensional domain, dominated by normal faults, (2) a down-dip contractional domain composed of folds and thrusts, and (3) a transitional domain that is either a broadly undeformed region (Corredor et al., 2005; Krueger and Gilbert, 2009) or a complex region composed of extensional and compressional features (Butler and Paton, 2010; de Vera et al., 2010). Deformation, or the lack thereof, in the transitional domain is often a result of the duration of time over which the collapse is active. Flexure of the margin over time changes the point of contact between the two opposing domains causing them to overlap. They deform through a combined process of gravity spreading and gravity gliding to decrease the gravitational potential energy (e.g., Peel, 2014).

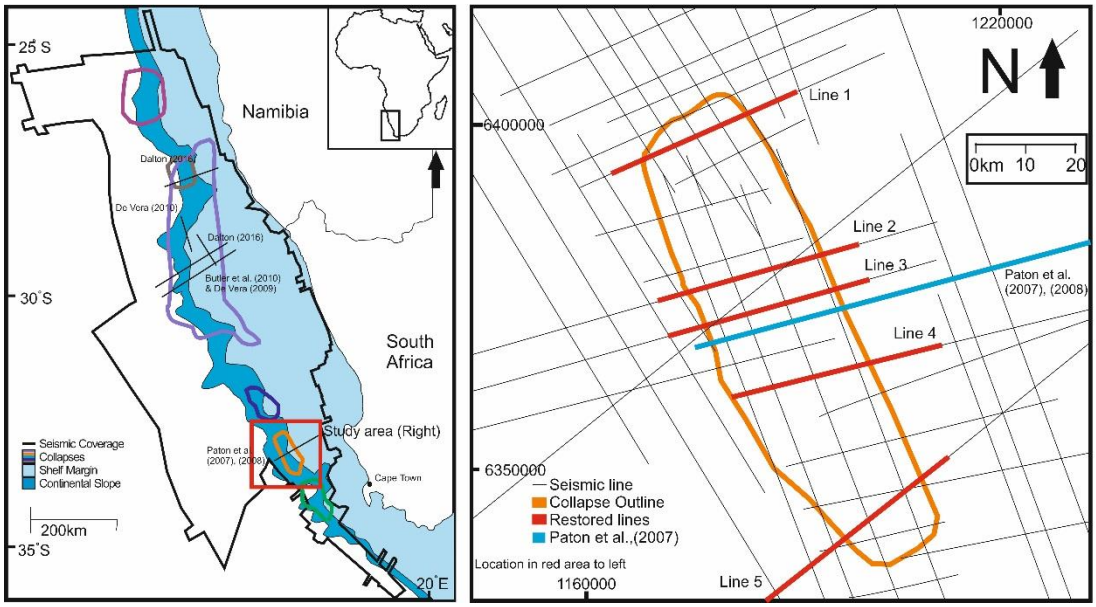

Figure 5.1 Location map of the study area showing the position of 2D seismic lines and the extent of the regional collapse features. Also highlighted are the location of lines used in previous studies in the area (Paton et al., 2007, 2008; Butler and Paton, 2010; Dalton et al., in review; De Vera et al., 2010).

Previous results of measurements of shale-detached gravity-driven collapse systems in the Orange Basin have identified a considerable imbalance between the up-dip extensional domain and the down-dip compressional domain (Butler and Paton, 2010; De Vera et al., 2010). This imbalance suggests significantly more extension than is compensated for by observed contractional features, resulting in a "missing strain component" between 10% and 25%. Both studies conclude that this is not a result of out-of-plane movements; rather, it is a systemic feature of these systems that may represent a strength-hardening phase. We test this premise by restoring multiple parallel sections to investigate whether the previous strain imbalance conclusion was an exceptional feature because both papers use the same seismic line, or if it is a common phenomenon in thin shale detachment systems.

Many studies of individual margin collapse focus on a single section of a system rather than considering the spatial variation in deformation. However, we examine five parallel seismic sections through a single collapse feature from the Orange Basin (Figure 5.1), to assess lateral variation in DWFTB geometry. We also restore these sections to measure and to test our understanding of how structures associated with the DWFTB develop through time. In doing so, we can address the existing enigma of how the

mismatch between extensional and contractional strain is accommodated. Furthermore, for the first time, we present a model that explains the temporal evolution of a DWFTB; our model has implications for understanding the complex interaction of sediments and structures on passive margins and also predicting the geomechanical response to deformation.

5.2 Regional setting

The geology of the Orange Basin is well documented by Muntingh and Brown (1993), Brown et al. (1995), Paton et al. (2007), Koopman et al. (2014), and Mohammed et al. (in press). The Orange Basin initiated with Jurassic to early Cretaceous rifting associated with the breakup of East and West Gondwana, progressing into the eventual continental separation of the South American and African plates. This resulted in a series of grabens and half-grabens that are orientated parallel to subparallel to the present-day continental margin (Paton et al., 2008). These graben were later filled by synrift sediments composed of siliciclastic, lacustrine sediments, and volcanic sequences throughout the Upper Jurassic to Hauterivian in the Lower Cretaceous (Brown et al., 1995). The progression from active rifting to the postrift thermal subsidence phase of the margin is characterized by a transitional sequence, which comprises Hauterivian-aged fluvial to deltaic sediments before reaching full marine conditions during the Barremian to Aptian. The main drift phase of the southern Atlantic is evident as a thick (up to 3.5 km) sequence of aggrading shale- and claystone-dominated sequences throughout the Upper Cretaceous (Gerrard and Smith, 1982). This Upper Cretaceous sequence is regionally truncated on the continental margin by the overlying Cenozoic sequence that progrades out into the basin and is 250–400 m thick on the margin and is 500–1400 m thick on the continental slope (Figure 5.2).

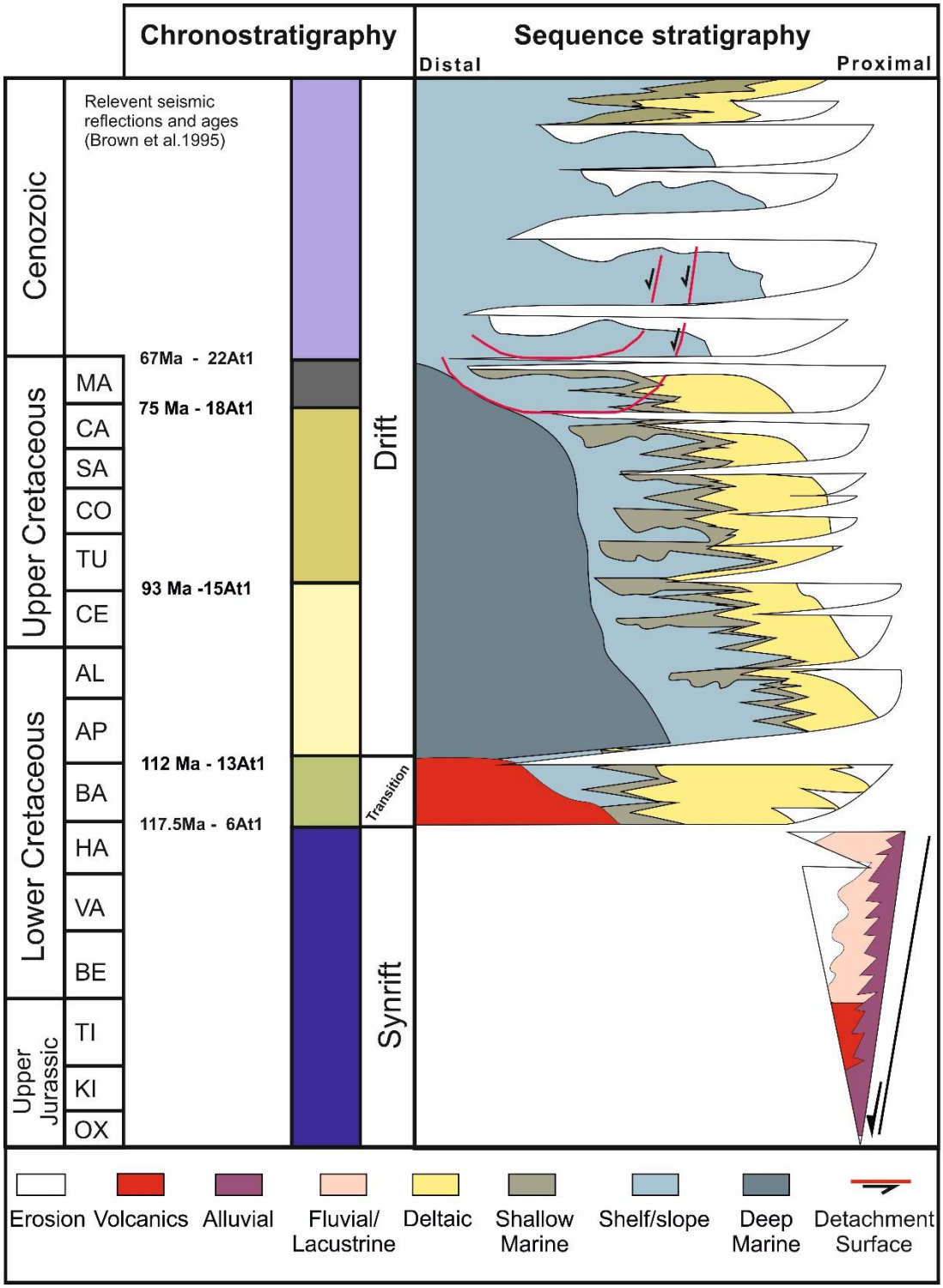

Figure 5.2 Chronostratigraphy for the Orange Basin with the main décollement horizons and collapse structures in this study identified (after Brown et al., 1995; Paton et al., 2008)

The postrift Cretaceous and Tertiary sedimentary sequences are deformed by a series of complex coupled gravity-collapse systems in which the up-dip extensional and down-dip contractional domains are very well imaged (Paton et al., 2007; Butler and Paton,

2010; De Vera et al., 2010; Dalton et al., 2016). Detachments exist at multiple levels within the Cretaceous sediments throughout the basin — the most significant being in the Aptian, Turonian, and Campanian. We focus on the southernmost collapse, which is approximately 90 km long in a north–south orientation and approximately 25 km wide (east–west).

5.3 Data and methods

The data used in this study comprise 39 2D PSTM/PSDM seismic lines (Figure 5.1) of which 27 delineate the gravity collapse structure. The seismic data are of various vintages from 1991 to 2012 and combine data from the Petroleum Agency of South Africa with recently acquired Spectrum multi-client data (2012). We use a megasequence interpretation approach of these data by using strata of cut-off, truncation, onlapping, and offlapping relationships of reflections and delineate stratal packages using definitions by Paton et al. (2008) (Figure 5.3) to show variations in timing and structural geometry laterally across the DWFTB.

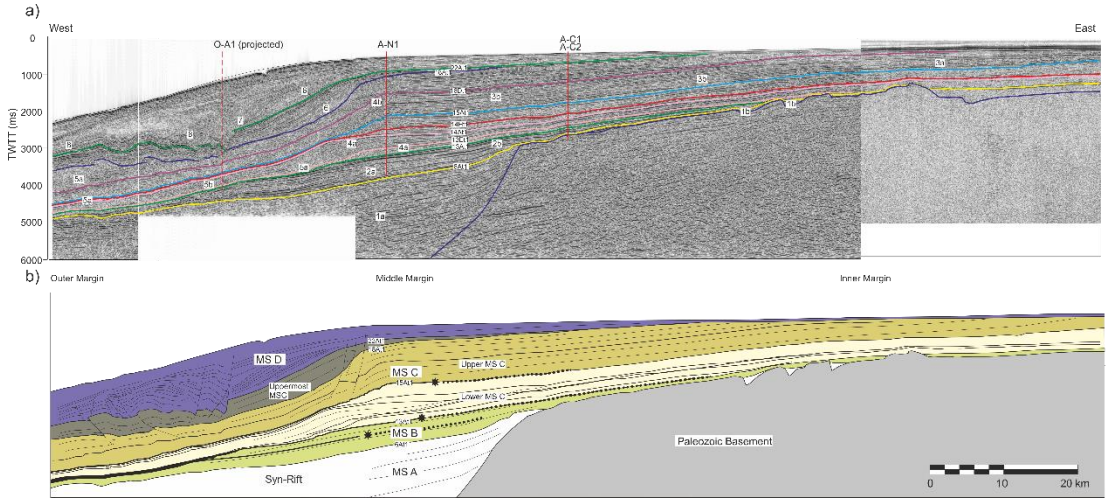

Figure 5.3. Cross section across the southern Orange Basin showing the key seismic horizons and megasequences (modified from Brown et al., 1995; Paton et al., 2007). The section traverses through the study area (Figure 5.1) and has been used to identify and date significant horizons in this study.

For this study, we pick the Hauterivian-Barremian-aged 6AT1 horizon to represent the top of the synrift (purple), the early Aptian 13AT1 horizon to represent the end of the transition package (green), the 15AT1 horizon representing the top of the Cenomanian (light yellow), the 18AT1 horizon defines the base of the Maastrichtian (dark yellow),

and the 22AT1 horizons represent the top of the Maastrichtian and are the uppermost Cretaceous package (grey). The seabed defines the top of the Tertiary megasequence (Figure 5.3).

To define the geometry and development of this gravity collapse structure, we interpret five dip-orientated seismic sections (Figures 5.4–5.9) that transect the entire collapse. The sections are spaced along the length of the collapse and are orientated parallel or subparallel (within 10°) to the transport direction of the collapse (Figures 5.1 and 5.9). Although the DWFTB in this study extends across the width of the margin, it is elongated along the margin as opposed to the bowl-shaped geometry that has been observed on other slides (e.g., Hesthammer and Fossen, 1999). We then restored the sections using the Upper Cretaceous- Tertiary (UCT) reflection (consistent with the 22At1 reflection) because its high-amplitude reflection character enables a confident correlation across the sections. The UCT refection is pre-kinematic to the onset of failure, which allows the restoration of this horizon to a realistic pre-collapse geometry equivalent to a continental margin slope system.

Kinematic restorations of PSDM data and depth-converted PSTM data, using Midland Valley Move 2013.1 software, allowed the measurement of throws and displacements to be consistent in the depth (m) domain. Through a process of sequential restoration of individual fault blocks (Lickorish and Ford, 1998; Bland et al., 2006), a realistic pre-deformation geometry is produced. For each of the five sections, the displacement on every seismically resolvable fault, in the extensional and contractional domains, is calculated and the cumulative displacements presented (Table 5.1).

5.4 Regional sections

We present five dip-orientated seismic sections from north to south along the western South African margin, which illustrate the geometry of the collapse structure (Figure 5.3). Each section is 35.7 km long and is plotted in TWTT (ms) with a vertical exaggeration of 3:1.

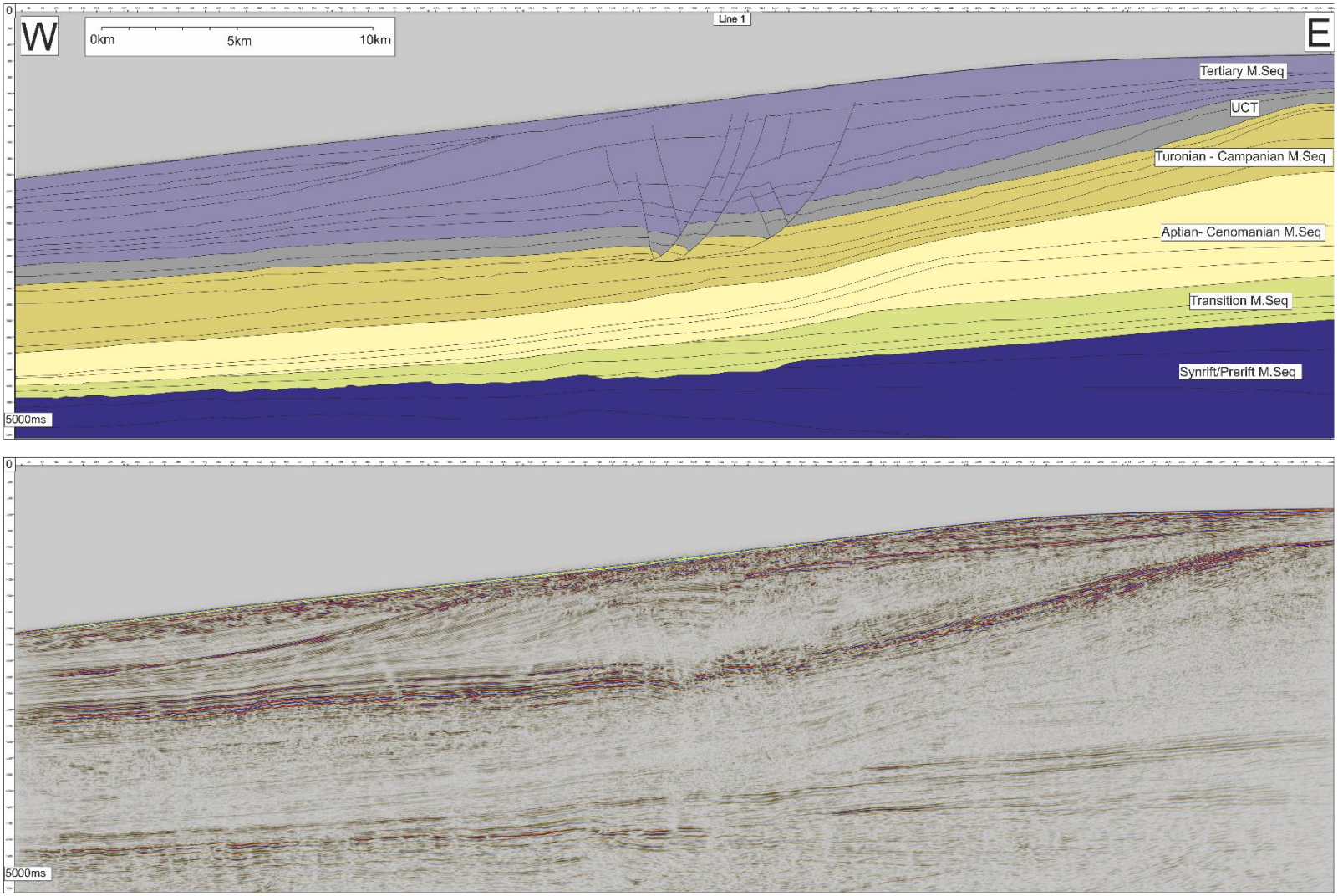

Figure 5.4. Line 1: seismic section, with interpretation. This is the most northerly line in which three west-dipping normal faults between a set of smaller antithetic east-dipping normal faults splaying from the larger faults are present. There is no contraction evident (Figure 5.1 for location).

Line 1 (Figure 5.4): This most northerly section is dominated by three large basin-dipping normal faults with displacements between 200 and 320 m, along with numerous, smaller conjugate or antithetic faults with 30–100 m of displacement. There are no apparent down-dip contractional features. The total extensional domain extends 10 km out into the basin. The larger faults detach onto to a common décollement in the Campanian claystones, which is identifiable by a set of downlapping reflections at the base of the fault blocks. Despite this considerable extensional domain, no corresponding seismically resolvable, contractional features are observed. The seismic packages show demonstrable thickening of growth strata during the Tertiary.

Line 2 (Figure 5.5): As in the previous section, the extensional domain contains three large normal faults, though most of the displacement is concentrated in the two most proximal faults (750 and 980 m) compared to the more distal fault (150 m). There is greater fault complexity in this section than in line 1, several small displacement (<30 m) normal faults can be interpreted as detaching onto the UCT in addition to a smaller number of corresponding thrusts that also detach onto the UCT. The contractional domain is defined by two large thrust faults (displacements of 220 and 490 m) that have a basal fault in the Campanian claystone and have west dipping ramp structures that propagate up through the Cretaceous sequence into the Tertiary. Reflections in the Tertiary cover show thickening of early packages into the normal faults; the same packages do not show thinning above the thrusts in the contractional domain.

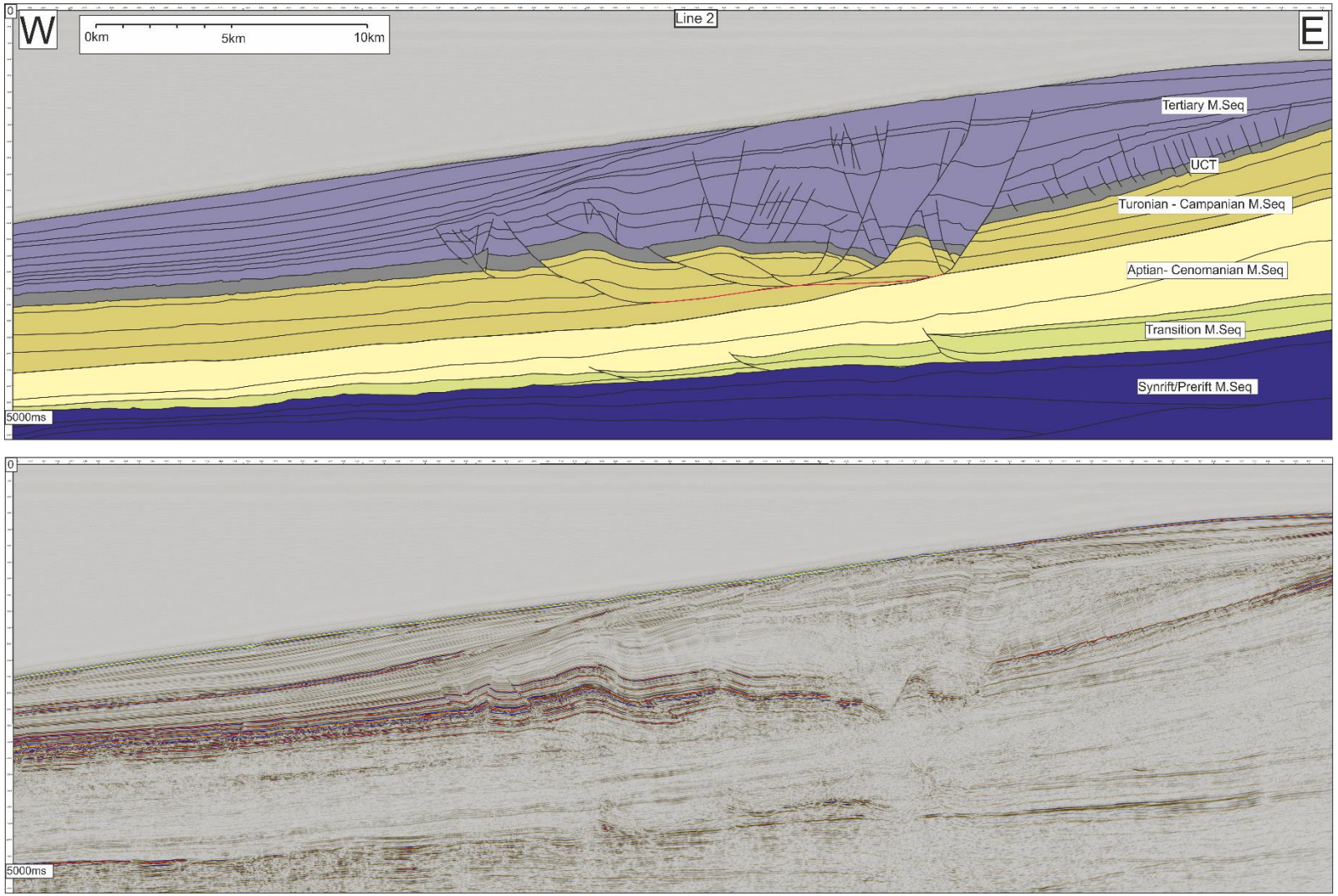

Figure 5.5. Line 2: seismic section, with interpretation of the section 22 km south of line 1. The large displacement normal faults are still evident as are the antithetic faults in the extensional zone. However, in down-dip, the reflections are folded and faulted by west verging thrust faults in a contractional zone.

Line 3 (Figure 5.6): The three normal faults that dominate the extensional domain in line 2 are again evident in this section; however, unlike the section 8 km to the north, most of the displacement is concentrated on the most landward/proximal fault (1140 m) with significantly lower displacements on the other two (480 and 500 m). Between these two lower displacement faults, the lowest Tertiary reflections downlap onto the UCT. Faults above the UCT are more common and have slightly larger displacements (30–80 m) compared to those observed in line 2 (less than 30 m) implying that more strain is being accommodated at this level.

Line 4 (Figure 5.7): The extent of the gravity collapse structure in this line is possibly incomplete with additional contraction potentially existing beyond the end of the section. We have, however, included it because it shows a significant change in the geometry of the failure relative to previous lines. Only two large normal faults that detach onto the Campanian claystones are present, and the corresponding contractional domain only contains a single major thrust. Deformation is now concentrated onto the UCT décollement, which shows considerable slip in the contractional (200– 1000 m) and extensional (500–2400 m) domains. Toe thrusts documented in the northern of the Orange Basin by Butler and Paton (2010) and De Vera et al. (2010) have formed above the UCT detachment immediately behind the fold formed by the underlying thrust fault that extends into the Campanian detachment.

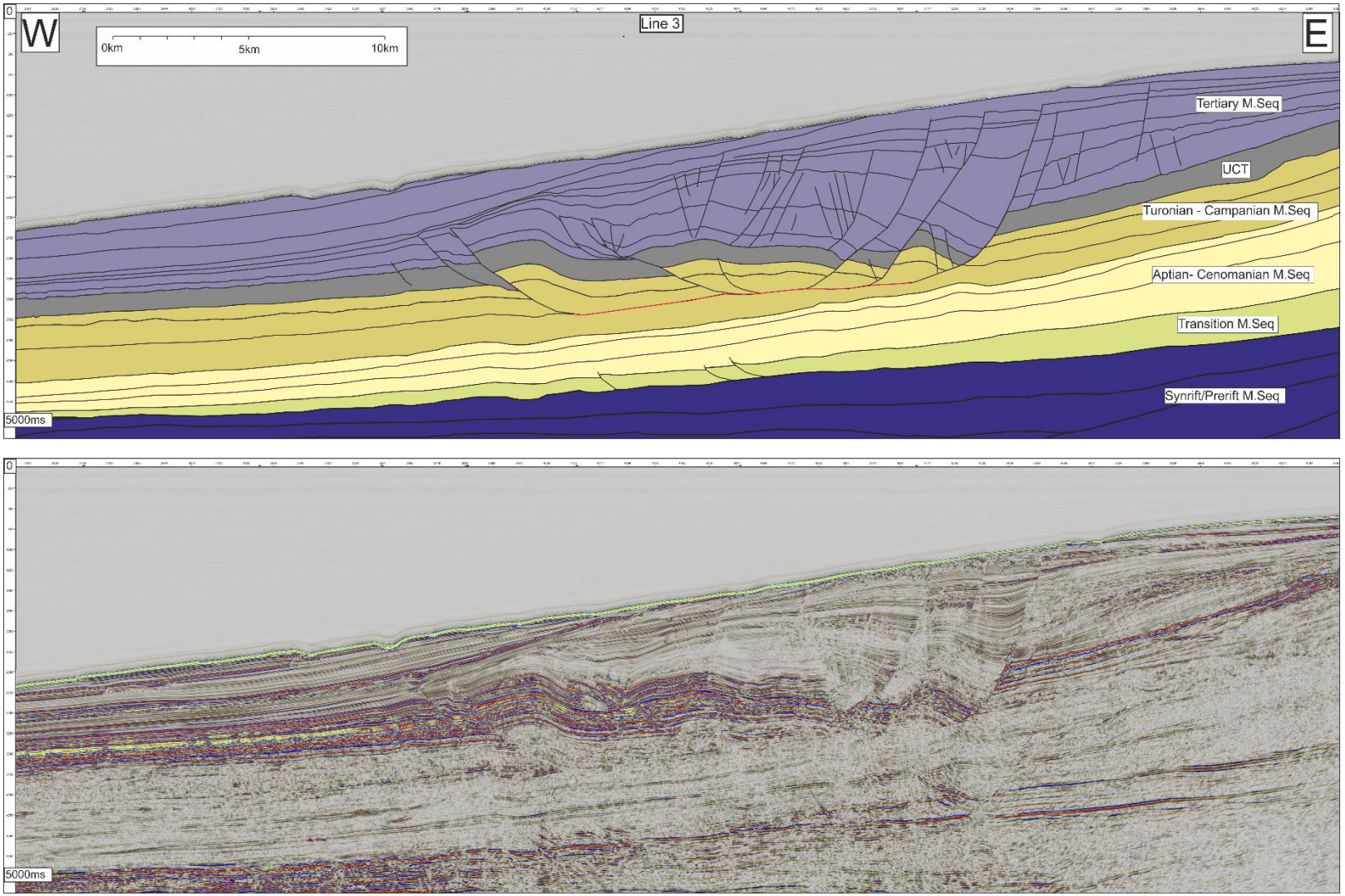

Figure 5.6. Line 3: seismic section, with interpretation of the section 5 km south of line 2. In this section, there is an increase in the number of extensional faults present, some of which detach on the UCT, although it is not clear whether the thrusts splay off the lower thrust or detach on the unconformity

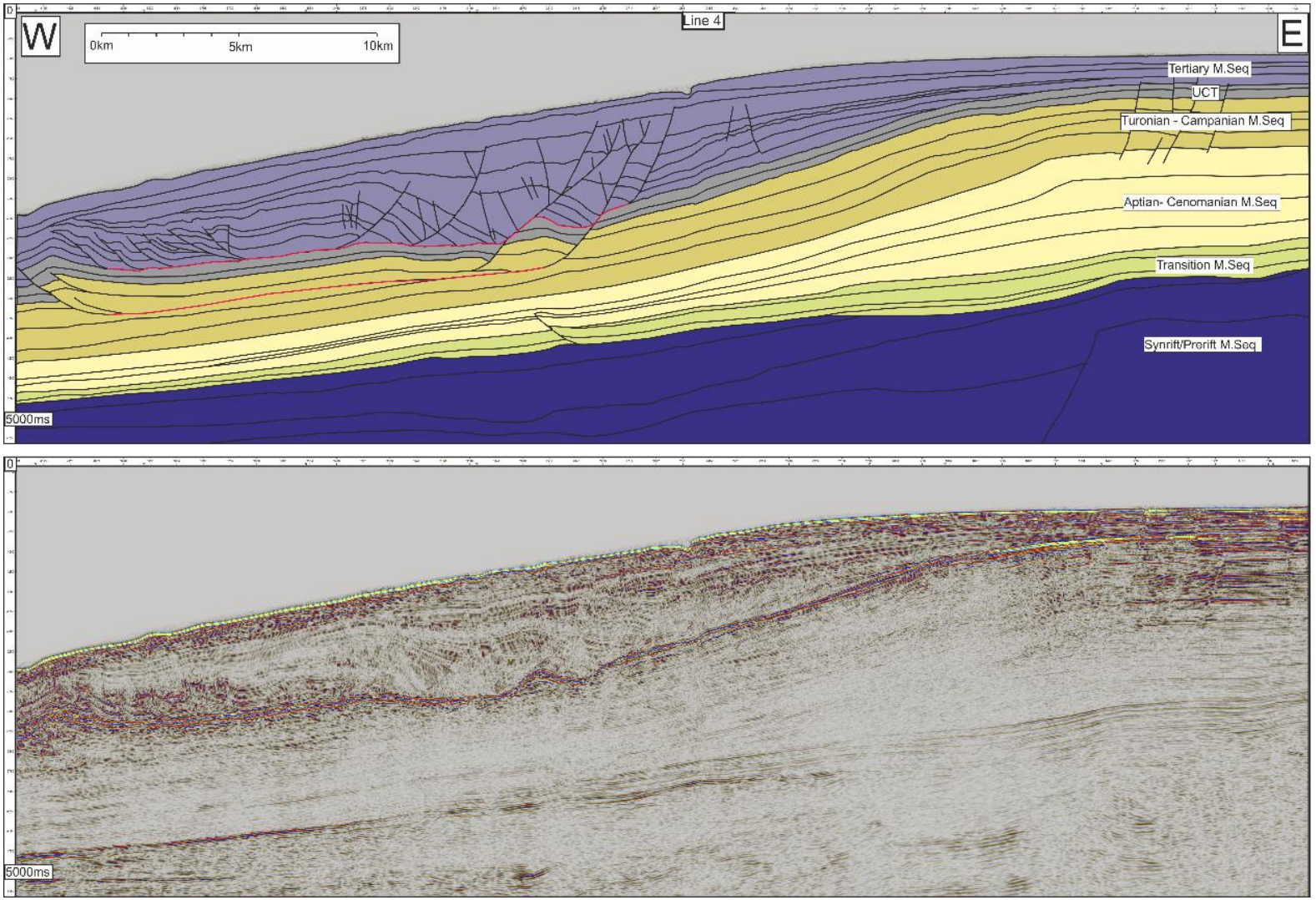

Figure 5.7. Line 4: seismic section, with interpretation, of the section 11.6 km south of line 7. This section is in the centre of the collapse and represents the maximum length of the system. It appears to have developed into a two-tier collapse with a second décollement forming on the UCT, this upper detachment taking up more of the slip.

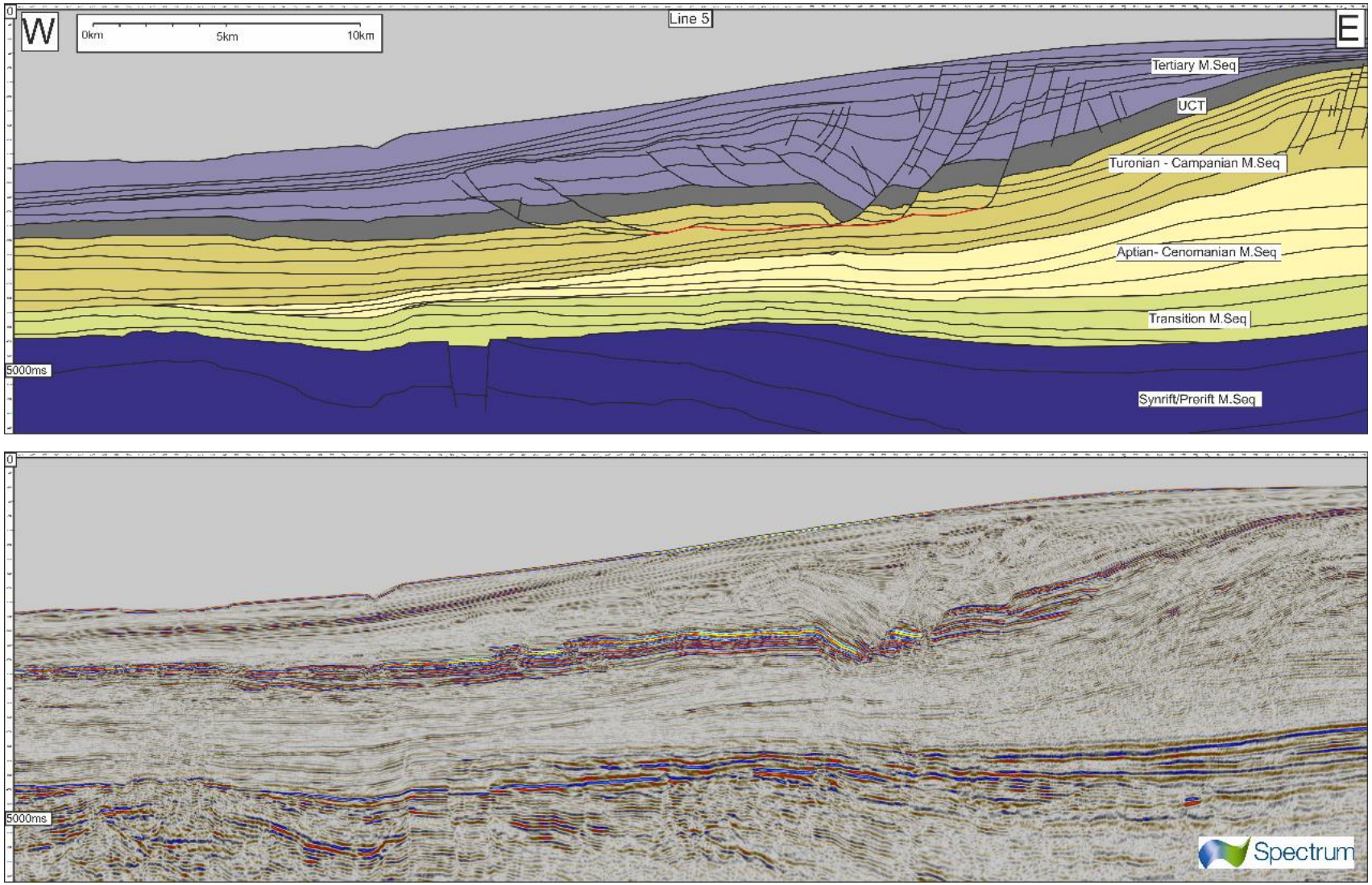

Figure 5.8. Line 5: seismic section, with interpretation, of the section 19.5 km south of line 4. This is the most southerly section that images the entire collapse structure

Line 5 (Figure 5.8): The southernmost complete seismic line within this collapse feature has comparatively similar geometries to lines 1–3; three large normal faults with displacements between 200 and 820 m, this time with the most distal normal fault containing the largest displacement in sediments along the Campanian detachment. Also along this surface, two large thrust faults are present with displacements of 280 and 520 m.

There is much less deformation above the UCT, though it is, unusually, dominated by thrust faults, the extensional strain being provided by the synchronous use of the Campanian detached normal fault planes. The UCT system as a whole is far less deformed than in line 4, with contractional displacements being 20– 100 m and extensional displacements being 160–220 m.

5.5 Restorations/data

We now present the results of the restorations undertaken on the depth-converted versions of the lines presented above (Figures 5.4–5.8), with the quantitative values presented in Table 5.1.

Values for total shortening and extension vary north to south along the collapse structure, increasing from line 1 in the north toward line 4 in the middle and reducing further south. The value for contraction in line 4 is lower due to the presence of only one thrust fault. Although additional thrusts could exist off section, the total length of the gravity failure here is comparable with the other sections, suggesting that this is likely to be its true extent. The net difference between total contraction and extension is, however, within a consistent range of 1000–1150 m regardless of these local variations. The fact that no section contains more contraction than extension confirms that this is not merely a factor related to out-of-plane deformation.

Butler and Paton (2010) calculate the missing strain as a proportion of the contractional domain length rather than the entire system. We calculate our missing strain value assuming it is distributed along its entire length, using the following equation:

$$\frac{(Total\ Extension\ (m) - Total\ Compaction(m))}{Length\ of\ DWFTB\ \ (m)} \times 100 = Missing\ Strain\ Component\ (\%)$$

To compare with previous results, we recalculate Butler and Paton (2010) and calculate values for De Vera et al (2010).

	Compression (m)	Extension (m)	Net (m)	DWFTB length	Missing Strain
Line 1	0	1008	1008	5917	100.0%
Line 2	943	2033	1090	19589	5.6%
Line 3	1043	2166	1123	21985	5.1%
Line 4	577	1673	1096	21767	5.0%
Line 5	818	1836	1018	20847	4.9%
de Vera et al	16000	24000	8000	145000	5.5%
Butler & Paton	25000	44000	19000	150000	12.7%

Table 5-1. Tabulated results of the cumulative contraction, extension and calculated net displacement, and missing strain for each section.

The measurements of the missing strain (4.9%–5.6%) agree with the previous results of 5.5% for De Vera et al. (2010) and 12.6% for Butler and Paton (2010). This implies that these results are consistent with larger gravity failures seen in the north detaching onto an earlier, Turonian-level detachment. Line 1, exhibiting no contractional domain, has a 100% missing strain component. It does, however, have an approximately 1 km value for net-missing strain, which is highly comparable to the other lines within the collapse.

5.6 Discussion

The variability of gravity collapse structures on a range of detachment lithologies has been well documented in previous studies (e.g., Rowan et al., 2004; Krueger and Gilbert, 2009; Morley et al., 2011). Although several of these studies document end-member models observed from 2D seismic examples, few record the variability observed within a single structure, however (Dalton et al., 2016). Previous studies have also presented restorations of 2D sections to establish likely deformation histories (Butler et al., 2010; De Vera et al., 2010). We have undertaken restorations of multiple parallel sections to gain a 3D understanding of the deformation history.
The repeated sequence of three normal faults with large displacements that extend close to the surface, in lines 1–3, suggests that these are the same faults in each section.

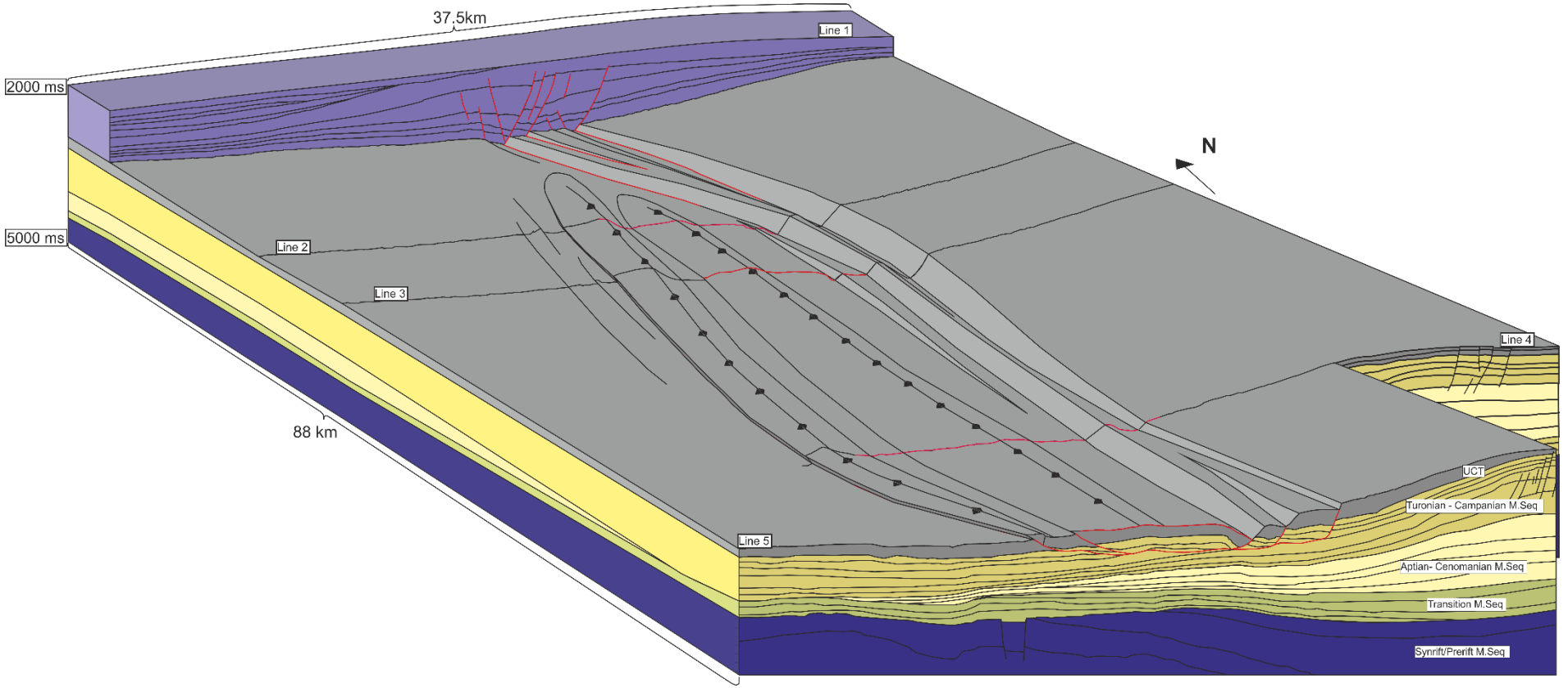

Figure 5.9. Cartoon illustrating the fault interactions of the Orange Basin gravity collapse structures in three dimensions for the UCT (18AT1) reflector.

Growth strata indicate the faults have propagated northward over time; however, the amount of displacement on each of these faults varies locally in each section. The largest faults are present across the margin (Figure 5.9) with two of the normal faults observable throughout but many of the smaller faults with displacements
> 100 m persist for shorter distances and are seemingly controlled by local variations in fold and fault geometries.

5.6.1 Comparisons with current models

The observations from the five sections outlined previously allow us to make a few interpretations regarding the development of this collapse structure as follows:
1) Line 1 does not conform to current models of gravity- driven collapse structures, and the absence of a down-dip contractional domain does not fit with our current understanding.
2) The earliest phase of deformation occurs in the centre of the structure near line 4 (Figure 5.7). Growth strata into the normal faults on lines 2 and 3 (Figures 5.5 and 5.6) indicate a Tertiary age for these faults, whereas crossline ties show that extensional faults in this section were active earlier than in line 1 (Figure 5.4). Note the relative thickness changes in the lowest purple unit in Figures 5.4 and 5.5. Furthermore, growth strata onto the thrust faults in line 3 suggest that although it is predated by the earliest phase of extension, crossline ties confirm that the contraction is also older toward the south
3) The extensional domain commences prior to the contractional domain: Reflections in line 2 (Figure 5.5) show thickening of early packages into the normal faults, whereas the same packages do not show thinning above the thrusts in the contractional domain.
4) The two detachments present in the system are active synchronously. In line 3 (Figure 5.6), downlaps onto the UCT between the two lower displacement faults indicate that the middle fault is active synchronously along the upper UCT décollement and along the deeper Campanian décollement. Furthermore, folding of the UCT décollement by the underlying Campanian décollement as seen in line 4 (Figure 5.7) curtailed the further deformation along it by altering its slip angle forcing

further deformation to occur proximal to its current position. This change in deformation geometry from a single detachment to a paired system may be due to changes in lithology, or it may possibly represent a lateral ramp (De Vera et al., 2010; Dalton et al., 2016) between two earlier separate collapse features that have subsequently coalesced.

5.6.2 Quantification of the strain imbalance

Previous studies have discussed that established concepts of balancing in cross sections do not apply when DWFTB systems are restored and that, commonly up-dip extension is approximately 10% greater than its equivalent toe-thrust system (Butler et al., 2010; De Vera et al., 2010). This missing strain is assumed to be a consequence of up-dip extension being initially accommodated by horizontal compaction of the downslope stratigraphy before deformation is localized onto discrete toe-thrust faults. This model is difficult to verify because these structures are often undrilled, and it would be difficult to prove that the equivalent amount of compaction has occurred. Our results, however, provide an alternative method to validate this model.

Despite the lateral variations in DWFTB geometry and the displacements of contraction and extension in our restorations, the net difference between these values remains consistently between 1000 and 1150 m. As each section displays DWFTB systems of similar total lengths of 19.5 to 22 km, we propose that, in this system, a value of approximately 1 km represents the maximum lateral compaction that can be accommodated prior to the strain being localized onto a discrete fault surface. From a temporal frame, line 1 is representative of the earliest stage of DWFTB development, at which point the extensional up-dip strain, generated by the collapse of the margin, is being entirely compensated for by lateral compaction down-dip. This amounts to a total of 1 km over 20 km of sediment (i.e., 5%). Lines 2–5 that are representative of the subsequent phase of development, show that subsequent extensional deformation is accommodated through discrete fault slip, thereby maintaining the approximately 1 km imbalance.

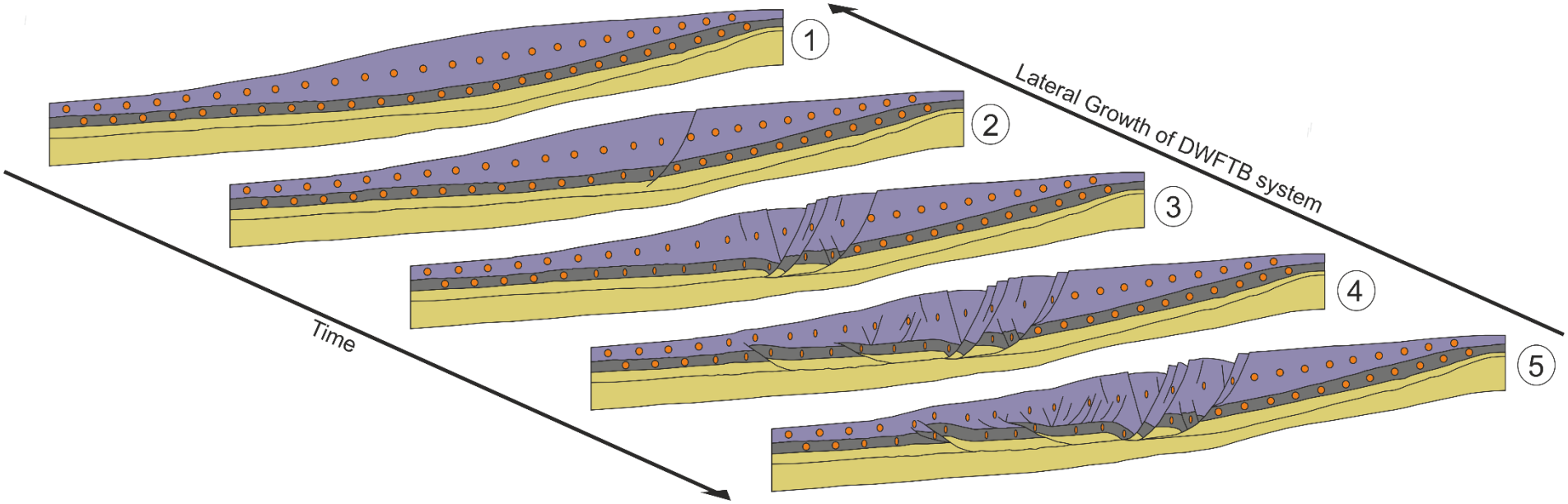

Figure 5.10. Model of initiation and propagation of a deepwater fold and thrust belt. (1) Normal faults develop and begin to laterally compact the margin sediments, (2) normal faults continue to grow and localize onto a common detachment, (3) because extension continues, the margin sediments become strength hardened and can no longer laterally compact leading to the formation of thrusts, (4) continued strain produced by the growth of normal faults is entirely absorbed by thrusts, and new faults that also form higher in the sequence begin to compact overlying under compacted pre-kinematic and syn-kinematic sedimentary packages. Orange ellipses represent strain for the sediments in the margin.

5.6.3 Model for growth of collapse

The gravity collapse system we describe in the Orange Basin is relatively simple, allowing a better understanding of the processes involved. Here, we present a temporal evolution model for the system (Figure 5.10). As demonstrated above, we can establish through the loop tying of reflections and restoration of multiple horizons the relative timing of individual structures within in the collapse. The analysis consistently shows that the first structures form in the centre of the system, with extension occurring prior to contraction. Lateral compaction occurs prior to the formation of a thrust domain. Given this premise, we consider that not only do the five lines represent a system that has increasing deformation toward the centre (e.g., line 4), but that they can also be viewed as an evolutionary sequence from lines 1 to 4:

1) Differential loading or tectonic uplift of a margin (e.g., Rowan et al., 2004; Paton, 2012) causes widespread instability leading to the formation of normal faults. The strain created by these faults is entirely accommodated via compaction of the down- dip margin stratigraphy.

2) Because extensional faulting continues, they coalesce onto a single efficient detachment that allows the effective translation of stress down dip. The resulting contractional strain produced by the translation of stress is compensated by lateral compaction of sediments downslope.

3) Continued margin instability leads to progressive growth of normal faults that in turn increase the strain that the down-dip system must accommodate. In this system, after approximately 5% strain, no further strain can be accommodated through compaction. At this point, deformation is accommodated through folds and thrusts extending off the detachment.

4) Once folding and thrusting have initiated, all new deformation is absorbed by faults, assuming the continued presence of a driving force. New normal faults form proximal to the margin, and thrust faults form ahead of the most distal thrust, whereas older faults continue to grow laterally creating a basin at its centre. Faults can only grow laterally where a slip surface exists. With increased deformation, other more advantageous slip horizons may present themselves leading to changes in detachment level (e.g., Dalton et al., 2016). Because systems continue to grow out into the basin, compaction of distal sediments will occur prior to the formation of additional distal thrusts.

5.6.4 Growth of larger systems

The net approximately 1 km seen in Table 5.1 is preserved throughout the continued development of the margin present as a missing strain component. This system is significantly smaller than the other collapse structures observed in the Orange Basin, in which systems can achieve widths of up to 160 km (Dalton et al., 2016). Despite this difference in scale, there appears to be a comparable 5% missing strain (De Vera et al., 2010) that is maintained, suggesting that the process may be independent of scale, although further analysis may be needed to determine the influence of the other boundary conditions, including detachment horizon, thickness of overburden, and relative timing of structures.

We consider that our model is applicable to other shale-detached DWFTB systems globally and conclude that once a compacted rock volume forms, it will continue to transmit strain down-dip; thereby, the zone of compaction in front of the emerging thrust front will continue to increase in width as the DWFTB size increases, given up-dip extension. This results in an approximate 5% missing strain regardless of the system's size. This value may vary on other margins, in direct relation to the mechanical behaviour of the stratigraphy involved. As noted by Dalton et al. (2016), the specific geometry of the DWFTB, and the faults contained within it, is also a function of the mechanical stratigraphy of the margin. Further studies are required to investigate the

role of fault evolution and stratigraphy in influencing spatial and temporal evolution of collapse systems.

5.7 Conclusions

The occurrence and geometry of DWFTBs are controlled by a number of well-established factors local to the margins on which they form. Despite these variations, the progression of the failure itself will follow a predictable pattern. Extension will occur in response to a margin imbalance, leading to the compaction of down-dip sediments that, once compacted, will localize continued deformation onto a discrete set of thrust planes. The compaction of the margin will be recorded in the imbalance between the amount of extension and contraction that will be approximately 5%. The systems' lateral growth will also conform to the same model, meaning that different stages of collapse will be observable across the margin at the same time.

5.8 Addendum to Chapter 5

This addendum to the published text has been included to discuss the mechanisms used to identify fault growth and fault timing.

5.8.1 Fault Growth Identification

The inference of syn-kinematic growth of sediments during periods of deformation on normal faults planes is established via the observation of growth strata represented by the thickening of packages into fault surfaces (Hardy et al., 1996; Suppe et al., 1992; Shaw et al., 2004). Figure 5.11a presents several examples of sediment packages thickening into fault planes. The reflector package Y (orange) shows clear thickening into the hanging wall of fault 4, creating a wedge geometry that thins towards the footwall of fault 3. If the fault 4 were inactive during the deposition of the Y, then the package should be of a similar thickness throughout. Though having been deposited on a slope, a similar geometry may be produced. In order to test these hypotheses, a simple block restoration of the Y is presented (Figure 5.11b).

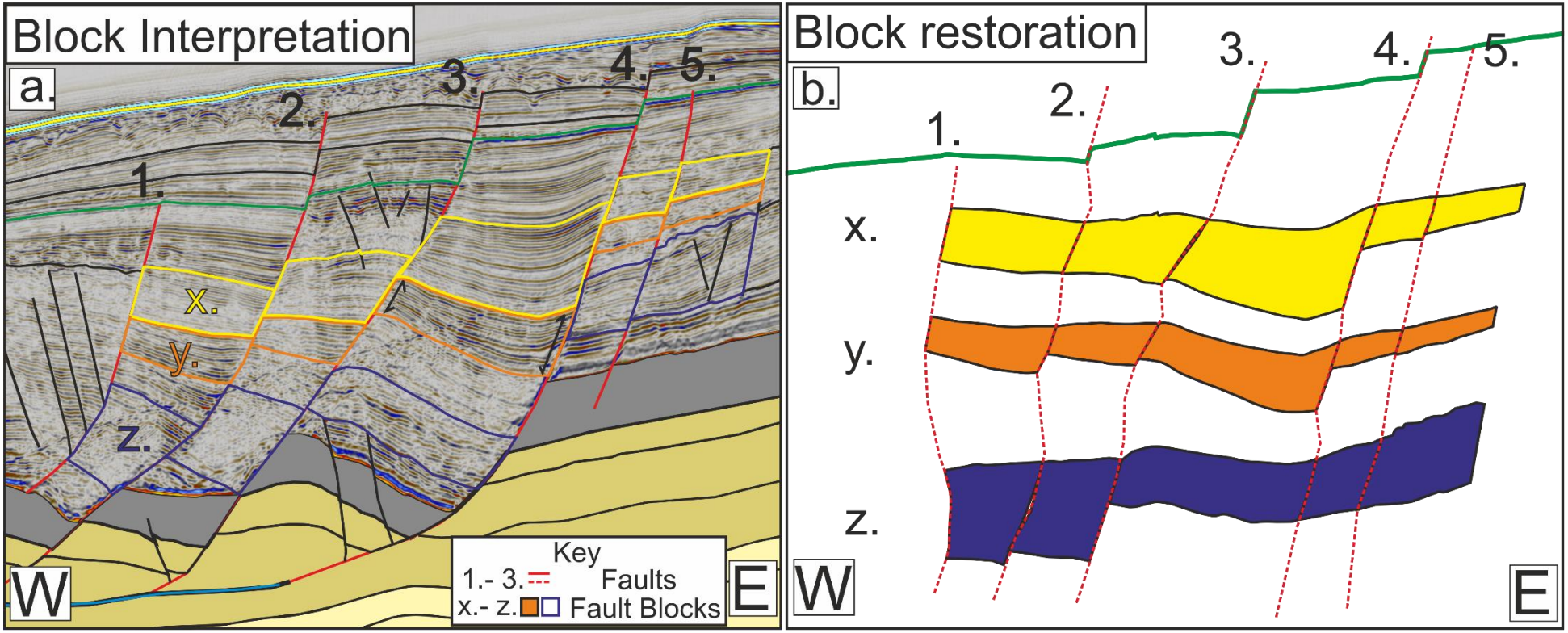

Figure 5.11. a) Interpretation of a faulted section of the extensional domain of Line 3 (Figure 5.6) displaying three packages X (Yellow), Y (Orange) and Z (Purple) b) a simple block restoration of the packages interpreted in a).

The thickness of Y varies either side of fault 4, and indicates more deposition occurred in its hanging wall. This proves the fault must have been active during the deposition of the Y, as it created the accommodation space into which sediments deposited. Put simply, where we see thicker deposits and rotation of the sediments in the hanging-walls of faults relative to their footwalls, we can infer the fault was active during the deposition of that sequence.

Biscke (1994) establish a mechanism for identifying and quantifying these as fault growth structures, by graphically representing the change in depth of a reflector between two wells and analysing the angle of the slope produced. Whilst absolute depths cannot be established due to an absence of well calibrations in appropriate locations a visual assessment of changes in depth of reflectors allows the identification of fault controlled strata and a temporal assessment of a faults activity and rate of deformation (Castelltort, et al., 2004).

5.8.2 Fault Growth Timing

The timing of fault structures is inferred through the observation of fault growth packages which are bounded between two identifiable horizons and can be traced between multiple sections. Figure 5.11b shows a simple block restoration of the reflector packages interpreted in Figure 5.11a. Where package thickness varies either side of faults 1-5, movement can be inferred to have occurred synchronous with the deposition of that package and *vice-versa*. From this we can see only faults 2 and 3 were active during the deposition of package Z (purple), faults 2-4 were active during deposition of Y and faults 3-5 were active during deposition of X. The green horizon shows that faults 2-5 were active or re-activated post the deposition of packages X-Z. From the faults are interpreted to activate progressively eastward (proximally).

However, this method can only identify a period of time in which the onset of deformation occurred. In order to determine the time at which deformation occurred more exactly an analysis of traceable individual seismic reflectors is required. The variable quality of the seismic used in the study and the presence of significant misties between lines prevents this style of detailed interpretation. Despite this two

observations support timing of relative onset; firstly, the thickest packages are present in the centre of the collapse structure (Figure 5.4-5.8), indicating they have displaced the most; secondly, packages between faults of the same section indicate proximal stepping of extensional displacement. In other words faults proximal to the earliest normal fault displaced later as no early growth packages are identifiable in their footwall (Figure 5.11b). In terms of the debate as to whether faults form their full length and then grow in displacement (Morley, 2002; Walsh et al., 2002; Jackson and Rotevatn, 2013; Jackson et al., 2017) or increase in length as they displace (Watterson, 1986, Walsh and Watterson, 1988: Cartwright et al., 1995) this analysis does not provide an answer, both models are potentially applicable to this study. Although the proximal stepping of faults and the absence of significantly thickened sequences in the north suggests that these faults formed later and grew northwards.

5.9 References

Ambrose, W. A., Wawrzyniec, T. F., Fouad, K., Sakurai, S., Jennette, D. C., Brown, Jr., L. F., Guevara, E. H., Dunlap, D. B., Talukdar, S. C., Garcia, M. A., Romano, U. H., Vega, J. A., Zamora, E. M., Ruiz, H. R., Hernandez, R. C., (2005). Neogene tectonic, stratigraphic and play framework of the southern Laguna Madre-Tuxpan continental shelf Gulf of Mexico: AAPG Bulletin, 89, 725–751, doi: 10.1306/01140504081.

Bilotti, F., and J. H. Shaw, (2005). Deepwater Niger Delta fold and thrust belt modelled as a critical-taper wedge: The influence of elevated basal fluid pressure on structural styles: AAPG Bulletin, 89, 1475–1491, doi: 10.1306/06130505002.

Bischke, R.E., (1994). Interpreting sedimentary growth structures from well log and seismic data (with examples). American Association of Petroleum Geologists Bulletin 78 (6), 873–892.

Bland, S., Griffiths, P., Hodge, d., Ravaglia, A., (2006). Restoring the seismic image: Geohorizons, 18–23.

Brown, L. F., Jr., Benson, J. M., Brink, G. J., Doherty, S., Jollands, E. H., Jungslager, A., Keenen, A., Muntingh, A., van Wyk, N. J. S., (1995). Sequence stratigraphy in offshore South African divergent basins - An atlas on exploration for Cretaceous lowstand traps Soekor (Pty) Ltd: AAPG, Studies in Geology 41.

Butler, R. W. H., and D. A. Paton, (2010). Evaluating lateral compaction in deepwater fold and thrust belts: How much are we missing from “nature’s sandbox”? : GSA Today, 20, 4–10, doi: 10.1130/GSATG77A.1.

Cartwright, J.A., Trudgill, B.D. & Mansfield, C.S. (1995). Fault growth by segment linkage: an explanation for scatter in maximum displacement and trace length data from the Canyonlands Grabens of SE Utah. Journal of Structural Geology, 17, 1319–1326.

Castelltort, S., Pochat, S., Van Den Driessche, J., (2004). Using T–Z plots as a graphical method to infer lithological variations from growth strata. Journal of Structural Geology 26 (8), 1425–1432.

Corredor, F., Shaw, J. H., Bilotti, F., (2005). Structural styles in the deep-water fold thrust belts of the Niger Delta: AAPG Bulletin, 89, 753–780, doi: 10.1306/02170504074.

Dalton, T. J. S., Paton, D. A., Needham, D. T. (2016). The influence of mechanical stratigraphy on multi-layer gravity collapse structures: insights from the Orange Basin, South Africa, in review. In: Sabato, Ceraldi, T., Hodgkinson, R. A. & Backe, G. (eds) Petroleum Geoscience of the West Africa Margin. Geological Society, London, Special Publications, 438. First published online January 19, 2016, http://doi.org/10.1144/SP438.4.

Deptuck, M. E., Kendell, K., Smith, P. (2009). Complex deep-water fold-belts in the SW Sable Sub-basin, offshore Nova Scotia. Frontiers innovation: Presented at the CSPG CSEG CWLS Convention.

De Vera, J., Granado, P., McClay, K., (2010). Structural evolution of the Orange basin gravity-driven system, offshore Namibia: Marine and Petroleum Geology, 27, 223–237, doi: 10.1016/j.marpetgeo.2009.02.003.

Gerrard, T., and G. C. Smith, (1982). Post-Palaeozoic succession and structure of the south-western African continental margin, in J. S. Watkins, and C. L. Drake, eds., Studies in continental margin geology: AAPG Memoir 34, 49–74.

Hardy, S., Poblet, J., McClay, K., Waltham, D., (1996). Mathematical modelling of growth strata associated with fault-related fold structures, in P. G. Buchanan and D. A. Nieuwland, eds., Modern developments in structural interpretation, Validation and modelling: Geological Society of London Special Publication 99, p. 265–282.

Hesthammer, J., and H. Fossen, (1999). Evolution and geometries of gravitational collapse structures with examples from the Statfjord Field, northern North Sea: Marine and Petroleum Geology, 16, 259–281, doi: 10.1016/S0264-8172(98)00071-3.

Hudec, M. R., and M. P. A. Jackson, (2004). Regional restoration across the Kwanza Basin, Angola: Salt tectonics triggered by repeated uplift of a metastable passive margin: AAPG Bulletin, 88, 971–990, doi: 10.1306/02050403061.

Jackson, M. P. A., Hudec, M. R., Jennette, D. C., Kilby, R. E., (2008). Evolution of the Cretaceous Astrid thrust belt in the ultra deep-water Lower Congo Basin, Gabon: AAPG Bulletin, 92, 487–511, doi: 10.1306/12030707074.

Jackson, C.A-L., Rotevatn, A., (2013). 3D seismic analysis of the structure and evolution of a salt-influenced normal fault zone: a test of competing fault growth models. Journal of Structural Geology, 54, 215–234

Jackson, C. A-L., Bell, R. E., Rotevatn, A., Tvedt, A. B. M., (2017). Techniques to determine the kinematics of synsedimentary normal faults and implications for fault growth models. Geometry and Growth of Normal Faults (Eds. C. C. Childs, R. E. Holdsworth, C. A.-L. Jackson, T. Manzocchi, J. J. Walsh and G. Yielding). *Geological Society of London Special Publications*, 439. doi:10.1144/SP439.22.

Koopmann, H., Schreckenberger, B., Franke, D., Becker, K., Schnabel, M., (2014). The late rifting phase and continental break-up of southern South Atlantic: The mode and timing of volcanic rifting and formation of earliest oceanic crust: Geological Society of London, Special Publications.

Krueger, A., and E. Gilbert, (2009). Deepwater fold-thrust belts: Not all the beasts are equal: AAPG Search and Discovery, Article 30085.

Lickorish, W. H., and M. Ford, (1998). Sequential restoration of the external Alpine Digne thrust system, SE France, constrained by kinematic data and synorogenic sediments, in Cenozoic Foreland Basins of Western Europe: Geological Society of London, Special Publications 134, 189–211.

Mohammed, M., Paton, D. A., Collier, R. E. L. I., Hodgson, N., Negonga, M., (2016). Interaction of crustal heterogeneity and lithospheric process in determining passive margin architecture on the Namibian margin. In: Sabato Ceraldi, T., Hodgkinson, R. A. & Backe, G. (eds) Petroleum Geoscience of the West Africa Margin. Geological Society, London, Special Publications, 438, http://doi.org/10.1144/SP438.9.

Morley, C.K., (2002). Evolution of large normal faults: evidence from seismic reflection data. American Association of Petroleum Geologists Bulletin, 86, 961–978.

Morley, C. K., King, R., Hillis, R., Tingay, M., Backe, G., (2011). Deepwater fold and thrust belt classification, tectonics, structure and hydrocarbon prospectivity: A review: Earth Science Review, 104, 41–91.

Muntingh, A., and L. F. J. Brown, (1993). Sequence stratigraphy of petroleum plays, post-rift Cretaceous rocks (lower Aptian to upper Maastrichtian), Orange Basin, South Africa: Siliciclastic sequence stratigraphy: Recent Applications of Siliciclastic Sequence Stratigraphy, in Siliciclastic sequence stratigraphy: Recent developments and applications 58, AAPG, 71–98.

Paton, D. A., (2012). Post rift deformation of the North East and South Atlantic margins: Are “passive margins” really passive?: in K. M. Busby, ed., Tectonics of sedimentary basins: Recent advances: Wiley, 249–269.

Paton, D. A., di Primio, R., Kuhlmann, G., van der Spuy, D., Horsfield, B., (2007). Insights into the petroleum system evolution of the southern Orange Basin, South Africa: South African Journal of Geology, 110, 261–274.

Paton, D. A., van der Spuy, D., di Primio, R., Horsfield, B. (2008). Tectonically induced adjustment of passive-margin accommodation space; influence on hydrocarbon potential of the Orange Basin, South Africa: AAPG Bulletin, 92, 589–609, doi: 10.1306/12280707023.

Peel, F. J., (2014). The engines of gravity-driven movement on passive margins: Quantifying the relative contribution of spreading vs. gravity sliding mechanisms: Tectonophysics, 633, 126–142, doi: 10.1016/j.tecto.2014.06.023.

Rowan, M. G., Peel, F. J., Vendeville, B. C., (2004). Gravity driven fold belts on passive margins, in K. R. McKay, ed., Thrust tectonics and hydrocarbon systems: AAPG, Memoir 82, 157–182.

Shaw, J. H., Novoa, E., Connors, C. D., (2004). Structural controls on growth stratigraphy in contractional fault-related folds, in K. R. McClay, ed., Thrust tectonics and hydrocarbon systems: AAPG Memoir 82, p. 400–412.

Suppe, J., Chou, T. T., Stephen, C. H., (1992). Rates of folding and faulting determined from growth strata in Thrust Tectonics, edited by K. R. McClay, pp 105-122, Chapman and Hall, New York.

Totterdell, J. M., and A. A. Krassay, (2003). The role of shale deformation and growth faulting in the Late Cretaceous evolution of the Bight Basin, offshore southern Australia, in Deep subsurface sediment mobilization: Geological Society of London, Special Publications 216, 429–442.

Walsh, J.J. & Watterson, J., (1988). Analysis of the relationship between displacements and dimensions of faults. Journal of Structural Geology, 10, 239–247.

Walsh, J.J., Nicol, A. & Childs, C., (2002). An alternative model for the growth of faults. Journal of Structural Geology, 24, 1669–1675.

Watterson, J., (1986). Fault dimensions, displacement and growth. Pure and Applied Geophysics, 124, 365–373

6 Chapter 6; The importance of missing strain in Deep Water Fold and Thrust Belts

[*This chapter is composed of a paper published by Marine and Petroleum Geology, Volume 82, Pages 163-177, in April 2017.*]

6.1 Abstract

Deep water fold and thrust belts (DWFTBs) are sedimentary wedges that accommodate plate-scale deformation on both active and passive continental margins. Internally, these wedges consist of individual structures that strongly influence sediment dispersal, bathymetry and fluid migration. Most DWFTB studies investigate basin- and intra-wedge- scale processes using seismic reflection profiles, yet are inherently limited by seismic resolution. Of critical importance is strain distribution and its accommodation on discrete faults compared to distributed deformation. Recent studies have considered strain distribution by investigating regional reflection DWFTBs profiles within coupled systems, which contain down-dip compression and up-dip extension. There is broad agreement of a mis-balance in compression versus extension, with ~5% excess in the latter associated with horizontal compaction, yet this remains unproven.

Using two exceptionally well exposed outcrops in the Spanish Pyrenees we consider deformation of DWFTB at a scale comparable to, and beyond, seismic resolution for the first time. By coupling outcrop observations (decametre to hectometre scale) with a re-evaluation of seismic profiles from the Orange Basin, South Africa, which contains one of the best imaged DWFTBs globally, we provide a unique insight into the deformation from metre to margin scale. Our observations reveal hitherto unrecognised second order structures that account for the majority of the previously recognised missing strain. This re-evaluation implies that ~5% missing strain should be accounted for in all DWFTBs, therefore existing studies using restorations of the sediment wedge will have underestimated crustal shortening in active margins, or sedimentary shortening in gravity driven systems by this amount. In contrast to previous studies, our observations imply that the majority of this strain is accommodated on discrete fault surfaces and

this can explain the occurrence and location of a range of intra-wedge processes that are intimately linked to structures including sediment dispersal, fluid migration pathways and reservoir compartmentalisation.

6.2 Introduction

Deep Water Fold and Thrust Belts (DWFTBs) occur on continental margins globally and are a consequence of the contraction of sedimentary sequences that are decoupled from underlying stratigraphy or basement by a décollement horizon (Rowan et al., 2004; Morley et al., 2011). The driving force that induces the contraction can occur either at a crustal scale, as is the case in an accretionary prism on an active margin (Type II; Morley et al., 2011), or within the decoupled sedimentary sequence as a consequence of gravitational processes, on an Atlantic-style passive margin (Type I: Morley et al., 2011). Regardless of the setting, processes that are intimately linked to the resulting deformation span the margin scale geometry of the fold and thrust belts including critical taper angle (e.g. Dahlen et al., 1984), the structural configuration and stratigraphic fill of associated sedimentary basins (Morley, 2007; Fillon et al., 2013) and the role of fluids that migrate through them (Saffer and Bekins, 2001). Quantifying the strain distribution across a DWFTB is therefore fundamental to understand these processes.

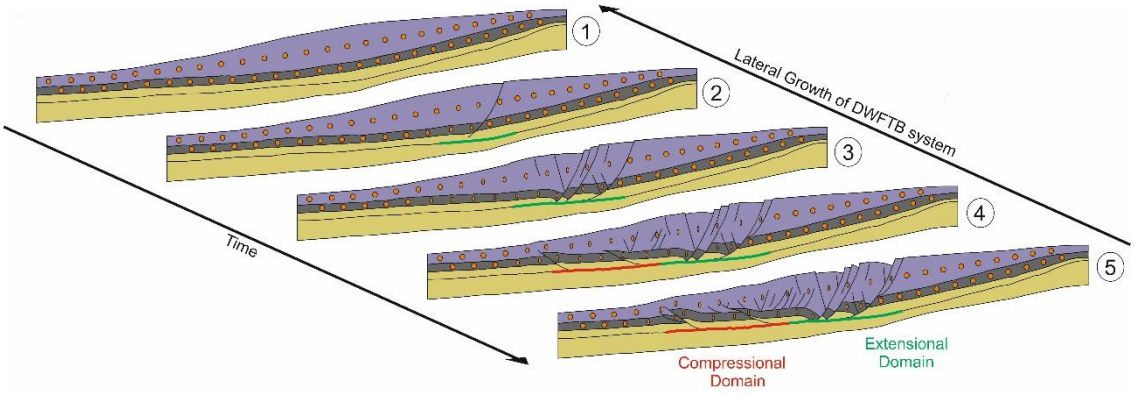

Figure 6.1. Conceptual model for the growth of a DWFTB in both space and time indicating the missing strain component is not explained by lateral deformation elsewhere along the margin, Dalton et al. (2015). The location of extensional and compressional domains are also shown along with Orange circles representing the lateral compaction of sediments in the wedge.

An entire DWFTB system comprises three domains: an up-dip extensional domain, a down-dip contractional domain and a transitional domain in-between (Krueger and Gilbert, 2009). An essential technique applied to understanding DWFTBs, and the distribution of strain across these three domains, is the kinematic restoration of stratigraphic sequences. This is commonly based upon interpretation of an increasing number of seismic reflection profiles covering DWFTBs. Conceptually shortening across the entire system should balance, however, recent studies document a 5-10% imbalance between extensional and contractional domains in favour of extension (Figure 6.1) and outline the importance of this value on our understanding the evolution of DWFTB systems (de Vera et al., 2010; Butler and Paton, 2010; Dalton et al., 2015). This 10% imbalance is calculated assuming the contraction due to the recorded missing strain component is distributed in both the extensional and contractional domains as per Dalton et al. (2015). This imbalance is implicit from the initiation of growth and throughout the growth of the structure as seen in Figure 6.1.

Although many of these recent studies have considered coupled extension and compressional systems, the same principles are as applicable to accretionary prisms as they are too passive margins. In the latter, for example, an accurate quantification of compression is important for both plate kinematic predictions as well as basin fill architecture in a range of settings including Sinu-Jacinto offshore Columbia, Barbados Ridge and Taiwan (Biju-Duval et al., 1982; Davis et al., 1983; Robertson and Burke, 1989; Toto and Kellogg, 1992; Vinnels et al., 2010). In certain settings where there is a complex interplay of accretionary prism and gravity collapse processes occurring (e.g. NW Borneo), differentiating between the two processes is essential to understanding the whole system evolution (Franke et al., 2008; Hesse et al., 2010; King et al., 2010).

Central to any analysis of a DWFTB, be it accretionary prism or gravity induced, is this mismatch in strain. In this study we couple field observations with seismic reflection examples of the extensional portion of DWFTB's to investigate this question. Through the identification of previously unrecorded contractional features present within the extensional domain we reconsider how strain is distributed across the system and discuss how this influences our current understanding of the associated processes.

6.3 Quantification of sub-seismic scale strain

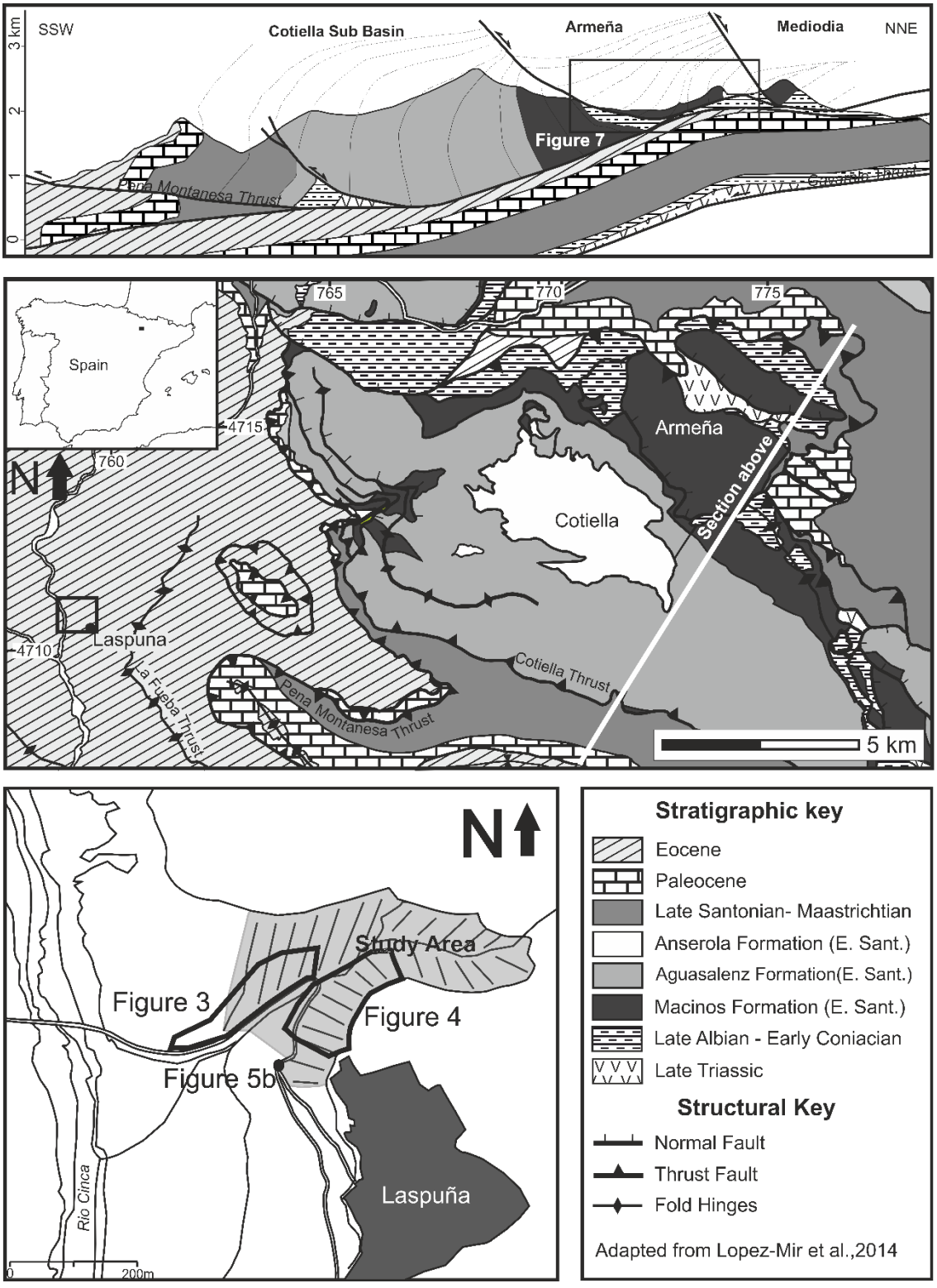

Figure 6.2. Location and geological map of the two areas used in this study along with a cross-section through the three faults in the Cotiella extension system; with the upper map displaying the location of both areas, adapted from Lopez-Mir et al. (2014); and the lower zoomed in map of the study area beneath Laspuña indicating the location of

Figures. 6.3, 6.4 and 6.5b. The cross section extends to the end of the Pena Montanessa thrust just off the edge of the geological map.

As most studies of DWFTBs are based upon seismic reflection profile analysis, an obvious limitation to quantifying the missing strain component in such profiles is the issue of how much strain is accommodated at a sub-seismic scale. Previous work in extensional settings has highlighted and quantified the potential impact of sub-seismic deformation on terms of both hydrocarbon exploration and production (Wood et al., 2015a, 2015b). Here we address the issue of sub-seismic deformation in DWFTBs by considering two well exposed outcrops in the Spanish Pyrenees that reveal as yet undocumented deformation across three orders of magnitude. The first is a decametre scale example in Laspuña (Figure 6.2). The second investigates a larger (hectometre) scale example at Armeña, Spain (Figure 6.2).

6.3.1 Case Study 1; Decametre Scale; Laspuña

A distinctive set of multiphase growth faults detaching onto a basal detachment is observed in the cliff section immediately to the west of the village of Laspuña. The syn-kinematic growth packages in the top of the normal faults seen in the cliff are indicative of the extensional domain of a DWFTB. This DWFTB is located on the then uplifting, north-eastern flank of the Ainsa Basin (Pickering and Bayliss, 2009) in the Spanish Pyrenees (Figure 6.2).

The stratigraphy that is deformed by the DWFTB comprises marls and fine sand slope deposits (Dreyer et al., 1999) and are of Early Ypresian age (Pickering and Corregidor, 2005). The slope sediments present at Laspuña were depositing whilst the Peña Montañesa, Cotiella and La Fueba thrusts systems were active (Munoz et al., 2013). The DWFTB presently sits structurally below these thrust faults (Figure 6.2), the slope was generally stable allowing deposition of successions of muddy sediments. The active tectonic system and a mud dominated semi-lithified slope provided the ideal conditions for gravitational collapse to occur. During phases of tectonic activity on the surrounding thrust systems stable paleo-slopes were uplifted and became mobilized, forming mass transport complexes (Dakin et al., 2012).

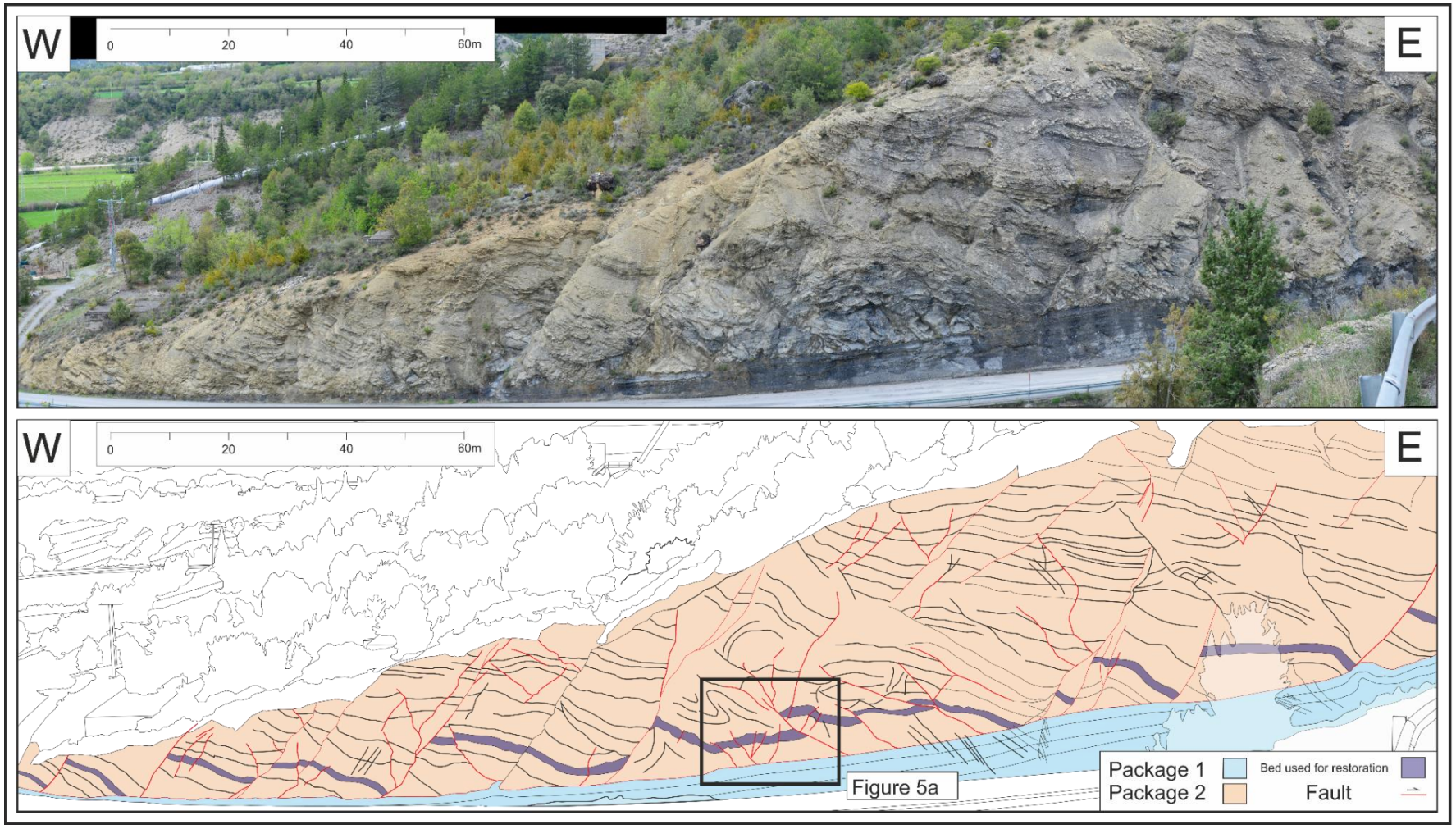

Figure 6.3 Image and interpretation of 240 m long cliff section in valley beneath Laspuña. Faults indicated in red, DWFTB package in orange, undeformed sub-detachment horizon in blue. For location see Figure 6.2.

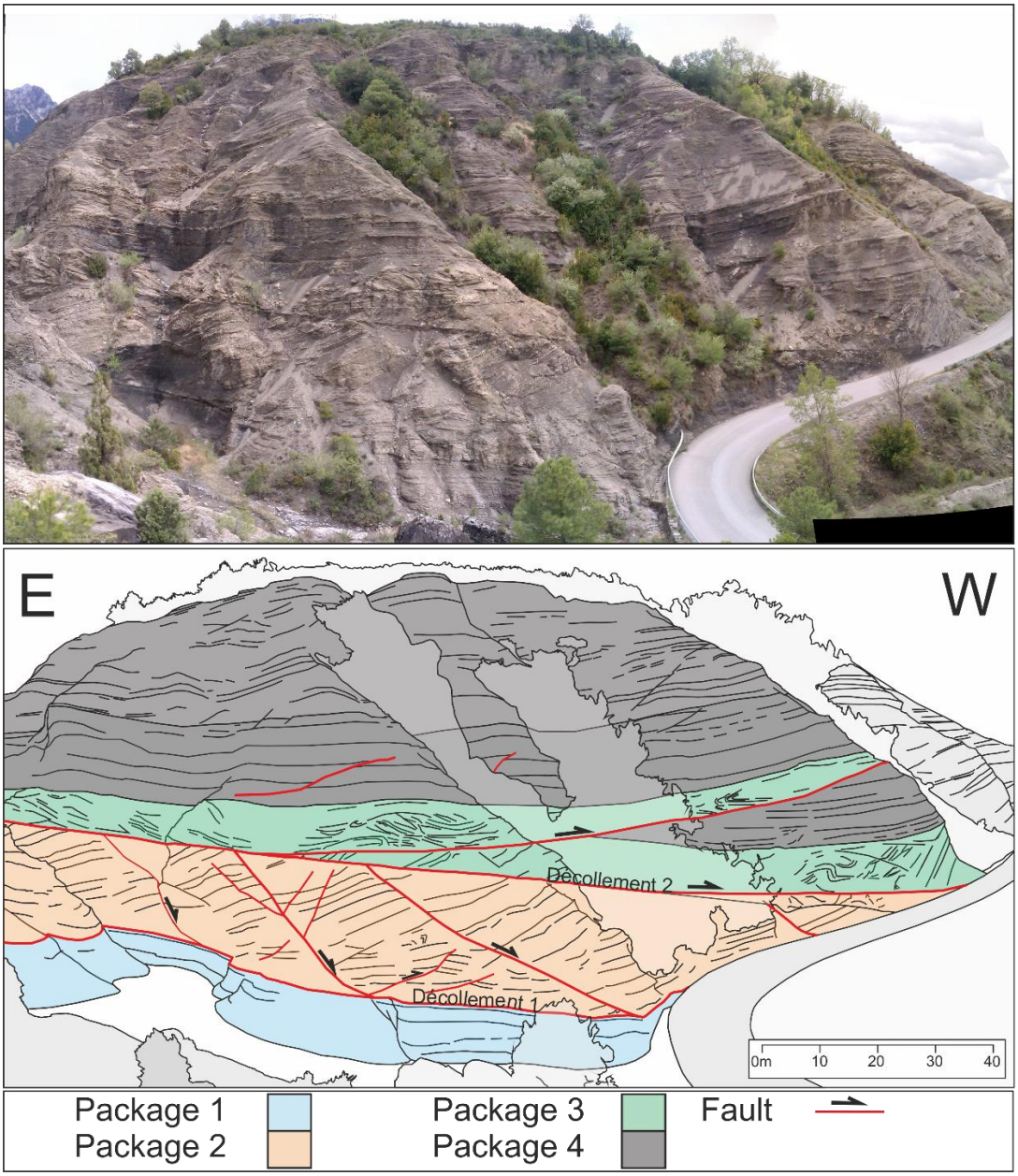

Figure 6.4. View of valley beneath Laspuna showing the overlying strata. Faults indicated in red, DWFTB package in orange, undeformed sub-detachment horizon in blue, chaotic package in green, planar concordant laminated beds in black. Also marked is the location Figure 6.5a. For location see Figure 6.2.

At Laspuña, failure of the slope did not result in mass transport remobilisation, but resulted in the formation of growth faults, indicative of multiple phases of extension and syn-deposition, shifting sediments south west downslope into the Ainsa Basin. This difference in deformation may be as a result of smaller uplift events occurring over a longer time period allowing a slower readjustment of surface slope geometry or an

effect of the presence of an underlying slip horizon making DWFTB formation more practical than outright slope failure.

The cliff section, in which the DWFTB is observed, is divided into four packages (1-4, bottom to top) based upon their stratigraphy and internal geometry. The lowest package (Package 1, Figure 6.3 and 6.4) is composed of a largely undeformed dark grey succession of more organically rich concordantly layered marls. Package 2 is defined by a sequence of light grey/brown muds with thin inter-beds of fine sands, which become thicker and more numerous towards the top of the cliff. Within this package also exhibits a set of west dipping listric normal faults with throws of 8– 15 m is observed. Striae on the fault planes indicate a westerly displacement of material into the Ainsa Basin. These faults detach onto a common décollement (décollement 1) along the upper surface of Package 1 (Figure 6.3); this is the extensional domain of the DWFTB. The top of Package 2 is truncated by a distinctive planar, gently west dipping fault surface, Décollement 2 (Figure 6.4). Above this is Package 3 which comprises a chaotic package of folded and faulted, muds and sands. This is topped by Package 4, a succession of dark grey planar concordant laminated beds. Packages 3 and 4 contain a set of evenly spaced thrust faults with displacements of up to 40 m, which detach onto Décollement 2 (Figure 6.4 and 5 b). These potentially form part of the contractional domain of a distal, later DWFTB for which the up-dip continuity does not crop-out.

The scale of the DWFTB systems present at Laspuña offers the opportunity to observe the internal structure of the fault blocks and in particular minor structures formed during deposition and deformation (Figure 6.5). Restorations of DWFTBs imply the preservation of pre-kinematic bedding within the fault blocks. However, we observe that significant internal deformation is present within the extensional and compressional blocks. Within the extensional fault blocks we observe multiple thrust features with throws of 0.2-3 m as well as significant folding (Figure 6.5 a). This smaller scale deformation is present equally in the contractional domain in Packages 3 & 4 which show smaller scale thrust faults with throws of 0.5-1 m and folding, in between larger thrusts (Figure 6.5 b). These smaller scale contractional features (<5 m throw) are largely unresolvable at the outcrop scale (Figure 6.4), yet detailed analysis reveals that

many of these surfaces that appear undeformed at outcrop scale contain kinematic indicators that show significant internal compression (Figure 6.5).

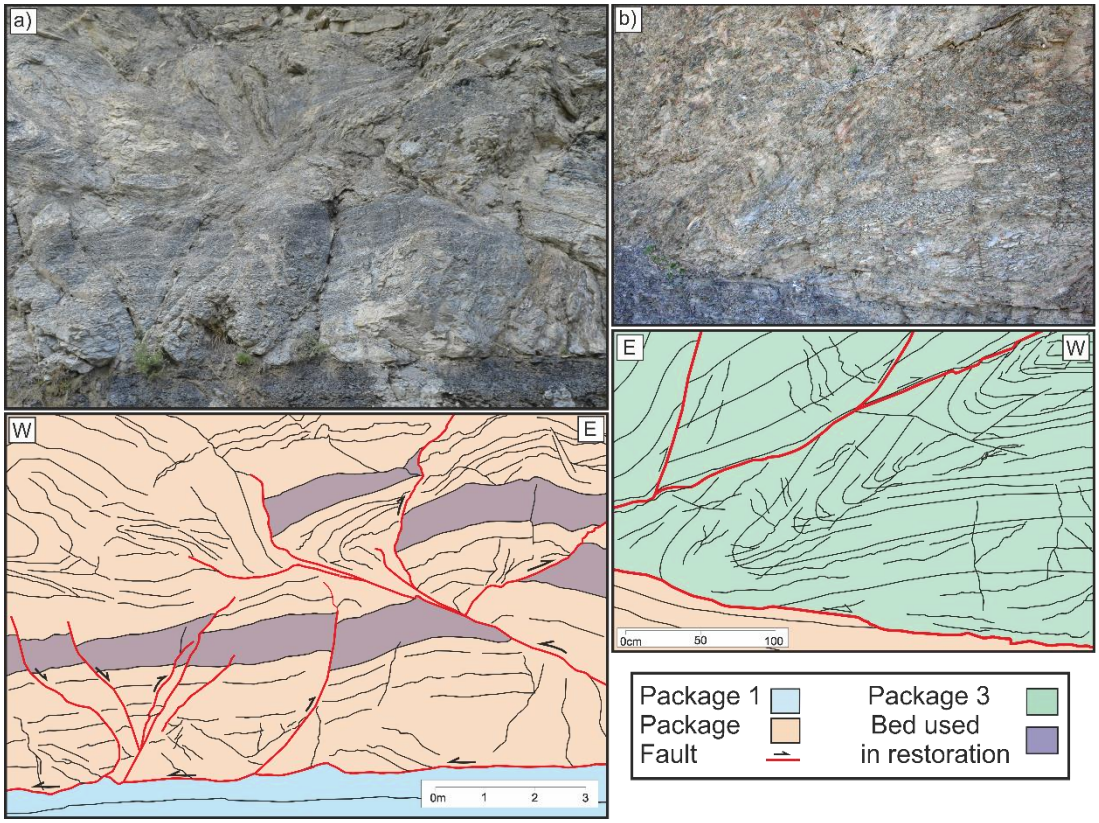

Figure 6.5. Interpreted and uninterpreted image of cliff section seen from base of the cliff showing the compaction of beds within normal fault blocks. The Purple horizon is the horizon used for the restoration. See Figure 6.3 and 6.4 for location.

These two sections in the Laspuña DWFTB system illustrate that not only does deformation occur at a range of scales, but more importantly, there is evidence of compression within the extensional domain. Such deformation has not been demonstrated before and is therefore not accounted for in current DWFTB restorations. To understand the impact of these smaller scale contractional structures on a restoration we present two interpretations of the same section (Figure 6.3). The first interpretation (Figure 6.6 a) is equivalent to existing DWFTB sections and does not incorporate these smaller contractional structures (i.e. equivalent to these structures being below observable resolution). While the second interpretation (Figure 6.6 b) is a detailed interpretation across the section including contractional features. It can be seen in Figure 6.6b that the contractional features are isolated within single fault blocks

and are thus not pre-existing deformation features. Both interpretations use the same distinct dark grey pre-kinematic bed that is present throughout the collapse (Figure 6.5 a). Slickensides on fault planes indicate this section is within 10_ of the transport direction, making it viable for restoration (Price, 1981). We then restore both sections to a pre-deformed geometry and calculate the extensional strain when the small scale contractions are ignored compared to when they are accounted for (Table 6.1).

	Original Lengths (m)	Current Length (m)	Displacement (m)	Extension
Yellow	200.5	240	39.5	16.5%
Green	211.5	240	28.5	11.9%
L Blue	195.9	240	44.1	18.4%
D. Blue	210	240	30	12.5%

	Without Compression	With Compression	Difference
Upper	16.5%	11.9%	4.6%
Lower	18.4%	12.5%	5.9%

Table 6-1. Table of results for the restorations undertaken of Figure 6.6 a) and b).

In Table 1 the significance of contractional features becomes clear, with the measurement of total displacement being 11-14 m less. The difference recorded in the total amount of strain ranges from 4.6 - 5.9% implying these sediments would be ~5% more compressed than expected. These figures are comparable with the missing strain component identified in seismic examples in Dalton et al. (2015) of ~5% and thus may offer an explanation for the observed miss-balance.

The Laspuña section is clearly small scale and therefore the validity of scaling these observations to larger examples is critical if we want to consider margin scale (>60 km long) DWFTBs. To address this we consider a larger (4 km wide) DWFTB that crops out approximately 25 km to the north-east of Laspuña at Armeña (Figure 6.2) as this allows us to observe whether similar contractional structures are present in larger systems.

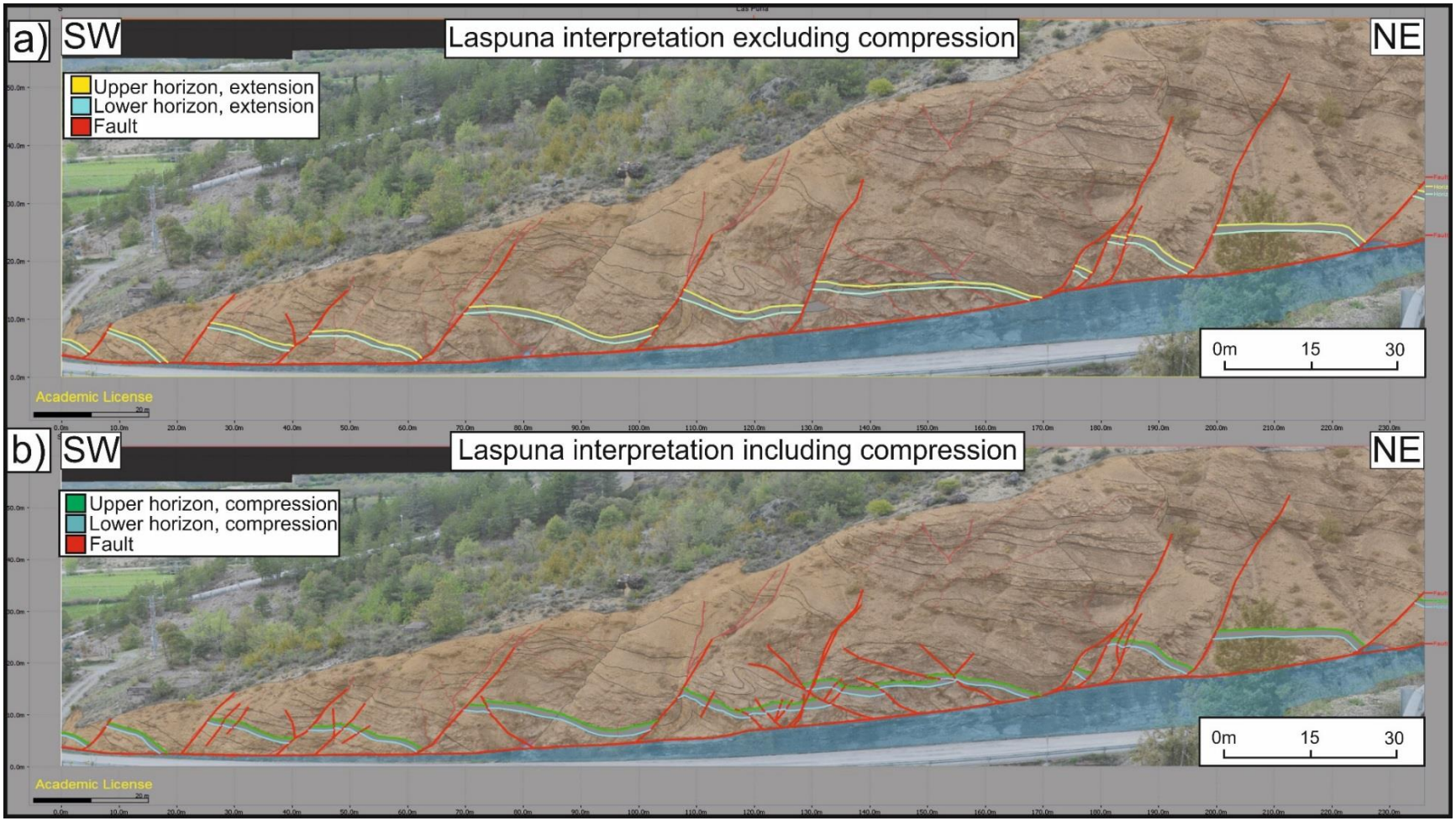

Figure 6.6. Two different interpretations of the Figure 6.3; a) based upon what can be seen from the opposite side of the valley, b) interpretation based upon data collected at road level. Both interpretations use the bed in Figure 6.5a for the purposes of restoration

6.3.2 Case Study 2; Hectometre Scale; Armeña

The gravity driven, growth fault system at Armeña, Huesca, Spain (Figure 6.2) has been described by McClay et al. (2004), Lopez-Mir et al. (2014, 2015) and Tavani et al. (2015). This growth fault forms part of the Cotiella extension system that formed in the Coniacian to Early Santonian during a post-rifting thermal subsidence phase of basin evolution (Verges et al., 2002). It comprises three listric growth faults traversing a 14 km section orientated NE-SW (Lopez-Mir et al., 2015, Figure 6.2). The best exposed of these three growth faults is the 4 km wide cliff section above the Refugio d'Armeña (Figure 6.7) referred to as the Armeña growth fault (Lopez-Mir et al.,2014). Extension initiated in the Coniacian and continued into the Early Santonian depositing up to 3 km of syn-kinematic carbonates and calcarenites which diverge towards the southwest, within the hanging wall of the controlling listric normal fault indicating a north easterly extension (Lopez-Mir et al., 2014). They are deposited above a pre-kinematic Upper Cenomanian to Turonian limestone succession (McClay et al., 2004). This overlies Late Triassic shales and evaporites that crops out at the northern end of the cliff section (Figure 6.8). The top of this Triassic sequence also forms the detachment horizon for all three growth faults.

The collapse structure at Laspuña implies that the most likely location for contractional features in extensional fault blocks is within the pre-kinematic sequence. Figure 6.8 shows the pre-kinematic Upper Cenomanian to Turonian limestone succession. The more competent limestones have better preserved bedding than the more mobile muds at Laspuña and so do not show the same amount of ductile deformation. Within these limestones multiple brittle contractional structures are present throughout, the largest being a ~100 m displacement thrust on the north-eastern flank (Figure 6.8). Multiple (10+) smaller intra-layer thrusts with throws of less than 10 m are also observed throughout the cliff. The orientation of these contractional features are consistent with a southwest to north-east transport direction (as indicated by striae on fault surfaces) and is therefore not related to the later phase of north east to south-west inversion. Despite later inversion Tavani et al. (2015) affirms syn-kinematic fracturing has been well preserved. Folding of beds in the hanging wall of the thrust and

the orientation of the throw are incompatible with the orientation of the inversion event.

Restorations of the three normal faults in Lopez-Mir et al. (2014), reveal a total extension of 8.1 km over 13.9 km. Assuming a missing strain component of 5% (Dalton et al., 2015) is compensated for by second order structures, compressive features totalling ~650 m should be present over the three faults, with ~215 m displacement being accommodated within the Armeña growth fault, assuming an equal distribution. The observation of a ~60 m displacement thrust and multiple smaller displacement (~10 m) contractional structures is in agreement with that prediction. From this we would suggest that 5% of measured extension is compensated by second order structures which should be prevalent in the extensional portion of DWFTBs.

The observation that 5% of the recorded extensional deformation is accommodated by smaller scale features in Armeña concurs with the observations made at Laspuña which are consistent with a scale invariant relationship. We now consider if these features are similarly present on margin-scale DWFTBs imaged on seismic reflection profiles.

6.3.3 Application to seismic scale; Orange Basin

We choose a DWFTB within the Orange Basin (Figure 6.9), offshore South Africa and Namibia, because the geological evolution of the margin has been well established (Gerrard and Smith, 1982; Brown et al., 1995; Mohammed et al., 2015) and DWFTBs are a well-documented and common feature found throughout the basin (Muntingh and Brown, 1993; Paton et al., 2008; Peel, 2014; Dalton et al., 2016). Restorations of these DWFTBs have been undertaken by de Vera et al. (2010), Butler and Paton (2010) and Dalton et al. (2015), all of which identified a shortfall in contractional features versus extensional. This imbalance, ~5% (Dalton et al., 2015), is equivalent to the 5% of strain recorded in the contractional features within the extensional domain of the DWFTB at Laspuña. Our field observations would suggest that contractional structures should be present within the larger extensional structures observed in the data presented by Dalton et al. (2015) although predict that they would be close to seismic resolution.

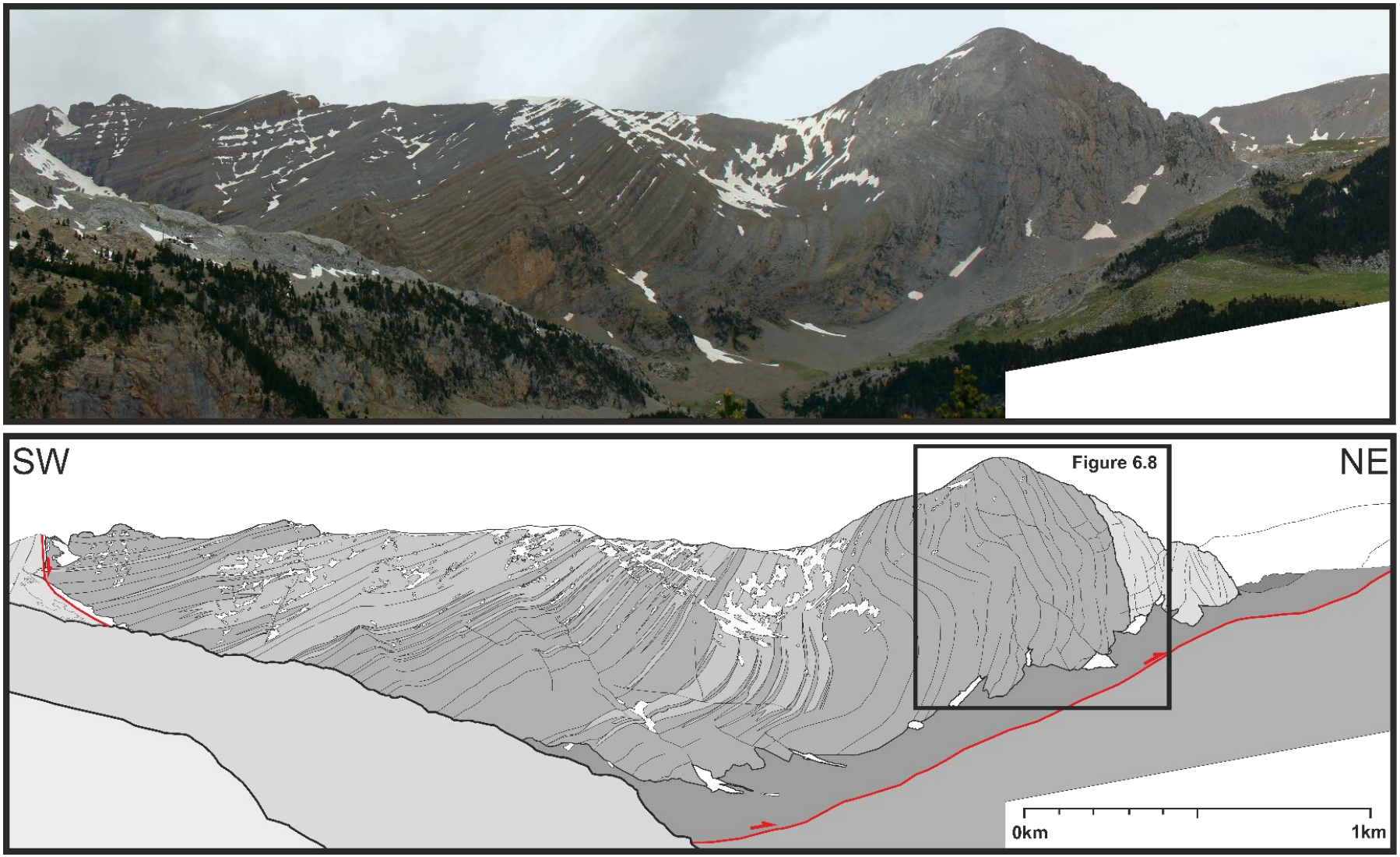

Figure 6.7. Interpretated and uninterpreted image of the growth fault at Armeña, location on Figure 6.2. The black box indicates the location of Figure 6.8.

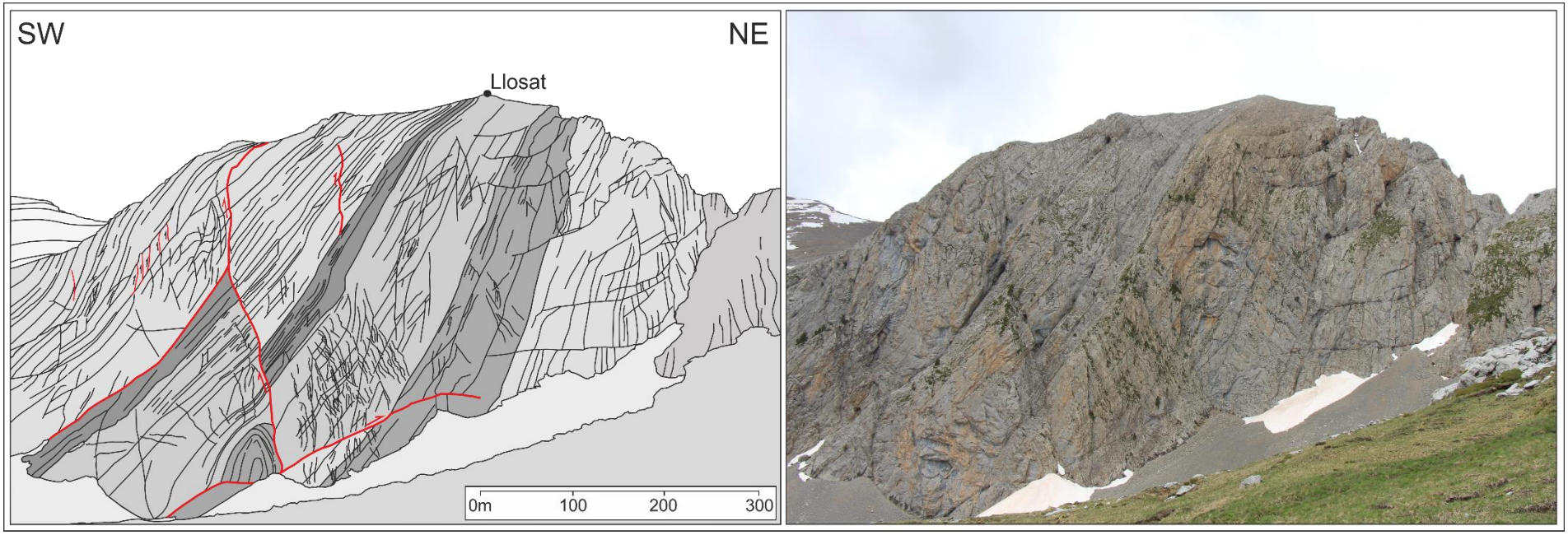

Figure 6.8. Interpreted and uninterpreted cliff section view of pre-kinematic Upper Cenomanian limestones viewed from beneath Llosat indicating contractional features. For location see Figure 6.7.

Our observations from Laspuña and Armeña suggest if these smaller contractional features are present, they are most likely to form in the pre-kinematic horizons towards the base of normal fault blocks. These portions of the collapse structures are frequently unresolvable, especially in more mature parts of the system where multiple phases of collapse have occurred and been overprinted. To overcome this difficulty we select a portion of an extensional domain (Figure 6.10 a, see Figure 6.9 for location) which contains later, more distal, normal faults and where seismic imaging is good. The reflections in the upper part of the collapse (Figure 6.10 a, light blue and yellow horizons) are broadly parallel and faulted in several places. The base of this package is picked by a high amplitude reflection (just below the blue horizon), which is the well documented Tertiary unconformity (Paton et al., 2008). The reflections beneath the unconformity have a shallow dip towards the south west, with multiple upper reflections truncating against the Tertiary unconformity heading progressively north east. These reflections are discontinuous in their horizontal extent and are broken by steeply dipping discontinuities that extend through the package. This style of response appears throughout the remainder of the section till the base where a number of broadly horizontal continuous reflections are present. The discontinuous packages represent Late Cretaceous sediments rotated by normal faults within the extensional domain. The termination of the discontinuous reflections defines the location of normal faults. The continuous reflections are beneath the horizon on which these faults detach and are thus undeformed.

At the scale of the regional section (Figure 6.9), previous restorations of the 156 km long section (de Vera et al., 2010; Butler and Paton, 2010) interpreted that the reflections are continuous between normal faults implying no internal deformation (Figure 6.10 c). However, when we consider these apparently low strain areas in more detail we observe that reflections are not parallel and show truncation and localised repetition of reflections that are best explained by the presence of thrust faults (Figure 6.10 b). These structures are most prevalent in pre-kinematic horizons at the base of fault blocks, as our observations at Laspuña and Armeña predict.

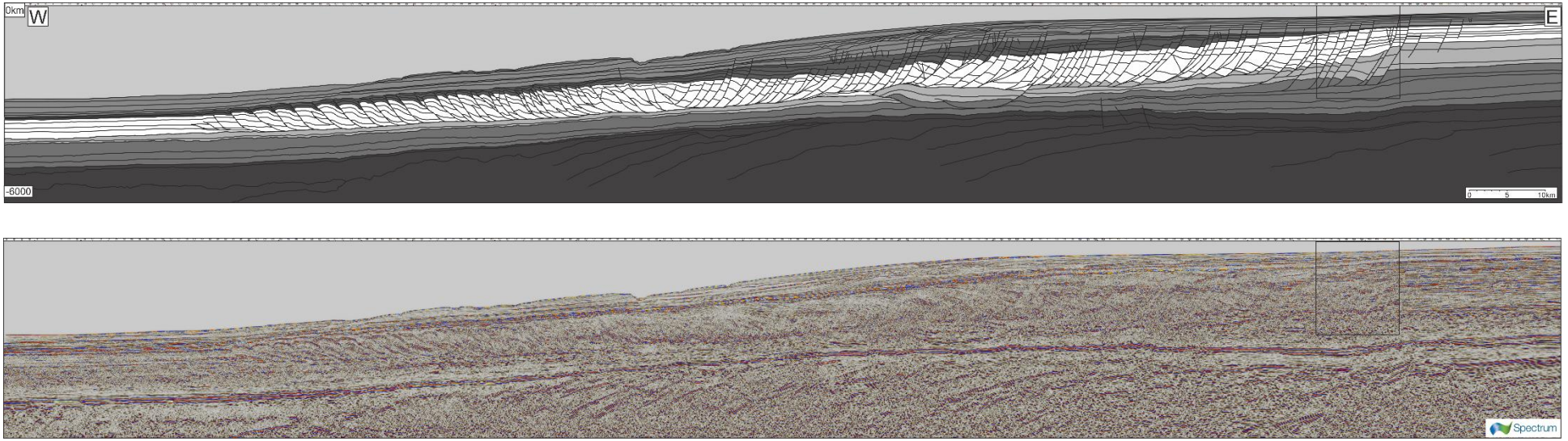

Figure 6.9. Shows a 196 km long seismic section through an entire DWFTB from the Orange Basin offshore Namibia. For Location see Figure 6.10.

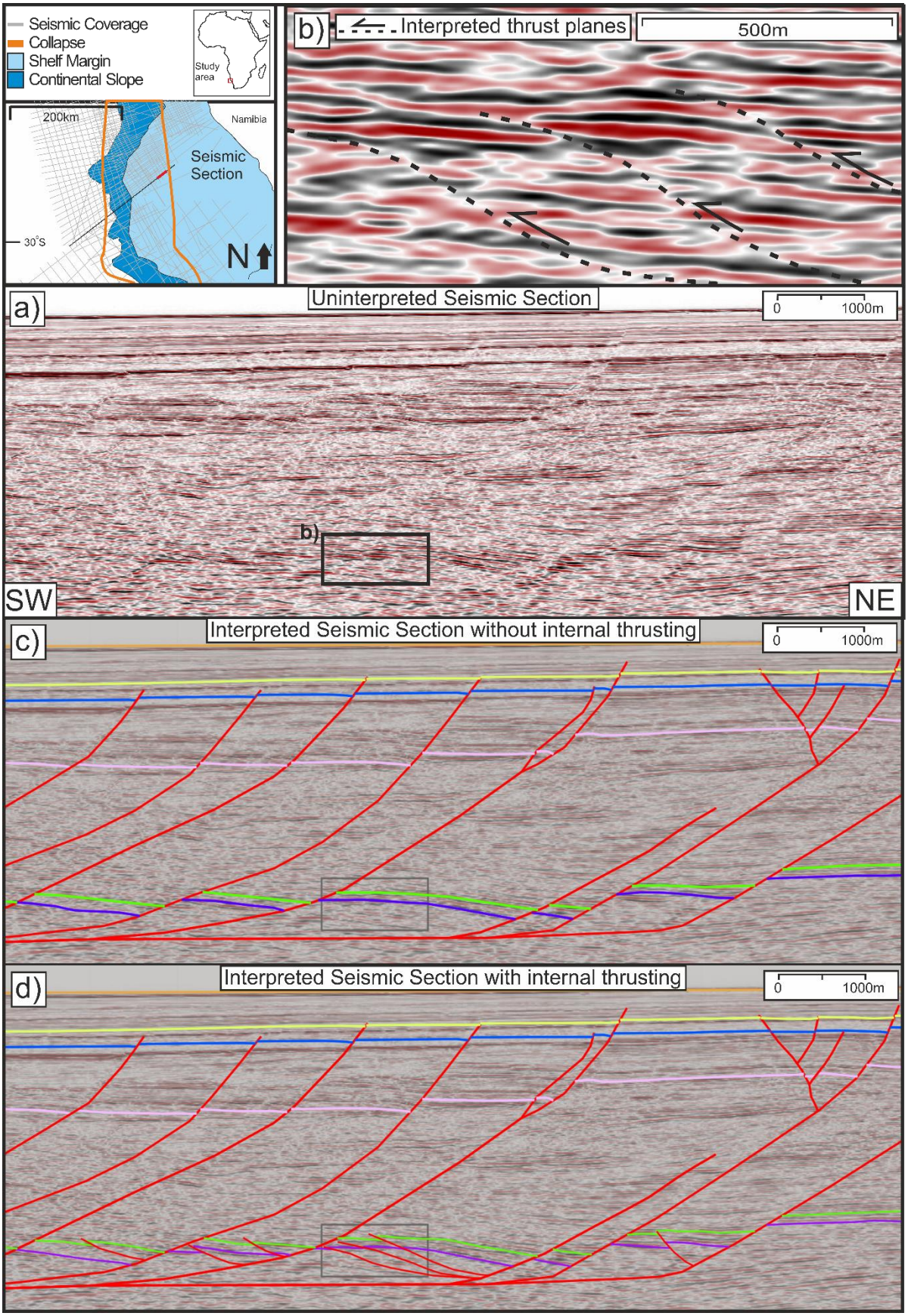

Figure 6.10. Multiple interpreted and uninterpreted seismic sections through the extensional domain of a DWFTB in the Orange Basin, Namibia ; a) Uninterpreted seismic

section used in this study; b) Zoomed in section of a) displaying potential compressional features; c) Interpreted section not accounting for contractional features; d) Interpreted section assuming features previously considered to be seismic artefacts are contractional features. All sections are presented without vertical exaggeration.

We choose two pre-kinematic horizons affected by these second order thrust faults as well as a number of higher horizons to make two interpretations. We apply the same method as at Laspuña and undertake one restoration that ignores contractional features (Figure 6.10 c) and a second (Figure 6.10 d) that accounts for the contractional features. The interpretation of the 1st order extensional faults remains the same for both. This allows us to isolate the effects of including the contractional features in the restoration.

	Original Length (m)	Present Length (m)	Displacement (m)	Extension (%)
Orange	10341.8	10341.8	0	0.0%
Yellow	10296.3	10341.8	45.5	0.4%
Blue	10193.6	10341.8	148.2	1.4%
Pink	9667.9	10341.8	673.9	6.5%
Green	8534	10341.8	1807.8	17.5%
Green Comp	8939.7	10341.8	1402.1	13.6%
Purple	8273.7	10341.8	2068.1	20.0%

	Without Compression (m)	With Compression (m)	Difference
Upper	17.5%	13.6%	3.9%
Lower	20.0%	14.7%	5.3%

Table 6-2. Table of results of restorations undertaken on sections in Figure 6.11 b) & c).

The results of the restorations (Table 6.2) show a marked increase in displacement down the length of the normal faults and thus through time. This reveals these faults have an extended growth history with multiple phases of deformation. Table 2 shows a difference of 4-5% between the interpretations including and excluding contractional features. This implies that 5% of the strain created by extension is compensated for within the extensional domain itself.

6.4 Discussion

6.4.1 Recognizing the missing strain

Recent analyses of DWFTBs involving gravity collapse broadly agree that there is an imbalance between extensional and contractional domains in favour of extension of ~5% (de Vera et al., 2010; Butler and Paton, 2010). Dalton et al., 2015 went further to look at a set of parallel lines (Figure 6.1) through a single collapse finding a consistent imbalance throughout, concluding the missing strain component is not an effect of out of plane movement but a crucial part of the growth mechanism. They suggested the imbalance represents a phase of strain hardening through compaction of more distal sediments relative to the primary normal fault. This phase predates the formation of down-dip thrusts, seismically resolvable as the contractional domain. It is this strain hardening phase which we have investigated. The missing strain component is likely to be near or below seismic resolution and should therefore be represented in field examples of DWFTB's.

The previously unpublished field location at Laspuña, whilst limited in extent displays many of the same features that we observe in seismic examples of extensional domains in DWFTBs. These include 1st order listric normal growth faults, a detachment surface above a relatively undeformed package and a separate overlying contractional domain composing imbricated thrusts. This implies a potential scalability in these structures that offers us an analogue to study the internal architecture of larger systems. The key observation from the Laspuña system (Figure 6.5), is the occurrence of 2nd order contractional features, present within both the extensional and compressional faulted blocks. This is contrary to seismic interpretation of thrust and normal fault blocks, which implies the preservation of pre-kinematic bedding. This both resolves the calculated missing strain component and suggests it is distributed across the entire structure and not limited to the contractional domain.

The results of the restoration of the seismic sections with and without contractional structures imply that 5% of the strain created by the extension is compensated for through contraction in the extensional domain itself. This would imply results of restorations of the entire DWFTB that do not account for this contraction will produce

missing strain components over the entire structure of 5%. This is highly comparable with the results of restorations undertaken at Laspuña and by de Vera et al. (2010) and Dalton et al. (2015). We conclude therefore that the contractional features interpreted in the Orange Basin are genuine rather than being artefacts of seismic processing.

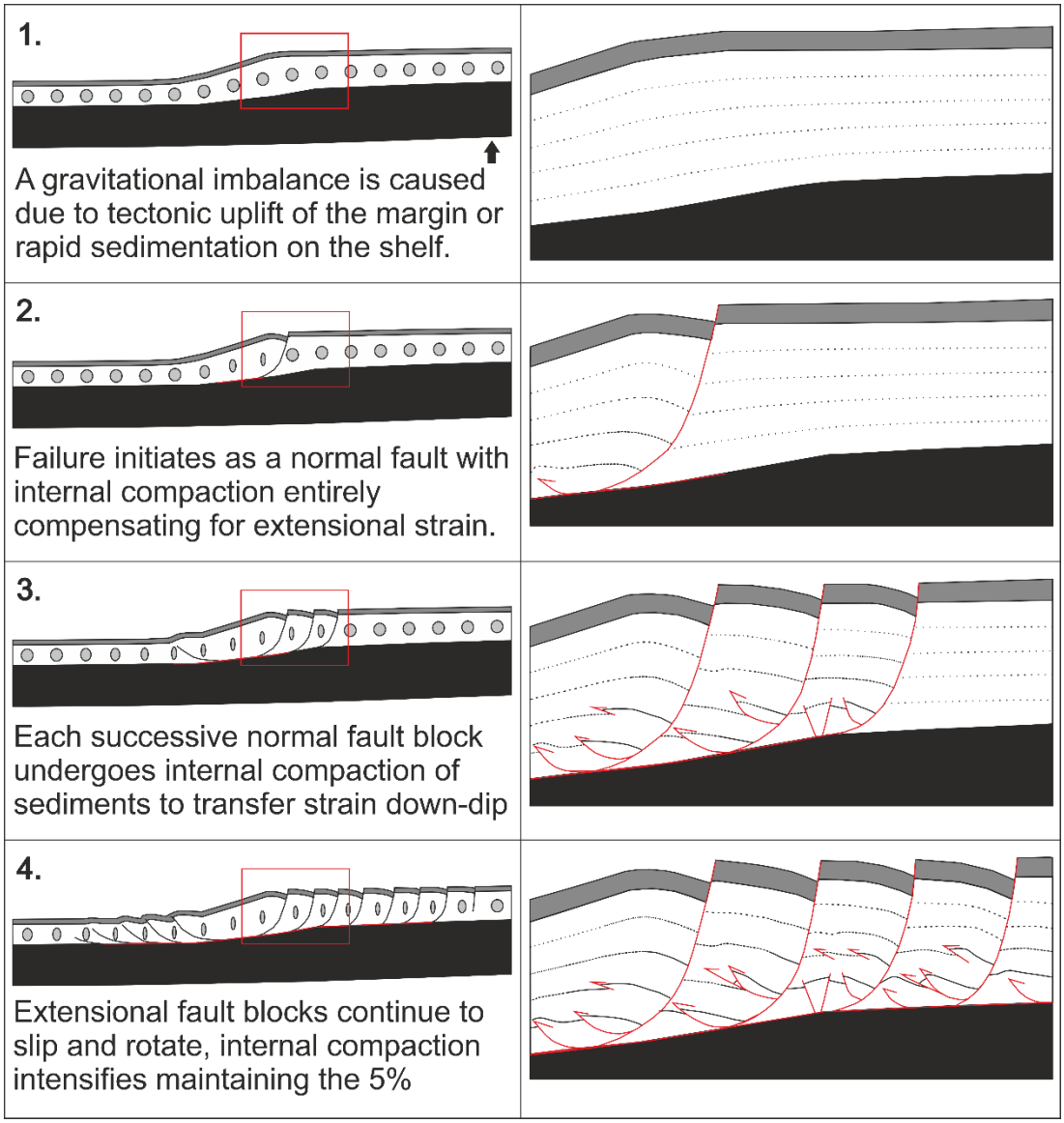

Figure 6.11. New model for the formation and development of DWFTBs accounting for internal compaction within the extensional domain.

Figure 6.11 shows a possible growth mechanism for DWFTBs showing how these contractional structures grow throughout the development of the collapse structure. This explains the observation made in Dalton et al. (2015) that notes the outer fringes of DWFTBs commonly lack a down-dip contractional domain, as the extensional strain created by the displacement of the normal faults is entirely compensated for internally

(Figure 6.1). We suggest this contraction is a necessary stage in the development of collapse structures and continues throughout their deformation history.

Given the dimensions of most DWFTBs (>100 km) it is unreasonable to expect restorations to include this level of detail. Indeed, such structures are only imaged in our dataset because of the high fidelity nature of our profiles where as in many examples the resolution of the data would preclude such analysis. We therefore suggest that when undertaking restorations of shale detached DWFTBs an internal shortening factor of 5% of the total strain produced through sub-seismic resolution deformation be implemented over the total length of the collapse.

6.4.2 Application of missing strain to gravity collapse and accretionary prisms

We consider that this 5% missing strain has important consequences for understanding the tectonic, structural, stratigraphic and fluid evolution of DWFTBs regardless of the driving mechanisms that induces them. As this estimate of the missing strain is sub-seismic and is predicted to be prevalent throughout a collapse structure it should be applicable in both compressional and extensional components of DWFTBs.

The critical taper model (Davis et al., 1983; Dahlen et al., 1984) describes the evolution of accretionary prisms and thrust belts as a self-similar wedge of sediment that is at Coulomb failure through the system and is often applied in a whole system context e.g. the critical taper angle between surface and the basal surface and its evolution in response to plate convergence rates, sedimentation rates, exhumation and climate (Willett et al., 2003; Roe et al., 2006; Stolar et al., 2006; Simpson, 2010; Fillon et al., 2013; von Hagke et al., 2014) In addition, a number of studies consider the internal geometry of the wedge, and the individual structures that interact through the fold and thrust belt. Our results imply that an additional, and unrecognized 5%, should be accounted for in such studies. We acknowledge that this may be within the errors of the analysis, however of particular note are studies in Niger and Baram Deltas and the Nankai Trough (Bangs et al., 2004; Bilotti and Shaw, 2005; Morley, 2009) that have coupled seismic reflection derived interpretation and restorations to understand bulk deformation and shortening amounts in a critical taper context. A further example is

the analysis of the broader Sabah system, NW Borneo in which evaluating the role of tectonic versus gravity driven deformation is critical both to the DWFTB and regional tectonic evolution (King et al., 2010). In such settings, where estimated shortening is low, in the order of ~1.8%, the sub-seismic deformation that we observe could play a significant role.

Although our focus here has been on the structural analysis, the quantification of a 5% missing strain will influence our understanding of the syn-kinematic evolution of sedimentary basins associated with DWFTBs. It is well established that in these settings there is an intimate link between the controlling structures, the accommodation space and the associated sedimentary basin fill. This is a consequence of the development of anticlines that act as transverse barriers to sediment moving down slope and the intervening synclines that not only control bathymetry and sediment distribution but can also influence the location of sand prone fairways and mass-transport complexes (McGilvery and Cook, 2003; Paton et al., 2007; Deville et al., 2015; Ortiz-Karpf et al., 2015). Our calculation of 5% missing strain is across an entire system and may therefore have a significant impact on specific structures, and sedimentary basins within a system. This agrees with the findings of Spikings et al. (2015) who conclude that the misinterpretation of structural features in sedimentary systems can lead to considerable underestimates of sediment volume and architecture.

A direct consequence of this missing 5% is that estimates of porosity and permeability of sediments within DWFTBs would be considerably less than previously predicted. This alters our understanding of the formation of these structures implying that prior to the translation of strain down-dip and thus the formation of a contractional domain a period of compaction and “strain hardening” must occur first. Most of the contractional structures persist in a single fault block towards the centre as opposed to being equally distributed amongst the blocks. This is possibly a feature of the local lithology being more prone to failure than the sediments in surrounding blocks. Internal variations in lithology may provide the opportunity for the formation of multiple higher slip horizons within fault blocks allowing DWFTBs with multiple detachments to form as described previously (Totterdell and Krassay, 2003; Rowan et al., 2004; Corredor et al., 2005;

Briggs et al., 2006). This process could produce vertical segmentation of normal fault blocks allowing for anomalous fault throws down a fault plane where higher throws may be recorded nearer the top of some faults as in Robson et al. (2016). This would add considerable uncertainty to the interpretation of the inner working of individual fault bounded blocks.

As a final consideration, faults within DWFTBs influence the location and migration of fluids through the system. The presence of water plays a major role in the dynamic evolution of accretionary prisms (Moore and Vrolijik, 1992; Saffer and Bekins, 1998) by increasing pore pressure and thereby altering the failure criterion at which Coulomb failure occurs, and by association the critical taper of systems. It is well established that faults play a critical role in localising fluid migration pathways and locations of future failure (Saffer and Bekins, 1998, 2001; Klaucke et al., 2016). In their study of Four Way Closure Ridge, offshore SW Taiwan, Klaucke et al. (2016) specifically discuss that water and methane (which subsequently feed Bottom Simulating Reflectors (BSRs)) exploit relatively permeable fault zones but note that these are poorly imaged. Permeability is dynamic over time (Maltman et al., 1997; Bolton and Maltman, 1998) as well as laterally variable (Maltman, 1998; Bolton et al., 1999) this potentially gives us a mechanism for internal shortening. Small scale contraction occurs where the fluid pressure drops and so local shortening occurs (i.e. the décollement locks). Sliding and extension occurs in areas where higher fluid pressures are maintained along the décollement horizon. Our observations highlight the importance of considering a range of fault sizes that are likely to be present in DWFTBs whether seismically resolvable or not and may all play a role in fluid migration through the system. The presence of hydrocarbon fluids is equally important in DWFTBs, although of course, much of the interest is in predicting areas in which it is retained rather than expulsed.

At the 2016 Tectonic Studies Group conference it was stated “it is not the faults that industry is interested in but the white spaces inbetween” (Peel pers comm, 2016) this statement perhaps most validates the outcome of this study. When we consider the white space between 1st order structures, we find a set of 2nd order structures precisely where our drilling targets are. Whilst previous research (Morley et al., 2011;

Futalan et al., 2012) indicates reservoirs are present in these areas we caution that reservoir intervals may be more structurally compartmentalised with lower permeabilities than predicted.

6.5 Conclusion

Through combining field observations from exceptionally well exposed outcrops with high fidelity seismic observations we are able to, for the first time, consider DWFTB deformation from the metre scale to the margin scale. Regardless of the scale of observation, we observe hitherto unrecognised compressional fault structures that are at a second order in scale compared to the principal structures. As our structural restorations suggest that they can account for ~5% of the overall strain irrespective of scale; we propose that this accounts for the missing strain that has been identified in previous studies but remained poorly understood. We conclude that the majority of this missing strain is accommodated on discrete faults rather than as distributed deformation as previous models invoke.

As our model for the evolution of these second order structures is scale invariant we propose that this 5% additional shortening is applicable to all DWFTBs and should be accounted for when shortening estimates are calculated in both active and passive margins. Furthermore, individual faults are important within an intra-wedge setting as they can control sedimentation, localise the position of fluid migration (brine or hydrocarbon), modify bathymetry and compartmentalise reservoir intervals. Yet often these processes are identified without an association with a visible fault structure in the seismic reflection data. Our conclusion, and resulting model, that these second order structures are discrete faults that are close to, or often beyond seismic resolution, provides a method for determining if these intra-wedge processes are indeed controlled by structures that are not necessarily resolvable in seismic data.

6.6 Acknowledgements

The authors of this research would like to thank Spectrum ASA for the release of seismic data for this study. This research took place under the patronage of the Basin Structure Group, we acknowledge the financial support of Geotech, BG Group and EON and the provision of software from Midland Valley and Schlumberger. We would also like to thank the reviewers of this paper and the Editor Bernard Colletta for their helpful comments and suggestions.

6.7 References

Biju-Duval, B., Le Quellec, P., Mascle A., Renard, V., Valery, P., (1982). Multibeam bathymetric survey and high resolution seismic investigations on the Barbados ridge complex (eastern Caribbean): A key to the knowledge and interpretation of an accretionary wedge. *Tectonophysics* 86.1 (1982): 275-304.

Bangs, N. L., Shipley, T. H., Gulick, S. P. S., Moore, G. F., Kuromoto, S., Nakamura, Y., (2004). Evolution of the Nankai Trough decollement from the trench into the seismogenic zone: Inferences from three-dimensional seismic reflection imaging. *Geology* 32.4 (2004): 273-276.

Bilotti, F., and Shaw, J. H., (2005). Deep-water Niger Delta fold and thrust belt modeled as a critical-taper wedge: The influence of elevated basal fluid pressure on structural styles. *AAPG Bulletin* 89.11 (2005): 1475-1491.

Bolton, A. J., Maltman, A., (1998). Fluid flow pathways in actively deforming sediments: the role of pore fluid pressures and volume change. Marine and Petroleum Geology 15(4): 281-297, DOI: 10.1015/S0264-8172(98)00025-7.

Bolton, A. J., Clennell, M., Maltman, A., (1999). Nonlinear stress dependence of permeability: A mechanism for episodic fluid flow in accretionary wedges. Geology 27(3), 239-242, DOI: 10.1130/0091-7613

Briggs, S. E., Davies, R. J., Cartwright, J. A., Morgan, R. (2006). Multiple detachment levels and their control on fold styles in the compressional domain of the deepwater west Niger Delta. Basin Research, 18, 435–450.

Brown Jr., L. F., Benson, J. M., Brink, G. J., Doherty, S., Jollands, E. H., Jungslagger, A., Keenen, A., Muntingh, A., van Wyk, N. J. S, (1995), Sequence Stratigraphy in Offshore South African Divergent Basins. An Atlas on Exploration for Cretaceous Lowstand Traps Soekor (Pty) Ltd: AAPG Studies in Geology, vol. 41 184 pp.

Butler, R. W. H. and D. A. Paton (2010), Evaluating lateral compaction in deepwater fold and thrust belts: how much are we missing from “nature's sandbox”?: GSA Today 20 (3), 4–10.

Corredor, F., Shaw, J. H. & Bilotti, F. (2005). Structural styles in the deep-water fold and thrust belts of the Niger Delta. AAPG Bulletin, 89, 735–780

Dahlen, F. A., J. Suppe, and D. Davis (1984). Mechanics of fold-and-thrust belts and accretionary wedges: Cohesive Coulomb Theory, J. Geophys. Res., 89(B12), 10087–10101, doi:10.1029/JB089iB12p10087.

Dakin, N., Pickering, K.T., Mohrig, D., Baylis, N.J., 2012. Channel-like features created by erosive submarine debris flows from the Middle Eocene Ainsa Basin. Mar. Petroleum Geol. 41, 62e71. http://dx.doi.org/10.1016/j.marpetgeo.2012.07.007.

Dalton, T. J. S., Paton, D. A., Needham, D. T. (2016). The influence of mechanical stratigraphy on multi-layer gravity collapse structures: insights from the Orange Basin, South Africa, in review. In: Sabato, Ceraldi, T., Hodgkinson, R.A. & Backe, G. (eds) Petroleum Geoscience of the West Africa Margin. Geological Society, London, Special Publications, 438. First published online January 19, 2016, http://doi.org/10.1144/SP438.4

Dalton, T. J. S., Paton, D. A., Needham, D. T., Hodgson, N., (2015), Temporal and spatial evolution of deepwater fold and thrust belts: Implications for quantifying strain imbalance, Interpretation, Vol.3, No. 4. doi: 10.1190/INT-2015-0034.1.

Davis, D., Suppe, J. and Dahlen, F. A., (1983). "Mechanics of fold-and-thrust belts and accretionary wedges." *Journal of Geophysical Research: Solid Earth* 88.B2 (1983): 1153-1172.

Deville, E., Mascle, A., Callec, Y., Huyghe, P., Lallemant, S. Lerat, O., Mathieu, X., Padron de Carillo, C., Patriat, M., Pichot, T., Loubrieux, B., Granjeon, D., (2015). Tectonics and sedimentation interactions in the east Caribbean subduction zone: an overview from the Orinoco delta and the Barbados accretionary prism. *Marine and Petroleum Geology* 64 (2015): 76-103.

de Vera, J., P. Granado, K. McClay (2010), Structural evolution of the Orange basin gravity-driven system, offshore Namibia: Mar. Petrol. Geol. 27, 233–237.

Dreyer, T., Corregidor, J., Arbues, P., Puigdefabregas, C. (1999), Architecture of the tectonically influenced Sobrarbe deltaic complex in the Ainsa Basin, northern Spain, *Sedimentary Geology,* 127, 127-169.

Fillon, C., Huismans, R. S., van der Beek, P. (2013), Syntectonic sedimentation effects on the growth of fold-and-thrust belts Geology, January 2013, v. 41, p. 83-86, first published on October 15, 2012, doi:10.1130/G33531.1.

Franke, D., Barckhausen, U., Heyde, I., Tingay, M., Ramli, N., (2008). Seismic images of a collision zone offshore NW Sabah/Borneo. *Marine and Petroleum Geology* 25.7 (2008): 606-624.

Futalan, K., Mitchell, A., Amos, K., Backe, G. (2012), Seismic facies analysis and structural interpretaion of the Sandakan sub-basin, Sulu sea, Philippines. Search and Discovery article #30254

Gerrard, T., and G.C. Smith (1982), Post-Palaeozoic succession and structure of the south-western African continental margin: Studies in continental margin geology: AAPG Memoir 34, p. 49–74.

Hesse, S., Back, S., and Franke, D. (2010). "The structural evolution of folds in a deepwater fold and thrust belt–a case study from the Sabah continental margin offshore NW Borneo, SE Asia." *Marine and Petroleum Geology* 27.2 (2010): 442-454.

Klaucke, I., Berndt, C., Crutchley, G., Chi, W. C., Lin, S., Muff, S., (2016). Fluid venting and seepage at accretionary ridges: the Four Way Closure Ridge offshore SW Taiwan. Geo-Marine Letters 36: 16 pp. 165-174. DOI 10.1007/s00367-015-0431-5.

King, R.C., Backe, G., Morley, C.K., Hillis, R.R., Tingay, M.R.P., (2010). Balancing deformation in NW Borneo: Quantifying plate-scale vs. gravitational tectonics in a delta and deepwater fold-thrust belt system. *Marine and Petroleum Geology* 27.1 (2010): 238-246.

Krueger, A., and E. Gilbert, (2009). Deepwater fold-thrust belts: Not all the beasts are equal: AAPG Search and Discovery, Article 30085.

Lopez-Mir, B., Muñoz, J. A., García-Senz, J. (2014). Restoration of basins driven by extension and salt tectonics: example from the Cotiella Basin in the central Pyrenees. Journal of structural geology 69, 147-162.

Lopez-Mir, B., Muñoz, J. A., García-Senz, J. (2015). Extensional salt tectonics in the partially inverted Cotiella post-rift basin (south-central Pyrenees): structure and evolution. Int J Earth Sci. (Geol Rundsch) 104:419-434. doi 10.1007/s00531-014-1091-9.

Maltman, A. J., (1998). Deformation structures from the toes of active accretionary prisms. Journal of the geological society, London Vol. 155, pp. 639-650, DOI: 10.1144/gsjgs.155.4.0639.

Maltman, A. J., Labaume, P., Housen, B., (1997). Structural geology of the décollement at the toe of the Barbados accretionary prism. Ed's Shipley, T. H., Ogawa, Y., Blum, P., Bahr, J. M. Proceedings of the Ocean Drilling Program, Scientific Results, Vol. 156, DOI: 102973/odp.proc.sr.156.037.1997.

McClay, K., Muñoz, J. A., García-Senz, J. (2004). Extensional salt tectonics in a contractional orogen: a newly identified tectonic event in the Spanish Pyrenees, Geology 32(9):737–740. doi:10.1130/G20565.1

McGilvery, T. A., Cook, D. L., (2003). The influence of local gradients on accommodation space and linked depositional elements across a stepped slope profile, Offshore Brunei. Shelf margin deltas and linked down slope petroleum systems: global significance and future exploration potential, GCSSEMP Foundation 23rd Annual Bob F. Perkins Research Conference, pp. 387‑419.

Mohammed, M., D. A. Paton, R. E. L. I. Collier, N. Hodgson, (2015) U. Utjavari, Interaction of crustal heterogeneity and lithospheric process in determining passive margin architecture on the Southern Namibian margin, Geological Society Special Publication, 438, DOI: 10.1016/S0264-8172 (03)00045.

Moore, J. C., and Vrolijk, P., (1992). Fluids in accretionary prisms. *Reviews of Geophysics* 30.2 (1992): 113-135.

Morley, C. K., (2007). "Interaction between critical wedge geometry and sediment supply in a deep-water fold belt." Geology 35.2): 139-142.

Morley, C. K., (2009). Geometry of an oblique thrust fault zone in a deepwater fold belt from 3D seismic data. Journal of Structural Geology 31 (12). 1540-1555.

Morley, C. K., R. King, R. Hillis, M. Tingay, G. Backe (2011), Deepwater fold and thrust belt classification, tectonics, structure and hydrocarbon prospectivity: a review. Earth Sci. Rev. 104, 41-91.

Muñoz J. A., (1992), Evolution of a continental collision belt: ECORS- Pyrenees crustal balanced cross-section. K.R. McClay (Ed.), Thrust Tectonics, Chapman & Hall, London, pp. 235-246.

Muñoz J. A., Beamud E., Fernández O., Arbués P., Dinarès-Turell J., Poblet J. (2013), The Ainsa Fold and thrust oblique zone of the Central Pyrenees: kinematics of a curved contractional system from paleomagnetic and structural data. Tectonics 32(5):1142–1175. doi: 10.1002/tect.20070

Muntingh, A. and L.F.J. Brown (1993), Sequence stratigraphy of petroleum plays, post-rift Cretaceous rocks (lower Aptian to upper Maastrichtian), Orange Basin, South Africa, Siliciclastic Sequence Stratigraphy. Recent Developments and Applications: American Association of Petroleum Geologists, Tulsa, Oklahoma, pp. 71–98.

Ortiz-Karpf, A., Hodgson D.M., McCaffrey, W. D., (2015). "The role of mass-transport complexes in controlling channel avulsion and the subsequent sediment dispersal patterns on an active margin: the Magdalena Fan, offshore Colombia." *Marine and Petroleum Geology* 64 (2015): 58-75.

Paton, D.A., Carr, M., Trudgill, B., Ortner, H., Medewedeff, D.A., (2007). Alpine-scale 3D geospatial modeling: Applying new techniques to old problems. *Geosphere* 3.6 (2007): 527-549.

Paton, D. A., D. van der Spuy, R. di Primio, B. Horsfield (2008), Tectonically induced adjustment of passive-margin accommodation space; influence on hydrocarbon potential of the Orange Basin, South Africa: AAPG Bulletin, v. 92, p. 589–609.

Peel, F. J., (2014), The engines of gravity-driven movement on passive margins: Quantifying the relative contribution of spreading vs. gravity sliding mechanisms: Tectonophysics 633, 126-142.

Pickering, K.T. and N.J. Bayliss (2009), Deconvolving tectono-climatic signals in deep-marine siliciclastics, Eocene Ainsa basin, Spanish Pyrenees: seesaw tectonics versus eustasy Geology, 37 (2009), pp. 203–206 http://dx.doi.org/10.1130/G25261A. 1

Pickering, K.T. and J. Corregidor (2005), Mass transport complex and tectonics control on confined basin-floor submarine fans, Middle Eocene, south Spanish Pyrenees, in: D.M. Hodgson, S.S. Flint (Eds.), Submarine Slope Systems: Process and Products, Geological Society Special Publication, vol. 244 (2005), pp. 51–74

Price, R.A., (1981), The Cordilleran foreland thrust and fold belt in the southern Canadian Rocky Mountains, in McClay, K.R., and Price, N.J., eds., Thrust and Nappe Tectonics: London Geological Society Special Publication 9, 427-448.

Robertson, P. and Burke, K., (1989). "Evolution of southern Caribbean plate boundary, vicinity of Trinidad and Tobago." *AAPG Bulletin* 73.4 (1989): 490-509.

Robson, A.G., King, R.C., Holford, S.P., (2016), 3D seismic analysis of gravity driven and basement influenced normal fault growth in the deepwater Otway Basin, Australia. Journal of Structural Geology 89, pg. 74-87.

Roe, G.H., Stolar, D.B., Willett, S.D., (2006). Response of a steady-state critical wedge orogen to changes in climate and tectonic forcing. *Geological Society of America Special Papers* 398 (2006): 227-239.

Rowan, M.G., F.J. Peel, B.C. Vendeville (2004), Gravity Driven fold belts on passive margins: Thrust tectonics and hydrocarbon systems, AAPG Mem, 82, pp 157-182.

Saffer, D.M., and Bekins B.A., (1998). Episodic fluid flow in the Nankai accretionary complex: Timescale, geochemistry, flow rates, and fluid budget. *Journal of Geophysical Research: Solid Earth* 103.B12 (1998): 30351-30370.

Saffer, D.M. and Bekins, B.A., (2001), Hydrologic controls on the morphology and mechanics of accretionary wedges. Geology, March, 2002, v. 30, p. 271-274, doi: 10.1130/00917613.

Simpson, G.D.H, (2010). Formation of accretionary prisms influenced by sediment subduction and supplied by sediments from adjacent continents. *Geology* 38.2 (2010): 131-134.

Spikings, A.L., Hodgson D.M., Paton D.A., Spychala Y.T. (2015) Palinspastic restoration of an exhumed deepwater system: A workflow to improve paleogeographic reconstructions, Interpretation-A Journal of Subsurface Characterization, 3, pp.SAA71-SAA87. doi: 10.1190/INT-2015-0015.1

Stolar, D.B., Roe, G.H., Willett, S.D., 2006. Controls on the patterns of topography and erosion rate in a critical orogen. Journal of Geophsyical Research, vol. 112 http://dx.doi.org/10.1029/2006JF000713.

Tavani, S., Lopez-Mir, B., Muñoz, J.A., 2015. Extensional fold-related fracturing in the Armeña rollover (Cotiella Massif, southern Pyrenees). Italian J. Geoscience 134. http://dx.doi.org/10.3301/IJG.2014.17.

Toto, E., and Kellogg, J. N., (1992). Structure of the Sinu-San Jacinto fold belt—An active accretionary prism in northern Colombia. *Journal of South American Earth Sciences* 5.2 (1992): 211-222

Totterdell, J.M. & Krassay, A.A. (2003), The role of shale deformation and growth faulting in the Late Cretaceous evolution of the Bight Basin, offshore southern Australia. In: Van Rensbergen, P., Hillis, R.R., Maltman, A.J. & Morley, C.K. (eds) Subsurface Sediment Mobilization. Geological Society, London, Special Publications, 216, 429–442, http://doi.org/10.1144/GSL.SP.2003.216.01.28

Vergés, J., Fernàndez, M. & Martínez, A. (2002), The Pyrenean orogen: pre-, syn-, and post-collisional evolution. In: Rosenbaum, G. and Lister, G.S. 2002. Reconstruction of the evolution of the Alpine-Himalayan Orogen. Journal of the Virtual Explorer, 5 – 7

Vinnels, J. S., Butler, R.W.H, McCaffrey, W.D., Paton, D.A., (2010). Depositional processes across the Sinu accretionary prism, offshore Colombia." *Marine and Petroleum Geology* 27.4 (2010): 794-809.

von Hagke, C., Oncken, O., Evseev, S., (2014). Critical taper analysis reveals lithological control of variations in detachment strength: an analysis of the Alpine basal detachment (Swiss Alps). *Geochemistry, Geophysics, Geosystems* 15.1 (2014): 176-191

Willett, S.D., Fisher, D., Fuller, C., En-Chao, Y., Chia-Yu, L., (2003). Erosion rates and orogenic-wedge kinematics in Taiwan inferred from fission-track thermochronometry. *Geology* 31.11 (2003): 945-948.

Wood, A. M., Paton, D. A., Collier, R. E. L., (2015a). The missing complexity in seismically imaged normal faults: what are the implications for geometry and production response? Geological Society, London, Special

Publications, 421, 213-230, http://doi.org/10.1144/SP421.12.

Wood, A. M., Paton, D. A., Collier, R. E. L., (2015b). Understanding regional-scale structural uncertainty: The onshore Gulf of Corinth rift as a hydrocarbon exploration analogue. Interpretation, 3(4), http://library.seg.org/doi/abs/10.1190/INT-2015-0046.1.

7 Discussion and Conclusions

This chapter synthesises the observations and conclusions reached in Chapters 3-6. As each data chapter contains its own discussion this chapter is intended to discuss aspects of this study that have not been previously covered and to tie together the understanding gleaned from all of the chapters. This chapter is broken into three sections, firstly the character and structure of the basin and DWFTBs within it, secondly the implications of this research for other shale detached systems, and finally I propose a 3D model for the initiation and growth of thin shale detached DWFTBs.

What follows is a brief discussion on how the research and conclusions reached in Chapters 4-6 help to answer the questions raised in the research objectives;

What role does stratigraphy play on DWFTBs?

The nature of the lithology of the detachment as a control on DWFTB development as discussed in Chapter 4 is well established in the literature (Davis et al., 1983; Davis & Engelder, 1985, Morley & Guerin, 1996; Rowan et al., 2004; Morley et al., 2011). Chapter 4 shows the effects a changeable stratigraphy across the margin, it links a number of significant shale deposits as identified by Brown et al. (1995) and Paton et al. (2007, 2008) with the location of significant DWFTBs along the margin. It also shows significant variation in the style of collapse present above these different detachment horizons. In identifying DWFTBs whose detachments switch between different stratigraphic horizons (Figure 4.4, 4.10, 5.7) it is clear that the role of variations in detachment lithology controls the location of décollements and the style of collapse.

What are the range of geometric structures possible in thin shale detached DWFTBs?

The interpreted seismic profiles included throughout this thesis (Figures 1.2, 2.1, 3.5 3.6, 3.16, 3.18, 4.4, 4.8, 4.9, 4.10, 5.4 - 8 & 6.10) indicate the huge variety of different geometries observable throughout the margin. They indicate a number of features that do not fit with a standard model of a DWFTB as outlined in Chapter 2, of an up-

dip extensional domain linked via a single detachment to a down-dip compressional domain. This study and previous authors have observed variations from a standard model such as: multiple detachment horizons (Figure 3.5, 3.6 c, e & f, 3.16, 3.18, 4.4, 4.9, 4.10, 5.6 - 8 & 6.10; Totterdell & Krassey, 2003; Rowan et al., 2004; Corredor et al., 2005; Briggs et al., 2006), seismic profiles with extensional domains with no contractional domains (Figures 3.6 a & g, 5.4 and Figure 7.3, Inline 1 & 5), multilevel slips within a single fault block (Figure 5.7 - 8; Robson et al., 2016), and stacked contractional domains (Figure 3.6c, 4.4, 4.10, 5.7, 5.8). The variety in different geometrical arrangements of DWFTBs is discussed in Chapter 4 with models that explain their variation and indicate the range of structures possible presented in Figures 4.11, 4.12 and 5.10.

Where is the strain taken up in DWFTB systems and what are we missing from seismic examples of DWFTBs?

It is well established in Chapter 5 and by a number of other authors (Granado et al., 2009; Butler & Paton 2010; de Vera et al. 2010) that there is a missing component of strain not compensated for by down-dip compression. This is particularly clear in Chapter 5 where the missing strain component was quantified as being 5 % of the extensional strain produced. The methodology applied in chapter 5 of using parallel sections through a collapse, proved the missing strain component was not compensated for by lateral compaction as proposed by Gonzalez-Mieres & Suppe (2006) and Butler & Paton (2010). This indicated the strain taken up by the system is compensated for internally by deforming the sediments of the wedge.

Chapter 6 identified significant 2nd order structures in the form of folds and thrusts, and quantified their effect as being equivalent to the missing strain component. This allows the prediction of what sub-seismic features may be present but are unobservable, in larger seismic examples of DWFTBs

7.1 The Structure of the DWFTBs and the Orange Basin

This study has observed and interpreted a larger range of DWFTB structures than in any published study of the Orange Basin. In looking at the basin on such a broad scale it is possible to compare a large range of structures that form under similar conditions as well as observe some of the effects of larger scale processes have on the margin's evolution. In this section I discuss two of observations of the wider scale margins behaviour, firstly the timing of DWFTB activity on the margin, and secondly the 3D structure of DWFTBs.

7.1.1 Timing of structural detachments

In this study I have identified and interpreted nine décollement horizons within the basin (Figures 3.3, 3.15 & 3.17). They range in depth from the top of the Transition Megasequence to the Cenozoic Megasequence and in activity from the Aptian to the Cenozoic. The timing of the onset of deformation on a DWFTB can be ascertained through determining and dating the earliest growth package within the structure. The final phase of deformation can be determined by looking for the latest sedimentary layer to be cut by a fault, whilst ignoring isolated local minor reactivations. This type of analysis is shown in Figure 7.1 where six interpreted seismic profiles through 8 of the 9 décollement surfaces are presented. Décollement E has not been presented as it is unclear when precisely it initiates. These sections show that growth packages pre-date the formation of a down-dip compressional domain as corresponding growth features do not present till upper sequences are deposited. It can also be noted that in the more proximal faults of the same sequences there are no growth packages indicating extensional deformation initiated towards the centre of the now larger systems, meaning later normal faults formed proximal to the first fault.

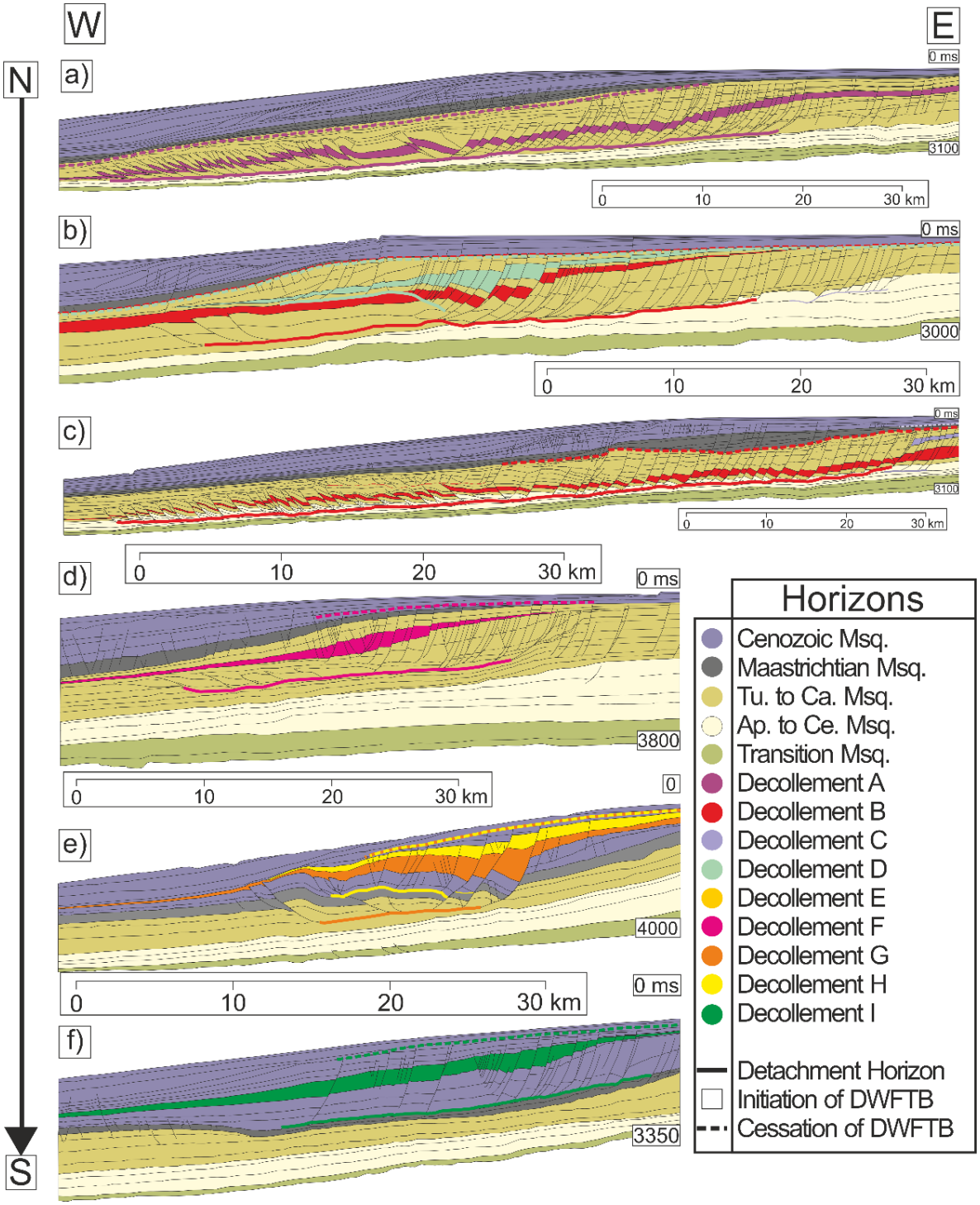

Figure 7.1. Six interpreted margin perpendicular PSTM seismic profiles made through Decollements A-D & F-I. Significant features have been coloured coded on each section to represent which detachment each feature relates too. These features are: the décollement horizon in a thick continuous line, a block coloured sequence containing the earliest growth fault representing the initiation of deformation along the detachment, and a dashed line representing the cessation of deformation on the DWFTB. The location of the profiles are shown in Figure 7.2 All section are vertically exaggerated 3:1.

Also observable in Figure 7.1 is a trend in the timing of initiation, growth and cessation of deformation from north to south. When the periods of DWFTB activity are plotted this trend can be seen more clearly (Figure 7.2).

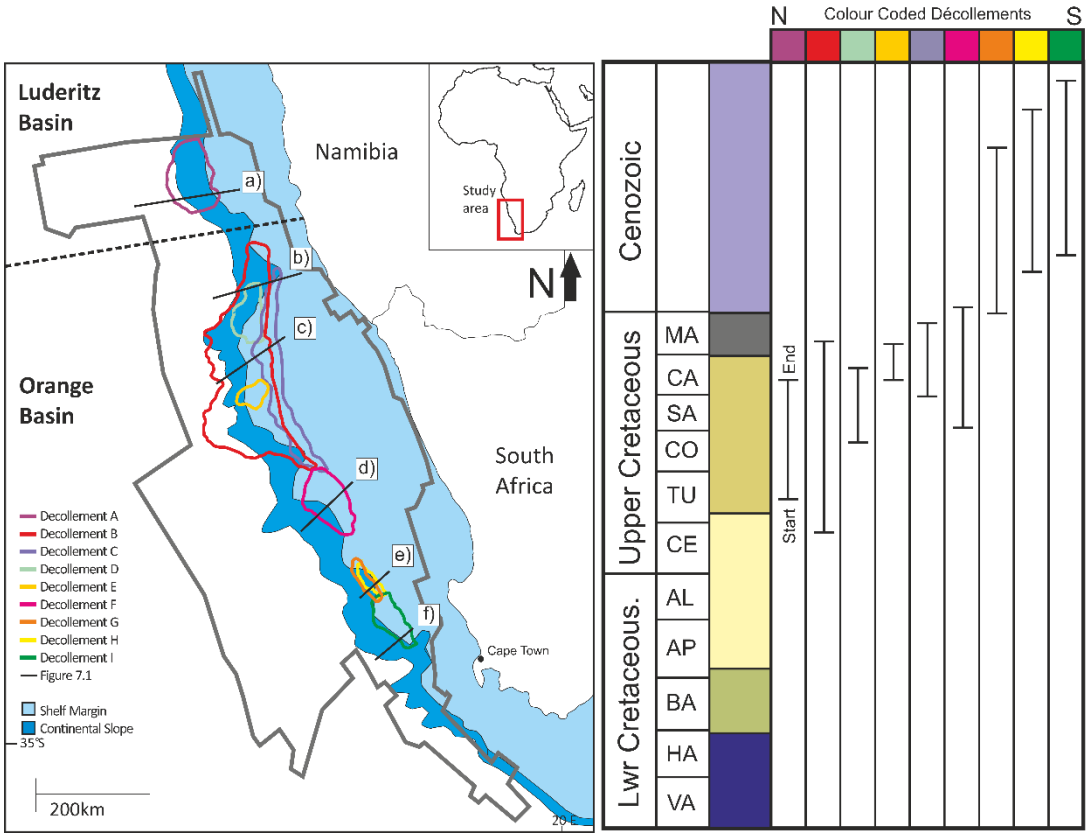

Figure 7.2. Map showing the locations and outline of detachments in the study area with a table indicating the timing of collapse on each structure. Colour code of décollements on map correspond to the coloured box at the top of the column and to Figure 7.1. Labelled lines relate to sections features in Figure 7.1.

In general the oldest collapses occurred in the north during the Cenomanian/ Turonian, then younger DWFTBs initiated progressively heading south with the latest collapse activity extending into the Late Tertiary. Most of the gravity collapse structures persist within the Turonian to Campanian Megasequence centred on the mouth of the Orange River. This may represent changes in sedimentation shifting along the basin or perhaps an indicator of the timing of a transient cratonic uplift, steepening the continental slope causing failure. These two concepts will be discussed further in section 7.2.

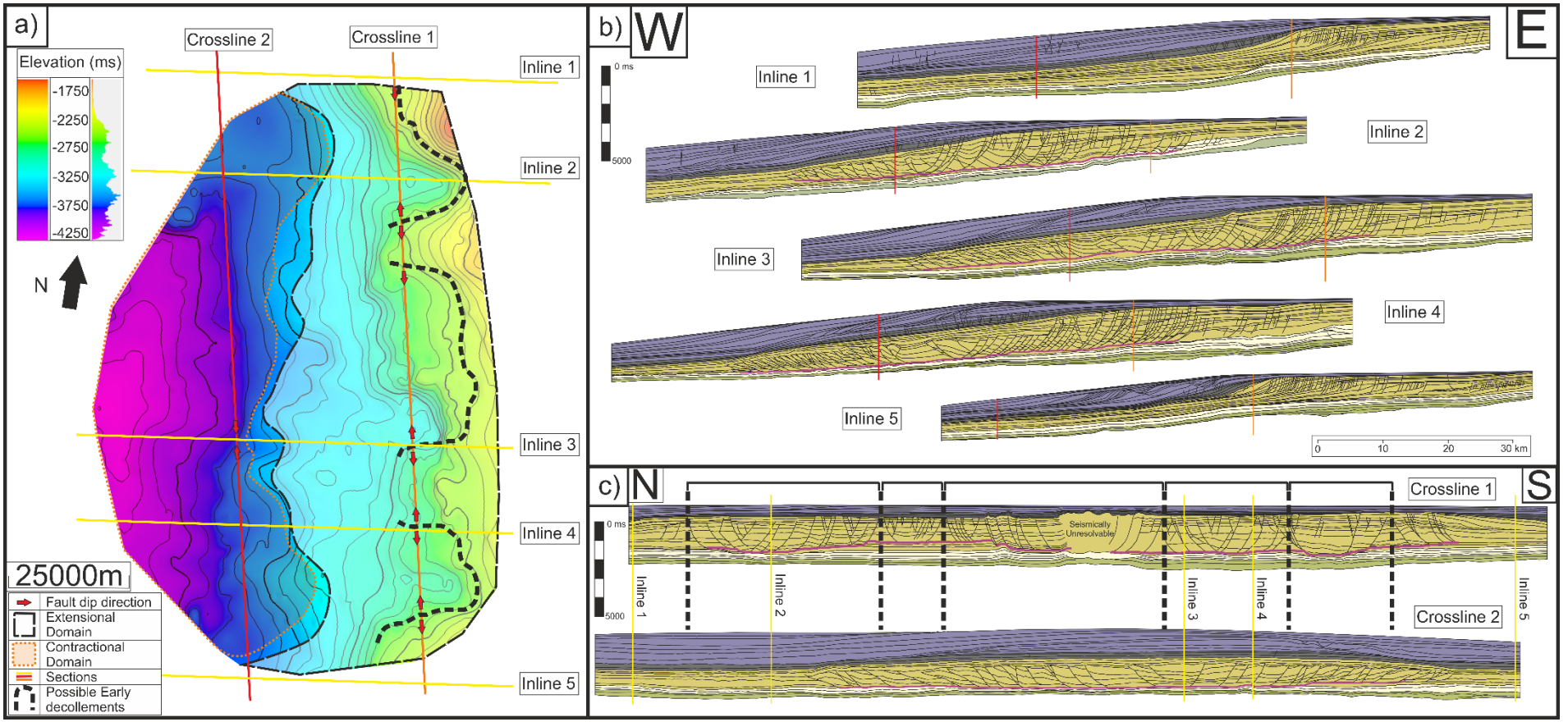

Figure 7.3. a) Map of Décollement A (Location in Figure 7.2) including the location of seven seismic profiles projected onto the surface. b) Five interpreted E-W transport parallel "Inline" seismic profiles through a collapse in the Luderitz Basin. c) Two interpreted N-S transport perpendicular "crossline" seismic profiles through a DWFTB in the Luderitz Basin, all profiles are presented in PSTM and have been vertically exaggerated 3:1 (larger version of crossline 1 included in Appendix).

7.2 3D Structure

Figure 7.3 shows a map of décollement A from Figure 3.17 and a set of seven sections through the DWFTB system located in the north of the study area in the Luderitz Basin (Figure 3.3 & 7.2). Of the seven sections, two are margin parallel “crosslines” that span the collapse perpendicular to the transport direction (Crossline 1, taken from Figure 3.16) and five are transport parallel “inlines” (Inlines 1 & 4 are from Figure 3.6 a & b, Inline 2 is from Figure 1.2) .

Unlike the collapse system presented in Chapter 6 the data used in Figure 7.3 are from a single survey which spans the entire structure and contains better imaging. The DWFTB in the Luderitz Basin is also simpler than the one presented in Chapter 6 with fewer detachments and a more classical geometry, this allows us to see the structure of the DWFTB more clearly. Inline 1 and 5 mark the limits of décollement A, both profiles show significant up-dip extensional faulting though no down-dip contractional domain. The extensional faulting within these profiles has not coalesced onto a single detachment horizon. The observation of a lack of coalescence and of an extensional domain with no contractional domain fits with the model discussed in Chapter 6. Inlines 2-4 all show profiles with extensional and contractional domains that detach onto a single décollement horizon. However, within each profile the stratigraphic level at which the décollement lies changes along the profile particularly within the extensional domains. When the intersection of these profiles are viewed in Crossline 1 the variations in the depth of the décollement can be seen to relate to changes in the orientation of fault dips.

So perhaps this collapse should be considered as a set of parallel collapses separated by lateral ramps, as discussed by de Vera et al. (2010) and Morley et al. (2011)? Looking at the map of the detachment, ridges in the up-dip easterly portion of the collapse could be interpreted as lateral ramps. However, the geometry of the collapse in Crossline 2 displays a continuous detachment with fault dips pivoting about a centre point, as opposed to showing consistent changes in orientation. When this observation is combined with the absence of ridged structures in the contractional domain of the detachment map it would seem the collapse is actually

a single homogenous structure. I propose that the ridges are remnant structures relating to earlier separate collapse that have coalesced into a single structure. I further suggest this is a standard characteristic of thin shale detached DWFTBs and is reflected in all of the décollements features across the margin. The remnant ridges appear as arcuate features on maps of detachment surfaces (Figure 3.15) and ally with changes in fault orientation (Figure 3.5). The relative age of the syn-kinematic sediments above the active faults further indicate the structures initiated as separate collapse systems. Later syn-kinematic sediments show no evidence of separate systems showing that these structures once separate now act as one system (Figure 3.16).

Rowan et al. (2004) discusses the active nature of collapse systems alters the effects of the driving factors of collapse. This principle is reflected in this study as we observe different portions of collapses and the margin being active at different times as well as behaving in a punctuated format. Displacement on fault blocks occurs slowly enough for thick syn-kinematic packages to be deposited and for fault blocks to erode. This implies deformation is a slow process and suggests the gravitational imbalances, once alleviated through deformation, are slowly rebuilt, either through continued high rates of sedimentation or a continuous process of tectonic uplift.

7.3 Structural controls on sedimentation or sedimentary controls on structural formation?

Sedimentation is a known driving factor of gravitational failure (Davis et al., 1983; Shaw et al., 2004; Rowan et al., 2004) and thus it would be expected for the location of DWFTB to be in areas with thick sediment accumulations. The concept is that a rapid influx of sediment from the Orange River leads to a gravitational imbalance between the shelf and the slope, over-steepening the continental slope leading to failure.

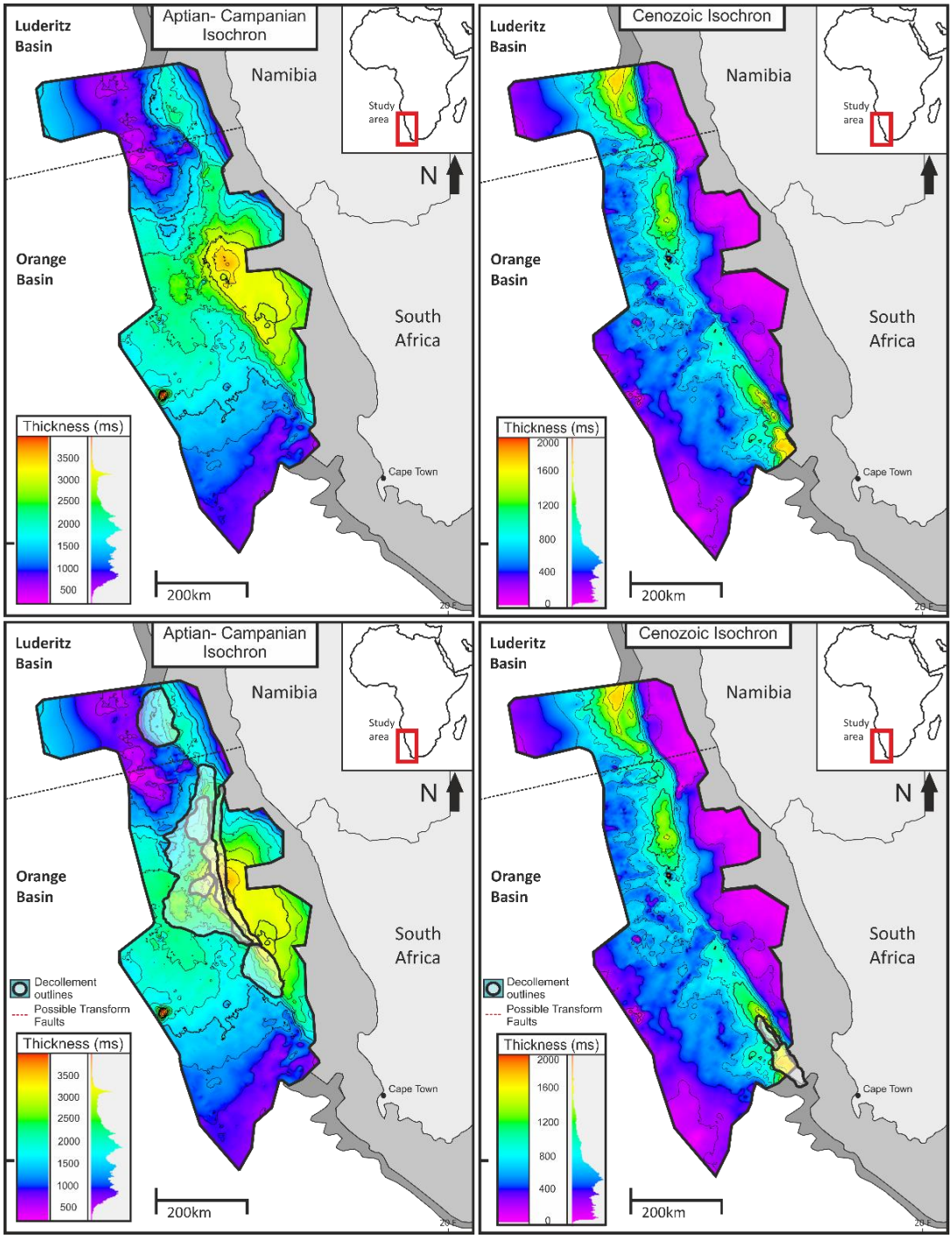

Figure 7.4. Isochrons of the Aptian- Campanian and the Cenozoic, projected on the lower image are the locations of DWFTBs active synchronously with deformation.

Figure 7.4 shows isochrons for the Aptian to Campanian and Cenozoic, which act as a proxy for sediment thickness. Projected onto these sections are the location of DWFTBs that were active during these time periods. The location of DWFTB development matches the location and timing of the thickest sediment accumulations in the basin. However, in the north of the Cenozoic isochron and in

the far south of the Aptian to Campanian isochron there are no DWFTBs despite having equivalent thick accumulations of sediment. This implies that whilst thick accumulations of sediment are necessary they are not necessarily the only factor for collapse in the basin. The dip of the detachment, the surface slope angle, the strength of the sediments in the wedge and the coefficient of friction of the detachment are known to exert a significant control on gravitational deformation (De Jong and Scholten, 1973; Ramberg, 1981; Rowan et al., 2004).

The slope angle of the original paleo-slope has been altered by the mid-Campanian uplift event (McMillan, 2003), which eroded up to 750 m of the mid-Aptian to Campanian sediments of the shelf (Paton et al., 2008). Measurements of paleo-slope post the uplift event indicate a range of surface slope angles from 1.0- 1.5^{o} in regions with limited or no Cenozoic-aged activity and 1.8- 2.3^{o} in the south where collapses were prevalent. This implies surface slope angle may play an integral part in DWFTB systems in this study.

The slope angles of detachments, based upon measurements made using PSDM data, varies across the basin from 1.0-2.5^{o} dipping outboard, as expected in Type Ia systems (Morley et al., 2011). By considering isochron time as a proxy for depth the variance in the dip of the décollement is observable in the detachment maps featured in Figures 3.15, 3.17 and 7.3. It is also seen in the interpreted seismic profiles, presented in this study, where the detachment can be seen cutting up and down stratigraphy (Figure 3.18, 4.4, 6.10). The detachment slope angle changes based upon the dip of the sediments of the margin and due to changes in the depth of a detachment as it switches between multiple advantageous slip horizons. The detachment slope angle has an impact on the viability of a DWFTB to form above a thin shale décollement (Dahlen et al., 1983, Morley et al., 2011) and a control on the length of the DWFTB that forms (Koyi and Vendeville, 2003). However, the variation of different dips and in dip consistency across the margin implies it is not the controlling factor for collapse.

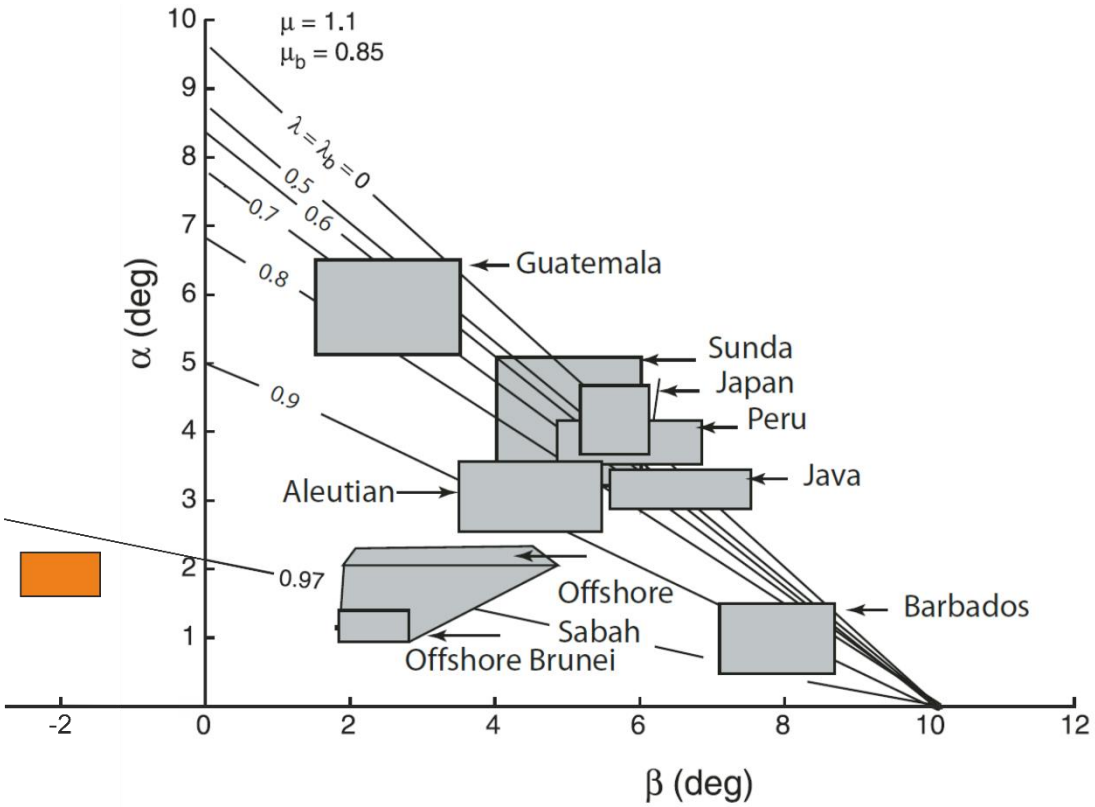

Figure 7.5. Graph adapted from Morley et al. (2007). Y-axis indicates surface slope angle, x-axis indicates detachment slope angles, and the lines indicate pore fluid pressure ratios. The boxes indicates the variation of slope angles in the different labelled DWFTB systems, the orange box indicates the DWFTBs in this study.

Figure 7.5 is adapted from Morley et al. (2007) and shows how the surface and detachment slope angles recorded in the margin compare to other DWFTB systems. The position of the study area DWFTB on this plot suggests that failure involved high pore fluid pressure ratio (Davis et al., 1983) implying the detachment is likely to be exceptionally weak. Overpressures have been implied within the horizons that form the detachments for DWFTBs within the basin (Paton et al., 2007). Overpressures along slip horizons and within the wedge can cause slip along a detachment with very low or no dip, given sufficiently high fluid pressures (Hubbert & Rubey, 1959; Davis et al. 1983). Lithologically controlled overpressures and steep surface slope dips are the most likely controls on the propagation of DWFTBs within this margin.

Steep surface slopes could either be caused by rapid sedimentation onto the shelf or by uplift and rotation of the proximal portion of the basin by tectonic processes. Returning to the observations made in Figures 7.1 and 7.2 about transient DWFTB formation, the southwards shift of failure could be caused by progressive steepening

of the shelf margin southwards. If sedimentation is the dominant cause of collapse along the margin then a question must be raised as to why the collapse structure in the far north above décollement A (Figure 7.1 a) did not reactivate in the Cenozoic. This is despite having similar sediment thicknesses deposited during the Cenozoic to those that caused failure, along the décollements G-I, in the far south contemporaneously (Figure 7.3). It is possible sufficient overpressures were not present to allow reactivation on the pre-existing DWFTB, or perhaps a sufficiently steep slope was not established to overcome the forces in the pre-deformed DWFTB. However, it is also possible that a tectonic uplift occurred during the Tertiary which had greatly more influence on the south of the margin than the north. Significant uplift events during the Cretaceous and the Tertiary, that control the modern topography, have been postulated by several authors (Paton et al., 2008; Burke & Gunnell, 2008; Mohammed 2013) though the precise amount of uplift is difficult to quantify due to a sparse record of Tertiary deposits on the shelf (Mohammed, 2013). Increases in the rates of sedimentation likely relate to tectonic uplift, which causes increased erosion on the continent. It is possible that the same uplift event that increased sedimentation rates also increases the surface slope angle further encouraging collapse.

7.4 Model for the formation and growth of DWFTBs

The models of collapse proposed by Krueger & Gilbert (2009) (Figure 2.5) described two end members for thin shale detached systems, those of discrete and non-discrete detachments. As observed in Chapter 4, and in multiple sections throughout the Orange Basin (Figures 1.2, 2.1, 3.5 3.6, 3.16, 3.18, 4.4, 4.9, 4.10, 5.4-8 & 6.10), both of these end members are in operation simultaneously. There are both significant slides that occur above discrete detachments (Figure 1.2, 2.1, 3.6 b, d & g, 5.4 & 5.5) and others that appear to range between a multitude of slip surfaces (Figure 3.5, 3.6 c, e & f, 3.16, 3.18, 4.4, 4.9, 4.10, 5.6-8 & 6.10). This would imply the Krueger and Gilbert (2009) model is not applicable to this margin, or perhaps more

broadly they are two end member models of the same suite of thin detached systems, as in Morley et al.'s (2011) description of Type 1a DWFTBs.

When the data from the basin are compared to the 3D models of collapse presented by de Vera et al (2010) and Scarselli et al. (2016) (Figure 2.6) these models are found to be insufficient for describing the range, variety and complexity of the DWFTBs. For example there is evidence of overlapping collapses systems (Figure 3.5, 3.16 & 7.3) and multilevel collapse systems (Figure 3.5, 3.6 c, e & f, 3.16, 3.18, 4.4, 4.9, 4.10, 5.6-8 & 6.10) which do not fit with these models. To expand on the findings from Chapter 5 and to incorporate the data from the detachment surfaces (Figure 7.3) it is necessary to construct an alternative model that fits these findings. The model presented in Figures 7.6-11 synthesises the findings of the entire study that preserves the complex understanding gleaned from the observations and interpretations made across the entire basin.

Figures 7.6-11 present a model for the initiation and growth of a thin shale detached DWFTB system incorporating growth of the system both oblique to and parallel to the basin. The figures are presented as 3D diagrams of a margin with an idealised margin perpendicular inline cross-section on the flank showing the growth and evolution of a DWFTB and a separate idealised margin parallel crossline cross-section. The inline section through the margin endeavours to encapsulate all the variations observed and described in Chapters 3-5 as well as express the compaction and 2nd order structures formed in the sediments of the wedge described in Chapter 6. The margin parallel crossline shows the evolution of the DWFTB laterally (north-south), this section is idealised to indicate interactions between two growing DWFTB systems. The upper surface of the box model shows the lateral growth and interaction of structures on the seabed as well as their influence on sedimentation through the creation of accommodation space. The model is composed of six figures (Figure 7.6 -11) presenting the evolution of two DWFTB systems:

a) Figure 7.6 presents a simple shelf margin with an aggradational geometry pre the formation of DWFTBs. Three thick shale horizons are present in the shelf, the lower two represent base of slope systems that extend along the full length of the margin, and the upper horizon is a maximum flooding surface, which thins out towards the north as indicated in the idealised crossline. The thick shale horizons are assumed to be overpressured and are thus ideal décollement horizons. The sediments above the thick shale horizons are assumed to have undergone vertical compaction through burial but are otherwise homogenous. These features represent the pre-kinematic phase of a margins observed development. Dependent upon which part of the study area this is equivalent to the megasequences in the: Aptian – Cenomanian in the north, the early Turonian- Campanian in the centre and the Maastrichtian in the south.

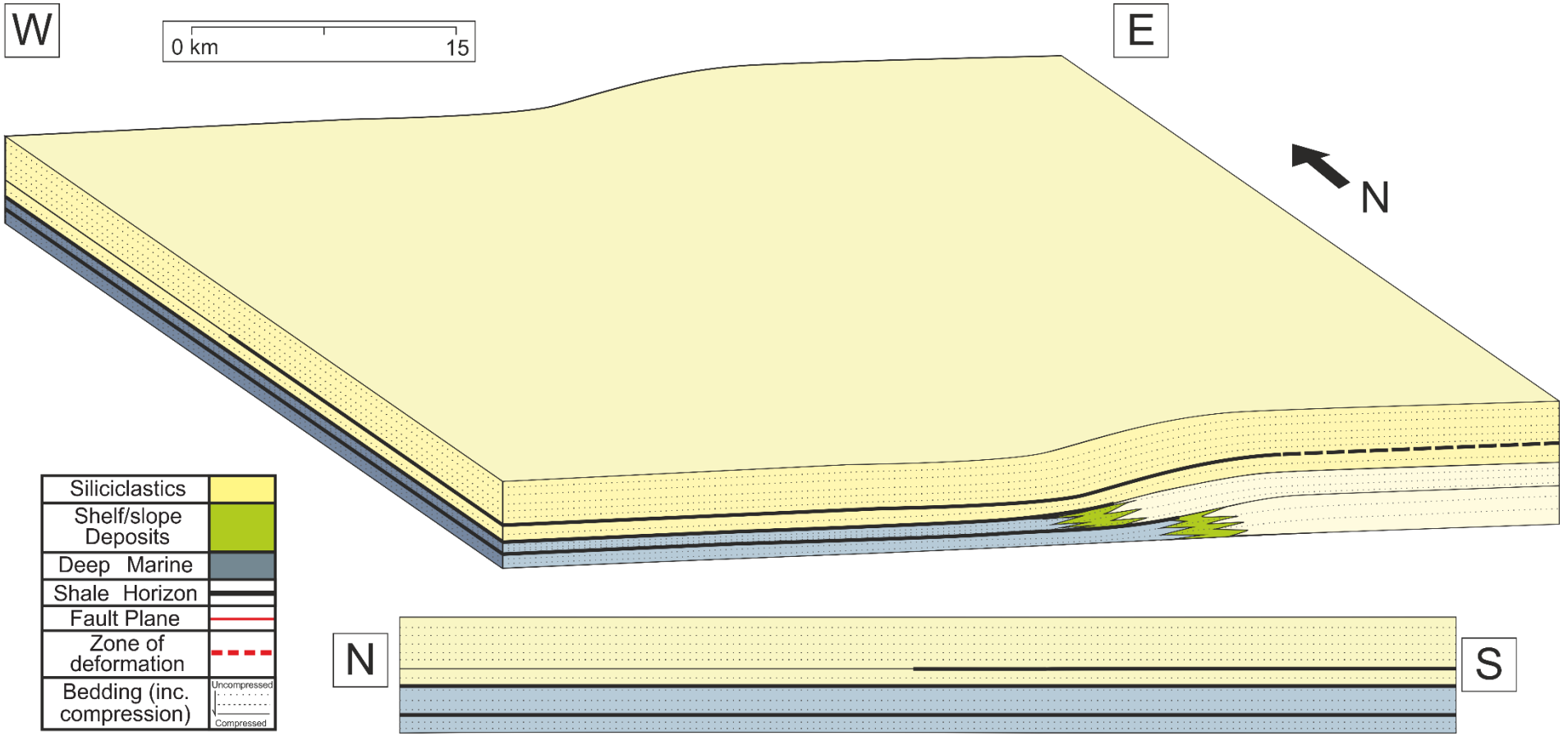

Figure 7.6. 3D Box model of a shelf margin presenting an inline section perpendicular to the margin and an idealised crossline. This is how the margin appears prior to the development of a gravitational instability

b) Figure 7.7 presents the earliest phase of DWFTB initiation. It assumes the margin presented in Figure 7.6 has undergone and is undergoing gravitationally induced deformation either due to uplift of the continental shelf or significant increases in the rate of sedimentation. Deformation initiates with the formation of a single normal fault located near the shelf margin. The fault will initially have a small displacement likely controlled by the ability for sediment in the hangingwall to compact, as discussed in Chapter 5 and seen in Figure 5.4. This compaction is absorbed by the formation of 2nd order structures (Chapter 6), as indicated by the minor thrust and fold seen in Figure 6.5 and 6.8, and by lateral compaction, as indicated by the change in line style from spaced dots to dashed lines to continuous lines. The dashed red line on the surface indicates that deformation is concentrated in the hangingwall of the normal fault and tapers towards the fault tip as compaction reduces relative to the reducing displacement on the fault. Displacement on the normal fault has created accommodation space on the seabed as well as forming a footwall scarp which will apply controls on the location of post and syn-kinematic sedimentation on the margin. This section most closely reflects the sections in Figures 3.6 a & g, 5.4 and Figure 7.3, Inline 1 & 5.

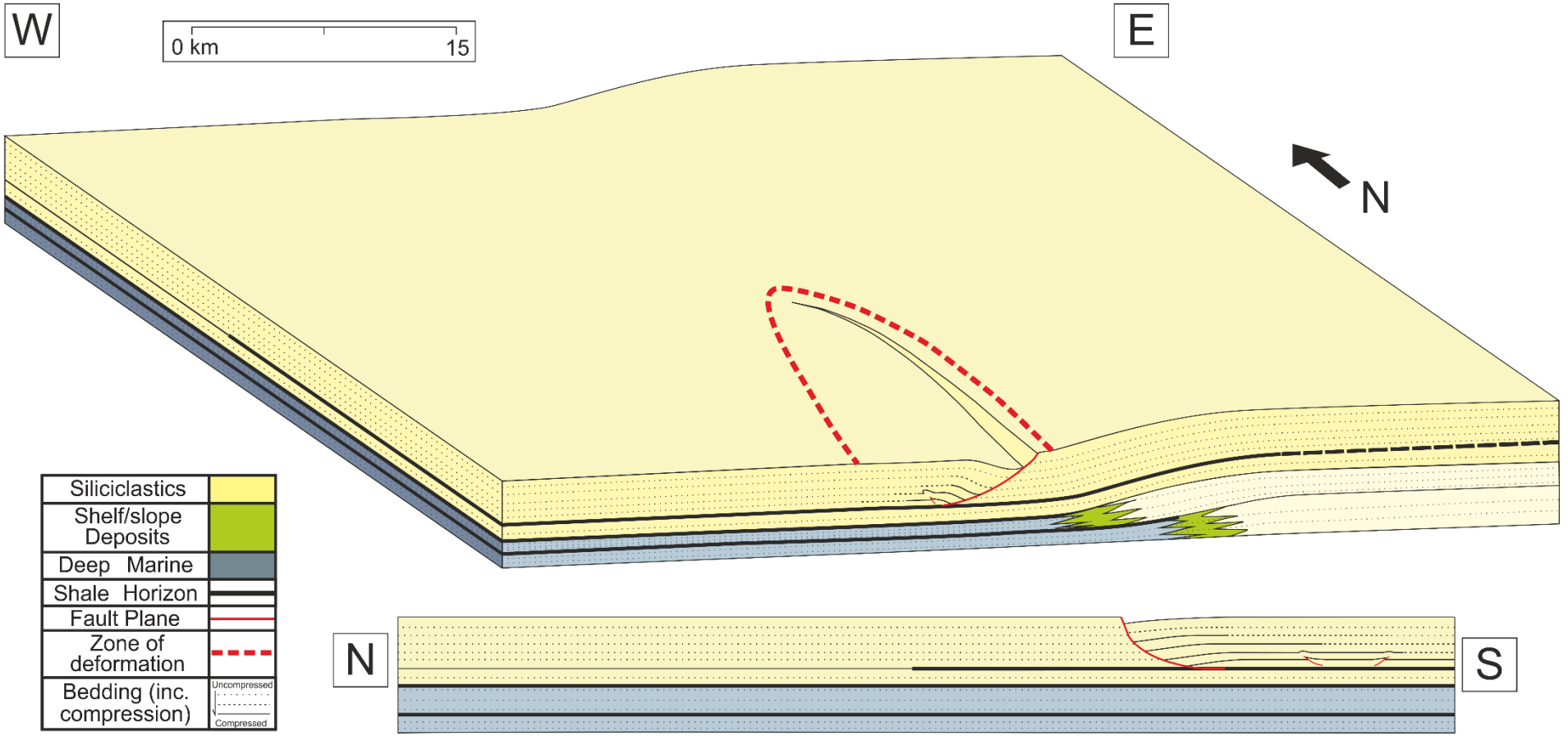

Figure 7.7. 3D Box model of shelf margin undergoing deformation due to the formation of a gravitational instability. Showing the formation of a single normal fault in the earliest phase of DWFTB development and its subsequent impact of the margins geometry.

c) In Figure 7.8, the effects of continued deformation on the margin as indicated by the formation of an additional normal fault that initiated and grew proximal to the active primary fault from Figure 7 7. As the new fault has grown it has compacted the sediment in the footwall of the primary fault. These faults coalesce onto a single advantageous slip horizon or décollement, these faults form the extensional domain of a DWFTB. The accommodation space created by the displacement on the normal faults has been filled by incoming syn-kinematic sediments indicate by growth packages. The sediments ahead of the extensional domain have continued to compact above the detachment horizon until the extensional strain could no longer be accommodated through internal compaction, which lead to the formation of a thrust. This thrust forms the contractional domain of this DWFTB at this point the inline section produced is analogous to the regional shale décollement model proposed by Krueger and Gilbert (2009). The propagation of the thrust has folded the overlying horizons and formed a pericline on the surface. Syn-kinematic sediments thin onto the uplifting pericline indicating the rate of sedimentation is higher than the rate of uplift caused by the folding. Though this also indicates the pericline is applying a control on sedimentation within the basin. The simplistic inline cross-section seen in Figure 7.7 would be replicated if a section were to be put through the northern part of the DWFTB. This shows that progressive increases in displacement in the extensional domain leads to lateral increases in the length of the fault, which initially grows through outboard compaction of sediments in the footwall as discussed in Chapter 5. This means the extensional domain grows laterally along the margin more rapidly than the compressional domain. The model in this Figure most closely matches the sections from Figures 1.2, 3.6 b & d and 5.5.

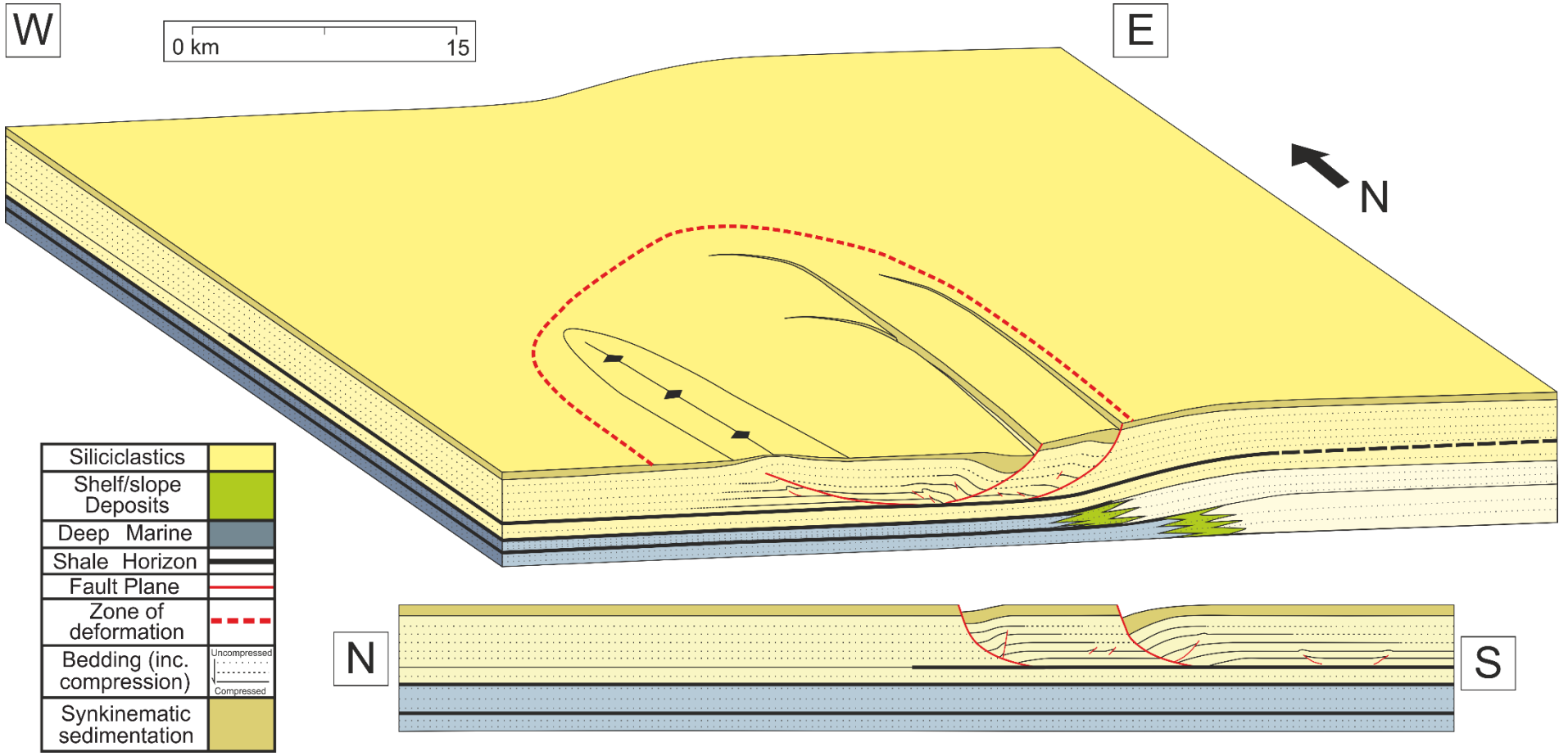

Figure 7.8. 3D Box model of shelf margin from Figure 7.7 undergoing continued gravitationally induced deformation. A second fault has formed along with a thrust fault causing changes to the seabed geometry

d) In Figure 7.9, the gravitational strain has been maintained causing the normal faults to continue to grow and new normal faults to form progressively more proximal to the basin. A counter regional antithetic fault has formed at the top of one of the extensional faults creating a mini basin at the top of the fault block exerting a further control on sedimentation. The most proximal normal fault has detached onto a lower base of slope shale horizon. The strain required to deform sediments above the upper detachment must be higher than that required to deform the underlying under-compacted sediments at this time making propagation along the lower detachment more favourable. Thrusts continue to propagate and initiate progressively more distal to the DWFTB. The faults in the extensional and contractional domain continue to grow northwards parallel to the margin, increasing the strain on relatively under-compacted sediments parallel to our inline section. This means parallel sections made through the flanks of a DWFTB will display progressively more simplistic earlier phases of DWFTB development as discussed in Chapter 5 and seen in Figure 5.4-9 and 7.3.

The gravitational stresses that produce DWFTBs are commonly regional. It is therefore likely that multiple separate DWFTB systems will form simultaneously along a single margin. As each of these discrete DWFTBs grow and expand along the margin they will interact with each other. In this figure we can see a northerly DWFTB (in blue) growing southwards towards the southern system (in red). The crossline shows the dip of the normal faults in the northerly and southerly DWFTBs have opposing orientations, with the northerly DWFTB faults dipping north and the faults in the southerly DWFTB dipping south. A region of undeformed sediments persists in-between separating the collapse systems. The inline section in this figure closely resembles the sections seen in Figures 2.1 and 4.10.

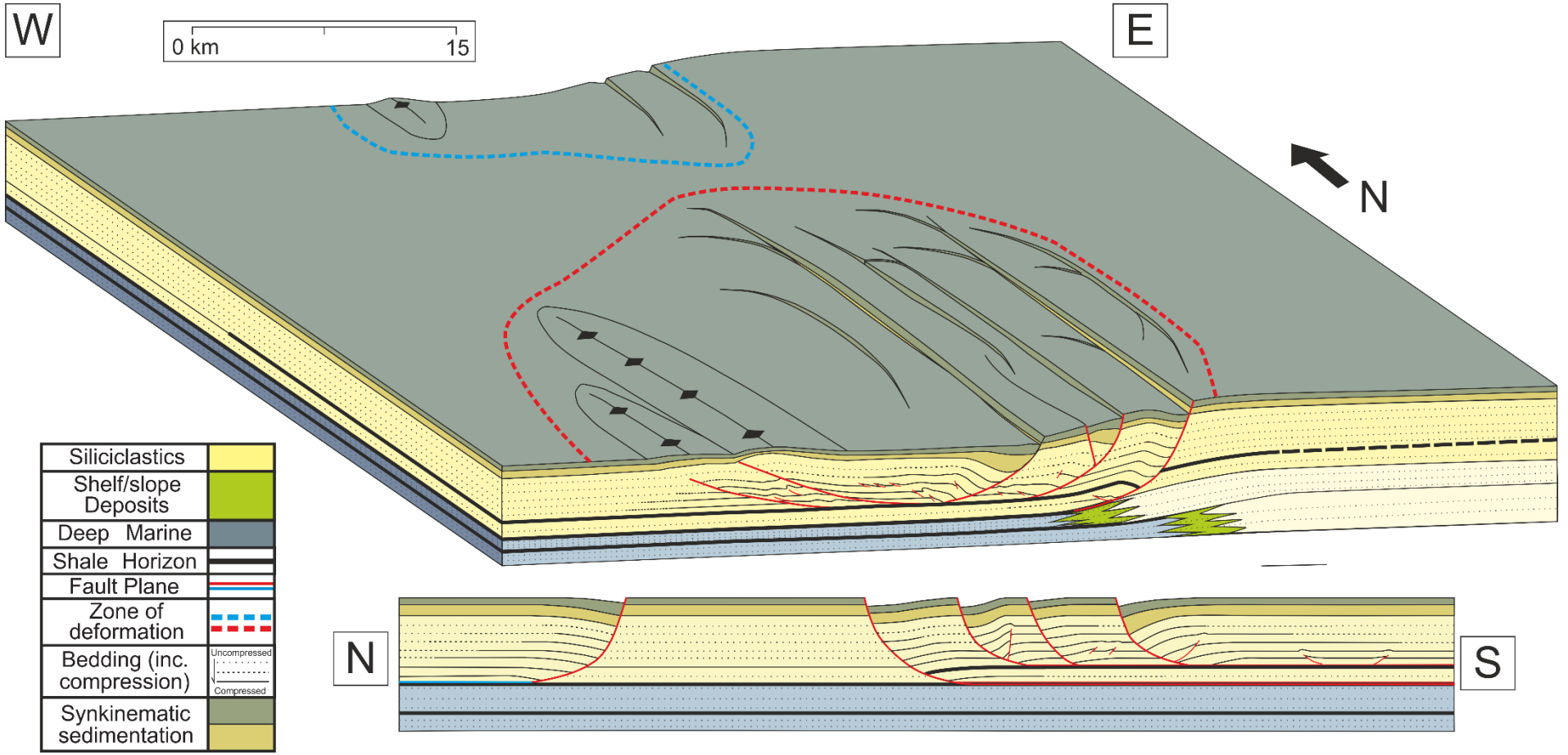

Figure 7.9. 3D box model of shelf margin from Figure 7.8 having undergone continued gravitationally induced deformation. Additional normal faults have formed, one detaching onto a lower base of slope shale horizon a second system has started to grow in the north of the model.

e) In Figure 7.10, the two DWFTB systems from Figure 7.9 are now significantly larger and more complex. The two regions affected by DWFTB induced deformation, defined by their zones of deformation, have now overlapped. The faults on the surface in this overlap zone can be seen truncating one another and begin to form single through going faults, similar to those in DWFTBs in the Otway Basin described by Robson et al. (2016). However, as seen in the crossline the systems are still in part separated by an undeformed region akin to those described as lateral ramps by de Vera et al. (2010) and Scarselli et al. (2016).

A third detachment is also being exploited by the most proximal normal fault in the inline. Switching between décollements may occur where the upper system has locked either due to: the force required to form additional thrust faults being higher than that required to slip on an alternative slip horizon; or local variations in the slip potential of a décollement preventing additional collapse from occurring for example due to dewatering. This has been observed in Figure 5.6 and 5.8 and has been discussed by Briggs et al. (2006).

Continued deformation along the lower detachment first exploited in d) has caused the formation of an underlying thrust that has folded the overlying collapse system, similar to that described in Figure 4.9. Thrusting along the upper detachment has continued to produce periclines on the surface. In the core of two of the periclines the previous syn-kinematic sediments are exposed on the surface, this could either be due to: the erosion of the top of the uplifting periclines: or that the rate of uplift due to fault propagation is outstripping the rate of sedimentation akin to the observations from Figure 4.7. The inline section in this figure most closely resembles the sections seen in Figures 3.6 c & f, 5.6, and 5.8.

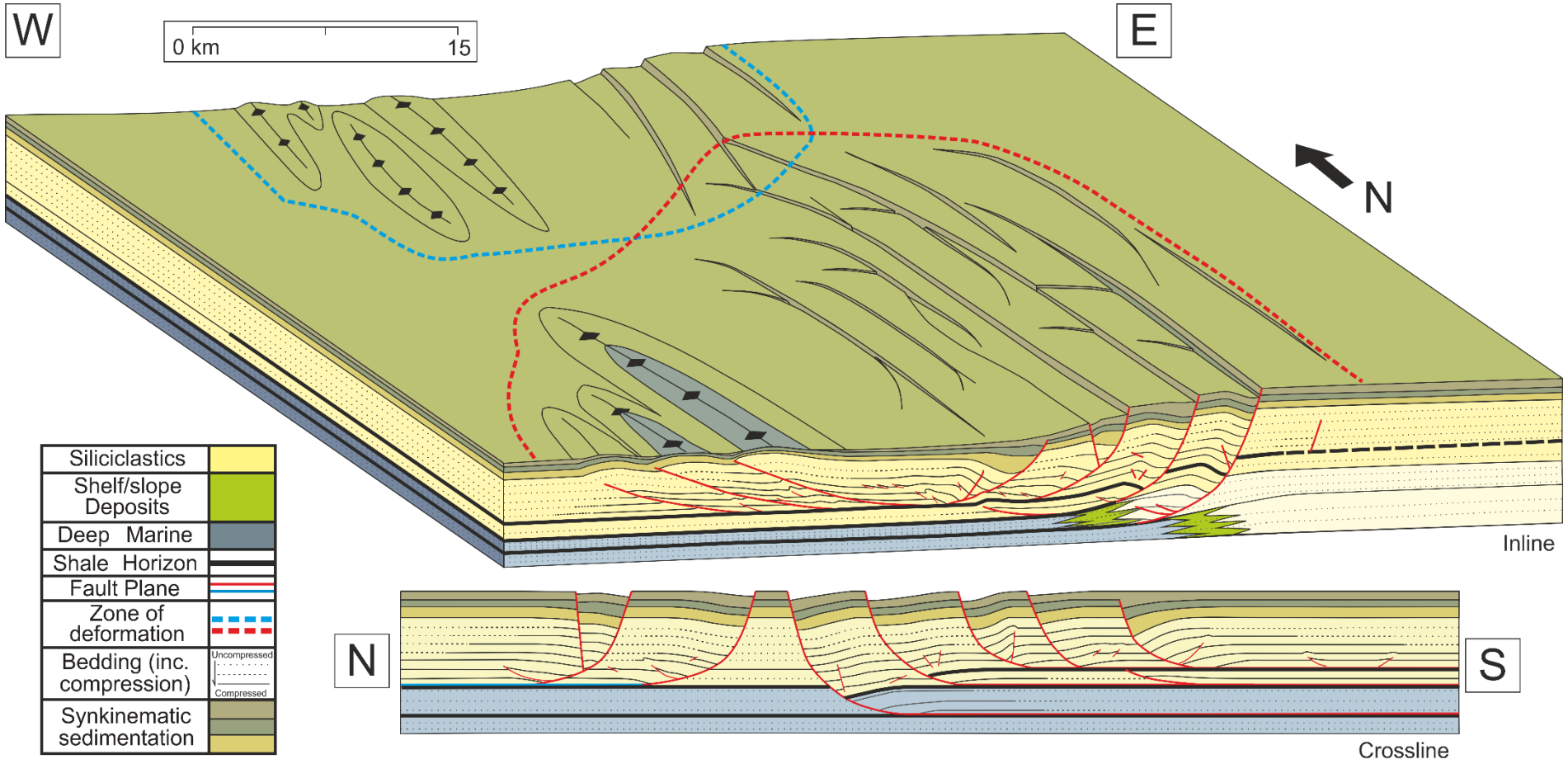

Figure 7.10. 3D box model of shelf margin from Figure 7.9 having undergone continued gravitationally induced deformation. The system continues to get increasing complex with a third detachment being exploited folding of the upper detachment and overlapping of the two DWFTB systems.

f) In Figure 7.11, the two previously separate systems in Figures 7.9 & 10 (blue and red) have now overlapped and amalgamated to form a single DWFTB system (in purple). New extensional faults have formed proximal to the earlier overlapping faults, which are also now through going. New thrust faults have also formed distally of the same overlap, advantaging from the under-compacted sediments present between the original systems. The origin of the two separate collapse systems can now only be implied from the crossline where faults of opposing dips persist and in places crosscut, similar to the sections in Figure 3.5 and Figure 3.15. The crossline also shows the systems exploiting different slip horizons leading to complex interactions between upper and lower décollements. This also creates the undulating décollement surfaces recorded in Figures 3.14, 3.16 and 7.3. It could be argued that rather than describe this as a single DWFTB it is in fact multiple stacked systems, and whilst true, continued deformation renders their separation into discrete systems impossible. Additionally as the system grows outwards, both distally and proximally, new faults form across the previous separation producing a homogenous feature preventing their identification. The overlaps may be within systems that are utilizing the same slip horizon in which case they amalgamate, this is unlike the models proposed by de Vera et al. (2010) and Scarselli et al. (2016) where the systems remain distinct, separated by lateral ramps.

The normal fault which first became active in Figure 7.9 has now ceased slipping on the middle detachment and is now slipping along the upper detachment, akin to the faults observed in Figure 5.7 and those described by Robson et al. (2016) in the Otway Basin. This can be attributed to a loss of overpressure in the middle detachment or an increase in overpressure along the upper detachment leading to more favourable conditions for slip. A thrust has also developed along the lowest detachment horizon which has reused the overlying thrust akin to a thrust in Figure 5.6. The increasing complexity of the fault network and 2nd order structures would lead to significant attenuation of seismic responses, particularly around the oldest extensional faults and lower detachments, a familiar problem presented in Figures 3.14 and 3.18. The inline section in this figure most closely resembles the interpreted sections in Figures 3.6 e, 3.18, 5.7 and 6.10.

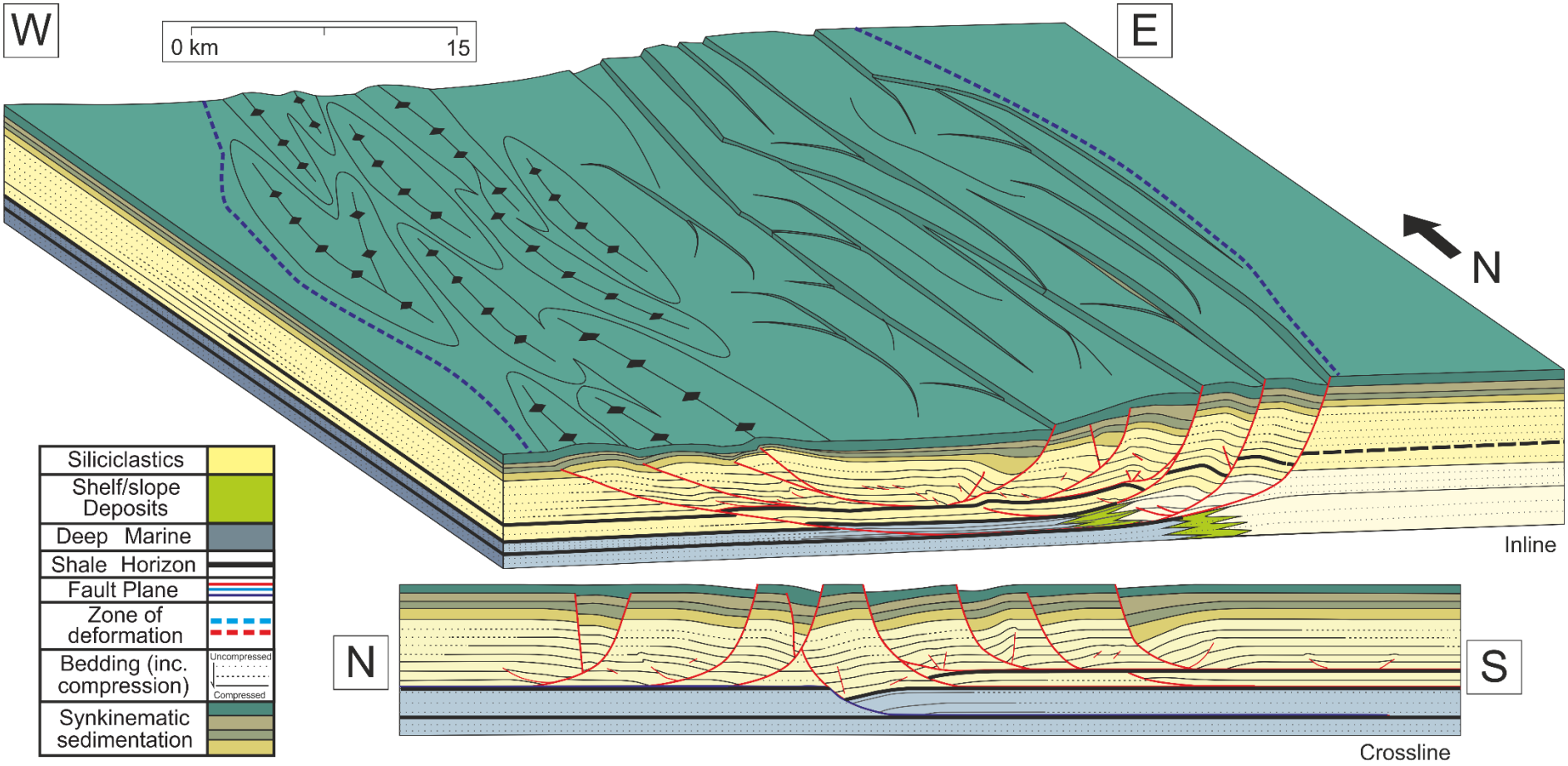

Figure 7.11. 3D box model of shelf margin from Figure 7.10 having undergone continued gravitationally induced deformation. The two DWFTBs have amalgamated to form a single collapse structure on the surface though the crossline shows stacked separate systems. However, the inline shows these multi-level systems are interacting.

Deformation will continue on the margin until the gravitationally instability is equalized by: the cessation of tectonic uplift, or the reduction in rate of sedimentation, or the loss of overpressure on the slip horizon. Reactivations of existing faults may occur locally later as either overpressure is re-established or due to local increases in sedimentation. This model provides an explanation for the broad range of different structures and geometries observed in thin shale detached DWFTBs. It shows how changes in lithology, overpressure and interactions with other systems can change the style of collapse. It also indicates where within DWFTBs sub-seismic features and areas of low permeability and porosity may persist as well as indicate how these structures impact on sedimentation and erosion.

7.5 Conclusions

Each chapter of this thesis has produced its own set of conclusions, what follows is a brief reassertion of the main points:

- Considerable variation exists in the geometry and structure of DWFTBs above thin shale detachments that has not been previously recognized.

- The role of stratigraphy plays a key role in the deformation of DWFTBs, especially the distribution of maximum flooding organic-rich units.

- Despite the huge variation in the geometry and style of collapse, DWFTBs follow a predictable pattern of deformation: extensional faults form in response to a margin imbalance, leading to the compaction of down-dip sediments of the margin, eventually causing the formation of a down-dip thrusts.

- Structural restorations of DWFTBs will produce a missing strain component between up-dip extension and down-dip contraction.

- The compaction phase of DWFTB development is recorded in the imbalance between the extensional and contractional domains and is approximately 5 %.

- The basinward evolution of a section through a DWFTB perpendicular to the transport direction will be reflected in parallel sections through the margin with earlier phases being observable in sections approaching the flanks of DWFTBs.

- Field outcrops of DWFTBs show scalability between structures making them useful as analogues for the interpretation of seismic scale examples.

- Internal compaction of sediments within DWFTBs is taken up by a range of geological processes from grain to grain interactions through to significant folding and thrusting.

- Internal deformation of sediments increases in proportion to the continued deformation of the DWFTB, maintaining ~5% of the total recorded extension.

- Smaller DWFTB systems will interact over time and amalgamate to form larger collapse systems.

- Changes in overpressure and lock-ups on previously advantageous slip planes cause multi-level multiphase collapses to occur over time.

7.6 Further Work

During the research for this project a number of ideas and concepts have been formulated for which time constraints has prevented from reaching fruition. Below are a number of ideas and concepts that could be explored to further this work.

The work in this study has been concentrated on the South African and Namibian margin but many results likely apply to other Type 1a DWFTBs and other systems. In particular internal compaction which likely impacts systems of all types. By using seismic data from other regions and undertaking the same analyses it should be possible to identify 2nd order deformation structures and further quantify the relationship between sediment wedge strength and the size of a DWFTB.

The observed southward shift in the occurrence of DWFTBs identified in this study requires additional research to determine an exact cause or causes. This could involve numerical modelling of the margin, fieldwork looking at paleo incision rates on the Orange River, and the integration of studies on sediment provenance relating to tectonostratigraphic sequences in the basin. This may reveal as yet unrecognized transient tectonic uplift events

Published restorations and this study concentrate on reconstructing the histories and quantifying the deformation on structures along 2D seismic profiles. Using the survey in the far north of the study area it should be possible to undertake a three dimensional volumetric restoration that reveals progressive deformation in the DWFTB occurring at different times. This would also reveal the 3D interplay between faults and how they relate to sedimentation. The interpretation of 3D surveys from the Orange Basin, such as the one presented by Scarselli et al. (2016) would allow exploration of these relationships.

Finally as opposed to looking a DWFTB systems in isolation it would be interesting to look at relationships across entire margins to see what they may reveal about larger scale tectonic processes. It is possible they may be usable as indicators of previously unrecognized regional scale tectonic uplift events.

Chapter 8; References

Ambrose, W. A., Wawrzyniec, T. F., Fouad, K., Sakurai, S., Jennette, D. C., Brown Jr., L. F., Guevara, E. H., Dunlap, D. B., Talukdar, S. C., Garcia, M. A., Romano, U. H., Vega, J. A., Zamora, E. M., Ruiz, H. R., Hernandez, R. C., (2005). Neogene tectonic, stratigraphic and play framework of the southern Laguna Madre-Tuxpan continental shelf Gulf of Mexico: AAPG Bulletin, 89, 725–751, doi: 10.1306/01140504081.

Austin, J. A., Uchupt, E., 1982. Continent-oceanic crustal transition off Southwest Africa. AAPG Bulletin, v.66, p. 1328-1347.

Bangs, N. L., Shipley, T. H., Gulick, S. P. S., Moore, G. F., Kuromoto, S., Nakamura, Y., (2004). Evolution of the Nankai Trough decollement from the trench into the seismogenic zone: Inferences from three-dimensional seismic reflection imaging. *Geology* 32.4 (2004): 273-276.

Bilotti, F., Shaw, J. H., (2005). Deepwater Niger Delta fold and thrust belt modelled as a critical-taper wedge: The influence of elevated basal fluid pressure on structural styles: AAPG Bulletin, 89, 1475–1491, doi: 10.1306/06130505002.

Biju-Duval, B., Le Quellec, P., Mascle A., Renard, V., Valery, P., (1982). Multibeam bathymetric survey and high resolution seismic investigations on the Barbados ridge complex (eastern Caribbean): A key to the knowledge and interpretation of an accretionary wedge. *Tectonophysics* 86.1 (1982): 275-304.

Bischke, R.E., (1994). Interpreting sedimentary growth structures from well log and seismic data (with examples). American Association of Petroleum Geologists Bulletin 78 (6), 873–892.

Bolton, A. J., Maltman, A., (1998). Fluid flow pathways in actively deforming sediments: the role of pore fluid pressures and volume change. Marine and Petroleum Geology 15(4): 281-297, DOI: 10.1015/S0264-8172(98)00025-7.

Bolton, A. J., Clennell, M., Maltman, A., (1999). Nonlinear stress dependence of permeability: A mechanism for episodic fluid flow in accretionary wedges. Geology 27(3), 239-242, DOI: 10.1130/0091-7613.

Bond, C. E., Gibbs, A. D., Shipton, Z. K., Jones, S., (2007). What do you think this is? "Conceptional uncertainty" in geoscience interpretation. GSA Today, V.17, No.11, doi:10.1130/GSAT01711A.1.

Bond, C. E., Lunn, R. J., Shipton, Z. K., Lunn, A. D., (2012). What makes an expert effective at interpreting seismic images? Geological Society of America, Geology v.40: no.1: p.75-78.

Bland, S., Griffiths, P., Hodge, D., A. Ravaglia, A., (2006). Restoring the seismic image. Journal of Society of Petroleum Geophysicists, India, Geohorizons, 18–23.

Briggs, S. E., Davies, R. J., Cartwright, J. A., Morgan, R. (2006). Multiple detachment levels and their control on fold styles in the compressional domain of the deepwater west Niger Delta. Basin Research, 18, 435–450, doi: 10.1111/j.1365-2117.2006.00300.x.

Brognon, G. P., Verrier, (1966). Oil and Geology in Cuanza Basin in Angola. AAPG Bulletin vol. 50, No.1, pp.108-158.

Brooks, J. M., Bryant, W. R., Bernard, B. B., Cameron, N. R., (2000). The nature of Gas hydrates on the Nigerian continental slope. Annals of the New York Academy of Sciences Third International Conference on Gas Hydrates, July 18-22, 1999, Park City, Utah. http://www.tdi-bi.com/our_publications/gas_hydrates/gas_hydrates.html.

Brown Jr., L. F., Benson, J. M., Brink, G. J., Doherty, S., Jollands, E. H., Jungslager, A., Keenen, A., Muntingh, A., van Wyk, N. J. S., (1995). Sequence Stratigraphy in Offshore South African Divergent Basins. An Atlas on Exploration for Cretaceous Lowstand Traps Soekor (Pty) Ltd: AAPG Studies in Geology, vol. 41 pp184.

Burke, K., Gunnel, Y., (2008). The African Erosion Surface: A Continental-Scale synthesis of Geomorphology, Tectonics, and Environmental Change over the past 180 million years. The Geological Society of America, Memoir 201, p.66, doi:10.1130/2008.1201.

Butler, R. W. H., Paton, D. A., (2010). Evaluating lateral compaction in deepwater fold and thrust belts: how much are we missing from “nature's sandbox”? : GSA Today 20 (3), 4–10, doi: 10.1130/GSATG77A.1.

Cartwright, J.A., Trudgill, B.D. & Mansfield, C.S. (1995). Fault growth by segment linkage: an explanation for scatter in maximum displacement and trace length data from the Canyonlands Grabens of SE Utah. Journal of Structural Geology, 17, 1319–1326.

Castelltort, S., Pochat, S., Van Den Driessche, J., (2004). Using T–Z plots as a graphical method to infer lithological variations from growth strata. Journal of Structural Geology 26 (8), 1425–1432.

Clemson, J., Cartwright, J., Booth, J., (1997). Structural segmentation and the influence of basement structure on the Namibian passive margin. Journal of the Geological Society, London Vol. 154, pp. 477-482.

Cobbold, P. R., Morgues, R., Boyd, K., (2004). Mechanism of thin skinned detachment in the Amazon assessing the importance of fluid overpressure and hydrocarbon generation. Marine and Petroleum Geology, vol.21, iss.8, p.1013-1025.

Costa, E., Vendeville, B. C. (2002). Experimental insights on the geometry and kinematics of fold-and thrust belts above weak, viscous evaporitic décollement. Journal of Structural Geology, 24, 1729–1739.

Corredor, F., Shaw, J. H., Bilotti, F., (2005). Structural styles in the deep-water fold thrust belts of the Niger Delta: AAPG Bulletin, 89, 753–780, doi: 10.1306/02170504074.

Dahlen, F. A., Suppe, J., Davis, D., (1984). Mechanics of fold-and-thrust belts and accretionary wedges: Cohesive Coulomb Theory. Journal of Geophysics Research, 89(B12), 10087–10101, doi:10.1029/JB089iB12p10087.

Dahlstrom, C. D. A., (1969). Balance cross sections. Canadian Journal of Earth Science, 6, p.743-757.

Dalton, T. J. S., Paton, D. A., Needham, D. T. (2016). The influence of mechanical stratigraphy on multi-layer gravity collapse structures: insights from the Orange Basin, South Africa. In: Sabato, Ceraldi, T., Hodgkinson, R. A. & Backe, G. (eds) Petroleum Geoscience of the West Africa Margin. Geological Society, London, Special Publications, 438. First published online January 19, 2016, http://doi.org/10.1144/SP438.4.

Dalton, T. J. S., Paton, D. A., Needham, D. T., Hodgson, N., (2015). Temporal and spatial evolution of deepwater fold and thrust belts: Implications for quantifying strain imbalance, Interpretation, Vol.3, No. 4. doi: 10.1190/INT-2015-0034.1.

Davis, D., Suppe, J., Dahlen, F. A., (1983). Mechanics of fold-and-thrust belts and accretionary wedges. *Journal of Geophysical Research: Solid Earth* 88.B2 (1983): 1153-1172.

Davis, D. M., Engelder, T., (1985). The role of salt in fold and thrust belts. Tectonophysics 119 p.67-88.

De Jong, K. A., Scholten, R., 1973, (1973). Preface. De Jong, K. A., Scholten, R. (Eds.), Gravity and Tectonics. John Wiley & Sons, New York, PP. IX-XVIII.

De Vera, J., Granado, P., McClay, K., (2010). Structural evolution of the Orange basin gravity-driven system, offshore Namibia: Marine and Petroleum Geology, 27, 223–237, doi: 10.1016/j.marpetgeo.2009.02.003.

Diegel, F. A., Karlo, J. F., Schuster, D. C., Shoup, R. C., Tauvers, P. R., (1995). Cenozoic structural evolution and tectono-stratigraphic framework of the northern Gulf coast continental margin, in Jackson, M. P. A., Roberts, D. G., Snelson, S., eds. Salt tectonics: a global perspective: AAPG Memoir 65, p. 109–151.

Dreyer, T., Corregidor, J., Arbues, P., Puigdefabregas, C. (1999). Architecture of the tectonically influenced Sobrarbe deltaic complex in the Ainsa Basin, northern Spain, *Sedimentary Geology,* 127, 127-169.

Deville, E., Mascle, A., Callec, Y., Huyghe, P., Lallemant, S. Lerat, O., Mathieu, X., Padron de Carillo, C., Patriat, M., Pichot, T., Loubrieux, B., Granjeon, D., (2015). Tectonics and sedimentation interactions in the east Caribbean subduction zone: an overview from

the Orinoco delta and the Barbados accretionary prism. *Marine and Petroleum Geology* 64 (2015): 76-103.

Deptuck, M. E., Kendell, K., Smith, P., (2009). Complex deep-water fold-belts in the SW Sable Sub-basin, offshore Nova Scotia. Frontiers innovation: Presented at the CSPG CSEG CWLS Convention.

Duval, B., Cramez, C., Jackson, M. P. A., (1992). Raft tectonics in the Kwanza Basin, Angola. Marine and Petroleum Geology, v.9, p.389-404.

Fillon, C., Huismans, R. S., van der Beek, P. (2013), Syntectonic sedimentation effects on the growth of fold-and-thrust belts Geology, January 2013, v. 41, p. 83-86, first published on October 15, 2012, doi:10.1130/G33531.1.

Franke, D., Barckhausen, U., Heyde, I., Tingay, M., Ramli, N., (2008). Seismic images of a collision zone offshore NW Sabah/Borneo. *Marine and Petroleum Geology* 25.7 (2008): 606-624.

Futalan, K., Mitchell, A., Amos, K., Backe, G. (2012). Seismic facies analysis and structural interpretation of the Sandakan sub-basin, Sulu Sea, Philippines. Search and Discovery article #30254.

Gerrard, T., Smith, G. C., (1982). Post-Palaeozoic succession and structure of the south-western African continental margin. In: Watkins, J. S. & Drake, C. L. (eds) Studies in Continental Margin Geology. AAPG Memoir, 34, 49–74.

Gonzalez-Mieres, R., Suppe, J., (2006). Relief and shortening in detachment folds. Journal of Structural Geology, v.28, p.1785-1807.

Granado, P., de Vera, J., McClay, K. R., (2009). Tectonostratigraphic evolution of the Orange Basin, SW Africa. Trabajos de Geologia, Univerisdad del Oviedo, 29: p321-328.

Hardy, S., Poblet, J., McClay, K., Waltham, D., (1996). Mathematical modelling of growth strata associated with fault-related fold structures, in P. G. Buchanan and D. A. Nieuwland, eds., Modern developments in structural interpretation, Validation and modelling: Geological Society of London Special Publication 99, p. 265–282.

Hesse, S., Back, S., Franke, D. (2010). "The structural evolution of folds in a deepwater fold and thrust belt–a case study from the Sabah continental margin offshore NW Borneo, SE Asia." *Marine and Petroleum Geology* 27.2 (2010): 442-454.

Hesthammer, J., Fossen, H., (1999). Evolution and geometries of gravitational collapse structures with examples from the Statfjord Field, northern North Sea: Marine and Petroleum Geology, 16, 259–281, doi: 10.1016/S0264-8172(98)00071-3.

Hirsch, K. K., Scheck-Wenderoth, M., van Wees, J. D., Kuhlmann, G. & Paton, D. A., (2010). Tectonic subsidence history and thermal evolution of the Orange Basin. Marine and Petroleum Geology, 27, 565–584.

Homza, T. X., Wallace, W. K., (1995). Geometric and kinematic models for detachment folds with fixed and variable detachment depths. Journal of Structural Geology, vol.17, no.4, pp.575-588.

Hubbert, M. K., Rubey, W. W., (1959). Role of fluid pressure in mechanics of overthrust faulting: 1. Mechanics of Fluid-filled solids and its application to overthrust fault, Bulletin of the Geological Society of America, Vol. 70, pp. 115-166.

Hudec, M. R., Jackson, M. P. A., (2004). Regional restoration across the Kwanza Basin, Angola: Salt tectonics triggered by repeated uplift of a metastable passive margin: AAPG Bulletin, 88, 971–990, doi: 10.1306/02050403061.

Imber, J., Childs, C., Nell, P. A. R., Walsh, J. J., Hodgetts, D., Flint, S., (2003). Hanging wall fault kinematics and footwall collapse in listric growth fault systems. Journal of Structural Geology, Vol. 25, P.197-208, doi;10.1016/S0191-8141(02)00034-2.

Jackson, M. P. A., Hudec, M. R., Jennette, D. C., Kilby, R. E., (2008). Evolution of the Cretaceous Astrid thrust belt in the ultra deep-water Lower Congo Basin, Gabon: AAPG Bulletin, 92, 487–511, doi: 10.1306/12030707074.

Jackson, C.A-L., Rotevatn, A., (2013). 3D seismic analysis of the structure and evolution of a salt-influenced normal fault zone: a test of competing fault growth models. Journal of Structural Geology, 54, 215–234

Jackson, C. A-L., Bell, R. E., Rotevatn, A., Tvedt, A. B. M., (2017). Techniques to determine the kinematics of synsedimentary normal faults and implications for fault growth models. Geometry and Growth of Normal Faults (Eds. C. C. Childs, R. E. Holdsworth, C. A.-L. Jackson, T. Manzocchi, J. J. Walsh and G. Yielding). *Geological Society of London Special Publications*, 439. doi:10.1144/SP439.22.

Jungslager, E. H. A. (1999). Petroleum habitats of the Atlantic margin of South Africa. In: Cameron, N. R., Bate, R. H. & Clure, V. S. (eds) The Oil and Gas Habitats of the South Atlantic. Geological Society, London, Special Publications, 153, 153–168, http://doi.org/10.1144/GSL.SP.1999.153.01.10.

Khani, H. F., Back, S., (2012). Temporal and lateral variation in the development of growth faults and growth strata in western Niger Delta, Nigeria. AAPG Bulletin, v.94, no.4, pp.595-614.

Khani, H. F., Back, S., (2015). The influence of pre-existing structure on the growth of syn-sedimentary normal faults in a deltaic setting, Niger Delta. Journal of Structural Geology, vol.73, p.18-32, doi:10.1016/j.jsg.2015.01.011.

Klaucke, I., Berndt, C., Crutchley, G., Chi, W. C., Lin, S., Muff, S., (2016). Fluid venting and seepage at accretionary ridges: the Four Way Closure Ridge offshore SW Taiwan. Geo-Marine Letters 36: 16 pp. 165-174. DOI 10.1007/s00367-015-0431-5.

King, R., C., Backe, G., (2010). A balanced 2D structural model of the Hammerhead Delta deepwater fold and thrust belt, Bight Basin, Australia. Australian Journal of Earth Sciences, 57:7, 1005-1012, doi:10.1080/08120099.2010.509409.

King, R. C., Backe, G., Morley, C. K., Hillis, R. R., Tingay, M. R. P., (2010). Balancing deformation in NW Borneo: Quantifying plate-scale vs. gravitational tectonics in a delta and deepwater fold-thrust belt system. *Marine and Petroleum Geology* 27.1 (2010): 238-246.

Koopmann, H., Franke, D., Schreckenberger, B., Schulz, H., Hartwig, A., Stollhofen, H., di Primio, R., (2013). Segmentation and volcano-tectonic characteristics along the SW Afircan continental margin, South Atlantic, as derived from multichannel seismic and potential field data. Marine and Petroleum Geology, v.50, p.22-39, doi:10.1016/j.marpetgeo.2013.10.016.

Koopmann, H., Schreckenberger, B., Franke, D., Becker, K., Schnabel, M., (2014). The late rifting phase and continental break-up of southern South Atlantic: the mode and timing of volcanic rifting and formation of earliest oceanic crust. In: Wright, T.J., Ayele, A., Ferguson, D.J., Kidane, T. & Vye-Brown, C. (eds) Magmatic Rifting and Active Volcanism. Geological Society, London, Special Publications, 420. First published online December 18, 2014, http://doi.org/10.1144/SP420.2.

Koyi, H. A., Vendeville, B. C., (2003). The effect of décollement dip on geometry and kinematics of model accretionary wedges. Journal of Structural Geology, Vol.25 P.1445-1450, doi:10.1016/S0191-8141(02)00202-x.

Krueger, A. C. V. A., Gilbert, E. (2006). Mechanics and kinematics of back thrusting in deep water fold-thrust belts – observations from the Niger Delta (abstract). 2006 AAPG Annual Meeting, Houston, TX, USA, Abstracts Volume, 15, 58.

Krueger, A. C. V. A., Gilbert, E. (2009). Deepwater fold-thrust belts: not all the beasts are equal. AAPG Datapages/Search and Discovery, Article #30085. http://www.searchanddiscovery.com/documents/2009/30085krueger/index.html.

Lickorish, W. H., Ford, M. (1998). Sequential restoration of the external Alpine Digne thrust system, SE France, constrained by kinematic data and synorogenic sediments, in Cenozoic Foreland Basins of Western Europe: Geological Society of London, Special Publications 134, 189–211.

Light, M. P. R., Maslanyj, M. P., Greenwood, R. J., Banks, N. L. (1993). Seismic sequence stratigraphy and tectonics offshore Namibia. In: Williams, G. D. & Dobb, A. (eds) Tectonics and Seismic Sequence Stratigraphy. Geological Society, London, Special Publications, 71, 163–191, http://doi.org/10.1144/GSL.SP.1993.071.01.08.

Lopez-Mir, B., Muñoz, J. A., García-Senz, J. (2014). Restoration of basins driven by extension and salt tectonics: example from the Cotiella Basin in the central Pyrenees. Journal of structural geology 69, 147-162.

Lopez-Mir, B., Muñoz, J. A., García-Senz, J. (2015). Extensional salt tectonics in the partially inverted Cotiella post-rift basin (south-central Pyrenees): structure and evolution. Int J Earth Sci. (Geol Rundsch) 104:419-434. doi 10.1007/s00531-014-1091-9.

Mahanjane, E. S., Franke, D., (2014). The Rovuma Delta deep water fold and thrust belt, offshore Mozambique. Tectonophysics 614 p91-99, doi.10.1016/j.tecto.2013.12.017.

Maltman, A. J., (1998). Deformation structures from the toes of active accretionary prisms. Journal of the geological society, London Vol. 155, pp. 639-650, DOI: 10.1144/gsjgs.155.4.0639.

Maltman, A. J., Bolton, A., (2003). How sediments become mobilized. Geological Society London Special Publications v.216, p. 9-20, doi.10.1144/GSL.SP.2003.216.01.02.

Maltman, A. J., Labaume, P., Housen, B., (1997). Structural geology of the décollement at the toe of the Barbados accretionary prism. Ed's Shipley, T. H., Ogawa, Y., Blum, P., Bahr, J. M. Proceedings of the Ocean Drilling Program, Scientific Results, Vol. 156, DOI: 102973/odp.proc.sr.156.037.1997.

Maslanyj, M. P., Light, M. P. R., Greenwood, R. J., Banks, N. L. (1992). Extension tectonics offshore Namibia evidence for passive rifting in the South Atlantic. Marine and Petroleum Geology Vol. 9, P. 590-601.

McClay, K., Muñoz, J. A., García-Senz, J. (2004). Extensional salt tectonics in a contractional orogen: a newly identified tectonic event in the Spanish Pyrenees, Geology 32(9):737–740. doi:10.1130/G20565.1.

McGilvery, T. A., Cook, D. L., (2003). The influence of local gradients on accommodation space and linked depositional elements across a stepped slope profile, Offshore Brunei. Shelf margin deltas and linked down slope petroleum systems: global significance and future exploration potential, GCSSEMP Foundation 23rd Annual Bob F. Perkins Research Conference, pp. 387‑419.

McGilvery, T. A. and Cook, D. L. (2004). Depositional elements of the slope/basin depositional system offshore Brunei. Proceedings of the Indonesia Petroleum Association Meeting, 7–8 December, Jakarta, Indonesia, 407–420.

McMillan, I. K., (2003). Forminiferally defined biostratigraphic episodes and sedimentation pattern of the Cretaceous drift succession (Early Barremian to Late Maastrictian) in seven basins on the South African and Namibian continental margin. South African Journal of science, issue 11 & 12 p.537-576.

Mello, M. R., Filho, N. D. A., Bender, A. A., Barbnti, S. M., Mohriak, W., Schmitt, P., De Jesus, C. L. C. (2012). The Namibian and Brazilian southern South Atlantic petroleum systems: are they comparable analogues? GSL Special Publications 10.1144/SP369.18.

Mohammed, M. M. (2013). Stratal Architecture and structural evolution of the Orange Basin, offshore Namibia: Implications on hydrocarbon prospectivity. PhD thesis, School of Earth and Environment, University of Leeds.

Mohammed, M., Paton, D. A., Collier, R. E. L., Hodgson, N., Negonga, M., (2016). Interaction of crustal heterogeneity and lithospheric process in determining passive margin architecture on the Namibian margin. In: Sabato Ceraldi, T., Hodgkinson, R. A. & Backe, G. (eds) Petroleum Geoscience of the West Africa Margin. Geological Society, London, Special Publications, 438, http://doi.org/10.1144/SP438.9.

Moore, J. C., and Vrolijk, P., (1992). Fluids in accretionary prisms. *Reviews of Geophysics* 30.2 (1992): 113-135.

Morgan, J. K., Karig, D. E., (1995). Kinematics and a balnced and restored cross-section across the toe of the eastern Nankai accretionary prism. Journal of Structural Geology, vol. 17, No.1, pp.31-45.

Morley, C. K. & Guerin, G., (1996). Comparison of gravity-deformation styles and behaviour associated with mobiles shales and salt. Tectonics, 15, 1154–1170.

Morley, C.K., (2002). Evolution of large normal faults: evidence from seismic reflection data. American Association of Petroleum Geologists Bulletin, 86, 961–978.

Morley, C. K., (2007). "Interaction between critical wedge geometry and sediment supply in a deep-water fold belt." Geology 35.2): 139-142.

Morley, C. K., (2009). Geometry of an oblique thrust fault zone in a deepwater fold belt from 3D seismic data. Journal of Structural Geology 31 (12). 1540-1555.

Morley, C. K., King, R., Hillis, R., Tingay, M., Backe, G., (2011). Deepwater fold and thrust belt classification, tectonics, structure and hydrocarbon prospectivity: a review. Earth Science Reviews, 104, 41–91.

Muñoz J. A., (1992). Evolution of a continental collision belt: ECORS- Pyrenees crustal balanced cross-section. K. R. McClay (Ed.), Thrust Tectonics, Chapman & Hall, London, pp. 235-246.

Muñoz, J. A., Beamud, E., Fernández, O., Arbués, P., Dinarès-Turell, J., Poblet, J., (2013). The Ainsa Fold and thrust oblique zone of the Central Pyrenees: kinematics of a curved contractional system from paleomagnetic and structural data. Tectonics 32(5):1142–1175. doi: 10.1002/tect.20070.

Muntingh, A., Brown, L. F. J., (1993). Sequence stratigraphy of petroleum plays, post-rift Cretaceous rocks (lower Aptian to upper Maastrichtian), Orange Basin, South Africa: Siliciclastic sequence stratigraphy: Recent Applications of Siliciclastic Sequence Stratigraphy, in Siliciclastic sequence stratigraphy: Recent developments and applications 58, AAPG, 71–98.

Nürnberg, D., Müller, R. D., (1991). The tectonic evolution of the South Atlantic from Late Jurassic to present. Tectonophysics, 191, 27-53.

Ortiz-Karpf, A., Hodgson D.M., McCaffrey, W. D., (2015). "The role of mass-transport complexes in controlling channel avulsion and the subsequent sediment dispersal patterns on an active margin: the Magdalena Fan, offshore Colombia." *Marine and Petroleum Geology* 64 (2015): 58-75.

Ortiz-Karpf, A., Hodgson, D. M., Jackson, C. A-L., McCaffrey, W. D., (2016). Mass-transport complexes as markers of deep water fold and thrust belt evolution: Insights

from the Southern Magdalena Fan, Offshore Columbia. Basin Research, doi:10.1111/bre.12208.

Paton, D. A., Carr, M., Trudgill, B., Ortner, H., Medewedeff, D. A., (2007). Alpine-scale 3D geospatial modeling: Applying new techniques to old problems. *Geosphere* 3.6 (2007): 527-549.

Paton, D. A., di Primio, R., Kuhlmann, G., van der Spuy, D., Horsfield, B., (2007). Insights into the petroleum system evolution of the southern Orange Basin, South Africa. South African Journal of Geology, 110, 261–274.

Paton, D. A., van der Spuy, D., di Primio, R., Horsfield, B., (2008). Tectonically induced adjustment of passive-margin accommodation space; influence on hydrocarbon potential of the Orange Basin, South Africa: AAPG Bulletin, v. 92, p. 589–609. doi: 10.1306/12280707023.

Paton, D. A., (2012). Post rift deformation of the North East and South Atlantic margins: Are “passive margins” really passive? : in K. M. Busby, ed., Tectonics of sedimentary basins: Recent advances: Wiley, 249–269.

Peel, F. J., C. J., Travis, Hossack, J. R., (1995). Genetic structural provinces and salt tectonics of the Cenozoic offshore US Gulf of Mexico: a preliminary analysis, in Jackson, M. P. A., Roberts, D. G., Snelson, S., eds. Salt Tectonics: a global perspective: AAPG Memoir 65, p.153-175.

Peel, F. J., (2014). The engines of gravity-driven movement on passive margins: Quantifying the relative contributions of spreading v. gravity sliding mechanisms. Tectonophysics, 633, 126–142, http://doi.org/10.1016/j.tecto.2014.06.023.

Pickering, K. T. and J. Corregidor (2005). Mass transport complex and tectonics control on confined basin-floor submarine fans, Middle Eocene, south Spanish Pyrenees, in: D.M. Hodgson, S.S. Flint (Eds.), Submarine Slope Systems: Process and Products, Geological Society Special Publication, vol. 244 (2005), pp. 51–74.

Pickering, K. T. and N. J. Bayliss, (2009). Deconvolving tectono-climatic signals in deep-marine siliciclastics, Eocene Ainsa basin, Spanish Pyrenees: seesaw tectonics versus eustasy. Geology, v.37, pp.203-206 http://dx.doi.org/10.1130/G25261A. 1.

Posamentier, H. W. and Kolla, V., (2003). Seismic geomorphology and stratigraphy of depositional elements in deep-water settings. Journal of Sedimentary Research,

73, 367–388.

Price, R. A., (1981). The Cordilleran foreland thrust and fold belt in the southern Canadian Rocky Mountains, in McClay, K. R., and Price, N. J., eds., Thrust and Nappe Tectonics: London Geological Society Special Publication 9, 427-448.

Ramberg, H., (1981). Gravity, Deformation and the Earths Crustin Theory, Experiments and Geological Application, 2nd Edition. Academic Press, London.

Robertson, P. and Burke, K., (1989). "Evolution of southern Caribbean plate boundary, vicinity of Trinidad and Tobago." *AAPG Bulletin* 73.4 (1989): 490-509.

Robson, A. G., King, R. C., Holford, S. P., (2016). 3D seismic analysis of gravity driven and basement influenced normal fault growth in the deepwater Otway Basin, Australia. Journal of Structural Geology 89, pg. 74-87.

Roe, G. H., Stolar, D. B., Willett, S. D., (2006). Response of a steady-state critical wedge orogen to changes in climate and tectonic forcing. *Geological Society of America Special Papers* 398 (2006): 227-239.

Rowan, M. G., Kligfield, R., (1989). Cross section restoration and balancing as aid to seismic interpretation in extensional terranes. AAPG Bulletin, vol. 73, p. 955-966.

Rowan, M. G., (1993). A systematic technique for the sequential restoration of salt structures. Tectonophysics, vol.228, Iss.3-4, p.331-348.

Rowan, M. G., Jackson, M. P. A., Trudgill, B. D., (1999). Salt related fault families and fault welds in the northern Gulf of Mexico. AAPG Bulletin, v.83, No. 9, p.1454-1484.

Rowan, M. G., Peel, F. J., Vendeville, B. C. (2004). Gravity-driven fold belts on passive margins. In: McClay, K. R. (ed.) Thrust Tectonics and Hydrocarbon Systems. AAPG Memoir, 82, 157–182.

Saffer, D. M., and Bekins B. A., (1998). Episodic fluid flow in the Nankai accretionary complex: Timescale, geochemistry, flow rates, and fluid budget. *Journal of Geophysical Research: Solid Earth* 103.B12 (1998): 30351-30370.

Saffer, D. M. and Bekins, B. A., (2001). Hydrologic controls on the morphology and mechanics of accretionary wedges. Geology, March, 2002, v. 30, p. 271-274, doi: 10.1130/00917613.

Sapin, F., Ringenbach, J-C., Rives T., Pubellier, M., (2012). Counter regional normal faults in shale-dominated deltas: Origin, mechanism and evolution. Marine and Petroleum Geology, vol.37, iss.1, p.121-128.

Scarselli, N., McClay, K., Elders, C., (2016). Seismic geomorphology Cretaceous megaslides offshore Namibia (Orange Basin): Insights into segmentation and degradation of gravity-driven linked systems. Marine and Petroleum Geology, vol. 75, p. 151-180, doi: 10.1016/j.marpetgeo.2016.03.012.

Serica Energy, (2014). The Namibian Atlantic margin south of the Walvis Ridge: piecing together the jigsaw of a potentially prospective new frontier. Tuesday 18th November 2014, PETEX 2014 Conference, London. http://www.serica-energy.com/downloads/presentations/PETEX%20Tues_18th_Nov_2014.pdf.

Shaw, J. H., Novoa, E., Connors, C. D., (2004). Structural controls on growth stratigraphy in contractional fault-related folds. In McClay, K. R. ed. Thrust tectonics and hydrocarbon systems AAPG Memoir 82, p.400-412.

Shaw, J. H., Connors, C. D., Suppe, J., (2005a). Seismic Interpretation of Contractional Fault-Related Folds. AAPG Seismic Atlas Studies in Geology #53.

Simpson, G. D. H, (2010). Formation of accretionary prisms influenced by sediment subduction and supplied by sediments from adjacent continents. *Geology* 38.2 (2010): 131-134.

Spikings, A. L**.,** Hodgson D. M., Paton D. A., Spychala Y. T., (2015). Palinspastic restoration of an exhumed deepwater system: A workflow to improve paleogeographic reconstructions*, Interpretation - A Journal of Subsurface Characterization*, 3**,** pp.SAA71-SAA87. doi: 10.1190/INT-2015-0015.1.

Suppe, J., Chou, T. T., Stephen, C. H., (1992). Rates of folding and faulting determined from growth strata in Thrust Tectonics, edited by K. R. McClay, pp 105-122, Chapman and Hall, New York.

Toto, E., and Kellogg, J. N., (1992). Structure of the Sinu-San Jacinto fold belt—An active accretionary prism in northern Colombia. *Journal of South American Earth Sciences* 5.2 (1992): 211-222.

Totterdell, J. M. and Krassay, A. A. (2003). The role of shale deformation and growth faulting in the Late Cretaceous evolution of the Bight Basin, offshore southern Australia. In: Van Rensbergen, P., Hillis, R. R., Maltman, A. J. & Morley, C. K. (eds) Subsurface Sediment Mobilization. Geological Society, London, Special Publications, 216, 429–442, http://doi.org/10.1144/GSL.SP.2003.216.01.28.

Van der Spuy, D., Ziegler, T., Bowyer, M., (2003). Deepwater 2D data reveal Orange Basin objectives off western South Africa. Oil & Gas Journal, 101, 44–49.

Vergés, J., Fernàndez, M., Martínez, A. (2002). The Pyrenean orogen: pre-, syn-, and post-collisional evolution. In: Rosenbaum, G. and Lister, G. S. 2002. Reconstruction of the evolution of the Alpine-Himalayan Orogen. Journal of the Virtual Explorer 08, doi:10.3809/jvirtex.2002.00058.

Vinnels, J. S., Butler, R. W. H, McCaffrey, W. D., Paton, D. A., (2010). Depositional processes across the Sinu accretionary prism, offshore Colombia." *Marine and Petroleum Geology* 27.4 (2010): 794-809.

von Hagke, C., Oncken, O., Evseev, S., (2014). Critical taper analysis reveals lithological control of variations in detachment strength: an analysis of the Alpine basal detachment (Swiss Alps). *Geochemistry, Geophysics, Geosystems* 15.1 (2014): 176-191.

Walsh, J.J. & Watterson, J., (1988). Analysis of the relationship between displacements and dimensions of faults. Journal of Structural Geology, 10, 239–247.

Walsh, J.J., Nicol, A. & Childs, C., (2002). An alternative model for the growth of faults. Journal of Structural Geology, 24, 1669–1675.

Watterson, J., (1986). Fault dimensions, displacement and growth. Pure and Applied Geophysics, 124, 365–373

Welbon, A. I. F., Brockbank, P. J., Brunsden, D., Olsen, T. S. (2007). Characterising and producing from reservoirs in landslides: challenges and opportunities. In: Jolley, S. J., Barr, D., Walsh, J. J. & Knipe, R. J. (eds) Structurally Complex Reservoirs. Geological Society, London, Special Publications, 292, 49–74, http://doi.org/10.1144/SP292.3.

Weijermars, R., Jackson, M. P. A., Vendeville, B., (1993). Rheological and tectonic modelling of salt provinces. Tectonophysics, Volume 217, issue 1-2, P.143-174, doi:10-1016/1951(93)90208-2.

Willett, S. D., Fisher, D., Fuller, C., En-Chao, Y., Chia-Yu, L., (2003). Erosion rates and orogenic-wedge kinematics in Taiwan inferred from fission-track thermochronometry. *Geology* 31.11 (2003): 945-948.

Williams, G. D., (1993). Tectonics and seismic sequence stratigraphy: an introduction. Eds Williams, G. D. & Dobb, A. Geological Society Special Publications No.71, p.1-13.

Wood, A. M., Paton, D. A., Collier, R. E. L., (2015a). The missing complexity in seismically imaged normal faults: what are the implications for geometry and production response? Geological Society, London, Special Publications, 421, 213-230, http://doi.org/10.1144/SP421.12.

Wood, A. M., Paton, D. A., Collier, R. E. L., (2015b). Understanding regional-scale structural uncertainty: The onshore Gulf of Corinth rift as a hydrocarbon exploration analogue. Interpretation, 3(4), http://library.seg.org/doi/abs/10.1190/INT-2015-0046.1.

Chapter 9. Appendix

Part A –

I: Published version of the paper featured in Chapter 4

II: Published version of the paper featured in Chapter 5

III: Published version of the paper featured in Chapter 6

Part B –

I: Larger versions of Sections within the thesis

II: Additional seismic sections

III: Décollement maps

Part C

I: Depth Conversions

II: Restorations

Part A –

I: Published version of the paper featured in Chapter 4

Influence of mechanical stratigraphy on multi-layer gravity collapse structures: insights from the Orange Basin, South Africa

T. J. S. DALTON[1]*, D. A. PATON[1] & D. T. NEEDHAM[2]

[1]*School of Earth and Environment, University of Leeds, Leeds LS2 9JT, UK*

[2]*Needham Geoscience Ltd, 10 Ghyll Wood, Ilkley LS29 9NR, UK*

**Corresponding author (e-mail: T.J.Dalton@leeds.ac.uk)*

Abstract: Gravity collapse structures are common features on passive margins and typically have a tripartite configuration including an updip extensional domain, a transitional domain and a downdip compressional domain with a common detachment underlying the system. A number of studies have classified these systems, yet few document the wide variations in geometry. This study documents the gravity collapse structures of the Namibian and South African Orange Basin; these structures represent some of the best imaged examples of this important process. We first demonstrate the geometry and kinematic evolution of these systems, focusing on examples of the tripartite configuration from a typical collapse. We then highlight the significant variability in the structures of the system and describe features such as cross-cutting in margin-parallel sections, portions of the system with multiple detachments, systems with stacked synchronous detachments and the temporal evolution of faults within the system. By integrating our observations from a number of sections, we present a model explaining the spatial and temporal evolution of the system. This enables us to discuss likely causes of collapse structures and also, by placing the system into a well-constrained stratigraphic context, how the presence of both maximum flooding surfaces and early margin deltaic sequences have a fundamental control on the resulting collapse geometry.

Deep water fold–thrust belts (DWFTBs) and their associated extensional systems occur in many passive margin systems throughout the world and provide an excellent opportunity to study the formation and development of both extensional and compressional faults. A considerable variation in the structural style of collapse systems is seen across different margins and this is generally accepted to result from differences in both the driving mechanisms for collapse and the geometry and nature of the detachment surface (Rowan *et al.* 2004; Krueger & Gilbert 2009; Morley *et al.* 2011).

Morley *et al.* (2011) classified DWFTBs into two broad categories: those controlled by near-field stress systems created by sediment loading and differential uplift/subsidence at passive margins (Type I) and those controlled by far-field stress regimes associated with active margins (Type II). Type I DWFTBs are further divided into Type Ia (shale detachment), such as those in the Orange Basin, and Type Ib (salt detachment), such as in Angola. Krueger & Gilbert (2009) proposed that DWFTBs should be divided into those found on active margins (caused by subduction) and those found on passive margins in a similar manner to the far- and near-field stress systems. Krueger & Gilbert (2009) then subdivided the passive margin systems into three categories based on the nature of their décollement: regional salt, regional shale and local non-discrete, where the local detachments are discontinuous and lead to a regional décollement crossing stratigraphic levels (Fig. 1).

In this study we focused on shale detachment systems that, regardless of the driving mechanism, commonly consist of three domains (Fig. 1): an updip extensional domain dominated by normal faulting; a downdip compressional domain composed of imbricate thrusts and folds; and a transitional domain. The transitional domain (sometimes referred to as the translational domain) is not referred to by all researchers, but is defined as an area between the extensional and compressional domains that is either a package of largely undeformed sediments (Corredor *et al.* 2005; Krueger & Gilbert 2009) or an area in which both compressional and extensional features overprint (Butler & Paton 2010; de Vera *et al.* 2010). This overprint arises from a shift in the location of the point of contact between the compressional and extensional domains. It is often difficult to resolve the internal geometry of the transitional domain because of limited seismic imaging. The basic premise of area balancing during deformation is expected to apply to these coupled systems; however, the work of de Vera *et al.* (2010) and Butler & Paton (2010) in the Orange Basin established an imbalance between the extension and compression domains of up to 25% in favour of extension, leaving a considerable

From: Sabato Ceraldi, T., Hodgkinson, R. A. & Backe, G. (eds) *Petroleum Geoscience of the West Africa Margin*. Geological Society, London, Special Publications, **438**, http://doi.org/10.1144/SP438.4

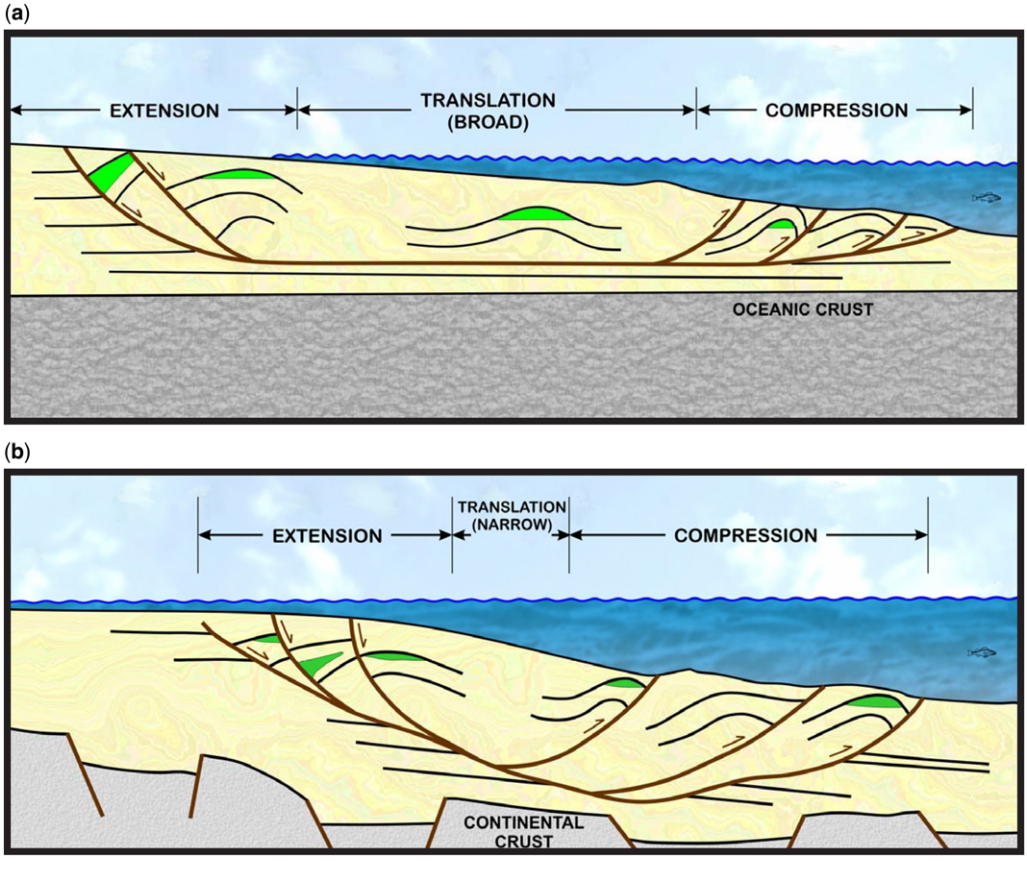

Fig. 1. Model of gravitational collapse (Krueger & Gilbert 2009). (**a**) Typical features and geometry of gravity system controlled by a regional detachment. (**b**) Geometry where no regional décollement is present.

missing component of contractional strain to be explained.

In this study, we looked in detail at the three domains along a typical section from the Orange Basin system and compared them with other portions of the same collapse structure to observe variations along-strike. From these observations we constructed a model to explain the temporal evolution of this important margin process. Finally, we considered how the margin stratigraphy played a critical role in the nature of the deformation and propose that this had a significant and, until now, unrecognized control on this process, which occurs on many passive margins.

Regional setting

The Orange Basin is the southernmost basin on the West African passive margin. It formed during the break-up of Gondwana and subsequent spreading of the South Atlantic Ocean (Muntingh & Brown 1993; Brown *et al.* 1995; Paton *et al.* 2008; Koopmann *et al.* 2014).

It underwent significant rifting during the Late Jurassic to Early Cretaceous, forming graben and half-graben infilled with synrift siliciclastic and lacustrine sediments (Jungslager 1999; Mohammed *et al.* 2015, this volume, in press). This was followed by continental break-up in the Barremian and the establishment of a passive continental margin, onto which a thick post-rift sedimentary sequence was deposited (Gerrard & Smith 1982). The thickness of the post-rift sediments ranges from 3 km in the south and north to up to 5.6 km in the centre of the basin. This sediment was largely sourced from the Orange River (Paton *et al.* 2008) and is broadly separated into two phases: black shales and claystones were deposited during an early drift phase and then a later drift phase deposited a thick succession of interbedded heterolithic sediments composed of shales and claystones

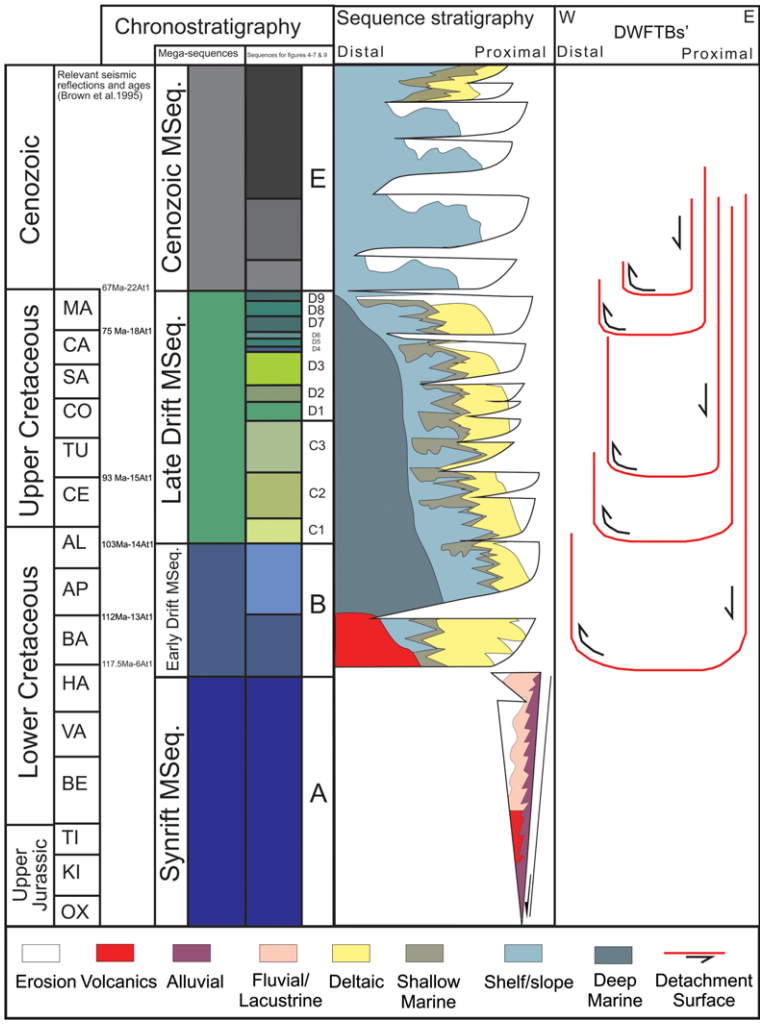

Fig. 2. Chronostratigraphy of Orange Basin adapted from Paton *et al.* (2008) showing the depths to which the deep water fold–thrust belts penetrate across the entire basin.

(Fig. 2). It is within the latter phase that we observed the greatest number of gravity collapse structures. Although much of the margin stratigraphy is claystone, we defined the system as dominated by a shale detachment because the décollement surfaces are shale intervals. These correspond to maximum flooding surfaces, with some identified as proved source rocks (van der Spuy *et al.* 2003). This Cretaceous succession underwent considerable tilting, up to 750 m in the inner margin (Paton *et al.* 2008), at the end of the Maastrichtian to produce a considerable proximal unconformity with the overlying Cenozoic sequence. Most of the Cenozoic sequence was deposited outboard into the basin and varies in thickness from 250 to 450 m on the margin and from 500 to 1400 m on the continental slope and beyond. The hydrocarbon system sequence stratigraphy and deeper structures of the Orange Basin are well established (Light *et al.* 1993; Muntingh & Brown 1993; Paton *et al.* 2007, 2008; Hirsch *et al.* 2010).

Data and methods

This study combined 38 480 km of vintage two-dimensional pre-stack time migration seismic data released by the Petroleum Agency of South Africa with 45 386 km of two-dimensional seismic data from Spectrum (Fig. 3), of which 24 042 km was

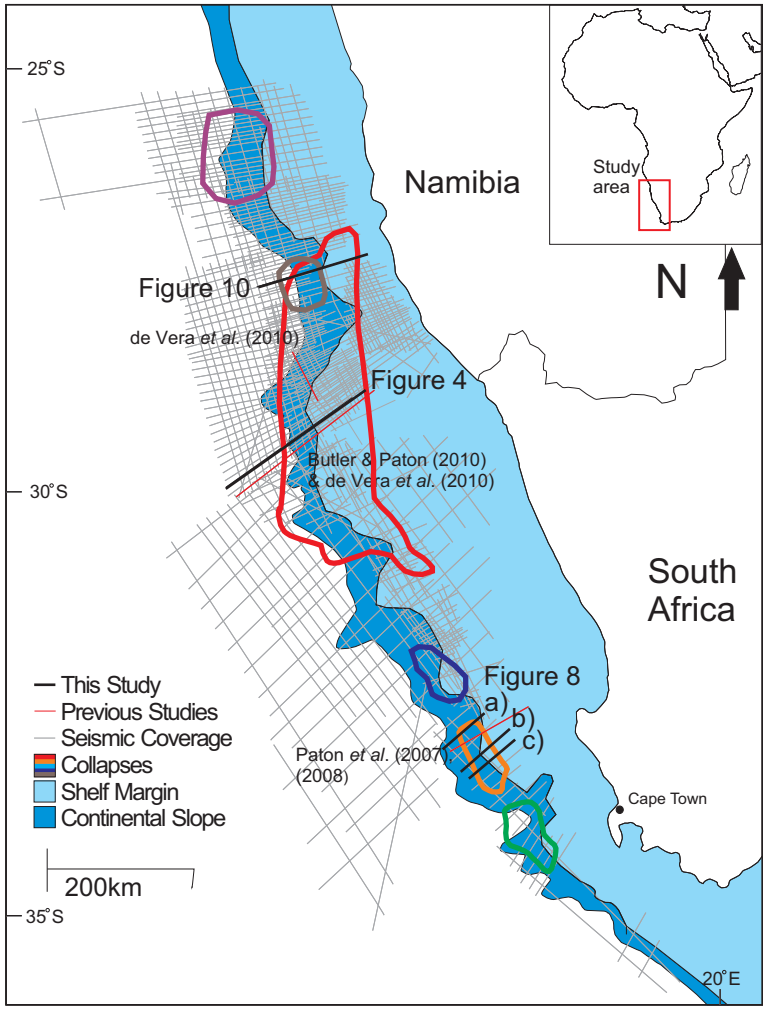

Fig. 3. Map of Orange Basin indicating the location of lines used in this study, the location of lines used in previous studies (Paton *et al.* 2007, 2008; Butler & Paton 2010; de Vera *et al.* 2010) and an outline representing the total data coverage used in this study.

pre-stack depth migration (PSDM) data obtained using fast-track Kirchoff migration. The maximum recording lengths were in the range 7–10 s two-way travel time; the vintage data were acquired between 1976 and 2012 and the Spectrum data were acquired in 2012. The line spacing of this deep seismic coverage was between 8 and 15 km and it provided unprecedented data coverage of the basin and allowed us to review the entire margin (Paton *et al.*, this volume, in press). We present here our interpretations of the Spectrum PSDM seismic lines because these provided better images. Well data for the basin are extensive, although limited to the shelf margin, and have been used in previous studies (e.g. Muntingh & Brown 1993; Paton *et al.* 2008) to define the margin stratigraphy and to define stratigraphic ages for our seismic intervals (Fig. 2). Stratigraphic megasequences and associated regional and local unconformities have been identified using reflection termination, cut-offs and onlap relationships with the sequence stratigraphic system based on the work of Muntingh & Brown (1993).

As we focused on the detailed architecture of the syn-kinematic packages, we subdivided the megasequences into sequences based on variations in the seismic character that indicated changes over time in the depositional or structural environment and rates of deposition. We used a unified

stratigraphic system to define these sequences across the margin (Fig. 2). We defined the packages regionally across the section as megasequences A–E and further subdivided megasequences C and D numerically in a temporal succession. However, because the packages were often isolated, any one section may not show a complete sequence.

Regional sections

We present here a 160 km long east–west-oriented regional seismic profile (Fig. 4) that illustrates both the main structural elements of the margin and one of the simpler collapse structures in the centre of the basin (Fig. 3). This is shown down to a depth of 6.4 km. Based on the previous regional interpretations of Paton *et al.* (2008), we divided the stratigraphy into four megasequences: Synrift, Late Jurassic to Hauterivian (A); Early Drift, Barremian to Aptian (B); Late Drift, Aptian to Maastrichtian (C and D); and Cenozoic (E). To aid the interpretation across the margin, including the structural features and local unconformities, we divided the megasequences into seismic sequences based on the character of internal seismic reflections. Although the synrift packages were imaged in the dataset (Paton *et al.*, this volume, in press), we focused on the sequences stratigraphically above the top-synrift reflection. The top of the synrift package was delineated by a package of high-amplitude parallel reflections, present across the basin, onto which Barremian-age stratigraphy was deposited. In this section, the nature of the contact was represented by an aggradational sequence of reflections conformable with the top of the synrift package. It is important to note that elsewhere in the basin this boundary has a progradational relationship marked by downlapping reflections onto the synrift sediments prior to an aggradational phase. The Late Drift megasequence is deposited conformably on the Early Drift package and is defined by its higher reflectivity.

Evident within this Late Drift megasequence are numerous unconformities represented by the truncation and onlapping of reflections. These unconformities only occur off the palaeoslope margin and are often restricted to fault blocks; they are therefore not regional in extent. Reflections within the centre of this package are both folded and faulted. In the proximal portion of the basin, westwards-dipping normal faults are identified by dislocated packages shifting downdip of one another (eastern end of Fig. 4); this is the extensional portion of the gravity collapse structure. Continuing westwards and downdip, the seismic character becomes increasingly chaotic and complex and we define this as the transition domain. The most distal part of the system, the compressional domain, is characterized by a series of east-dipping thrust faults identifiable by high-amplitude, steeply dipping reflections that appear to be stacking packages on top of one another.

These structural features will be discussed in more detail later; however, it is important to note at this point that although the main décollement for this collapse (red reflection in Fig. 4) is broadly coincident with the top of the Early Drift megasequence, it does not have a constant slope and shows significant changes in the direction and angle of dip. The décollements are picked based on where the faults terminate, as identified through cut-offs and changes in the dip of the reflections. The Late Drift megasequence is capped by a regional truncation at the top of the palaeoshelf picked out by the top of the uppermost green package (Fig. 4), whereas these sequences are conformable at the base of the palaeoslope. The unconformity is, however, still interpretable by a change from a low- to a high-amplitude reflection along this boundary. The Cenozoic package is defined by a change in the location of deposition from proximal to a more distal position on the continental slope. The package is considerably thinner than the Cretaceous sequence on the central margin and thickens significantly to the west. Each of the structural elements is considered in more detail in the following sections.

Extensional domain

To define the structures in more detail, we subdivided the megasequence into a number of sequences (A–E, Fig. 2). Figure 5 shows a typical interpreted section from the upper portions of the extensional system, where the latest faults formed prior to detaching onto a regional décollement. This interpretation focuses on the upper part of the extensional portion of the structure and shows a more detailed breakdown of the Late Drift megasequence (sequences C and D). These packages are defined based on the internal seismic facies and reflection termination and reveal relative changes in sediment supply and fault-controlled accommodation space (Brown *et al.* 1995).

Internally, sequence C3 has an absence of seismic impedance contrast, resulting in only limited internal geometry being imaged, but it is conformable with the high-amplitude reflections at the base of sequence D1 and is truncated by sequence D3. This suggests that D1 was being deposited as the upper portions of C3 were being eroded and that the discontinuity was a direct result of faulting. D3 has a thick package of high-amplitude reflections that allow several horizons to be tracked internally. When restored, sequence D3 forms a westwards-thickening wedge. Changes in spacing between

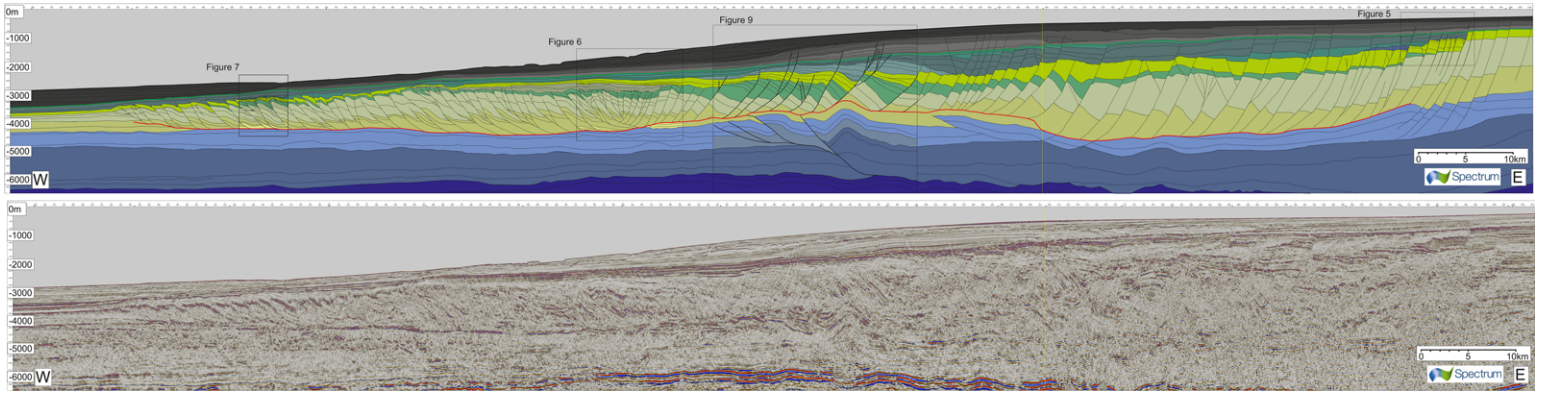

Fig. 4. Pre-stack depth migrated uninterpreted and interpreted sections of Line 1 (see Fig. 3 for location) shown with a vertical exaggeration of 3:1. The colours correspond to each megasequence (Fig. 2). The Synrift megasequence is purple, the Early Drift megasequence is blue, the Late Drift megasequence is green and the Cenozoic megasequence is grey; different shades correspond to discrete packages within each megasequence. The detachments are picked out in red.

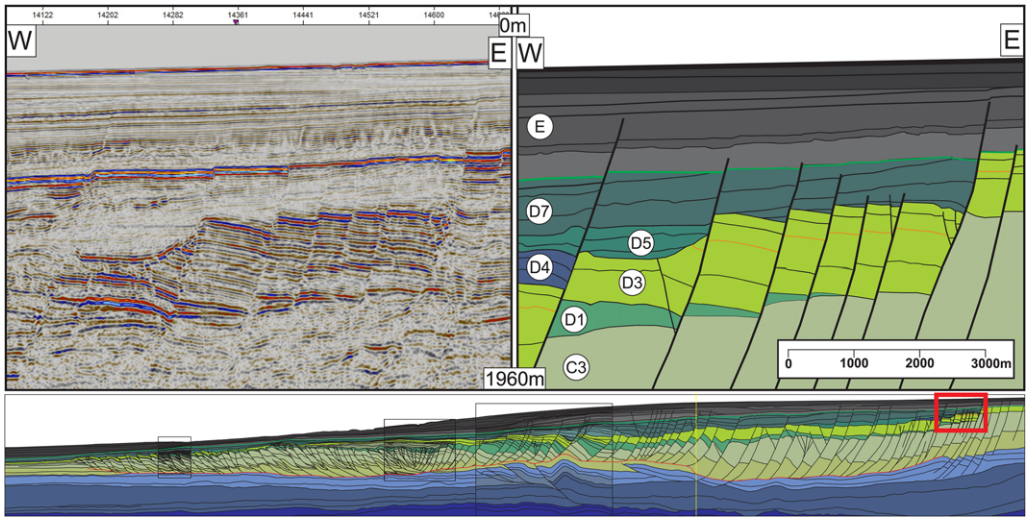

Fig. 5. Detailed interpreted and uninterpreted sections of the extensional domain from Figure 4. Section is vertically exaggerated 3:1.

traceable horizons in D3 show slight changes in thickness along its length, indicating that different faults were active at different points. Of particular note are the small changes in thickness in the packages above and below the orange horizon (Fig. 5), which indicate the movement of small faults in the package between two faults with far larger throws. As the largest thickness changes occur on the faults on which D4 and D7 truncate, this implies that the deformation tends to concentrate onto a few larger, more widely spaced faults – that is, large faults become large and stay large, thus stopping smaller faults from growing. Sequence D4, defined by a package of low-amplitude reflections, reinforces this point. Its presence in only the west of the section abutting a large fault plane implies that it grew more rapidly at this point than faults to the east. This created a larger accommodation space that was rapidly infilled, as indicated by folding of the reflections into the fault. D3 is clearly truncated by the base of sequence D5 with a rugose contact that appears to represent the collapse of the top of the fault block. D5 has chaotic and poorly imaged reflectance that infills the eroded section truncated at the top of D4. As shown in Figure 4, D5 extends for 16 km west of Figure 5 and continues to erode earlier fault blocks. Its chaotic seismic character and erosive base suggest that it is a mass transport complex (MTC). Several similar MTCs can be seen throughout the extensional portion of the collapse features (e.g. Posamentier & Kolla 2003; McGilvery & Cook 2004).

Sequence D7 is defined by a series of reflections that onlap onto the top of D4 and D5 and are clearly imaged on the tops of the fault blocks. This implies that fault movement outstripped sediment supply at this point. It also appears that several of the faults had switched off by this time. As the sediment supply increased and the faults switched off, the sediments began to bury the fault blocks and deformation was again concentrated into the larger faults, where we observed some limited sediment growth into the fault plane. The truncation of D7 by megasequence E – that is, the boundary between the Late Drift and Cenozoic megasequences – can be seen throughout the palaeo-continental margin and the upper palaeoslope. It is unclear how much sediment has been eroded, although Paton *et al.* (2008) suggested it may have been as much as 750 m. Only the two largest faults were active after this unconformity formed, although they offset it with only small throws.

Transitional domain

The section in Figure 6 shows the point at which the extensional domain changed into the compressional domain and indicates that this occurred predominantly within megasequences C and D.

Megasequence B contains the high-amplitude parallel reflections that denote the top of the Early Drift megasequence, although these reflections become less distinct immediately beneath the most deformed section of the transition zone, probably due to signal attenuation. These reflections are composed of coarsening upwards silt–medium sandstone packages (Paton *et al.* 2007) that represent the progradation of the Aptian deltaic margin and

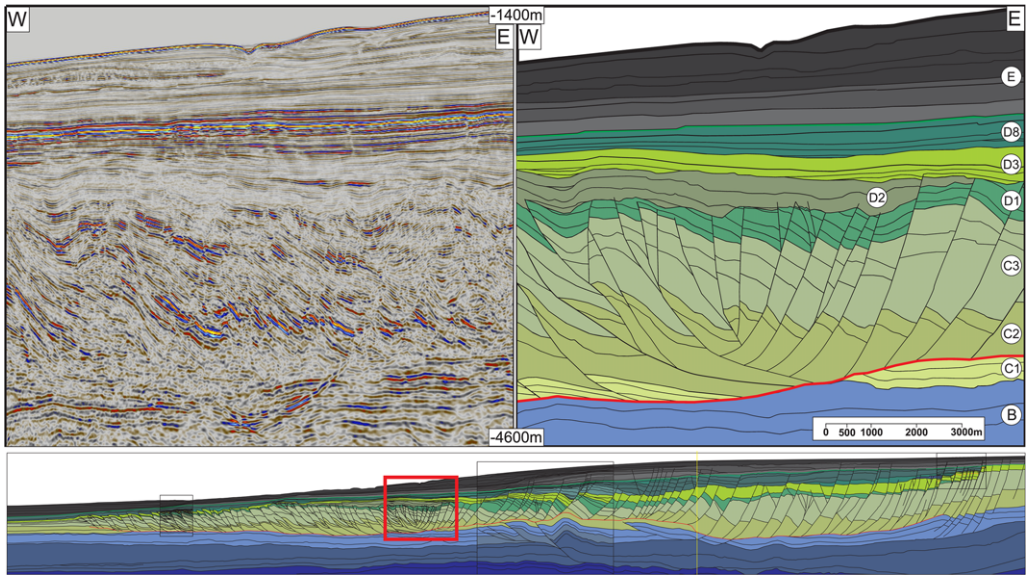

Fig. 6. Detailed interpreted and uninterpreted sections of the transitional domain from Figure 4. Section is vertically exaggerated 3:1.

are capped by a maximum flooding surface that forms the detachment. Sequence C1 is defined as a set of lower amplitude parallel reflections that have a variable relationship across the section with the surrounding sequences. In the east of the section they are conformable with megasequence B; the reflections become truncated towards the west by the base of sequence C2. They reappear in the west as a set of reflections conformable with C2 and downlap onto megasequence B. We interpret this as a shift in the depth of the main décollement that is immediately above B in the east and cuts down to an inter-megasequence B layer with the consequence of translating the C1 package downslope by *c.* 2300 m towards the west.

C2 is defined by low-amplitude, largely discontinuous reflections and is conformable with C3, which consists of higher amplitude, more continuous reflections. The lowest reflections in C2 to the east and centre downlap onto B and C1 and are directly above the detachment at this point; they are conformable with C1 in the west as the detachment cuts down-sequence, as described earlier. The division between the C2 and C3 intervals is identifiable by an easily correlated, high-amplitude reflection package. This allows us to define fault cut-offs with confidence. In the east, these faults dip steeply landwards with normal offsets and detach onto the main basal décollement. Progressing west they become more closely spaced and detach onto a shallow basinwards-dipping thrust fault located above the regional décollement. A shift from extensional to compressional tectonics occurs on top of this thrust fault. The low amplitudes at the base of C2 are probably a result of the coalescing of multiple faults at this level, causing increased stress at this depth. The thickness of C2/C3 is largely maintained throughout the margin, including the area of intense faulting, which suggests that it is largely a pre-kinematic sequence deposited prior to collapse, although some reflections in the top of C3 show limited thickening into fault planes, suggesting some degree of syn-kinesis.

Sequence D1 is defined here by a set of low-amplitude reflections that are largely conformable with C3; as in the previous sequence, cut-offs are used to define the location of faults. Many packages have wedge-like geometries that thicken into fault planes, implying fault growth during deposition and making this a syn-kinematic succession. From the position of cut-offs in the region in which normal faulting gives way to thrusting, it can be seen that several faults stopped moving. The upper boundary is truncated by sequence D2. This sequence is defined upwards by a series of low-amplitude continuous reflections that onlap onto the erosional truncation defining the top of D1. They form a tapering wedge to the east, where the formation onlaps onto significant faults with throws of *c.* 120 and *c.* 250 m. There appear to be numerous minor truncations of horizons against one another within the formation, possibly due to limited deposition in

what are effectively minibasins. Some faults do persist into the base of D2, but most are truncated by it, implying an erosional episode followed by progressive infill during which limited reactivation occurred, causing minor folding as opposed to faulting in the overlying sequence. At this point of the section, sequence D3 is defined by low-amplitude continuous reflections that downlap onto D2, infilling its uneven upper surface, before latterly adopting a more aggradational geometry. Minor folding of some reflections at the western end of the section imply limited localized reactivation on some thrusts. Sequence D8 is composed of high-amplitude reflections conformable with D3. The contact between these two horizons can be traced into the compressional domain downdip. The top of D8 appears conformable with megasequence E (Cenozoic).

The transitional domain in the centre of Figure 6 generally picks out a large fold structure detaching onto a thrust above the regional décollement. The back-limb of the fold is cut by normal faults, which progressively become thrust faults towards the crest, some of which are likely to be inverted normal faults. The precise contact between the compressional and extensional domains (e.g. the transitional zone) is narrow, similar to the modes proposed by Corredor *et al.* (2005) and Krueger & Gilbert (2009); however, the possible inversion may imply a more complex structural style, as suggested by de Vera *et al.* (2010) and Butler & Paton (2010).

Compressional domain

Figure 7 is a typical section from the distal end of the compressional domain and we have divided it into nine packages. Megasequence B, which is correlated from the transitional domain, is defined by several near-horizontal reflections that show a consistent increase in amplitude from east to west, probably reflecting a progressive change in its petrophysical properties. Sequences C1–C3, despite being of varying amplitudes, have the same geometry of stacked, steeply east-dipping reflections (*c.* 35° using PSDM data) that shallow and flatten with depth to become parallel with the top reflection of megasequence B. Definable packages of reflections stack with discrete cut-offs that pick out a set of imbricate thrusts. Sequence D1 is defined by a set of discontinuous low-amplitude reflections that onlap the thrust planes and downlap onto C3. The reflections are folded and have been truncated by both sequence D3 and by one another. The variation in thickness and the associated onlap onto anticlines of D1 suggest that thrusting was active during the deposition of D3 and was frequently emergent, leading to folding and erosion of the depositing sediments in a syn-kinematic fashion. This onlap implies that the deformation rates were greater than the sedimentation rates during this interval. D3 truncates D1 with a set of low-amplitude, but continuous, reflections. These reflections are folded above the underlying thrust planes, but are only cut

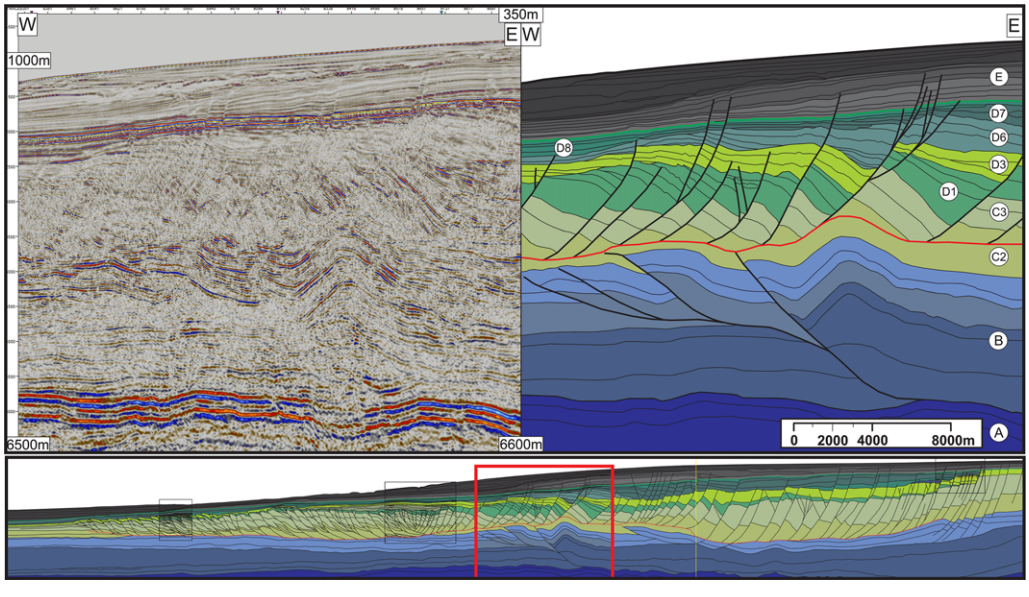

Fig. 7. Detailed interpreted and uninterpreted sections of the compressional domain from Figure 4, image is vertically exaggerated 3:1.

by two of the thrusts with far smaller throws. Although it is clear that the faults remained active during this period, the rate of deformation relative to sedimentation had slowed significantly.

Sequence D8 truncates the crests of the folded reflections in D3 and onlaps in the synclines formed by the dipping reflections on the back-limb of the thrust faults. This suggests the end of deformation in this part of the compressional domain, with sediment infilling the remnant topography, although the sediment supply is insufficient to entirely fill the bathymetric lows. The last of these lows were filled by small onlapping packages at the base of sequence D9, which is otherwise conformable with D8. As with the transitional domain, the contact between the Late Drift (D) and the Cenozoic megasequences (E) is conformable. In a broader context, when viewing the compressional domain in Figure 4, the imbricates have a relatively equal spacing and become progressively less deformed away from the transition zone, while also deforming ever-younger sequences. The dips of the faults shallow from 40–50° at the transitional domain to 15–25° at the frontal thrusts. They progressively deform younger sequences, implying that once the dip of the thrusts becomes too high, it is preferential to deform more distal sediments.

Variations in DWFTB geometry

Having summarized the structural elements that comprise a typical section for gravity collapse, we now outline how the styles of deformation deviate from this typical section by looking at variations along the margin, as illustrated by a number of additional sections.

Lateral variation

The three sections in Figure 8 are modified from Dalton *et al.* (2015) and show three slip-parallel 35 km long sections running north–south (see Fig. 3 for locations) through a DWFTB in the southern portion of the Orange Basin. Growth strata indicate that collapse initiated during the deposition of the Cenozoic megasequence, which detaches onto a maximum flooding surface at the top of the Campanian in the Late Drift megasequence (Paton *et al.* 2008). Section (a) consists of an extensional domain with no corresponding compressional domain. Section (b) has a more classical geometry with both extensional and compressional domains detached onto the Campanian décollement; however, an additional set of thrusts detach onto the contact between the Cenozoic and Late Drift megasequences. Section (c) indicates that this upper detachment is far more developed with a separate set of normal faults detaching onto the base of the Cenozoic megasequence. The geometries of reflections in the extensional domain indicate slip occurring along both detachments synchronously, suggesting that gravitationally driven strain is distributed between both systems. The Campanian detachment has larger throws, suggesting that it has taken more of the strain, although the folding of the Cenozoic reflections in the far west appears to restrict its westerly development. The imbalance between the two detachments in section (c) suggests that the Cenozoic detachment is more efficient; however, as the system grows northwards the Campanian detachment becomes more important. This may relate to local variations in the slip potential of the detachment surfaces, such as changes in thickness, overpressure or lithology.

Multiple detachments

The presence of multiple detachment horizons in gravity collapse systems has been recognized previously (e.g. Totterdell & Krassay 2003; Rowan *et al.* 2004; Corredor *et al.* 2005; Briggs *et al.* 2006), but few studies have documented how the position and interaction of different slip horizons creates a range of complex geometries indicating changes in the timing and location of deformation.

Sub-Aptian failure. The focus of previous studies of the Orange Basin collapse structures (Butler & Paton 2010; de Vera *et al.* 2010) has been on the system contained within the Late Drift megasequence. Figure 9 presents a more detailed interpretation of a portion of the extensional domain of the collapse (see Fig. 4 for location). We see here that the main detachment in the Late Drift megasequence is underlain by a set of thrusts detaching onto the top of the Synrift megasequence. This lower detachment is formed along a maximum flooding surface between the top of the Synrift megasequence (Hauterivian) and the base of the Early Drift megasequence (Barremian) identified by Brown *et al.* (1995). Folding of the upper detachment and overlying horizons by the developing underlying thrusts imply that they formed later. In addition, thickening in sequence D6 into the fault immediately above the fold suggests that its inception led to reactivation of this fault. The lack of significant thickening of sequence D7 suggests that thrusting had largely ceased by the time of its deposition. This suggests that although the upper system was initiated first, both systems existed coevally. The vergence of these lower thrusts is consistent with the same basinwards translation as the upper system. The most proximal normal faults present in the east of the section clearly penetrate into the Early Drift megasequence and are likely to link directly to these

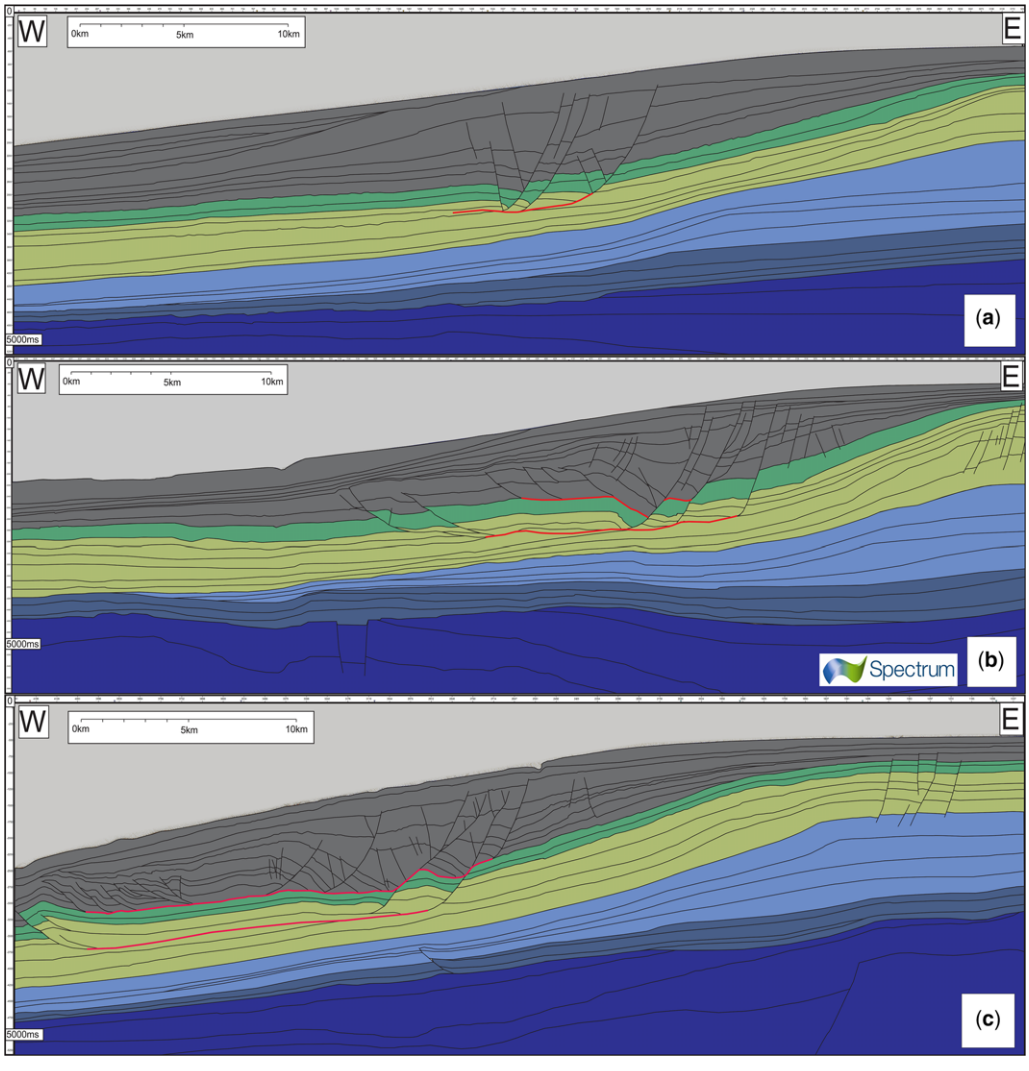

Fig. 8. Three interpreted sections (**a–c**) from the south of the Orange Basin (Fig. 3) adapted from Dalton *et al.* (2015). All sections are 35 km long and are presented as pre-stack time-migrated with vertical exaggerations of 3:1.

thrusts, although the seismic resolution prevents clear confirmation. D6 is not present above these faults (Fig. 5) and may have either been eroded out or not been deposited; however, the infilling of the subsequent D7 into the fault planes suggests that these faults were most active prior to its deposition.

Stacked detachments. Sections through the far north of the largest collapse structure provide further insights into the multi-layer detachment systems (Figs 3 & 10). In Figure 10, an 83 km long section shows several different detachment surfaces at a number of stratigraphic intervals, picked by the identification of mutual fault terminations. In the east of the section, a 30 km long package of normal faults extends up to 2.5 km from a detachment layer within the Early Drift megasequence to the Cenozoic horizon. A second smaller extensional domain, 12 km long with faults extending vertically 600 m up from the detachment, is seen downdip and is contained entirely within the Early Drift megasequence, representative of an early phase of collapse. Two compressional domains also exist: a lower detachment in the Early Drift megasequence, along the Aptian–Barremian maximum flooding surface (Muntingh & Brown 1993), contains thrusts penetrating up to 1.1 km into the overlying Late Drift

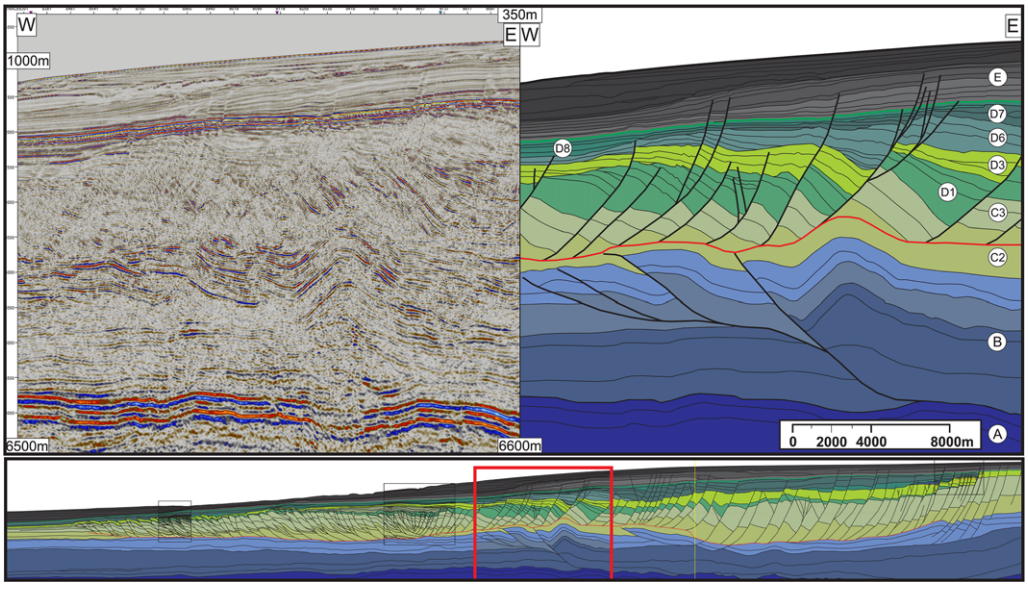

Fig. 9. Detailed interpreted and uninterpreted section from Figure 4 showing folding of the upper detachment by and lower detachment system. Section is vertically exaggerated 3:1.

megasequence, whereas an upper 45 km long detachment, along the Cenomanian–Turonian maximum flooding surface (Paton *et al.* 2007), consists of widely spaced thrusts extending 700 m up from the detachment and is entirely within the Late Drift megasequence. Reflections in the lower compressional domain demonstrate two periods of activity; one period is synchronous with the lower extensional system, with which it shares a detachment and a later phase of reactivation leading to thrusting and folding of the Late Drift megasequence. The upper detachment may have been active synchronously with the lower compressional domain, but remained active for longer, as indicated by thrusting and folding of the uppermost Late Cretaceous package. It is interesting to note that the upper system terminates at the location at which the first thrust of the lower system emerges. Altering the slope angle of the upper detachment at this point may have made further slip along it non-viable. The upper extensional system remained active throughout the Late Drift megasequence and clearly transferred considerable strain downdip. However, the upper compressional domain remained active during this period, although this domain does not appear to be genetically linked at this point, so the process of transmission of strain between the upper and lower compressive domains is not clear. No genetic link emerged in reviewing parallel sections; in fact, the lower system disappeared relatively rapidly. The transition from extensional to compressional domains along the upper detachment in this section was of a very different character to that seen in Figure 6 and appeared as a zone of largely deformed sediments, as described by Corredor *et al.* (2005) and Krueger & Gilbert (2009).

Discussion

The presence of gravity collapse structures has been documented on many margins and some of the inherent variability has been discussed in detail elsewhere (Morley & Guerin 1996; Rowan *et al.* 2004; Krueger & Gilbert 2009; Morley *et al.* 2011). Studies that have focused on systems driven by thin shale detachments generally propose that they are relatively coherent bodies presenting little variation within a single system. We discuss here how the observed lateral variability in geometries observed in this study has influenced our understanding of thin shale detachment systems. We also consider the greater complexity observed in these features to synthesize a new temporal model of collapse development in the Orange Basin.

Model for the temporal evolution of a collapse structure

Variations in the style and character of deformation appear consistently across the width of the Orange Basin, including the spacing between thrusts, the

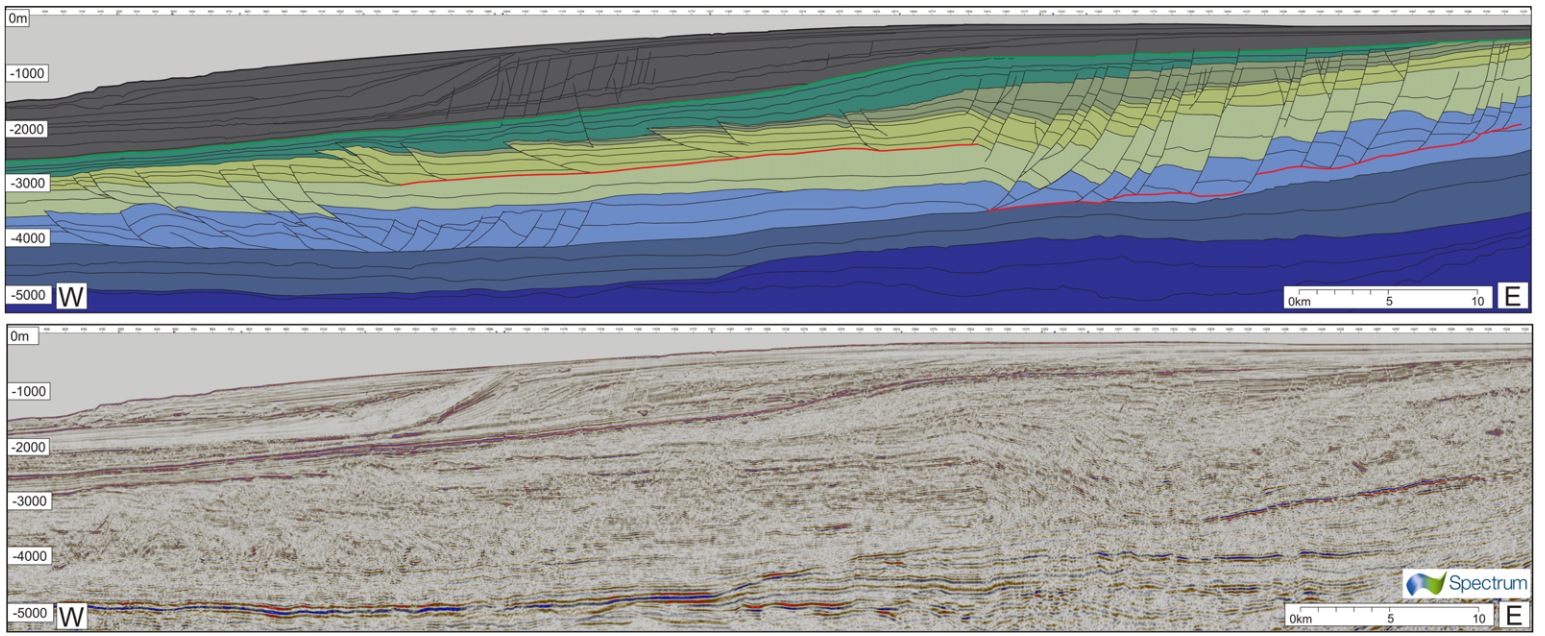

Fig. 10. Interpreted section taken from northern portion of the same collapse structure as featured in Figure 4. Section is vertically exaggerated 3:1

depth and location of slip detachment surfaces, and the nature of the transition zone. Although there is also considerable variation in the thickness of the Upper Cretaceous sediments across the basin, the same regional detachment is present throughout. This means that the changes in the styles of deformation observed are present within a single DWFTB so that any single end-member model is not applicable. Dalton *et al.* (2015) have demonstrated that the extensional domain was initiated prior to the formation of a later compressional phase. In this study, we have shown through growth packages that the earliest phase of collapse was located in the centre around the transition zone. For example, D8 in Figure 6 is a post-kinematic horizon, but in Figure 7 it is clearly a syn-kinematic package and is entirely eroded out to the west, where the overlying D9 package, here post-kinematic, becomes syn-kinematic, showing that later phases of movement occur progressively more distally than earlier phases. Few sequences can be tracked throughout the entire structure as they are either truncated by later sequences or are only locally present. However, analyses on the megasequence scale and of larger traceable sequences reinforce this finding. New faults formed and grew at the outer extents of the collapse, although older faults were still active with a reduction in offset. Successive younger faults formed out from the transition zone, downdip to the west in the case of the compressional domain and updip to the east in the case of the extensional domain. The high fidelity of the seismic imaging of our data showed that the transition domain represents a short-wavelength change from extensional to compressional tectonics as opposed to being a zone of overprinted regimes and, more importantly, that it appears to remain fixed. In general, the position of maximum strain migrates away from the transition domain, although we do observe fault reactivation occurring (Fig. 9).

It is similarly clear that if we can relate later, more proximal, movements to ever more distal thrusts, then this would reinforce the concept that these regimes preserve the original contact between them as a block of material that ceases to deform, allowing the translation of strain downslope. Observations of the underlying thrust systems, and the timing of structures above and beneath in Figure 9, indicate a synchronous relationship between the systems – that is, the overlying detachment was folded by the underlying system, which remained active throughout. This suggests that they are both part of a single system as opposed to being two stacked systems of different ages.

Although many studies make reference to multiple detachment horizons (Rowan *et al.* 2004; Krueger & Gilbert 2006; Morley *et al.* 2011; Peel 2014), their presence is generally not included in models of gravity collapse systems. Growth strata indicate that these alternative detachments are often not merely spatially and temporally separate collapse events, but are linked integral portions of the same system. They thus have an important role in terms of strain distribution. They preferentially appear on more mature systems and link to the youngest, most proximal, normal faults. This implies that they form after a point at which continued deformation along the extant distal compressional regime is no longer as efficient as linking to a lower detachment. Sequence-scale observations show that these structures take a long time to form and experience multiple reactivations, which control deposition and erosion along the margin. With this in mind, we have produced a model for the formation and growth of these systems in thin shale detachment systems (Fig. 11).

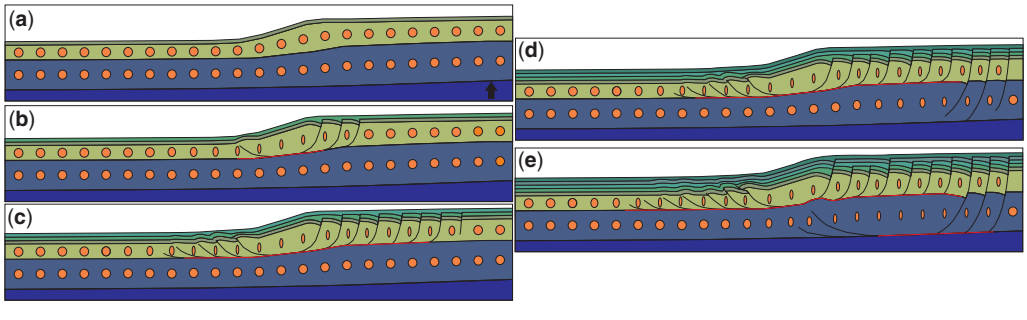

Fig. 11. Multistage model of gravity collapse culminating in the formation of a lower detachment. Orange ellipses represent the distribution of strain within the DWFTB and reflect the findings of Dalton *et al.* (2015) that considerable compaction of the margin is required prior to the formation of the compressional domain. (**a**) Undeformed margin; (**b**) initiation of failure and formation of primary thrust; (**c**) new normal faults form proximal to basin with thrust faults forming in response increasingly more distal; (**d**) upper system becomes increasingly more difficult to slide along, normal faults penetrate down to alternative lower slip surface and compact lower sediments; (**e**) once compacted sufficiently, a lower compressional domain develops.

Our model assumes that continued lateral compaction and deformation of the sediments above and ahead of the original detachment reaches a point at which it is no longer the most efficient way of accommodating the gravitationally induced stress. Assuming that the underlying sediments are comparatively under-compacted and in the presence of an appropriate alternative slip horizon, strain is now accommodated along a lower décollement. However, it is not clear how the strain is transferred from normal faults connected to a lower system. The strain recorded in the upper compressional domain is shown in Figure 10, where both the upper compressional regime and the most proximal normal faults deform age-equivalent sediments and thus must be linked. The extensional domain in Figure 8c shows two slip surfaces that have been exploited by the same faults at different times and it is possible that the same relationships exist in the more mature system in Figure 10, although continued deformation has made this relationships difficult to ascertain.

Brown *et al.* (1995) indicated that our detachment horizons are maximum flooding surfaces, presumably composed of low basal friction shales, which, as long as they are sufficiently thick and continuous, will continue to allow slip (Rowan *et al.* 2004). If the shale thins or is absent from a section, then the system will lock up. This locking up of the system while the overburden builds up sufficiently to lead to the re-initiation of failure by overcoming frictional cohesion results in the development of isolated sediment imbalances at the head of fault scarps (de Vera *et al.* 2010). This, in turn, leads to the formation of MTCs, which rework the sediments of the upper portion of the extensional domain. This explains why we tend to see the large-scale development of MTCs only on mature systems prone to more lock ups. They become more prevalent stepping back towards the coast, where fewer shale

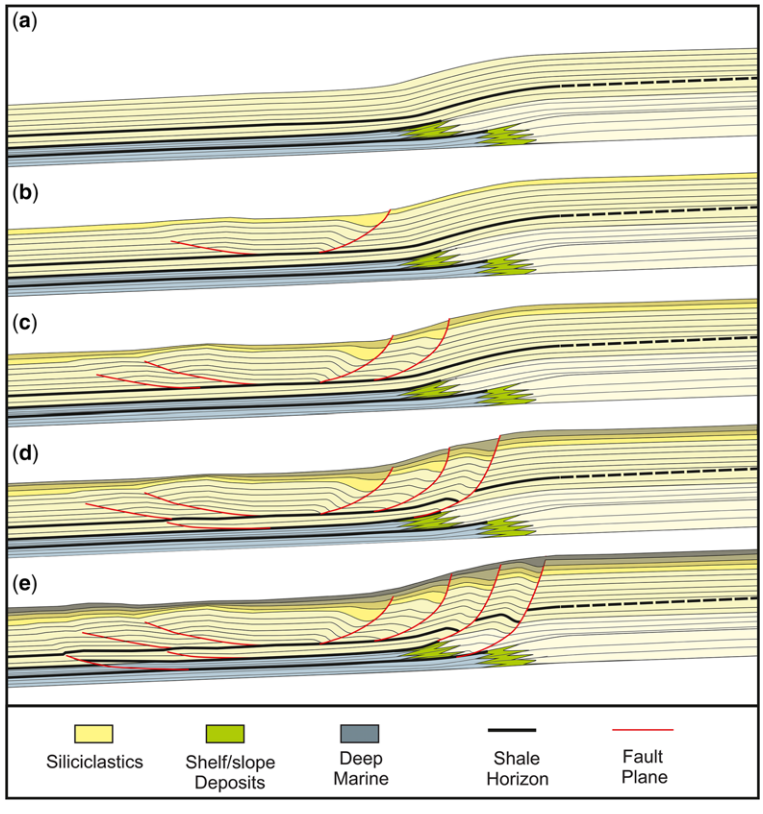

Fig. 12. Model explaining the role of deposition on the location and development of detachment horizons. (**a**) Section through a typical margin showing three stacked sequences, two with shale horizons at the base of slope and the upper shale horizon representing a maximum flooding surface. (**b**) Development of a simple single detachment system slipping along the maximum flooding surface. (**c**) System matures with the development of additional faults and eventually locks up. (**d**) In response to system locking up, alternative slip horizons along the lower base of slope shale are used instead. (**e**) Even lower detachment horizons are sought as the shale in (d) is restricted depositionally.

intervals were deposited, and provide potential slip surfaces on what were palaeo-continental margins.

The initial geometries are controlled by the original local accumulations of sediments. The most amenable slip horizons – for example, the shale with the lowest frictional cohesion – will be used in preference to other slip horizons. This cohesion may, however, vary across the basin depending on the original depositional conditions and better slip horizons may be used elsewhere (Dalton *et al.* 2015). The collapse systems in this study were commonly associated with maximum flooding surfaces or the base of slope systems.

Stratigraphic controls on margin collapse

Although the majority of the passive margin stratigraphy on the Orange Basin is claystone, our observations imply that there is a strong control on the location and evolution of the collapse structures from variations in stratigraphy. The principle slip surfaces have been well documented as being relatively thin (*c.* 100 m), organic-rich shale horizons (e.g. Muntingh & Brown 1993; Paton *et al.* 2008) that act as low friction surfaces. This depositionally controlled variation in the basin can be related to the two end-member model for gravity collapse structures on shale detachments (Krueger & Gilbert 2009). One end-member suggests slip along a single detachment horizon, whereas in the second end-member the detachment switches between local over-pressured shale horizons as variations in depositional occurrence and slip potential allow. In the Orange Basin, examples of both end-members are observed with the upper compressional domain in Figure 10. There is clearly slipping along a single regional plane, while the easterly extensional domain has a highly undulating character suggestive of smaller localized slip horizons.

The model presented by Morley *et al.* (2011) characterizes the collapse systems within the Niger Delta and Orange Basin as being of equivalent types (Type 1a). Both are detached on shale and, although there is much discussion as to the existence of shale diapirism, there appears to be distinct differences in the style of deformation between the two basins. The implications of a thick shale interval versus a thin horizon, as commented on by Rowan *et al.* (2004), alters the nature of the failure. Critical wedge concepts (Bilotti & Shaw 2005; Briggs *et al.* 2006) assume the oceanwards propagation of the system. As long as there is low basal friction, then the system will continue to propagate. If there is a thick detachment layer, then it will localize all of the deformation on to the basal system. For example, where the Akata shale in the Niger delta is thick, it internally deforms and the whole overburden can behave as a mechanically strong unit (Corredor *et al.* 2005). This could cause long wavelength folding with some localized faulting (Costa & Vendeville 2002) and would not require significant intra-stratigraphic deformation. In the Orange Basin, in contrast, and in other basins dominated by interbedded heterolithic sediments with thin detachments, the mechanically strong unit above the detachment will need to undergo considerable intra-stratigraphic deformation, such as folding and intra-layer thrusting, to allow it to transfer strain downdip (Dalton *et al.* 2015).

Our observations also show that the collapse is controlled not just by the detachment thickness, but also by variations in the margin stratigraphy. Existing stratigraphic studies of the Orange Basin (Brown *et al.* 1995; Paton *et al.* 2007, 2008) show that there are two key stratigraphic variations in the evolution of the basin. During the Aptian (megasequence B in this study), the stratigraphy facies consists of a landwards-stepping clastic front. This results in the landward migration of the delta foreset to marine shale transition. Overlying the delta system is the main shelf margin sequence with interbedded organic-rich shale horizons. This results in a complex distribution of the décollement horizons and corresponding multiphase development, which is described in the following parts of Figure 12:

(a) Stratigraphic distribution of the stable passive margin.
(b) Extensional faulting initiates on the continental slope, detaching onto an advantageous shale horizon and subsequently leading to thrusting downdip on the abyssal plain.
(c) Continued gravitational imbalance on the margin leads to additional faults forming proximal and distal to the original collapse, which continues itself to deform.
(d) The ability of the upper detachment to redistribute strain downdip becomes less efficient and so new extensional faults penetrate down to a lower shale horizon to compact lower, relatively under-compacted, sediments.
(e) This process continues to exploit lower shale horizons to redistribute strain; the original systems may also continue to deform, although lower systems may alter the structural development of the overlying systems. The propagation of the faults to the lower packages is, in part, controlled by the stratigraphy of the margin and the location of the delta front.

Conclusions

Using very well imaged examples of gravity collapse structures from the Namibian and South African Atlantic passive margin, we have illustrated

the significant variation in the structures present in these tripartite systems. This variation includes the typical updip extensional faults and downdip thrust faults, but also multi-detachment faulting and folding, stacked detachments, cross-cutting and the complex progressive evolution of the system.

As this system is dominated by a series of relatively thin detachments, we suggest that the role of stratigraphy, especially the distribution of maximum flooding organic-rich units, plays a fundamental role in both the style and spatial distribution of the deformation. We propose that such a model helps to explain the differences that occur in thick shale systems, salt systems and thinly bedded heterolithic systems.

References

Bilotti, F. & Shaw, J.H. 2005. Deep-water Niger Delta fold and thrust belt modelled as a critical-taper wedge: the influence of elevated basal fluid pressure on structural styles. *AAPG Bulletin*, **89**, 1475–1491.

Briggs, S.E., Davies, R.J., Cartwright, J.A. & Morgan, R. 2006. Multiple detachment levels and their control on fold styles in the compressional domain of the deepwater west Niger Delta. *Basin Research*, **18**, 435–450.

Brown, L.F., Jr, Benson, J.M. *et al.* 1995. *Sequence Stratigraphy in Offshore South African Divergent Basins. An Atlas on Exploration for Cretaceous Lowstand Traps by Soekor (Pty) Ltd.* AAPG Studies in Geology, **41**.

Butler, R.W.H. & Paton, D.A. 2010. Evaluating lateral compaction in deepwater fold and thrust belts: how much are we missing from 'nature's sandbox'? *GSA Today*, **20**, 4–10.

Corredor, F., Shaw, J.H. & Bilotti, F. 2005. Structural styles in the deep-water fold and thrust belts of the Niger Delta. *AAPG Bulletin*, **89**, 735–780.

Costa, E. & Vendeville, B.C. 2002. Experimental insights on the geometry and kinematics of fold-and-thrust belts above weak, viscous evaporitic décollement. *Journal of Structural Geology*, **24**, 1729–1739.

de Vera, J., Granado, P. & McClay, K. 2010. Structural evolution of the Orange basin gravity-driven system, offshore Namibia. *Marine and Petroleum Geology*, **27**, 233–237.

Dalton, T.J.S., Paton, D.A., Needham, D.T. & Hodgson, N. 2015. Temporal and spatial evolution of deepwater fold thrust belts: implications for quantifying strain imbalance. *Interpretation*, **3**, SAA71–SAA87.

Gerrard, T. & Smith, G.C. 1982. Post-Palaeozoic succession and structure of the south-western African continental margin. *In*: Watkins, J.S. & Drake, C.L. (eds) *Studies in Continental Margin Geology*. AAPG Memoir, **34**, 49–74.

Hirsch, K.K., Scheck-Wenderoth, M., van Wees, J.-D., Kuhlmann, G. & Paton, D.A. 2010. Tectonic subsidence history and thermal evolution of the Orange Basin. *Marine and Petroleum Geology*, **27**, 565–584.

Jungslager, E.H.A. 1999. Petroleum habitats of the Atlantic margin of South Africa. *In*: Cameron, N.R., Bate, R.H. & Clure, V.S. (eds) *The Oil and Gas Habitats of the South Atlantic*. Geological Society, London, Special Publications, **153**, 153–168, http://doi.org/10.1144/GSL.SP.1999.153.01.10

Koopmann, H., Schreckenberger, B., Franke, D., Becker, K. & Schnabel, M. 2014. The late rifting phase and continental break-up of southern South Atlantic: the mode and timing of volcanic rifting and formation of earliest oceanic crust. *In*: Wright, T.J., Ayele, A., Ferguson, D.J., Kidane, T. & Vye-Brown, C. (eds) *Magmatic Rifting and Active Volcanism*. Geological Society, London, Special Publications, **420**. First published online December 18, 2014, http://doi.org/10.1144/SP420.2

Krueger, A.C.V.A. & Gilbert, E. 2006. Mechanics and kinematics of back thrusting in deep water fold-thrust belts – observations from the Niger Delta (abstract). *2006 AAPG Annual Meeting*, Houston, TX, USA, Abstracts Volume, **15**, 58.

Krueger, A. & Gilbert, E. 2009. Deepwater fold-thrust belts: not all the beasts are equal. *AAPG Datapages/Search and Discovery*, Article #30085. http://www.searchanddiscovery.com/documents/2009/30085krueger/index.html

Light, M.P.R., Maslanyj, M.P., Greenwood, R.J. & Banks, N.L. 1993. Seismic sequence stratigraphy and tectonics offshore Namibia. *In*: Williams, G.D. & Dobb, A. (eds) *Tectonics and Seismic Sequence Stratigraphy*. Geological Society, London, Special Publications, **71**, 163–191, http://doi.org/10.1144/GSL.SP.1993.071.01.08

McGilvery, T.A. & Cook, D.L. 2004. Depositional elements of the slope/basin depositional system offshore Brunei. *Proceedings of the Indonesia Petroleum Association Meeting*, 7–8 December, Jakarta, Indonesia, 407–420.

Mohammed, M., Paton, D.A., Collier, R.E.L.I., Hodgson, N. & Negonga, M. In press. Interaction of crustal heterogeneity and lithospheric process in determining passive margin architecture on the Namibian margin. *In*: Sabato Ceraldi, T., Hodgkinson, R.A. & Backe, G. (eds) *Petroleum Geoscience of the West Africa Margin*. Geological Society, London, Special Publications, **438**, http://doi.org/10.1144/SP438.9

Morley, C.K. & Guerin, G. 1996. Comparison of gravity-deformation styles and behaviour associated with mobiles shales and salt. *Tectonics*, **15**, 1154–1170.

Morley, C.K., King, R., Hillis, R., Tingay, M. & Backe, G. 2011. Deepwater fold and thrust belt classification, tectonics, structure and hydrocarbon prospectivity: a review. *Earth Science Reviews*, **104**, 41–91.

Muntingh, A. & Brown, L.F.J. 1993. Sequence stratigraphy of petroleum plays, post-rift Cretaceous rocks (Lower Aptian to Upper Maastrichtian), Orange Basin, South Africa. *In*: Masterson, A.R. (ed.) *Siliciclastic Sequence Stratigraphy. Recent Developments and Applications*. AAPG Memoir, **58**, 71–98.

Paton, D.A., di Primio, R., Kuhlmann, G., van der Spuy, D. & Horsfield, B. 2007. Insights into the petroleum system evolution of the southern Orange

Basin, South Africa. *South African Journal of Geology*, **110**, 261–274.

PATON, D.A., VAN DER SPUY, D., DI PRIMIO, R. & HORSFIELD, B. 2008. Tectonically induced adjustment of passive-margin accommodation space; influence on hydrocarbon potential of the Orange Basin, South Africa. *AAPG Bulletin*, **92**, 589–609.

PATON, D.A., MORTIMER, E.J. & HODGSON, N. In press. The missing piece of the South Atlantic jigsaw: when continental break-up ignores crustal heterogeneity. *In*: SABATO CERALDI, T., HODGKINSON, R.A. & BACKE, G. (eds) *Petroleum Geoscience of the West Africa Margin*. Geological Society, London, Special Publications, **438**, http://doi.org/10.1144/SP438.8

PEEL, F.J. 2014. The engines of gravity-driven movement on passive margins: quantifying the relative contributions of spreading v. gravity sliding mechanisms. *Tectonophysics*, **633**, 126–142, http://doi.org/10.1016/j.tecto.2014.06.023

POSAMENTIER, H.W. & KOLLA, V. 2003. Seismic geomorphology and stratigraphy of depositional elements in deep-water settings. *Journal of Sedimentary Research*, **73**, 367–388.

ROWAN, M.G., PEEL, F.J., VENDEVILLE, B.C. 2004. Gravity-driven fold belts on passive margins. *In*: MCCLAY, K.R. (ed.) *Thrust Tectonics and Hydrocarbon Systems*. AAPG Memoir, **82**, 157–182.

TOTTERDELL, J.M. & KRASSAY, A.A. 2003. The role of shale deformation and growth faulting in the Late Cretaceous evolution of the Bight Basin, offshore southern Australia. *In*: VAN RENSBERGEN, P., HILLIS, R.R., MALTMAN, A.J. & MORLEY, C.K. (eds) *Subsurface Sediment Mobilization*. Geological Society, London, Special Publications, **216**, 429–442, http://doi.org/10.1144/GSL.SP.2003.216.01.28

VAN DER SPUY, D., ZIEGLER, T. & BOWYER, M. 2003. Deepwater 2D data reveal Orange Basin objectives off western South Africa. *Oil & Gas Journal*, **101**, 44–49.

Part A –

II: Published version of the paper featured in Chapter 5

Temporal and spatial evolution of deepwater fold thrust belts: Implications for quantifying strain imbalance

Tobias James Scott Dalton[1], Douglas. A. Paton[1], Timothy Needham[2], and Neil Hodgson[3]

Abstract

Deepwater fold and thrust belts (DWFTBs) occur in a large number of active and passive continental margins, and their occurrence play an important role in controlling the structural configuration and stratigraphic evolution of margins. Although DWFTBs that are located on passive margins are a coupled system, in which updip extension is linked to downdip contraction, many studies have established a significant imbalance between these two domains in favor of net extensional strain. We have sequentially restored a series of parallel sections from the Orange Basin, South Africa, to quantify the amount of extension and contraction along a single collapse system. We found there to be a constant shortfall in the amount of contraction relative to extension in these features, which allowed us to quantify the lateral compaction of the margin as 5%. We also established a temporal model for the development and growth of thin shale detachment gravity collapse structures on passive margins. This model had implications not only for the kinematic and geometric evolution of these systems but also on the geomechanical process involved, in particular the accommodation of strain through compactional processes rather than discrete faulting.

Introduction

The development of deepwater fold and thrust belts (DWFTBs) on passive continental margins is an important process that has been recognized on a number of margins globally, including the Gulf of Mexico, the Scotia Basin, the Bight Basin (e.g., Totterdell and Krassy, 2003; Ambrose et al., 2005; Deptuck et al., 2009), and many South Atlantic margins, in particular, Brazil, Angola, Niger Delta, Congo, and the Orange Basin (e.g., Hudec and Jackson, 2004; Bilotti and Shaw, 2005; Corredor et al., 2005; Jackson et al., 2008). DWFTBs are linked fault systems of updip extension and downdip contraction that often share a common detachment and result from gravitationally induced margin instability. As proposed by Morley et al. (2011), DWFTBs can be classified in a number of ways, including driving mechanism, sediment thickness, and basal detachment characteristics. This in part explains the significant structural variety that has been previously identified within DWFTBs (e.g., Rowan et al., 2004; Krueger et al., 2009; Morley et al., 2011). This variety is caused by differences in lithology, failure mechanisms, detachment geometries, and detachment lithologies. Most studies (e.g., Rowan et al., 2004; Morley et al., 2011) separate margin collapses into two broad categories based on detachment lithologies: salt-detached and shale-detached systems. Shale systems are further subdivided into thin shale detachment and thick or mobile shale detachments (Morley et al., 2011).

The Orange Basin, located on the Namibian and South African sector of the West African passive margin, is an excellent environment to study the formation and growth of thin shale DWFTBs and their associated extensional fault systems. Gravity collapse structures can be broadly divided into three tectonic regions: (1) an updip extensional domain, dominated by normal faults, (2) a downdip contractional domain composed of folds and thrusts, and (3) a transitional domain that is either a broadly undeformed region (Corredor et al., 2005; Krueger et al., 2009) or a complex region composed of extensional and compressional features (Butler and Paton, 2010; De Vera et al., 2010). Deformation, or the lack thereof, in the transitional domain is often a result of the duration of time over which the collapse is active. Flexure of the margin over time changes the point of contact between the two opposing domains causing them to overlap. They deform through a combined process of gravity spreading and gravity gliding to decrease the gravitational potential energy (e.g., Peel, 2014).

[1]University of Leeds, Basin Structure Group, School of Earth and Environment, UK. E-mail: t.j.dalton@leeds.ac.uk; d.d.paton@leeds.ac.uk.
[2]University of Leeds, Basin Structure Group, School of Earth and Environment; and Geoscience Limited, Ghyll Wood, Ilkley, UK. E-mail: d.t.needham@leeds.ac.uk.
[3]Spectrum, Dukes Court, Woking, UK. E-mail: neil.hodgson@spectrumasa.com.

Manuscript received by the Editor 4 February 2015; revised manuscript received 10 April 2015; published online 24 July 2015. This paper appears in *Interpretation*, Vol. 3, No. 4 (November 2015); p. SAA59–SAA70, 10 FIGS., 1 TABLE.
http://dx.doi.org/10.1190/INT-2015-0034.1.

Previous results of measurements of shale-detached gravity-driven collapse systems in the Orange Basin have identified a considerable imbalance between the updip extensional domain and the downdip compressional domain (Butler and Paton, 2010; De Vera et al., 2010). This imbalance suggests significantly more extension than is compensated for by observed contractional features, resulting in a "missing strain component" between 10% and 25%. Both studies conclude that this is not a result of out-of-plane movements; rather, it is a systemic feature of these systems that may represent a strength-hardening phase. We test this premise by restoring multiple parallel sections to investigate whether the previous strain imbalance conclusion was an exceptional feature because both papers use the same seismic line, or if it is a common phenomenon in thin shale detachment systems.

Many studies of individual margin collapse focus on a single section of a system rather than considering the spatial variation in deformation. However, we examine five parallel seismic sections through a single collapse feature from the Orange Basin (Figure 1), to assess lateral variation in DWFTB geometry. We also restore these sections to measure and to test our understanding of how structures associated with the DWFTB develop through time. In doing so, we can address the existing enigma of how the mismatch between extensional and contractional strain is accommodated. Furthermore, for the first time, we present a model that explains the temporal evolution of a DWFTB; our model has implications for understanding the complex interaction of sediments and structures on passive margins and also predicting the geomechanical response to deformation.

Regional setting

The geology of the Orange Basin is well documented by Muntingh and Brown (1993), Brown et al. (1995), Paton et al. (2007), Koopman et al. (2014), and M. Mohammed, personal communication (2015). The Orange Basin initiated with Jurassic to early Cretaceous rifting associated with the breakup of East and West Gondwana, progressing into the eventual continental separation of the South American and African plates. This resulted in a series of grabens and half-grabens that are orientated parallel to subparallel to the present-day continental margin (Paton et al., 2008). These graben were later filled by synrift sediments composed of siliciclastic, lacustrine sediments, and volcanic sequences throughout the Upper Jurassic to Hauterivian in the Lower Cretaceous (Brown et al., 1995). The progression from active rifting to the postrift thermal subsidence phase of the margin is characterized by a transitional sequence, which comprises Hauterivian-aged fluvial to deltaic sediments before reaching full marine conditions during the Barremian to Aptian. The main drift phase of the southern Atlantic is evident as a thick (up to 3.5 km) sequence of aggrading shale- and claystone-dominated sequences throughout the Upper Cretaceous (Gerrard and Smith, 1982). This Upper Cretaceous sequence is regionally truncated on the

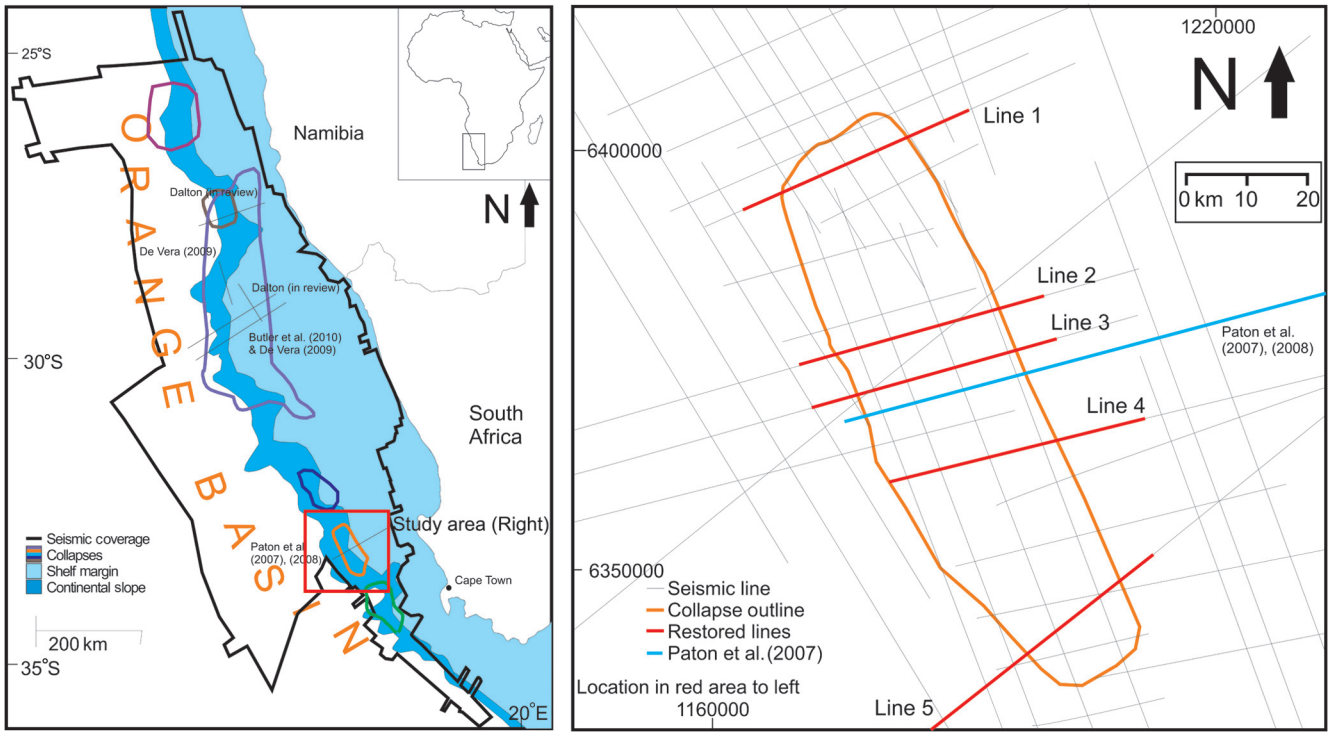

Figure 1. Location map of the study area showing the position of 2D seismic lines and the extent of the regional collapse features. Also highlighted are the location of lines used in previous studies in the area (Paton et al., 2007, 2008; Butler and Paton, 2010; De Vera et al., 2010; T. Dalton, personal communication, 2015).

continental margin by the overlying Cenozoic sequence that progrades out into the basin and is 250–400 m thick on the margin and is 500–1400 m thick on the continental slope (Figure 2).

The postrift Cretaceous and Tertiary sedimentary sequences are deformed by a series of complex coupled gravity-collapse systems in which the updip extensional and downdip contractional domains are very well imaged (Paton et al., 2007; Butler and Paton, 2010; De Vera et al., 2010; T. Dalton, personal communication, 2015). Detachments exist at multiple levels within the Cretaceous sediments throughout the basin — the most significant being in the Aptian, Turonian, and Campanian. We focus on the southernmost collapse, which is approximately 90 km long in a north–south orientation and approximately 25 km wide (east–west).

Data and methods

The data used in this study comprise 39 2D prestack time migrated (PSTM)/prestack depth migrated (PSDM) seismic lines (Figure 1) of which 27 delineate the gravity collapse structure. The seismic data are of various vintages from 1991 to 2012 and combine data from the Petroleum Agency of South Africa with recently acquired Spectrum multiclient data (2012). We use a megasequence approach to these data by using stratal cut-off, truncation, onlapping, and offlapping relationships of reflections and delineate stratal packages using definitions by Paton et al. (2008) (Figure 3) to show variations in timing and structural geometry laterally across the DWFTB.

For this study, we pick the Hauterivian-/Barremian-aged 6AT1 horizon to represent the top of the synrift (purple), the early Aptian 13AT1 horizon to represent the end of the transition package (green), the 15AT1 horizon representing the top of the Cenomanian (light yellow), the 18AT1 horizon defines the base of the Maastrichtian (dark yellow), and the 22AT1 horizons represent the top of the Maastrichtian and are the uppermost Cretaceous package (gray). The seabed defines the top of the Tertiary megasequence (Figure 3).

To define the geometry and development of this gravity collapse structure, we interpret five dip-orientated seismic sections (Figures 4–9) that transect the entire collapse. The sections are spaced along the length of the collapse and are orientated parallel or subparallel (within 10°) to the transport direction of the collapse (Figures 1 and 9). Although the DWFTB in this study extends across the width of the margin, it is elongated along the margin as opposed to the bowl-shaped geometry that has been observed on other slides (e.g., Hesthammer and Fossen, 1999). We then restored the sections using the Upper Cretaceous-Tertiary (UCT) reflection (consistent with the 22At1 reflection) because its high-amplitude reflection character enables a confident correlation across the sections. The UCT refection is prekinematic to the onset of failure, which allows the restoration of this horizon to a realistic precollapse geometry equivalent to a continental margin slope system.

Kinematic restorations of PSDM data and depth-converted PSTM data, using Midland Valley Move 2013.1 software, allowed the measurement of throws and displacements to be consistent in the depth (m) domain. Through a process of sequential restoration of individ-

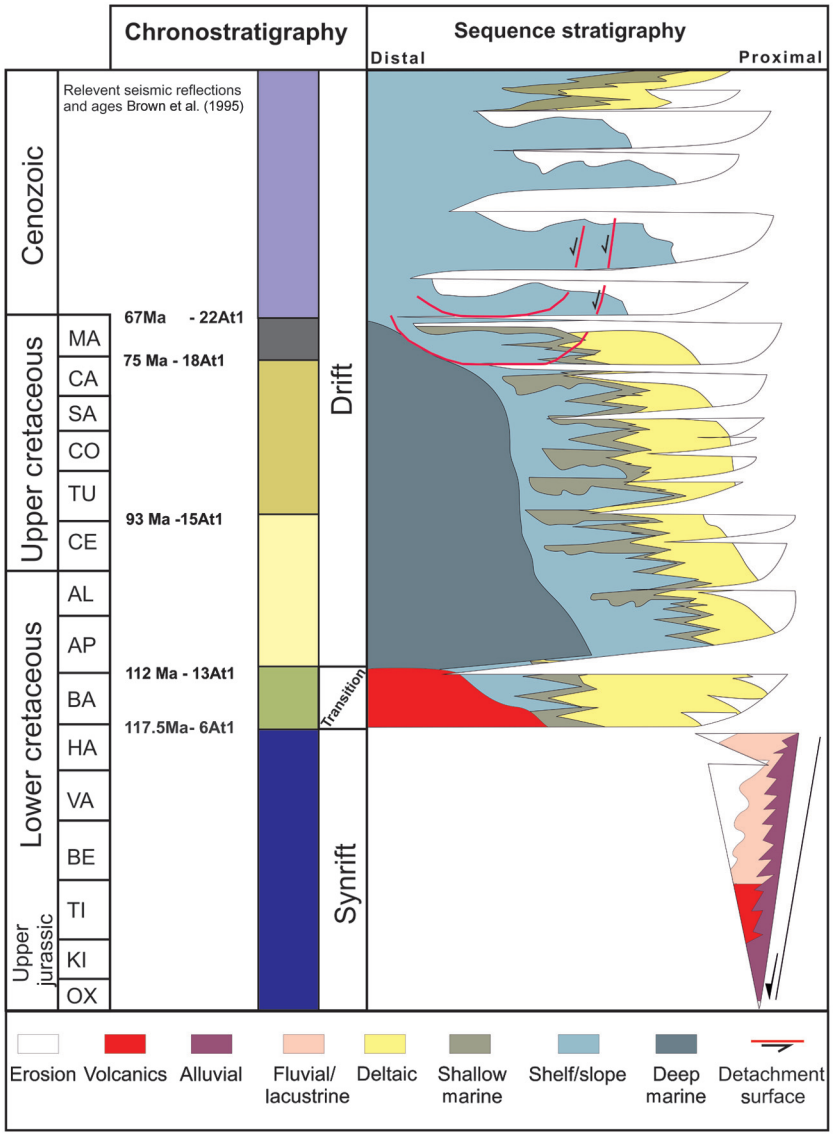

Figure 2. Chronostratigraphy for the Orange Basin with the main décollement horizons and collapse structures in this study identified (after Brown et al., 1995; Paton et al., 2008).

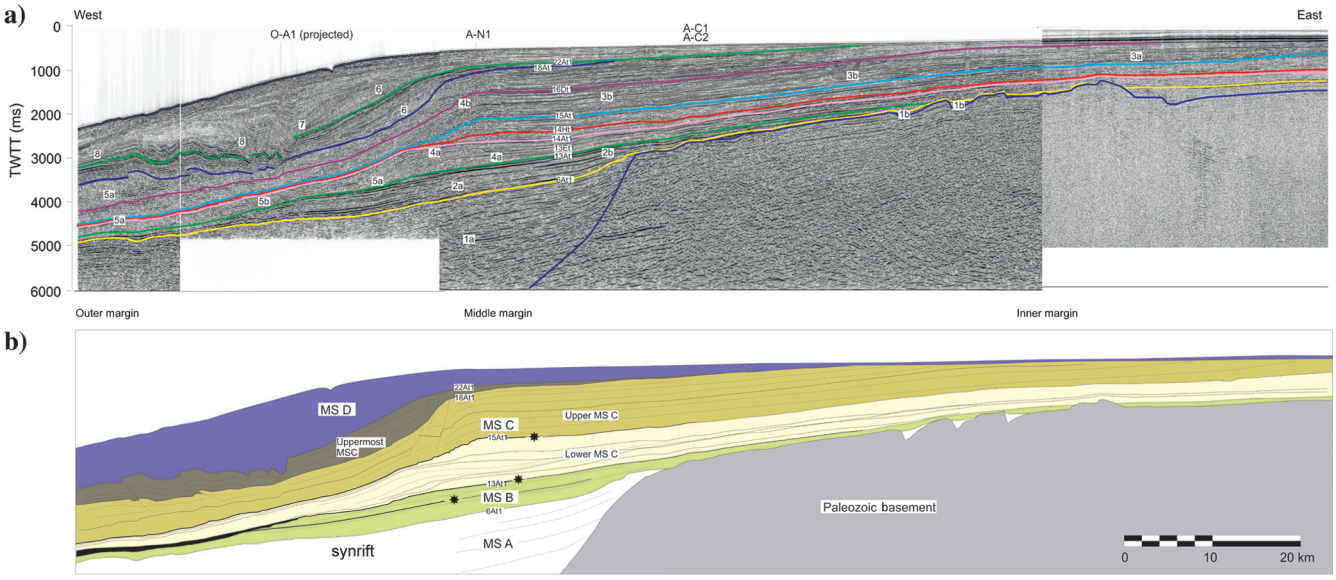

Figure 3. Cross section across the southern Orange Basin showing the key seismic horizons and megasequences (modified from Brown et al., 1995; Paton et al., 2007). The section traverses through the study area (Figure 3) and has been used to identify and date significant horizons in this study.

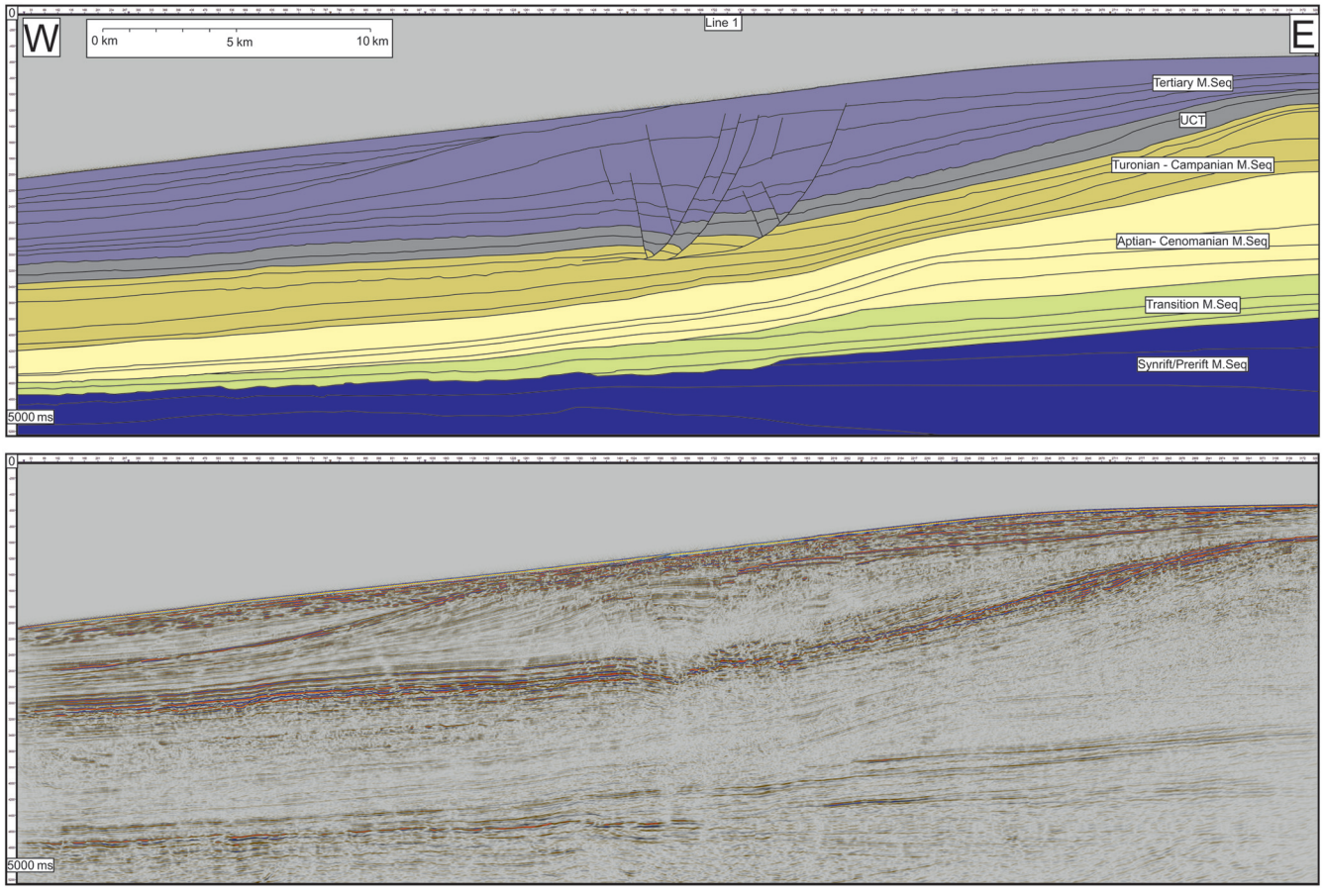

Figure 4. Line 1: seismic section, with interpretation. This is the most northerly line in which three west-dipping normal faults between a set of smaller antithetic east-dipping normal faults splaying from the larger faults are present. There is no contraction evident (Figure 1 for location).

ual fault blocks (Lickorish and Ford, 1998; Bland et al., 2006), a realistic predeformation geometry is produced. For each of the five sections, the displacement on every seismically resolvable fault, in the extensional and contractional domains, is calculated and the cumulative displacements presented (Table 1).

Regional sections

We present five dip-orientated seismic sections from north to south along the western South African margin, which illustrate the geometry of the collapse structure (Figure 3). Each section is 35.7 km long and is plotted in two-way traveltime (ms) with a vertical exaggeration of 3:1

Line 1 (Figure 4): This most northerly section is dominated by three large basin-dipping normal faults with displacements between 200 and 320 m, along with numerous, smaller conjugate or antithetic faults with 30–100 m of displacement. There are no apparent downdip contractional features. The total extensional domain extends 10 km out into the basin. The larger faults detach onto to a common décollement in the Campanian claystones, which is identifiable by a set of downlapping reflections at the base of the fault blocks. Despite this considerable extensional domain, no corresponding seismically resolvable, contractional features are observed. The seismic packages show demonstrable thickening of growth strata during the Tertiary.

Line 2 (Figure 5): As in the previous section, the extensional domain contains three large normal faults, though most of the displacement is concentrated in the two most proximal faults (750 and 980 m) compared to the more distal fault (150 m). There is greater fault complexity in this section than in line 1, several small displacement (<30 m) normal faults can be interpreted as detaching onto the UCT in addition to a smaller number of corresponding thrusts that also detach onto the UCT. The contractional domain is defined by two large thrust faults (displacements of 220 and 490 m) that have a basal fault in the Campanian claystone and have west-dipping ramp structures that propagate up through the Cretaceous sequence into the Tertiary. Reflections in the Tertiary cover show thickening of early packages into the normal faults; the same packages do not show thinning above the thrusts in the contractional domain.

Line 3 (Figure 6): The three normal faults that dominate the extensional domain in line 2 are again evident in this section; however, unlike the section 8 km to the north, most of the displacement is concentrated on

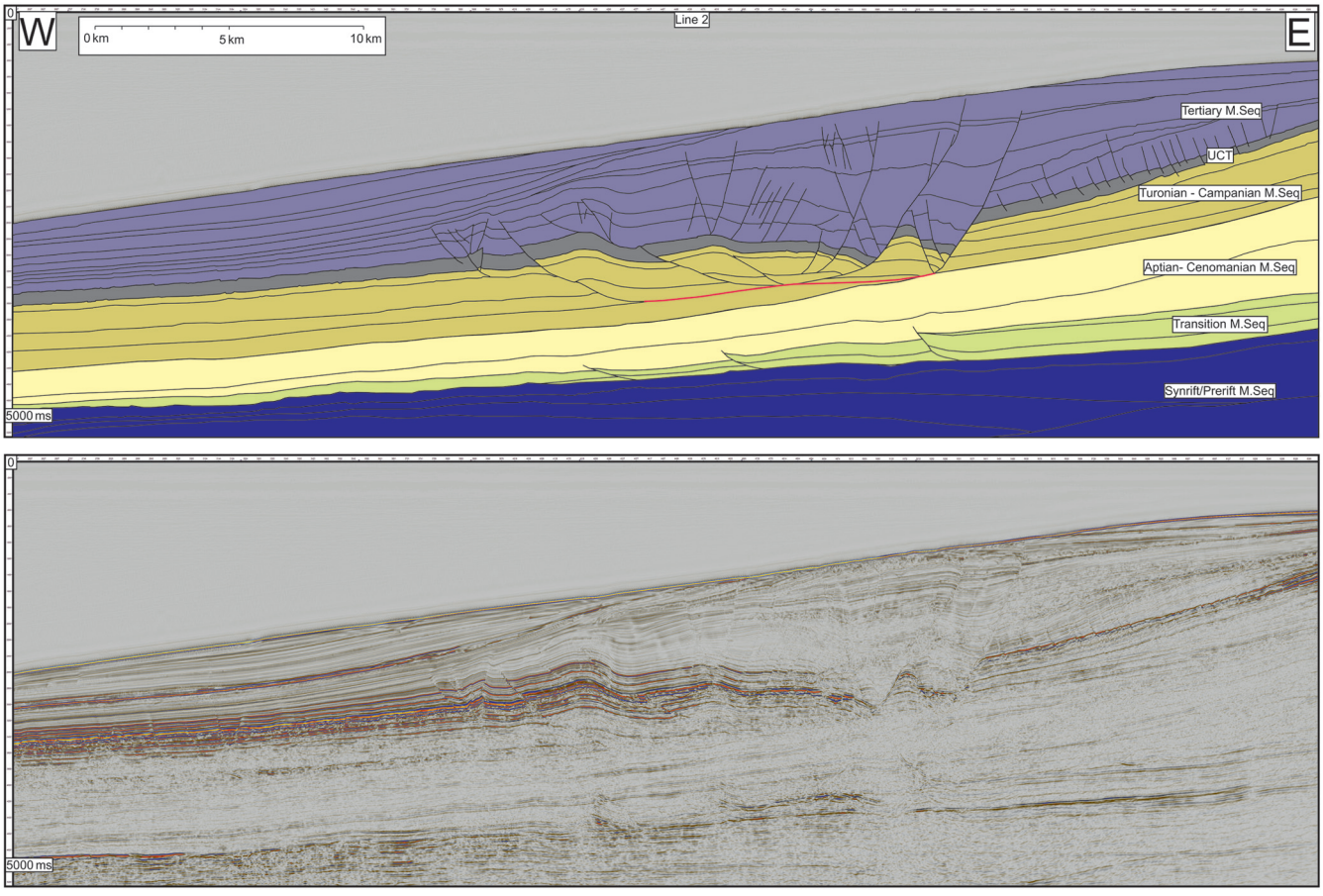

Figure 5. Line 2: seismic section, with interpretation of the section 22 km south of line 1. The large displacement normal faults are still evident as are the antithetic faults in the extensional zone. However, in downdip, the reflections are folded and faulted by west-verging thrust faults in a contractional zone.

the most landward/proximal fault (1140 m) with significantly lower displacements on the other two (480 and 500 m). Between these two lower displacement faults, the lowest Tertiary reflections downlap onto the UCT. Faults above the UCT are more common and have slightly larger displacements (30–80 m) compared to those observed in line 2 (less than 30 m) implying that more strain is being accommodated at this level.

Line 4 (Figure 7): The extent of the gravity collapse structure in this line is possibly incomplete with additional contraction potentially existing beyond the end of the section. We have, however, included it because it shows a significant change in the geometry of the failure relative to previous lines. Only two large normal faults that detach onto the Campanian claystones are present, and the corresponding contractional domain only contains a single major thrust. Deformation is now concentrated onto the UCT décollement, which shows considerable slip in the contractional (200–1000 m) and extensional (500–2400 m) domains. Toe thrusts documented in the northern of the Orange Basin by Butler and Paton (2010) and De Vera et al. (2010) have formed above the UCT detachment immediately behind the fold formed by the underlying thrust fault that extends into the Campanian detachment.

Line 5 (Figure 8): The southernmost complete seismic line within this collapse feature has comparatively similar geometries to lines 1–3; three large normal faults with displacements between 200 and 820 m, this time with the most distal normal fault containing the largest displacement in sediments along the Campanian detachment. Also along this surface, two large thrust faults are present with displacements of 280 and 520 m.

There is much less deformation above the UCT, though it is, unusually, dominated by thrust faults, the extensional strain being provided by the synchronous use of the Campanian detached normal fault planes. The UCT system as a whole is far less deformed than in line 4, with contractional displacements being 20–100 m and extensional displacements being 160–220 m.

Restorations/data

We now present the results of the restorations undertaken on the depth-converted versions of the lines presented above (Figures 4–8), with the quantitative values presented in Table 1.

Values for total shortening and extension vary north–south along the collapse structure, increasing from line 1 in the north toward line 4 in the middle and reducing further south. The value for contraction in line 4 is

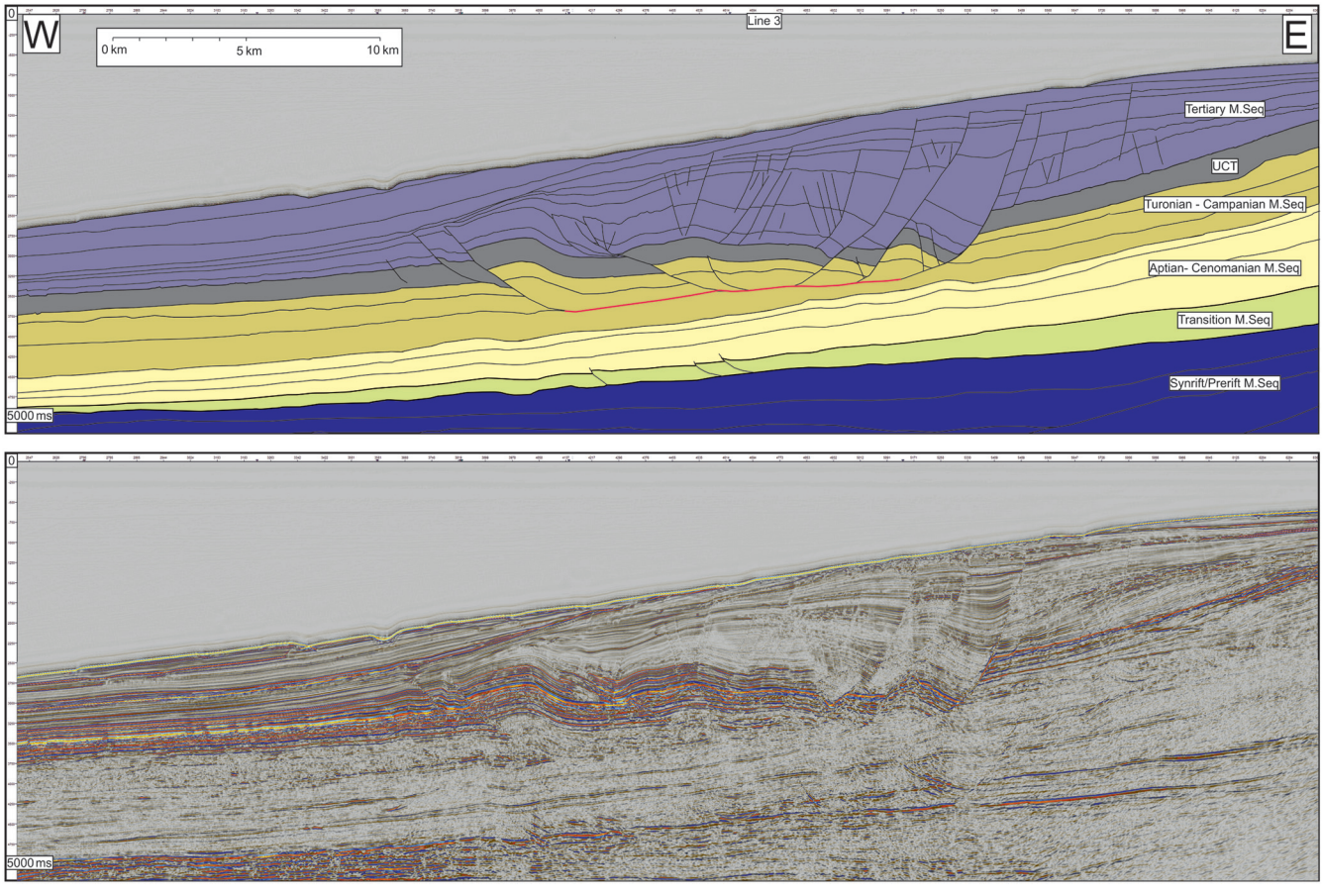

Figure 6. Line 3: seismic section, with interpretation of the section 5 km south of line 2. In this section, there is an increase in the number of extensional faults present, some of which detach on the UCT, although it is not clear whether the thrusts splay off the lower thrust or detach on the unconformity.

lower due to the presence of only one thrust fault. Although additional thrusts could exist off section, the total length of the gravity failure here is comparable with the other sections, suggesting that this is likely to be its true extent. The net difference between total contraction and extension is, however, within a consistent range of 1000–1150 m regardless of these local variations. The fact that no section contains more contraction than extension confirms that this is not merely a factor related to out-of-plane deformation.

Butler and Paton (2010) calculate the missing strain as a proportion of the contractional domain length rather than the entire system. We calculate our missing strain value assuming it is distributed along its entire length, using the following equation:

$$\frac{(\text{total extension(m)} - \text{total compaction(m)})}{\text{length of DWFTB(m)}} \times 100 = \text{missing strain component(\%)} \quad (1)$$

To compare with previous results, we recalculate Butler and Paton (2010) and calculate values for De Vera et al (2010).

The measurements of the missing strain (4.9%–5.6%) agree with the previous results of 5.5% for De Vera et al. (2010) and 12.6% for Butler and Paton (2010). This implies that these results are consistent with larger gravity failures seen in the north detaching onto an earlier, Turonian-level detachment. Line 1, exhibiting no contractional domain, has a 100% missing strain component. It does, however, have an approximately 1 km value for net-missing strain, which is highly comparable to the other lines within the collapse.

Discussion

The variability of gravity collapse structures on a range of detachment lithologies has been well documented in previous studies (e.g., Rowan et al., 2004; Krueger and Gilbert, 2009; Morley et al., 2011). Although several of these studies document end-member models observed from 2D seismic examples, few record the variability observed within a single structure, however (T. Dalton, personal communication, 2015). Previous studies have also presented restorations of 2D sections to establish likely deformation histories (Butler et al., 2010; De Vera et al., 2010). We have undertaken resto-

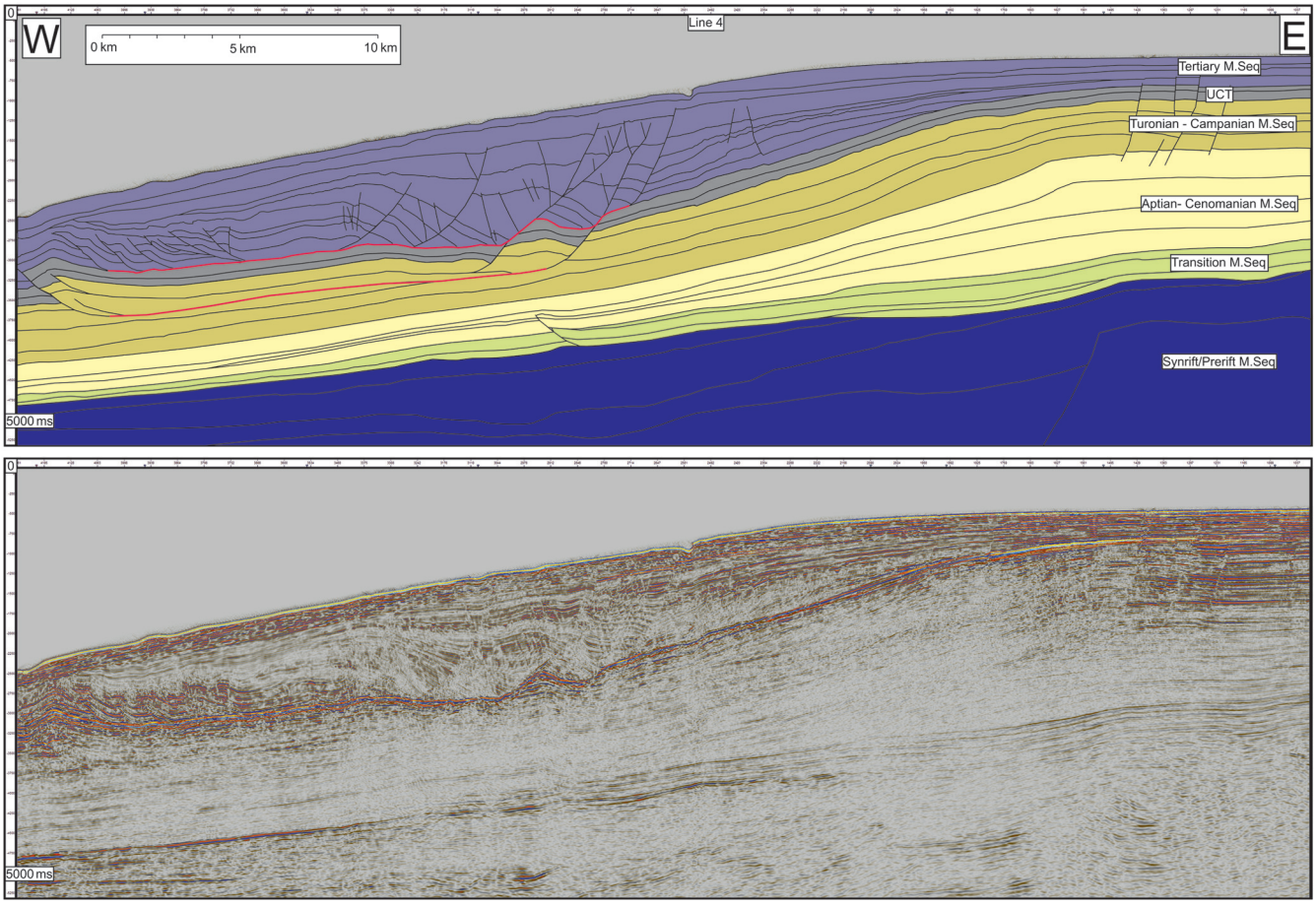

Figure 7. Line 4: seismic section, with interpretation, of the section 11.6 km south of line 7. This section is in the centre of the collapse and represents the maximum length of the system. It appears to have developed into a two-tier collapse with a second décollement forming on the UCT, this upper detachment taking up more of the slip.

rations of multiple parallel sections to gain a 3D understanding of the deformation history.

The repeated sequence of three normal faults with large displacements that extend close to the surface, in lines 1–3, suggests that these are the same faults in each section.

Growth strata indicate the faults have propagated northward over time; however, the amount of displacement on each of these faults varies locally in each section. The largest faults are present across the margin (Figure 9) with two of the normal faults observable throughout but many of the smaller faults with displacements > 100 m persist for shorter distances and are seemingly controlled by local variations in fold and fault geometries.

Comparisons with current models

The observations from the five sections outlined previously allow us to make a few interpretations regarding the development of this collapse structure as follows:

1) Line 1 does not conform to current models of gravity-driven collapse structures, and the absence of a downdip contractional domain does not fit with our current understanding.
2) The earliest phase of deformation occurs in the center of the structure near line 4 (Figure 7). Growth strata into the normal faults on lines 2 and 3 (Figures 5 and 6) indicate a Tertiary age for these faults, whereas crossline ties show that extensional faults in this section were active earlier than in line 1 (Figure 4). Note the relative thickness changes in the lowest purple unit in Figures 4 and 5. Furthermore, growth strata onto the thrust faults in line 3 suggest that although it is predated by the earliest phase of extension, crossline ties confirm that the contraction is also older toward the south
3) The extensional domain commences prior to the contractional domain: Reflections in line 2 (Figure 5) show thickening of early packages into the normal faults, whereas the same packages do not show thinning above the thrusts in the contractional domain.
4) The two detachments present in the system are active synchronously. In line 3 (Figure 6), downlaps onto the UCT between the two lower displacement faults indicate that the middle fault is active synchronously along the upper UCT décollement and along the deeper Campanian décollement. Furthermore, folding of the UCT décollement by the underlying Campanian décollement as seen in line 4 (Figure 7) curtailed the further deformation along

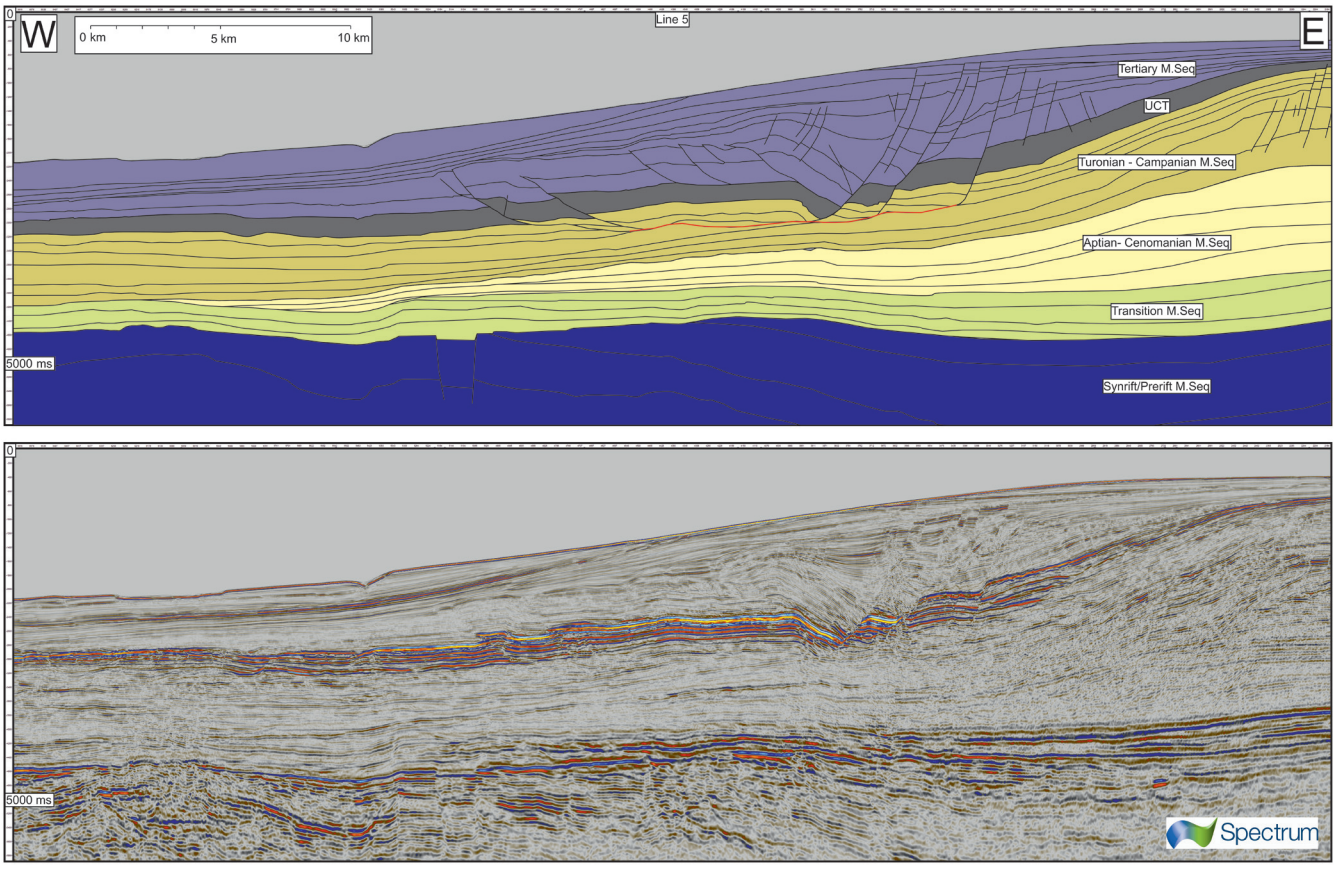

Figure 8. Line 5: seismic section, with interpretation, of the section 19.5 km south of line 4. This is the most southerly section that images the entire collapse structure.

it by altering its slip angle forcing further deformation to occur proximal to its current position. This change in deformation geometry from a single detachment to a paired system may be due to changes in lithology, or it may possibly represent a lateral ramp (De Vera et al., 2010; T. Dalton, personal communication, 2015) between two earlier separate collapse features that have subsequently coalesced.

Quantification of the strain imbalance

Previous studies have discussed that established concepts of balancing in cross sections do not apply when DWFTB systems are restored and that, commonly, updip extension is approximately 10% greater than its equivalent toe-thrust system (Butler et al., 2010; De Vera et al., 2010). This missing strain is assumed to be a consequence of updip extension being initially accommodated by horizontal compaction of the downslope stratigraphy before deformation is localized onto discrete toe-thrust faults. This model is difficult to verify because these structures are often undrilled, and it would be difficult to prove that the equivalent amount of compaction has occurred. Our results, however, provide an alternative method to validate this model.

Despite the lateral variations in DWFTB geometry and the displacements of contraction and extension in our restorations, the net difference between these values remains consistently between 1000 and 1150 m. As each section displays DWFTB systems of similar total lengths of 19.5 to 22 km, we propose that, in this system, a value of approximately 1 km represents the maximum lateral compaction that can be accommodated prior to the strain being localized onto a discrete fault surface. From a temporal frame, line 1 is representative of the earliest stage of DWFTB development, at which point the extensional updip strain, generated by

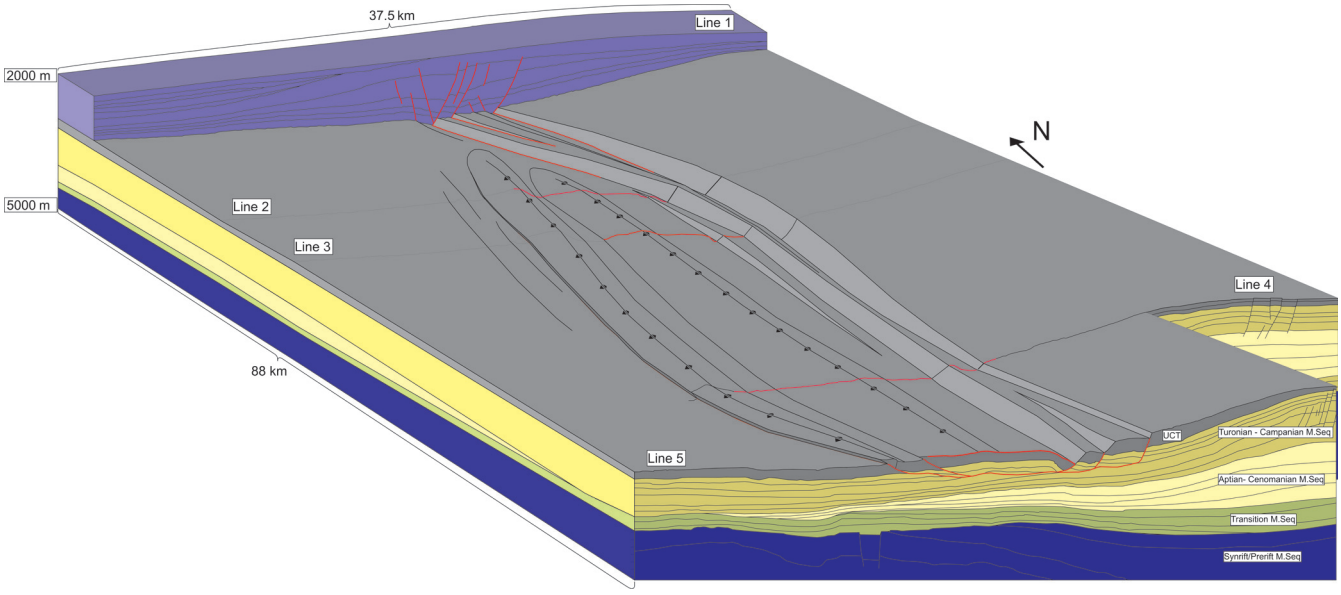

Figure 9. Cartoon illustrating the fault interactions of the Orange Basin gravity collapse structures in three dimensions for the UCT (18AT1) reflector.

Table 1. Tabulated results of the cumulative contraction, extension and calculated net displacement, and missing strain for each section.

	Compression (m)	Extension (m)	Net (m)	DWFTB length (m)	Missing strain (%)
Line 1	0	1008	1008	5917	100.0
Line 2	943	2033	1090	19,589	5.6
Line 3	1043	2166	1123	21,985	5.1
Line 4	577	1673	1096	21,767	5.0
Line 5	818	1836	1018	20,847	4.9
De Vera	16,000	24,000	8000	145,000	5.5
Butler and Paton (2010)	25,000	44,000	19,000	150,000	12.6

the collapse of the margin, is being entirely compensated for by lateral compaction downdip. This amounts to a total of 1 km over 20 km of sediment (i.e., 5%). Lines 2–5 that are representative of the subsequent phase of development, show that subsequent extensional deformation is accommodated through discrete fault slip, thereby maintaining the approximately 1 km imbalance.

Model for growth of collapse

The gravity collapse system we describe in the Orange Basin is relatively simple, allowing a better understanding of the processes involved. Here, we present a temporal evolution model for the system (Figure 10). As demonstrated above, we can establish through the loop tying of reflections and restoration of multiple horizons the relative timing of individual structures within in the collapse. The analysis consistently shows that the first structures form in the center of the system, with extension occurring prior to contraction. Lateral compaction occurs prior to the formation of a thrust domain. Given this premise, we consider that not only do the five lines represent a system that has increasing deformation toward the center (e.g., line 4), but that they can also be viewed as an evolutionary sequence from lines 1 to 4:

1) Differential loading or tectonic uplift of a margin (e.g., Rowan et al., 2004; Paton, 2012) causes widespread instability leading to the formation of normal faults. The strain created by these faults is entirely accommodated via compaction of the downdip margin stratigraphy.
2) Because extensional faulting continues, they coalesce onto a single efficient detachment that allows the effective translation of stress down dip. The resulting contractional strain produced by the translation of stress is compensated by lateral compaction of sediments downslope.
3) Continued margin instability leads to progressive growth of normal faults that in turn increase the strain that the downdip system must accommodate. In this system, after approximately 5% strain, no further strain can be accommodated through compaction. At this point, deformation is accommodated through folds and thrusts extending off the detachment.
4) Once folding and thrusting have initiated, all new deformation is absorbed by faults, assuming the continued presence of a driving force. New normal faults form proximal to the margin, and thrust faults form ahead of the most distal thrust, whereas older faults continue to grow laterally creating a basin at its center. Faults can only grow laterally where a slip surface exists. With increased deformation, other more advantageous slip horizons may present themselves leading to changes in detachment level (e.g., T. Dalton, personal communication, 2015). Because systems continue to grow out into the basin, compaction of distal sediments will occur prior to the formation of additional distal thrusts.

Growth of larger systems

The net approximately 1 km missing strain seen in Table 1 is preserved throughout the continued development of the margin present as a missing strain component. This system is significantly smaller than the other collapse structures observed in the Orange Basin, in which systems can achieve widths of up to 160 km (T. Dalton, personal communication, 2015). Despite this difference in scale, there appears to be a comparable 5% missing strain (De Vera et al., 2010) that is maintained, suggesting that the process may be independent of scale, although further analysis may be needed to determine the influence of the other boundary conditions,

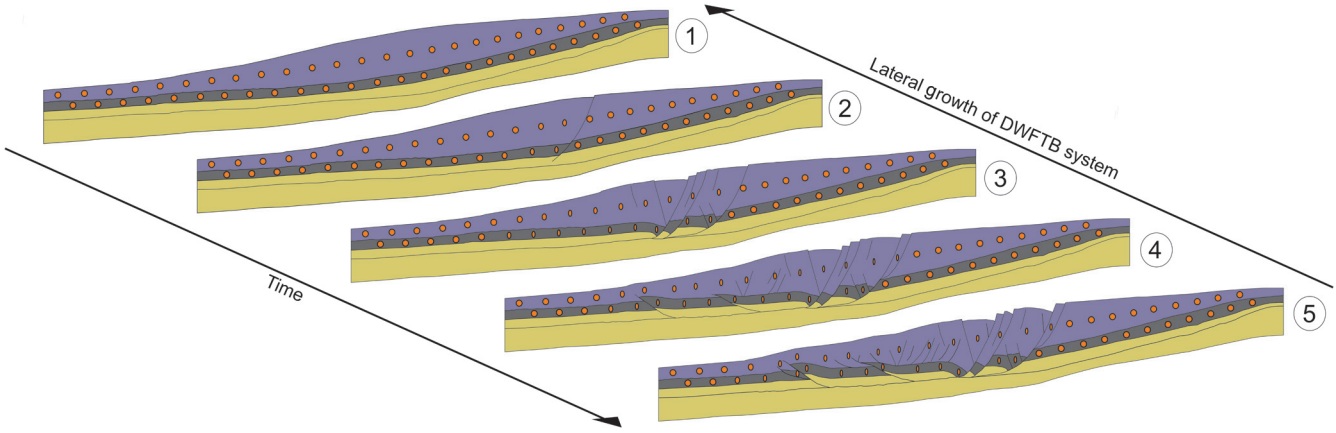

Figure 10. Model of initiation and propagation of a deepwater fold and thrust belt. (1) Normal faults develop and begin to laterally compact the margin sediments, (2) normal faults continue to grow and localize onto a common detachment, (3) because extension continues, the margin sediments become strength hardened and can no longer laterally compact leading to the formation of thrusts, (4) continued strain produced by the growth of normal faults is entirely absorbed by thrusts, and new faults that also form higher in the sequence begin to compact overlying under compacted prekinematic and synkinematic sedimentary packages. Orange ellipses represent strain for the sediments in the margin.

including detachment horizon, thickness of overburden, and relative timing of structures.

We consider that our model is applicable to other shale-detached DWFTB systems globally and conclude that once a compacted rock volume forms, it will continue to transmit strain downdip; thereby, the zone of compaction in front of the emerging thrust front will continue to increase in width as the DWFTB size increases, given updip extension. This results in an approximate 5% missing strain regardless of the system's size. This value may vary on other margins, in direct relation to the mechanical behavior of the stratigraphy involved. As noted by T. Dalton (personal communication, 2015), the specific geometry of the DWFTB, and the faults contained within it, is also a function of the mechanical stratigraphy of the margin. Further studies are required to investigate the role of fault evolution and stratigraphy in influencing spatial and temporal evolution of collapse systems.

Conclusions

The occurrence and geometry of DWFTBs are controlled by a number of well-established factors local to the margins on which they form. Despite these variations, the progression of the failure itself will follow a predictable pattern. Extension will occur in response to a margin imbalance, leading to the compaction of downdip sediments that, once compacted, will localize continued deformation onto a discrete set of thrust planes. The compaction of the margin will be recorded in the imbalance between the amount of extension and contraction that will be approximately 5%. The systems' lateral growth will also conform to the same model, meaning that different stages of collapse will be observable across the margin at the same time.

Acknowledgments

The authors of this study would like to thank Spectrum ASA and the Petroleum Agency of South Africa for releasing the seismic data used in this study. This study was undertaken under the auspices of the Basin Structure Group, and we acknowledge financial support from Getech, BG Group, and EON and the provision of software licences from Midland Valley and Schlumberger. We would also like to thank the editors of this paper, T. Hearon and O. Fernandez, for their insights and comments.

References

Ambrose, W. A., T. F. Wawrzyniec, K. Fouad, S. Sakurai, D. C. Jennette, L. F. Brown, Jr., E. H. Guevara, D. B. Dunlap, S. C. Talukdar, M. A. Garcia, U. H. Romano, J. A. Vega, E. M. Zamora, H. R. Ruiz, and R. C. Hernandez, 2005, Neogene tectonic, stratigraphic and play framework of the southern Laguna Madre-Tuxpan continental shelf Gulf of Mexico: AAPG Bulletin, **89**, 725–751, doi: 10.1306/01140504081.

Bilotti, F., and J. H. Shaw, 2005, Deepwater Niger Delta fold and thrust belt modelled as a critical-taper wedge: The influence of elevated basal fluid pressure on structural styles: AAPG Bulletin, **89**, 1475–1491, doi: 10.1306/06130505002.

Bland, S., P. Griffiths, D. Hodge, and A. Ravaglia, 2006, Restoring the seismic image: Geohorizons, **11**, 18–23.

Brown, L. F., Jr., J. M. Benson, G. J. Brink, S. Doherty, E. H. Jollands, A. Jungslagger, A. Keenen, A. Muntingh, and N. J. S. van Wyk, 1995, Sequence stratigraphy in offshore South African divergent basins — An atlas on exploration for Cretaceous lowstand traps Soekor (Pty) Ltd: AAPG, Studies in Geology 41.

Butler, R. W. H., and D. A. Paton, 2010, Evaluating lateral compaction in deepwater fold and thrust belts: How much are we missing from "nature's sandbox"?: GSA Today, **20**, 4–10, doi: 10.1130/GSATG77A.1.

Corredor, F., J. H. Shaw, and F. Bilotti, 2005, Structural styles in the deep-water fold thrust belts of the Niger Delta: AAPG Bulletin, **89**, 753–780, doi: 10.1306/02170504074.

Deptuck, M. E., K. Kendell, and P. Smith, 2009, Complex deep-water fold-belts in the SW Sable Subbasin, offshore Nova Scotia, Frontiers innovation: Presented at the CSPG CSEG CWLS Convention.

De Vera, J., P. Granado, and K. McClay, 2010, Structural evolution of the Orange basin gravity-driven system, offshore Namibia: Marine and Petroleum Geology, **27**, 223–237, doi: 10.1016/j.marpetgeo.2009.02.003.

Gerrard, T., and G. C. Smith, 1982, Post-Palaeozoic succession and structure of the south-western African continental margin, *in* J. S. Watkins, and C. L. Drake, eds., Studies in continental margin geology: AAPG Memoir 34, 49–74.

Hesthammer, J., and H. Fossen, 1999, Evolution and geometries of gravitational collapse structures with examples from the Statfjord Field, northern North Sea: Marine and Petroleum Geology, **16**, 259–281, doi: 10.1016/S0264-8172(98)00071-3.

Hudec, M. R., and M. P. A. Jackson, 2004, Regional restoration across the Kwanza Basin, Angola: Salt tectonics triggered by repeated uplift of a metastable passive margin: AAPG Bulletin, **88**, 971–990, doi: 10.1306/02050403061.

Jackson, M. P. A., M. R. Hudec, D. C. Jennette, and R. E. Kilby, 2008, Evolution of the Cretaceous Astrid thrust belt in the ultra deep-water Lower Congo Basin, Gabon: AAPG Bulletin, **92**, 487–511, doi: 10.1306/12030707074.

Koopmann, H., B. Schreckenberger, D. Franke, K. Becker, and M. Schnabel, 2014, The late rifting phase and continental break-up of southern South Atlantic: The mode and timing of volcanic rifting and formation of earliest oceanic crust: Geological Society of London, Special Publications vol. 420.

Krueger, A., and E. Gilbert, 2009, Deepwater fold-thrust belts: Not all the beasts are equal: AAPG Search and Discovery, Article 30085.

Lickorish, W. H., and M. Ford, 1998, Sequential restoration of the external Alpine Digne thrust system, SE France, constrained by kinematic data and synorogenic sediments, *in* A. Mascle, C. Puidefabregas, H.P. Lutebacher, and M. Fernandez, eds., Cenozoic Foreland Basins of Western Europe: Geological Society of London, Special Publications 134, 189–211.

Morley, C. K., R. King, R. Hillis, M. Tingay, and G. Backe, 2011, Deepwater fold and thrust belt classification, tectonics, structure and hydrocarbon prospectivity: A review: Earth Science Review, **104**, 41–91.

Muntingh, A., and L. F. J. Brown, 1993, Sequence stratigraphy of petroleum plays, post-rift Cretaceous rocks (lower Aptian to upper Maastrichtian), Orange Basin, South Africa: Siliciclastic sequence stratigraphy: Recent Applications of Siliciclastic Sequence Stratigraphy, *in* P. Weimer, and H. Postmentier, eds., Siliciclastic sequence stratigraphy: Recent developments and applications 58, AAPG, 71–98.

Paton, D. A., 2012, Post rift deformation of the North East and South Atlantic margins: Are "passive margins" really passive?: *in* K. MBusby, ed., Tectonics of sedimentary basins: Recent advances: Wiley, 249–269.

Paton, D. A., R. di Primio, G. Kuhlmann, D. van der Spuy, and B. Horsfield, 2007, Insights into the petroleum system evolution of the southern Orange Basin, South Africa: South African Journal of Geology, **110**, 261–274.

Paton, D. A., D. van der Spuy, R. di Primio, and B. Horsfield, 2008, Tectonically induced adjustment of passive-margin accommodation space; influence on hydrocarbon potential of the Orange Basin, South Africa: AAPG Bulletin, **92**, 589–609, doi: 10.1306/12280707023.

Peel, F. J., 2014, The engines of gravity-driven movement on passive margins: Quantifying the relative contribution of spreading vs. gravity sliding mechanisms: Tectonophysics, **633**, 126–142, doi: 10.1016/j.tecto.2014.06.023.

Rowan, M. G., F. J. Peel, and B. C. Vendeville, 2004, Gravity driven fold belts on passive margins, *in* K. R. McKay, ed., Thrust tectonics and hydrocarbon systems: AAPG, Memoir **82**, 157–182.

Totterdell, J. M., and A. A. Krassay, 2003, The role of shale deformation and growth faulting in the Late Cretaceous evolution of the Bight Basin, offshore southern Australia, *in* P. Van Rensbergen, R. R. Hillis, A.J. Maltman, and C.K. Morley, eds., Deep subsurface sediment mobilization: Geological Society of London, Special Publications 216, 429–442.

Biographies and photographs of the authors are not available.

Part A –

III: Published version of the paper featured in Chapter 6

Marine and Petroleum Geology 82 (2017) 163–177

Contents lists available at ScienceDirect

Marine and Petroleum Geology

journal homepage: www.elsevier.com/locate/marpetgeo

Research paper

The importance of missing strain in Deep Water Fold and Thrust Belts

T.J.S. Dalton [a, *], D.A. Paton [a], S.J. Oldfield [a], D.T. Needham [a, b], A.M. Wood [a, c]

[a] Basin Structure Group, School of Earth and Environment, University of Leeds, UK
[b] Needham Geoscience Ltd., 10 Ghyll Wood, Ilkley, LS29 9NR, UK
[c] Shell Global Solutions Netherlands, Rijswijk, The Netherlands

ARTICLE INFO

Article history:
Received 14 September 2016
Received in revised form
13 January 2017
Accepted 16 January 2017
Available online 19 January 2017

Keywords:
Deep water fold thrust belts
Orange basin
Pyrenee's: Sesimic interpretation
Restorations: Gravity driven collapse

ABSTRACT

Deep water fold and thrust belts (DWFTBs) are sedimentary wedges that accommodate plate-scale deformation on both active and passive continental margins. Internally, these wedges consist of individual structures that strongly influence sediment dispersal, bathymetry and fluid migration. Most DWFTB studies investigate basin- and intra-wedge- scale processes using seismic reflection profiles, yet are inherently limited by seismic resolution. Of critical importance is strain distribution and its accommodation on discrete faults compared to distributed deformation. Recent studies have considered strain distribution by investigating regional reflection DWFTBs profiles within coupled systems, which contain down-dip compression and up-dip extension. There is broad agreement of a mis-balance in compression versus extension, with ~5% excess in the latter associated with horizontal compaction, yet this remains unproven.

Using two exceptionally well exposed outcrops in the Spanish Pyrenees we consider deformation of DWFTB at a scale comparable to, and beyond, seismic resolution for the first time. By coupling outcrop observations (decametre to hectometre scale) with a re-evaluation of seismic profiles from the Orange Basin, South Africa, which contains one of the best imaged DWFTBs globally, we provide a unique insight into the deformation from metre to margin scale. Our observations reveal hitherto unrecognised second order structures that account for the majority of the previously recognised missing strain. This re-evaluation implies that ~5% missing strain should be accounted for in all DWFTBs, therefore existing studies using restorations of the sediment wedge will have underestimated crustal shortening in active margins, or sedimentary shortening in gravity driven systems by this amount. In contrast to previous studies, our observations imply that the majority of this strain is accommodated on discrete fault surfaces and this can explain the occurrence and location of a range of intra-wedge processes that are intimately linked to structures including sediment dispersal, fluid migration pathways and reservoir compartmentalisation.

1. Introduction

Deep Water Fold and Thrust Belts (DWFTBs) occur on continental margins globally and are a consequence of the contraction of sedimentary sequences that are decoupled from underlying stratigraphy or basement by a décollement horizon (Rowan et al., 2004; Morley et al., 2011). The driving force that induces the contraction can occur either at a crustal scale, as is the case in an accretionary prism on an active margin (Type II; Morley et al., 2011), or within the decoupled sedimentary sequence as a consequence of gravitational processes, on an Atlantic-style passive margin (Type I: Morley et al., 2011). Regardless of the setting, processes that are intimately linked to the resulting deformation span the margin-scale geometry of the fold and thrust belts including critical taper angle (e.g. Dahlen et al., 1984), the structural configuration and stratigraphic fill of associated sedimentary basins (Morley, 2007; Fillon et al., 2013) and the role of fluids that migrate through them (Saffer and Bekins, 2001). Quantifying the strain distribution across a DWFTB is therefore fundamental to understand these processes.

An entire DWFTB system comprises three domains: an up-dip extensional domain, a down-dip contractional domain and a transitional domain in-between (Krueger and Gilbert, 2009). An essential technique applied to understanding DWFTBs, and the

Abbreviations: DWFTBs, Deep water fold thrust belt.

* Corresponding author.
E-mail address: T.J.Dalton@leeds.ac.uk (T.J.S. Dalton).

http://dx.doi.org/10.1016/j.marpetgeo.2017.01.013
0264-8172/

distribution of strain across these three domains, is the kinematic restoration of stratigraphic sequences. This is commonly based upon interpretation of an increasing number of seismic reflection profiles covering DWFTBs. Conceptually shortening across the entire system should balance, however, recent studies document a 5–10% imbalance between extensional and contractional domains in favour of extension (Fig. 1) and outline the importance of this value on our understanding the evolution of DWFTB systems (de Vera et al., 2010; Butler and Paton, 2010; Dalton et al., 2015). This 5–10% imbalance is calculated assuming the contraction due to the recorded missing strain component is distributed in both the extensional and contractional domains as per Dalton et al. (2015). This imbalance is implicit from the initiation of growth and throughout the growth of the structure as seen in Fig. 1.

Although many of these recent studies have considered coupled extension and compressional systems, the same principles are as applicable to accretionary prisms as they are to passive margins. In the latter, for example, an accurate quantification of compression is important for both plate kinematic predictions as well as basin fill architecture in a range of settings including Sinu-Jacinto offshore Columbia, Barbados Ridge and Taiwan (Biju-Duval et al., 1982; Davis et al., 1983; Robertson and Burke, 1989; Toto and Kellogg, 1992; Vinnels et al., 2010). In certain settings where there is a complex interplay of accretionary prism and gravity collapse processes occurring (e.g. NW Borneo), differentiating between the two processes is essential to understanding the whole system evolution (Franke et al., 2008; Hesse et al., 2010; King et al., 2010).

Central to any analysis of a DWFTB, be it accretionary prism or gravity induced, is this mismatch in strain. In this study we couple field observations with seismic reflection examples of the extensional portion of DWFTB's to investigate this question. Through the identification of previously unrecorded contractional features present within the extensional domain we reconsider how strain is distributed across the system and discuss how this influences our current understanding of the associated processes.

2. Quantification of sub-seismic scale strain

As most studies of DWFTBs are based upon seismic reflection profile analysis, an obvious limitation to quantifying the missing strain component in such profiles is the issue of how much strain is accommodated at a sub-seismic scale. Previous work in extensional settings has highlighted and quantified the potential impact of sub-seismic deformation on terms of both hydrocarbon exploration and production (Wood et al., 2015a, 2015b). Here we address the issue of sub-seismic deformation in DWFTBs by considering two well exposed outcrops in the Spanish Pyrenees that reveal as yet undocumented deformation across three orders of magnitude. The first is a decametre scale example in Laspuña (Fig. 2). The second investigates a larger (hectometre) scale example at Armeña, Spain (Fig. 2).

2.1. Case study 1; decametre scale; Laspuña

A distinctive set of multiphase growth faults detaching onto a basal detachment is observed in the cliff section immediately to the west of the village of Laspuña. The syn-kinematic growth packages in the top of the normal faults seen in the cliff are indicative of the extensional domain of a DWFTB. This DWFTB is located on the then uplifting, north-eastern flank of the Ainsa Basin (Pickering and Bayliss, 2009) in the Spanish Pyrenees (Fig. 2).

The stratigraphy that is deformed by the DWFTB comprises marls and fine sand slope deposits (Dreyer et al., 1999) and are of Early Ypresian age (Pickering and Corregidor, 2005). The slope sediments present at Laspuña were depositing whilst the Peña Montañesa, Cotiella and La Fueba thrusts systems were active (Muñoz et al., 2013). The DWFTB presently sits structurally below these thrust faults (Fig. 2), the slope was generally stable allowing deposition of successions of muddy sediments. The active tectonic system and a mud dominated semi-lithified slope provided the ideal conditions for gravitational collapse to occur. During phases of tectonic activity on the surrounding thrust systems stable paleo-slopes were uplifted and became mobilized, forming mass transport complexes (Dakin et al., 2012). At Laspuña, failure of the slope did not result in mass transport remobilisation, but resulted in the formation of growth faults, indicative of multiple phases of extension and syn-deposition, shifting sediments south west downslope into the Ainsa Basin. This difference in deformation may be as a result of smaller uplift events occurring over a longer time period allowing a slower readjustment of surface slope geometry or an effect of the presence of an underlying slip horizon making DWFTB formation more practical than outright slope failure.

The cliff section, in which the DWFTB is observed, is divided into four packages (1–4, bottom to top) based upon their lithology and internal geometry. The lowest package (Package 1, Figs. 3 and 4) is composed of a largely undeformed dark grey succession of more

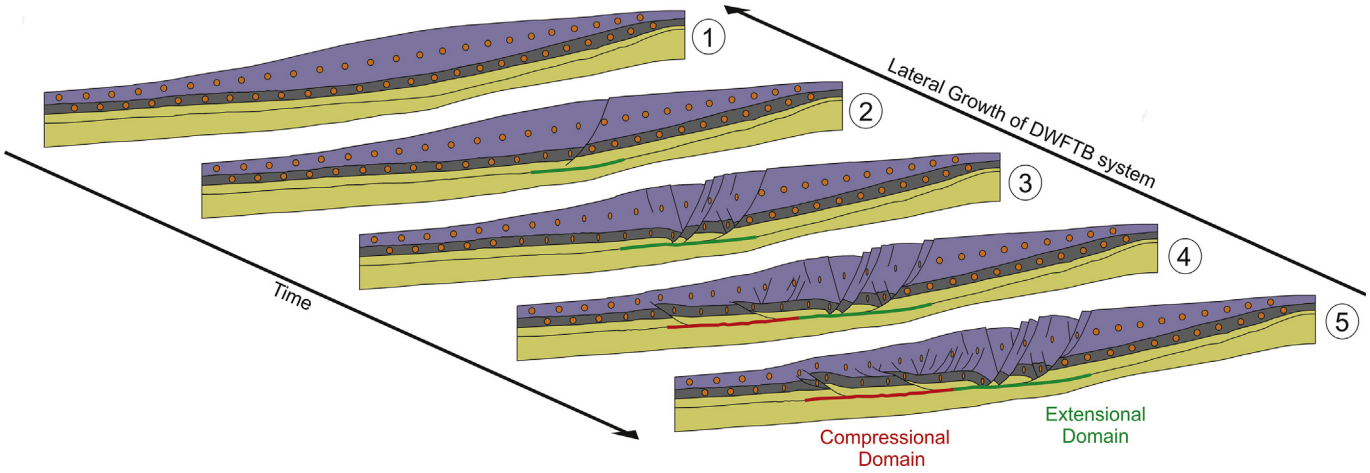

Fig. 1. Conceptual model for the growth of a DWFTB in both space and time indicating the missing strain component is not explained by lateral deformation elsewhere along the margin, Dalton et al. (2015). The location of extensional and compressional domains are also shown along with Orange circles representing the lateral compaction of sediments in the wedge. (For interpretation of the references to colour in this figure legend, the reader is referred to the web version of this article.)

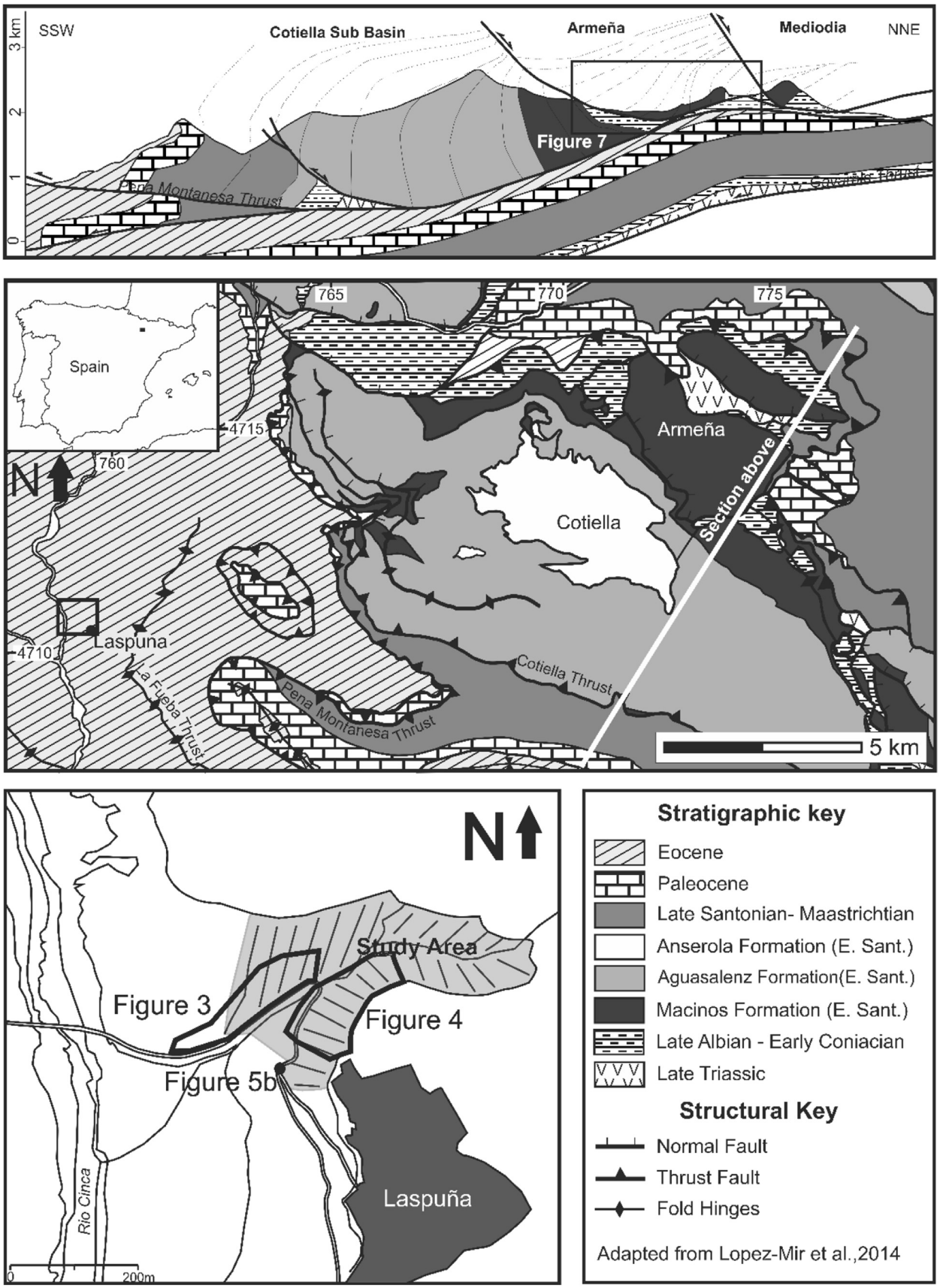

Fig. 2. Location and geological map of the two areas used in this study along with a cross-section through the three faults in the Cotiella extension system; with the upper map displaying the location of both areas, adapted from Lopez-Mir et al. (2014); and the lower zoomed in map of the study area beneath Laspuña indicating the location of Figs. 3, 4 and 5b. The cross section extends to the end of the Pena Montanessa thrust just off the edge of the geological map.

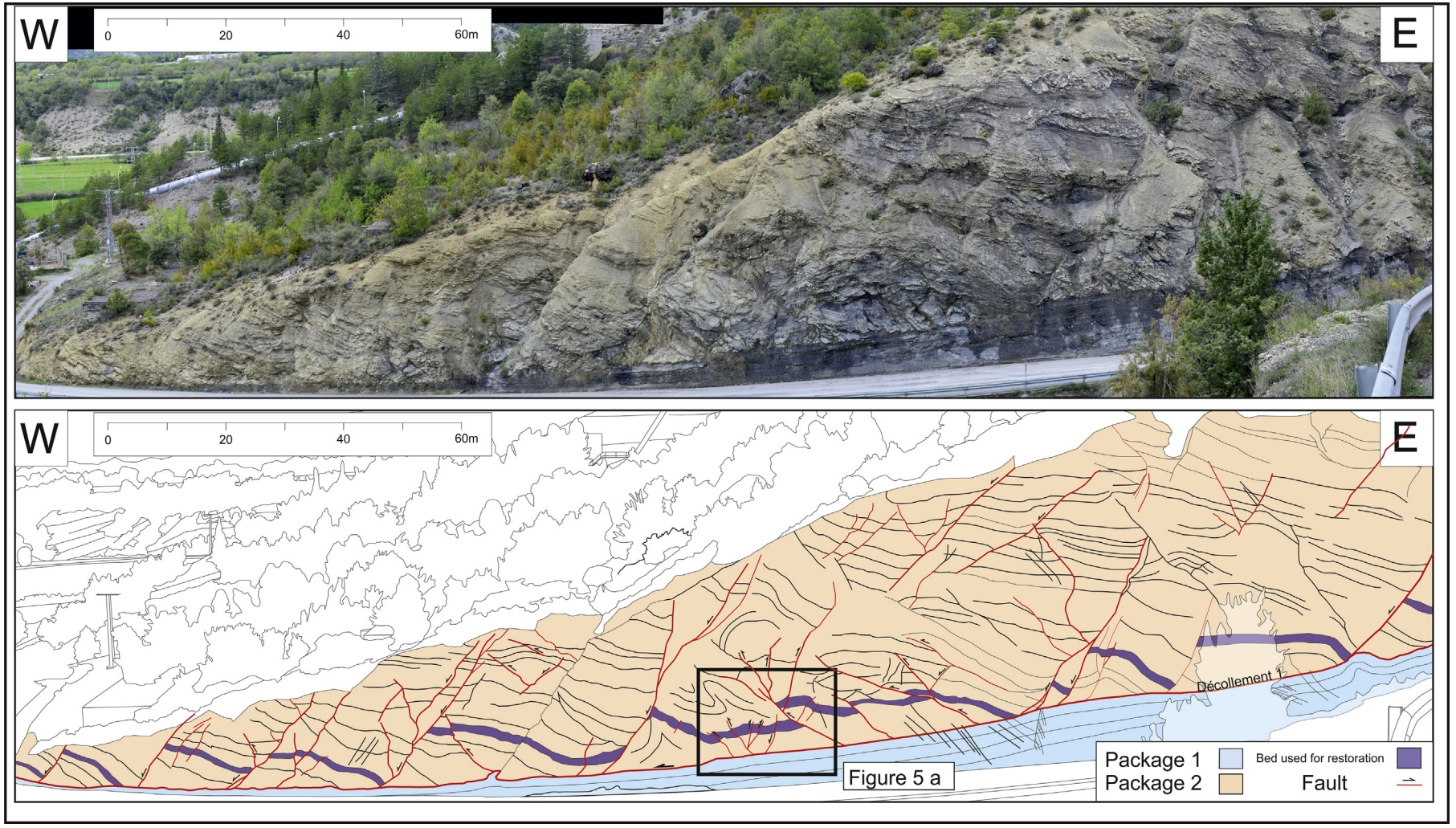

Fig. 3. Image and interpretation of the 240 m long cliff section in the valley beneath Laspuña. Faults are indicated in red, DWFTB package in orange, undeformed sub-detachment horizon in blue. For location see Fig. 2. (For interpretation of the references to colour in this figure legend, the reader is referred to the web version of this article.)

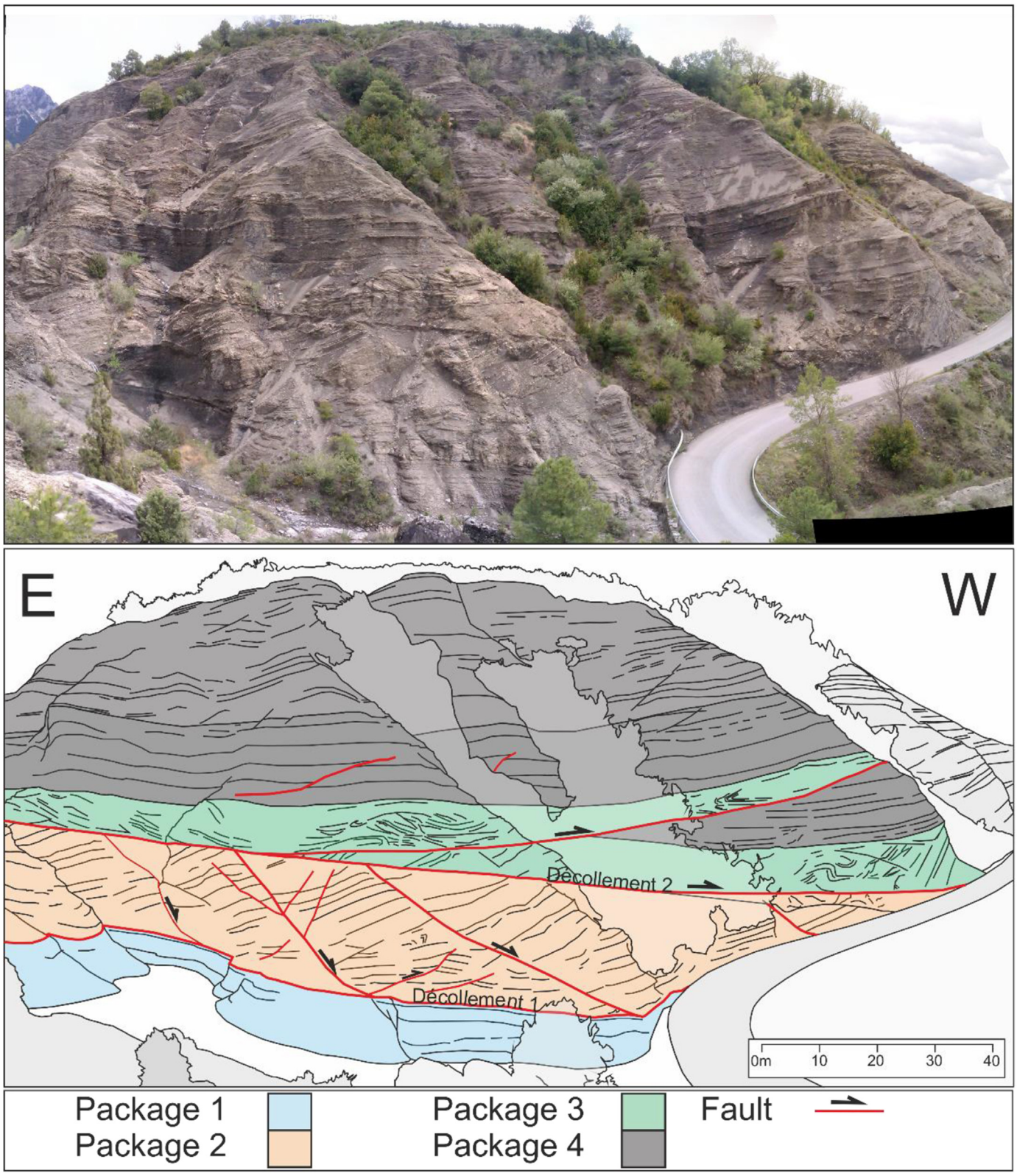

Fig. 4. View of the valley beneath Laspuña showing the stratigraphy that overlies that observed in Fig. 3. Faults are indicated in red, DWFTB package in orange, undeformed sub-detachment horizon in blue, chaotic package in green, planar concordant laminated beds in black. Also marked is the location Fig. 5a. For location of profile see Fig. 2. (For interpretation of the references to colour in this figure legend, the reader is referred to the web version of this article.)

organically rich concordantly layered marls. Package 2 is defined by a sequence of light grey/brown muds with thin inter-beds of fine sands, which become thicker and more numerous towards the top of the cliff. Within this package a set of west dipping listric normal

faults with throws of 8–15 m is observed. Striae on the fault planes indicate a westerly displacement of material into the Ainsa Basin. These faults detach onto a common décollement (Décollement 1) along the upper surface of Package 1 (Fig. 3); this is the extensional domain of the DWFTB. The top of Package 2 is truncated by a distinctive planar, gently west dipping fault surface, Décollement 2 (Fig. 4). Above this is Package 3 which comprises a chaotic package of folded and faulted, muds and sands. This is topped by Package 4, a succession of dark grey planar concordant laminated beds. Packages 3 and 4 contain a set of evenly spaced thrust faults with displacements of up to 40 m, which detach onto Décollement 2 (Figs. 4 and 5 b). These potentially form part of the contractional domain of a distal, later DWFTB for which the up-dip continuity does not crop-out.

The scale of the DWFTB systems present at Laspuña offers the opportunity to observe the internal structure of the fault blocks and in particular minor structures formed during deposition and deformation (Fig. 5). Restorations of DWFTBs imply the preservation of pre-kinematic bedding within the fault blocks. However, we observe that significant internal deformation is present within the extensional and compressional blocks. Within the extensional fault blocks we observe multiple thrust features with throws of 0.2–3 m as well as significant folding (Fig. 5 a). This smaller scale deformation is present equally in the contractional domain in Packages 3 & 4 which show smaller scale thrust faults with throws of 0.5–1 m and folding, in between larger thrusts (Fig. 5 b). These smaller scale contractional features (<5 m throw) are largely unresolvable at the outcrop scale (Fig. 4), yet detailed analysis reveals that many of these surfaces that appear undeformed at outcrop scale contain kinematic indicators that show significant internal compression (Fig. 5).

These two sections in the Laspuña DWFTB system illustrate that not only does deformation occur at a range of scales, but more importantly, there is evidence of compression within the extensional domain. Such deformation has not been demonstrated before and is therefore not accounted for in current DWFTB restorations. To understand the impact of these smaller scale contractional structures on a restoration we present two interpretations of the same section (Fig. 3). The first interpretation (Fig. 6 a) is equivalent to existing DWFTB sections and does not incorporate these smaller contractional structures (i.e. equivalent to these structures being below observable resolution). While the second interpretation (Fig. 6 b) is a detailed interpretation across the section including contractional features. It can be seen in Fig. 6

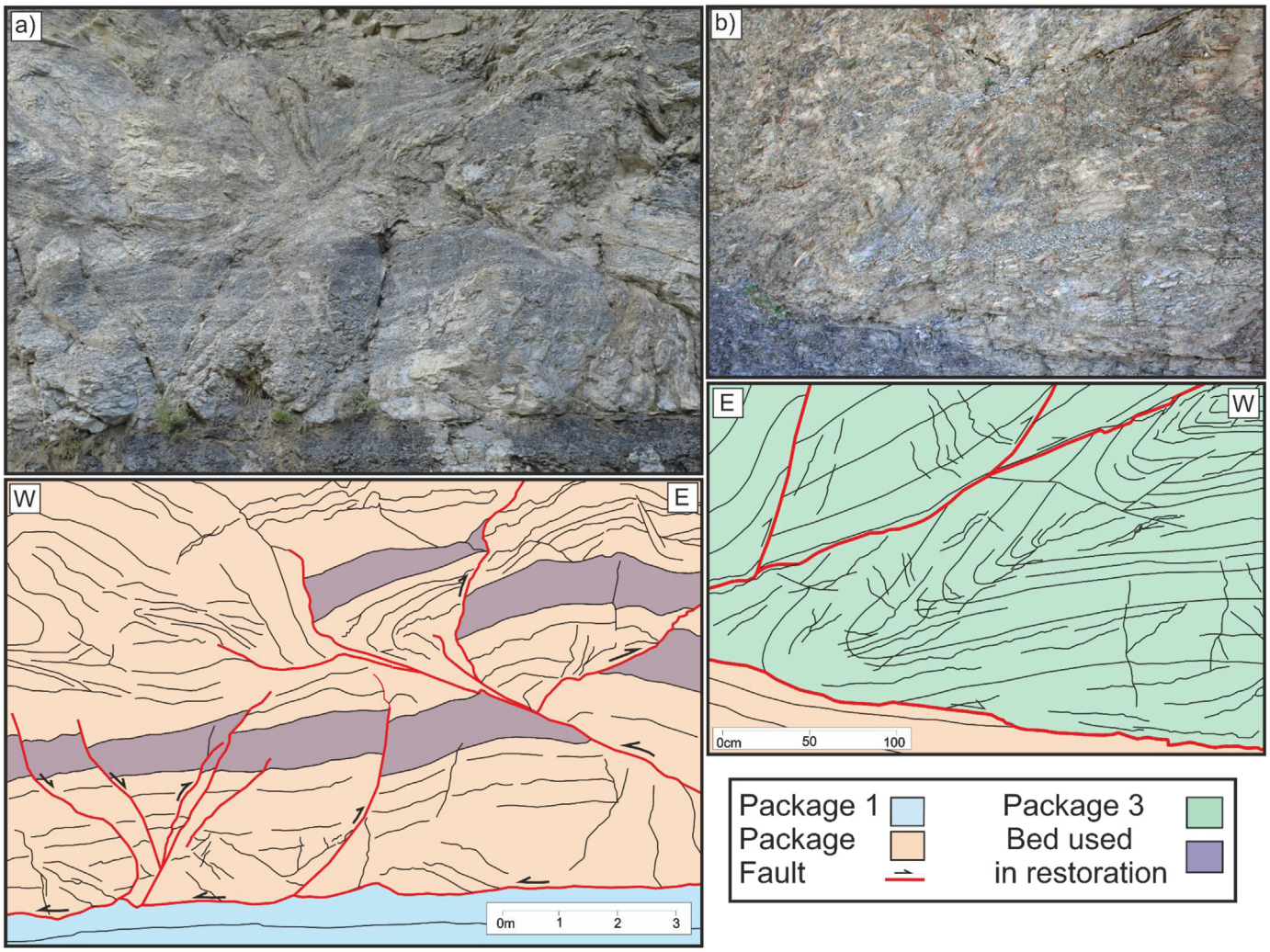

Fig. 5. Interpreted and uninterpreted image of cliff sections seen from base of the cliff showing: a) the compaction of beds within normal fault blocks, b) the contraction of beds within thrust fault blocks. The purple horizon is the horizon used for the restoration. See Fig. 3 and 4 for location. (For interpretation of the references to colour in this figure legend, the reader is referred to the web version of this article.)

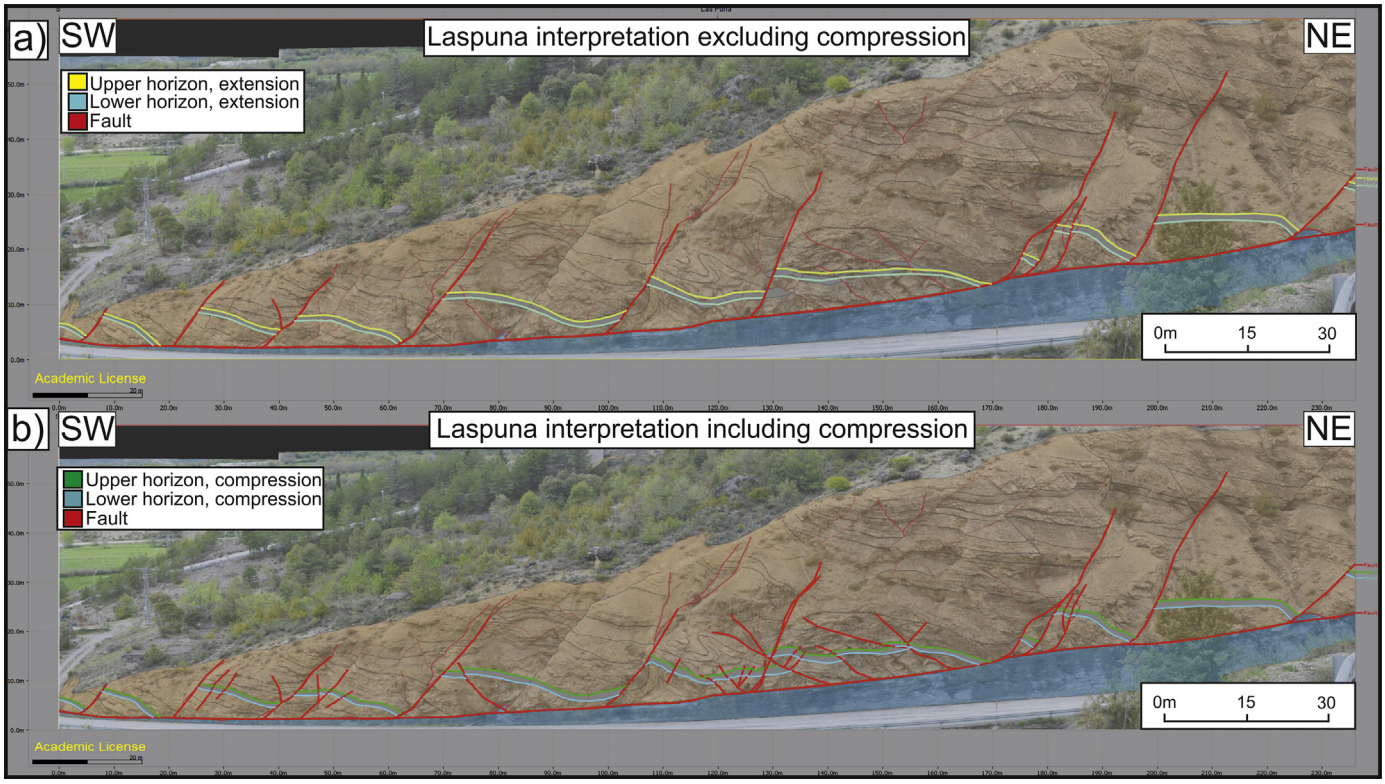

Fig. 6. Two different interpretations of the section in Fig. 3; a) based upon what is observed from the opposite side of the valley where only large scale structures can be interpreted, b) interpretation based upon data collected from the outcrop itself, at road level. Both interpretations use the bed in Fig. 5a for the purposes of restoration.

b that the contractional features are isolated within single fault blocks and are thus not pre-existing deformation features. Both interpretations use the same distinct dark grey pre-kinematic bed that is present throughout the collapse (Fig. 5 a). Slickensides on fault planes indicate this section is within 10° of the transport direction, making it viable for restoration (Price, 1981). We then restore both sections to a pre-deformed geometry and calculate the extensional strain when the small scale contractions are ignored compared to when they are accounted for (Table 1).

In Table 1 the significance of contractional features becomes clear, with the measurement of total displacement being 11–14 m less. The difference recorded in the total amount of strain ranges from 4.6 - 5.9% implying these sediments would be ~5% more compressed than expected. These figures are comparable with the missing strain component identified in seismic examples in Dalton et al. (2015) of ~5% and thus may offer an explanation for the observed miss-balance.

The Laspuña section is clearly small scale and therefore the validity of scaling these observations to larger examples is critical if we want to consider margin scale (>60 km long) DWFTBs. To address this we consider a larger (4 km wide) DWFTB that crops-out approximately 25 km to the north-east of Laspuña at Armeña (Fig. 2) as this allows us to observe whether similar contractional structures are present in larger systems.

2.2. Case study 2; hectometre scale; Armeña

The gravity driven, growth fault system at Armeña, Huesca, Spain (Fig. 2) has been described by McClay et al. (2004), Lopez-Mir et al. (2014, 2015) and Tavani et al. (2015). This growth fault forms part of the Cotiella extension system that formed in the Coniacian to Early Santonian during a post-rifting thermal subsidence phase of basin evolution (Vergés et al., 2002). It comprises three listric growth faults traversing a 14 km section orientated NE-SW (Lopez-Mir et al., 2015, Fig. 2). The best exposed of these three growth faults is the 4 km wide cliff section above the Refugio d'Armeña (Fig. 7) referred to as the Armeña growth fault (Lopez-Mir et al., 2014). Extension initiated in the Coniacian and continued into the

Table 1
Table of results for the restorations undertaken of Fig. 6a) and b).

	Original lengths (m)	Current length (m)	Displacement (m)	Extension
Upper Horizon Comp.	200.5	240	39.5	**16.5%**
Upper Horizon Extension	211.5	240	28.5	**11.9%**
Lower Horizon Comp.	195.9	240	44.1	**18.4%**
Lower Horizon Extension	210	240	30	**12.5**
	With compression	Without compression		Difference
Upper	16.5%	11.9%		**4.6%**
Lower	18.4%	12.5%		**5.9%**

Figures in bold show the results of the analysis.

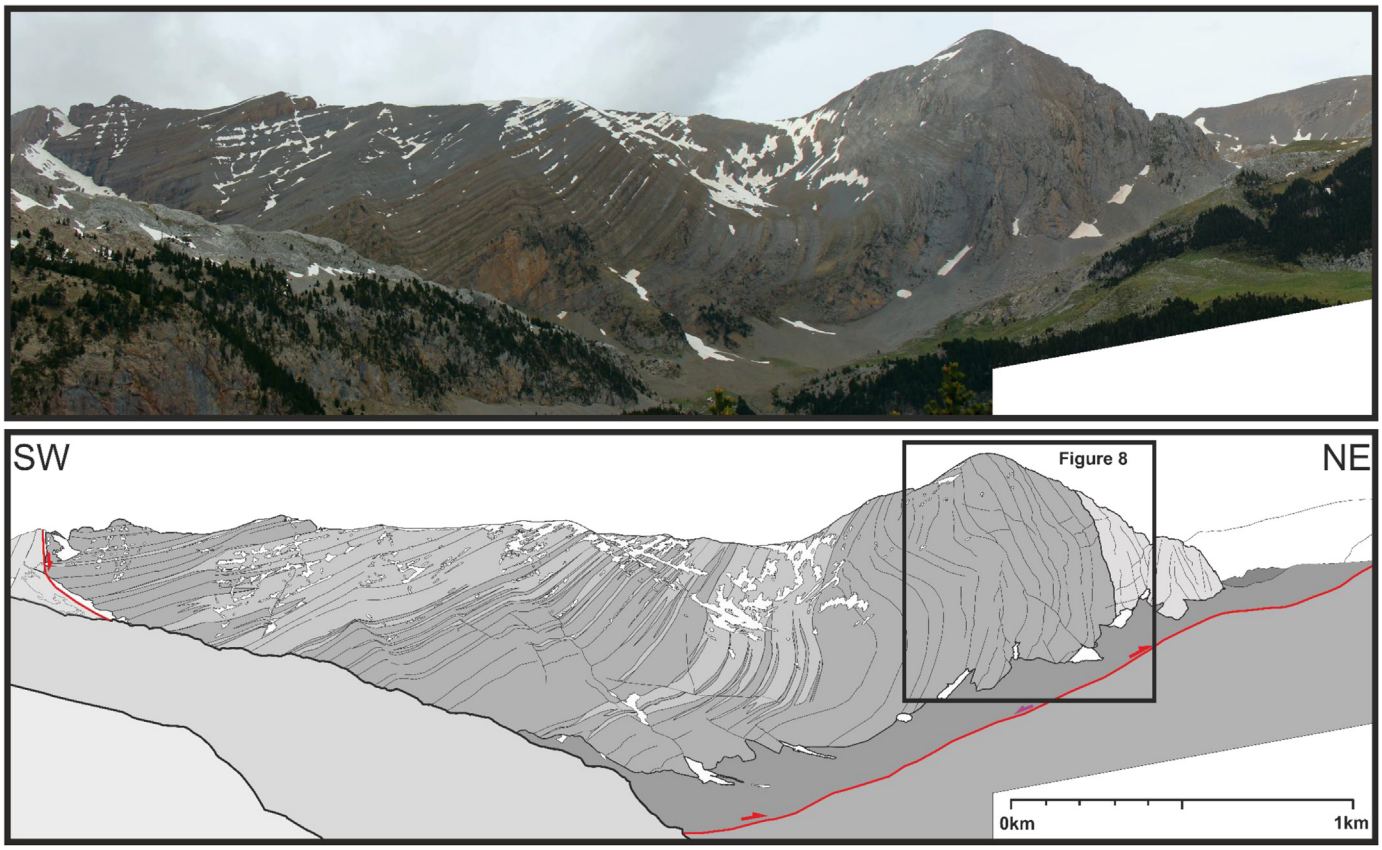

Fig. 7. Interpretated and uninterpreted image of the growth fault at Armeña, location on Fig. 2. The red box indicates the location of Fig. 8. (For interpretation of the references to colour in this figure legend, the reader is referred to the web version of this article.)

Early Santonian depositing up to 3 km of syn-kinematic carbonates and calcarenites which diverge towards the southwest, within the hanging wall of the controlling listric normal fault indicating a north easterly extension (Lopez-Mir et al., 2014). They are deposited above a pre-kinematic Upper Cenomanian to Turonian limestone succession (McClay et al., 2004). This overlies Late Triassic shales and evaporites that crops out at the northern end of the cliff section (Fig. 8). The top of this Triassic sequence also forms the detachment horizon for all three growth faults.

The collapse structure at Laspuña implies that the most likely location for contractional features in extensional fault blocks is within the pre-kinematic sequence. Fig. 8 shows the pre-kinematic Upper Cenomanian to Turonian limestone succession. The more competent limestones have better preserved bedding than the more mobile muds at Laspuña and so do not show the same amount of ductile deformation. Within these limestones multiple brittle contractional structures are present throughout, the largest being a ~100 m displacement thrust on the north-eastern flank (Fig. 8). Multiple (10+) smaller intra-layer thrusts with throws of less than 10 m are also observed throughout the cliff. The orientation of these contractional features are consistent with a south-west to north-east transport direction (as indicated by striae on fault surfaces) and is therefore not related to the later phase of north east to south-west inversion. Despite later inversion Tavani et al. (2015) affirms syn-kinematic fracturing has been well preserved. Folding of beds in the hanging wall of the thrust and the orientation of the throw are incompatible with the orientation of the inversion event.

Restorations of the three normal faults in Lopez-Mir et al. (2014), reveal a total extension of 8.1 km over 13.9 km. Assuming a missing strain component of 5% (Dalton et al., 2015) is compensated for by second order structures, compressive features totalling ~650 m should be present over the three faults, with ~215 m displacement being accommodated within the Armeña growth fault, assuming an equal distribution. The observation of a ~60 m displacement thrust and multiple smaller displacement (~10 m) contractional structures is in agreement with that prediction. From this we would suggest that 5% of measured extension is compensated by second order structures which should be prevalent in the extensional portion of DWFTBs.

The observation that 5% of the recorded extensional deformation is accommodated by smaller scale features in Armeña concurs with the observations made at Laspuña which are consistent with a scale invariant relationship. We now consider if these features are similarly present on margin-scale DWFTBs imaged on seismic reflection profiles.

3. Application to seismic scale; Orange Basin

We choose a DWFTB within the Orange Basin (Fig. 9), offshore South Africa and Namibia, because the geological evolution of the margin has been well established (Gerrard and Smith, 1982; Brown et al., 1995; Mohammed et al., 2015) and DWFTBs are a well-documented and common feature found throughout the basin (Muntingh and Brown, 1993; Paton et al., 2008; Peel, 2014; Dalton et al., 2016). Restorations of these DWFTBs have been undertaken by de Vera et al. (2010), Butler and Paton (2010) and Dalton et al. (2015), all of which identified a shortfall in contractional features versus extensional. This imbalance, ~5% (Dalton et al., 2015), is equivalent to the 5% of strain recorded in the contractional features

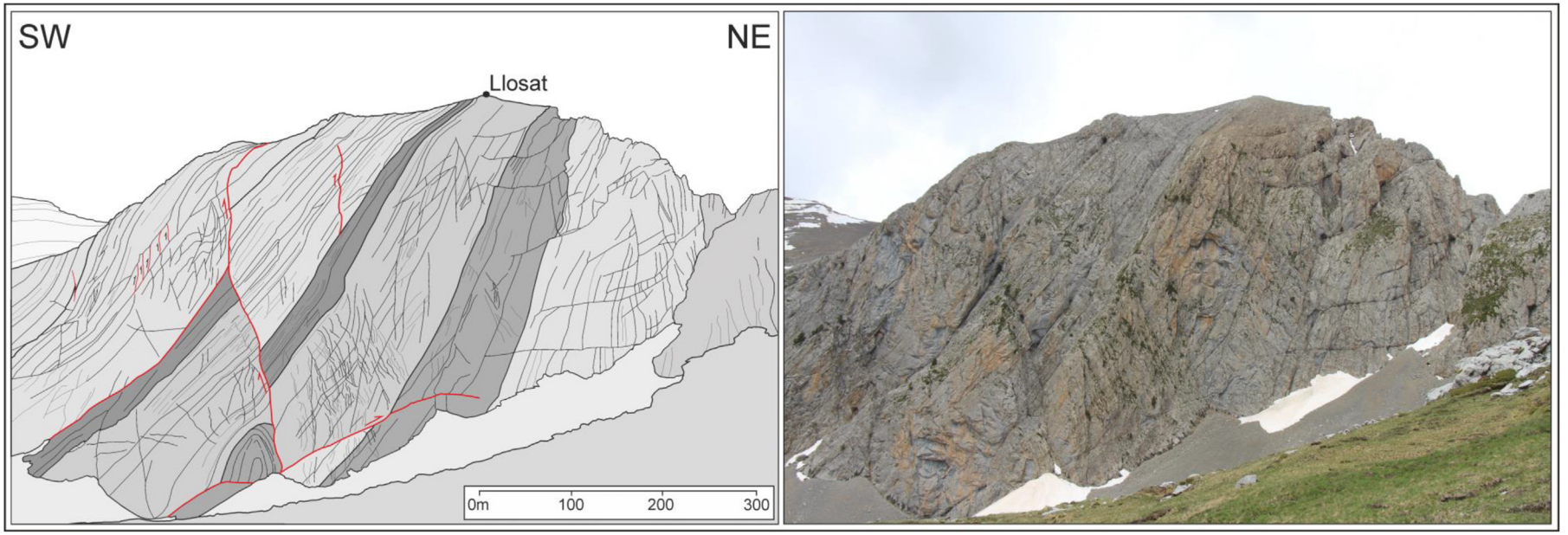

Fig. 8. Interpreted and uninterpreted cliff section view of pre-kinematic Upper Cenomanian limestones viewed from beneath Llosat indicating contractional features. Larger contractional faults associated with the extensional phase of DWFTB formation have been picked out in red. For location see Fig. 7. (For interpretation of the references to colour in this figure legend, the reader is referred to the web version of this article.)

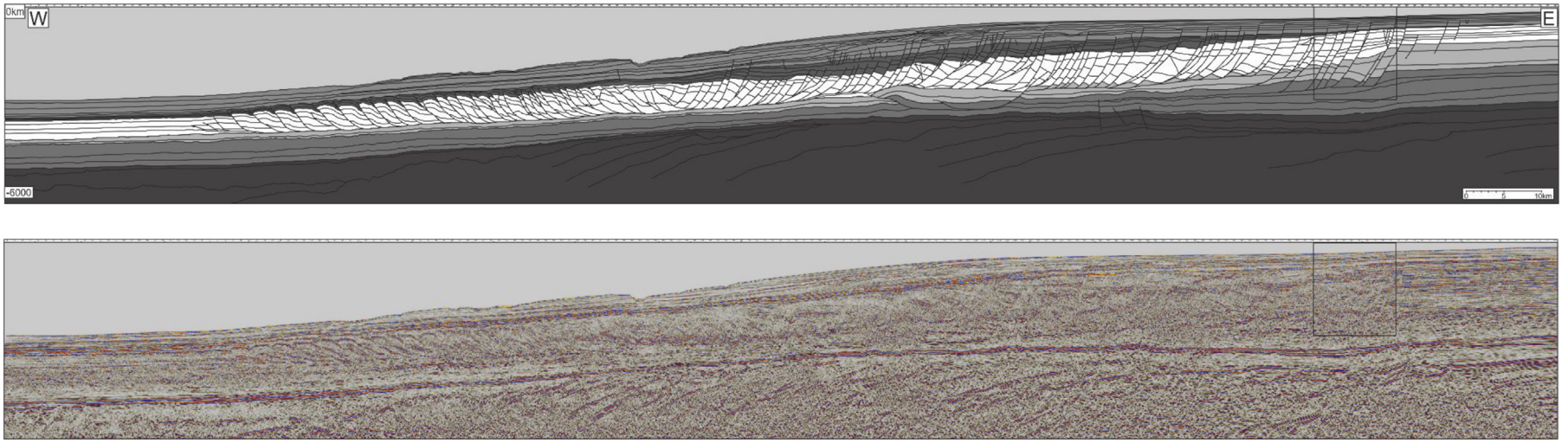

Fig. 9. A 196 km long seismic section through an entire DWFTB from the Orange Basin offshore Namibia. For Location see Fig. 10. The seismic profile is courtesy of Spectrum.

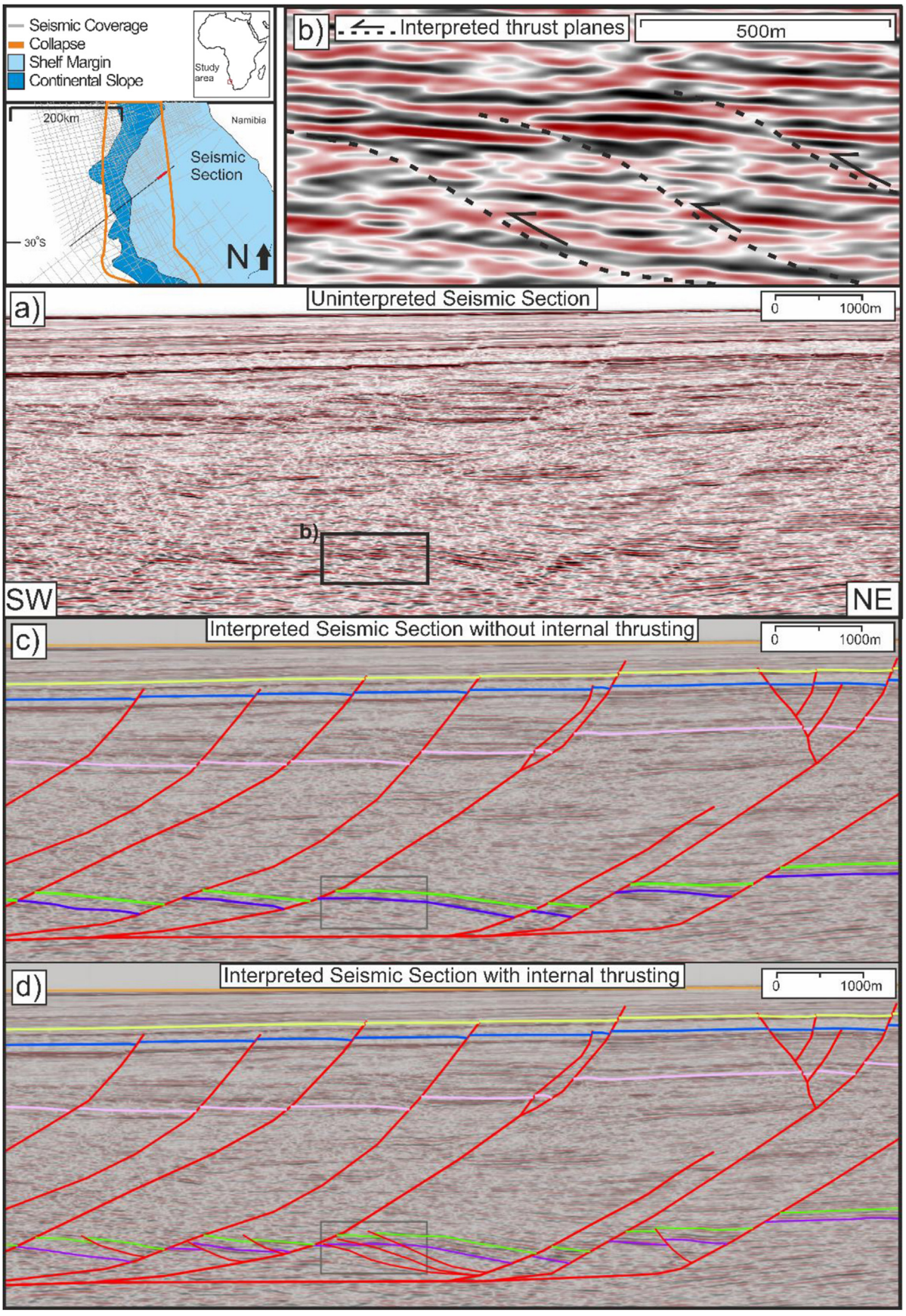

Fig. 10. Interpreted and uninterpreted seismic sections through the extensional domain of a DWFTB in the Orange Basin, Namibia; **a)** Uninterpreted seismic section used in this study; **b)** Zoomed in section of a) displaying potential compressional features; **c)** Interpreted section not accounting for contractional features; **d)** Interpreted section assuming

within the extensional domain of the DWFTB at Laspuña. Our field observations would suggest that contractional structures should be present within the larger extensional structures observed in the data presented by Dalton et al. (2015) although predict that they would be close to seismic resolution.

Our observations from Laspuña and Armeña suggest if these smaller contractional features are present, they are most likely to form in the pre-kinematic horizons towards the base of normal fault blocks. These portions of the collapse structures are frequently unresolvable, especially in more mature parts of the system where multiple phases of collapse have occurred and been overprinted. To overcome this difficulty we select a portion of an extensional domain (Fig. 10 a, see Fig. 9 for location) which contains later, more distal, normal faults and where seismic imaging is good. The reflections in the upper part of the collapse (Fig. 10 a, light blue and yellow horizons) are broadly parallel and faulted in several places. The base of this package is picked by a high amplitude reflection (just below the blue horizon), which is the well documented Tertiary unconformity (Paton et al., 2008). The reflections beneath the unconformity have a shallow dip towards the south west, with multiple upper reflections truncating against the Tertiary unconformity heading progressively north east. These reflections are discontinuous in their horizontal extent and are broken by steeply dipping discontinuities that extend through the package. This style of response appears throughout the remainder of the section till the base where a number of broadly horizontal continuous reflections are present. The discontinuous packages represent Late Cretaceous sediments rotated by normal faults within the extensional domain. The termination of the discontinuous reflections defines the location of normal faults. The continuous reflections are beneath the horizon on which these faults detach and are thus undeformed.

At the scale of the regional section (Fig. 9), previous restorations of the 156 km long section (de Vera et al., 2010; Butler and Paton, 2010) interpreted that the reflections are continuous between normal faults implying no internal deformation (Fig. 10 c). However, when we consider these apparently low strain areas in more detail we observe that reflections are not parallel and show truncation and localised repetition of reflections that are best explained by the presence of thrust faults (Fig. 10 b). These structures are most prevalent in pre-kinematic horizons at the base of fault blocks, as our observations at Laspuña and Armeña predict.

We choose two pre-kinematic horizons affected by these second order thrust faults as well as a number of higher horizons to make two interpretations. We apply the same method as at Laspuña and undertake one restoration that ignores contractional features (Fig. 10 c) and a second (Fig. 10 d) that accounts for the contractional features. The interpretation of the 1st order extensional faults remains the same for both. This allows us to isolate the effects of including the contractional features in the restoration.

The results of the restorations (Table 2) show a marked increase in displacement down the length of the normal faults and thus through time. This reveals these faults have an extended growth history with multiple phases of deformation. Table 2 shows a difference of 4–5% between the interpretations including and excluding contractional features. This implies that 5% of the strain created by extension is compensated for within the extensional domain itself.

4. Discussion

4.1. Recognizing the missing strain

Recent analyses of DWFTBs involving gravity collapse broadly agree that there is an imbalance between extensional and contractional domains in favour of extension of ~5% (de Vera et al., 2010; Butler and Paton, 2010). Dalton et al., 2015 went further to look at a set of parallel lines (Fig. 1) through a single collapse finding a consistent imbalance throughout, concluding the missing strain component is not an effect of out of plane movement but a crucial part of the growth mechanism. They suggested the imbalance represents a phase of strain hardening through compaction of more distal sediments relative to the primary normal fault. This phase predates the formation of down-dip thrusts, seismically resolvable as the contractional domain. It is this strain hardening phase which we have investigated. The missing strain component is likely to be near or below seismic resolution and should therefore be represented in field examples of DWFTB's.

The previously unpublished field location at Laspuña, whilst limited in extent displays many of the same features that we observe in seismic examples of extensional domains in DWFTBs. These include 1st order listric normal growth faults, a detachment surface above a relatively undeformed package and a separate overlying contractional domain composing imbricated thrusts. This implies a potential scalability in these structures that offers us an analogue to study the internal architecture of larger systems. The key observation from the Laspuña system (Fig. 5), is the occurrence of 2nd order contractional features, present within both the extensional and compressional faulted blocks. This is contrary to seismic interpretation of thrust and normal fault blocks, which implies the preservation of pre-kinematic bedding. This both resolves the calculated missing strain component and suggests it is distributed across the entire structure and not limited to the contractional domain.

The results of the restoration of the seismic sections with and without contractional structures imply that 5% of the strain created by the extension is compensated for through contraction in the extensional domain itself. This would imply results of restorations of the entire DWFTB that do not account for this contraction will produce missing strain components over the entire structure of 5%. This is highly comparable with the results of restorations undertaken at Laspuña and by de Vera et al. (2010) and Dalton et al. (2015). We conclude therefore that the contractional features interpreted in the Orange Basin are genuine rather than being artefacts of seismic processing.

Fig. 11 shows a possible growth mechanism for DWFTBs showing how these contractional structures grow throughout the development of the collapse structure. This explains the observation made in Dalton et al. (2015) that notes the outer fringes of DWFTBs commonly lack a down-dip contractional domain, as the extensional strain created by the displacement of the normal faults is entirely compensated for internally (Fig. 1). We suggest this contraction is a necessary stage in the development of collapse structures and continues throughout their deformation history.

Given the dimensions of most DWFTBs (>100 km) it is unreasonable to expect restorations to include this level of detail. Indeed, such structures are only imaged in our dataset because of the high fidelity nature of our profiles where as in many examples the

features previously considered to be seismic artefacts are contractional features. The green and blue horizons are pre-kinematic horizons used for the restoration, the pink light blue and yellow horizons are syn-kinematic and indicate there have been multiple phases of activity on the faults. All sections are pre-stack depth migrated seismic reflection profiles, presented without vertical exaggeration and are courtesy of Spectrum. (For interpretation of the references to colour in this figure legend, the reader is referred to the web version of this article.)

Table 2
Table of results of restorations which were undertaken on sections presented in Fig. 11c) and d).

	Original length (m)	Present length (m)	Displacement (m)	Extension (%)
Orange	10341.8	10341.8	0	**0.0%**
Yellow	10296.3	10341.8	45.5	**0.4%**
Blue	10193.6	10341.8	148.2	**1.4%**
Pink	9667.9	10341.8	673.9	**6.5%**
Green	8534.0	10341.8	1807.8	**17.5%**
Green Comp	8939.7	10341.8	1402.1	**13.6%**
Purple	8273.7	10341.8	2068.1	**20.0%**
Purple Comp	8822.7	10341.8	1519.1	**14.7%**

	Without compression	With compression	Difference
Upper	17.5%	13.6%	3.9%
Lower	20.0%	14.7%	5.3%

Figures in bold show the results of the analysis.

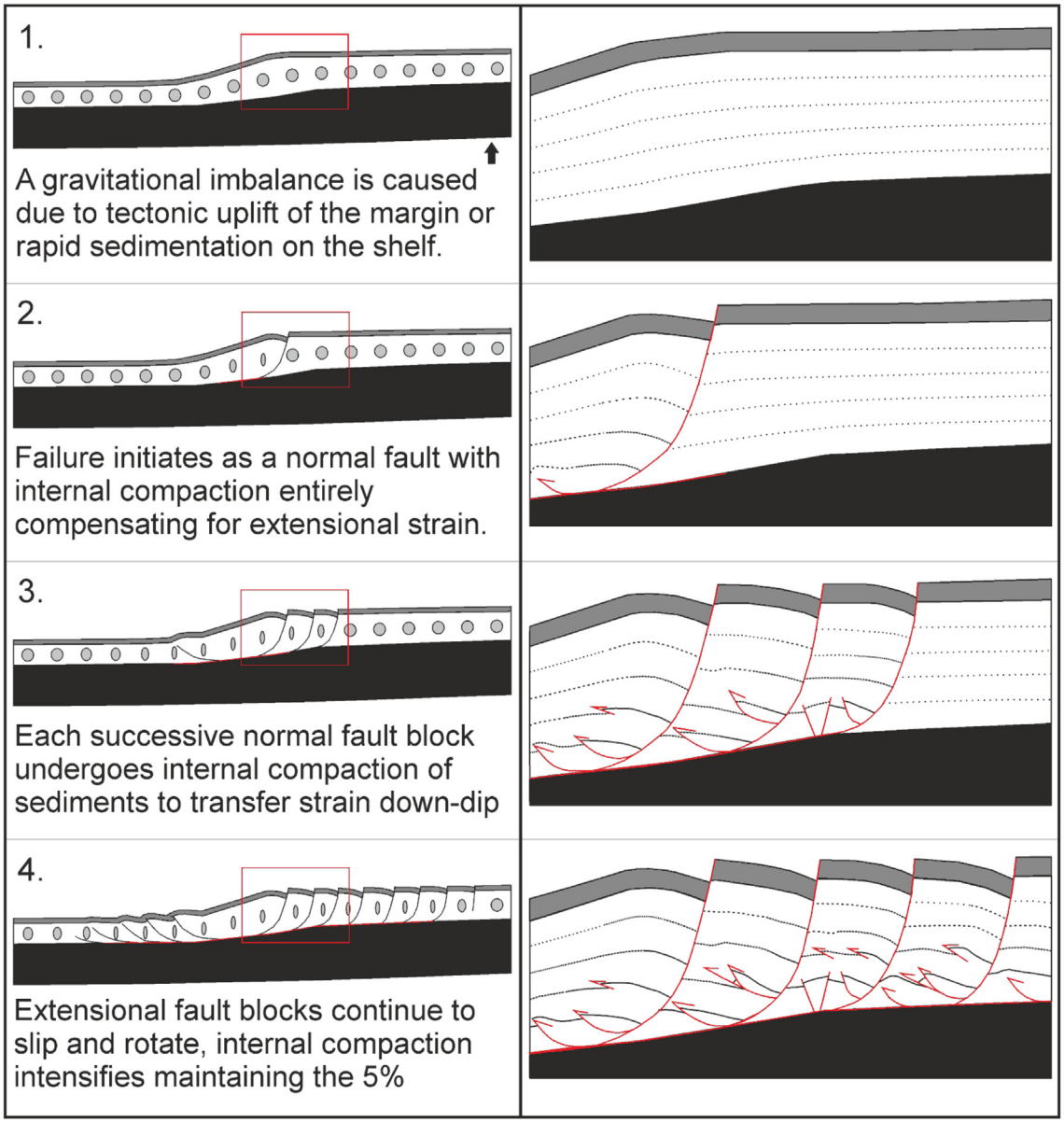

Fig. 11. New model for the formation and development of DWFTBs accounting for internal contraction within the extensional domain.

resolution of the data would preclude such analysis. We therefore suggest that when undertaking restorations of shale detached DWFTBs an internal shortening factor of 5% of the total strain produced through sub-seismic resolution deformation be implemented over the total length of the collapse.

4.2. Application of missing strain to gravity collapse and accretionary prisms

We consider that this 5% missing strain has important consequences for understanding the tectonic, structural, stratigraphic and fluid evolution of DWFTBs regardless of the driving mechanisms that induces them. As this estimate of the missing strain is sub-seismic and is predicted to be prevalent throughout a collapse structure it should be applicable in both compressional and extensional components of DWFTBs.

The critical taper model (Davis et al., 1983; Dahlen et al., 1984) describes the evolution of accretionary prisms and thrust belts as a self-similar wedge of sediment that is at Coulomb failure through the system and is often applied in a whole system context e.g. the critical taper angle between surface and the basal surface and its evolution in response to plate convergence rates, sedimentation rates, exhumation and climate (Willett et al., 2003; Roe et al., 2006; Stolar et al., 2006; Simpson, 2010; Fillon et al., 2013; von Hagke et al., 2014) In addition, a number of studies consider the internal geometry of the wedge, and the individual structures that interact through the fold and thrust belt. Our results imply that an additional, and unrecognized 5%, should be accounted for in such studies. We acknowledge that this may be within the errors of the analysis, however of particular note are studies in Niger and Baram Deltas and the Nankai Trough (Bangs et al., 2004; Bilotti and Shaw, 2005; Morley, 2009) that have coupled seismic reflection derived interpretation and restorations to understand bulk deformation and shortening amounts in a critical taper context. A further example is the analysis of the broader Sabah system, NW Borneo in which evaluating the role of tectonic versus gravity driven deformation is critical both to the DWFTB and regional tectonic evolution (King et al., 2010). In such settings, where estimated shortening is low, in the order of ~1.8%, the sub-seismic deformation that we observe could play a significant role.

Although our focus here has been on the structural analysis, the quantification of a 5% missing strain will influence our understanding of the syn-kinematic evolution of sedimentary basins associated with DWFTBs. It is well established that in these settings there is an intimate link between the controlling structures, the accommodation space and the associated sedimentary basin fill. This is a consequence of the development of anticlines that act as transverse barriers to sediment moving down slope and the intervening synclines that not only control bathymetry and sediment distribution but can also influence the location of sand prone fairways and mass-transport complexes (McGilvery and Cook, 2003; Paton et al., 2007; Deville et al., 2015; Ortiz-Karpf et al., 2015). Our calculation of 5% missing strain is across an entire system and may therefore have a significant impact on specific structures, and sedimentary basins within a system. This agrees with the findings of Spikings et al. (2015) who conclude that the misinterpretation of structural features in sedimentary systems can lead to considerable underestimates of sediment volume and architecture.

A direct consequence of this missing 5% is that estimates of porosity and permeability of sediments within DWFTBs would be considerably less than previously predicted. This alters our understanding of the formation of these structures implying that prior to the translation of strain down-dip and thus the formation of a contractional domain a period of compaction and “strain hardening” must occur first. Most of the contractional structures persist in a single fault block towards the centre as opposed to being equally distributed amongst the blocks. This is possibly a feature of the local lithology being more prone to failure than the sediments in surrounding blocks. Internal variations in lithology may provide the opportunity for the formation of multiple higher slip horizons within fault blocks allowing DWFTBs with multiple detachments to form as described previously (Totterdell and Krassay, 2003; Rowan et al., 2004; Corredor et al., 2005; Briggs et al., 2006). This process could produce vertical segmentation of normal fault blocks allowing for anomalous fault throws down a fault plane where higher throws may be recorded nearer the top of some faults as in Robson et al. (2016). This would add considerable uncertainty to the interpretation of the inner working of individual fault bounded blocks.

As a final consideration, faults within DWFTBs influence the location and migration of fluids through the system. The presence of water plays a major role in the dynamic evolution of accretionary prisms (Moore and Vrolijik, 1992; Saffer and Bekins, 1998) by increasing pore pressure and thereby altering the failure criterion at which Coulomb failure occurs, and by association the critical taper of systems. It is well established that faults play a critical role in localising fluid migration pathways and locations of future failure (Saffer and Bekins, 1998, 2001; Klaucke et al., 2016). In their study of Four Way Closure Ridge, offshore SW Taiwan, Klaucke et al. (2016) specifically discuss that water and methane (which subsequently feed Bottom Simulating Reflectors (BSRs)) exploit relatively permeable fault zones but note that these are poorly imaged. Permeability is dynamic over time (Maltman et al., 1997; Bolton and Maltman, 1998) as well as laterally variable (Maltman, 1998; Bolton et al., 1999) this potentially gives us a mechanism for internal shortening. Small scale contraction occurs where the fluid pressure drops and so local shortening occurs (i.e. the décollement locks). Sliding and extension occurs in areas where higher fluid pressures are maintained along the décollement horizon. Our observations highlight the importance of considering a range of fault sizes that are likely to be present in DWFTBs whether seismically resolvable or not and may all play a role in fluid migration through the system. The presence of hydrocarbon fluids is equally important in DWFTBs, although of course, much of the interest is in predicting areas in which it is retained rather than expulsed.

At the 2016 Tectonic Studies Group conference it was stated “it is not the faults that industry is interested in but the white spaces in-between” (Peel pers comm, 2016) this statement perhaps most validates the outcome of this study. When we consider the white space between 1st order structures, we find a set of 2nd order structures precisely where our drilling targets are. Whilst previous research (Morley et al., 2011; Futalan et al., 2012) indicates reservoirs are present in these areas we caution that reservoir intervals may be more structurally compartmentalised with lower permeabilities than predicted.

5. Conclusion

Through combining field observations from exceptionally well-exposed outcrops with high fidelity seismic observations we are able to, for the first time, consider DWFTB deformation from the metre scale to the margin scale. Regardless of the scale of observation, we observe hitherto unrecognised compressional fault structures that are at a second order in scale compared to the principal structures. As our structural restorations suggest that they can account for ~5% of the overall strain irrespective of scale; we propose that this accounts for the missing strain that has been identified in previous studies but remained poorly understood. We conclude that the majority of this missing strain is accommodated

on discrete faults rather than as distributed deformation as previous models invoke.

As our model for the evolution of these second order structures is scale invariant we propose that this 5% additional shortening is applicable to all DWFTBs and should be accounted for when shortening estimates are calculated in both active and passive margins. Furthermore, individual faults are important within an intra-wedge setting as they can control sedimentation, localise the position of fluid migration (brine or hydrocarbon), modify bathymetry and compartmentalise reservoir intervals. Yet often these processes are identified without an association with a visible fault structure in the seismic reflection data. Our conclusion, and resulting model, that these second order structures are discrete faults that are close to, or often beyond seismic resolution, provides a method for determining if these intra-wedge processes are indeed controlled by structures that are not necessarily resolvable in seismic data.

Acknowledgements

The authors of this research would like to thank Spectrum ASA for the release of seismic data for this study. This research took place under the patronage of the Basin Structure Group, we acknowledge the financial support of Getech, BG Group and EON and the provision of software from Midland Valley and Schlumberger. We would also like to thank the reviewers of this paper and the Editor Bernard Colletta for their helpful comments and suggestions.

References

Biju-Duval, B., Le Quellec, P., Mascle, A., Renard, V., Valery, P., 1982. Multibeam bathymetric survey and high resolution seismic investigations on the Barbados ridge complex (eastern Caribbean): a key to the knowledge and interpretation of an accretionary wedge. Tectonophysics 86 (1), 275–304.

Bangs, N.L., Shipley, T.H., Gulick, S.P.S., Moore, G.F., Kuromoto, S., Nakamura, Y., 2004. Evolution of the Nankai Trough decollement from the trench into the seismogenic zone: inferences from three-dimensional seismic reflection imaging. Geology 32 (4), 273–276.

Bilotti, F., Shaw, J.H., 2005. Deep-water Niger Delta fold and thrust belt modeled as a critical-taper wedge: the influence of elevated basal fluid pressure on structural styles. AAPG Bull. 89 (11), 1475–1491.

Bolton, A.J., Maltman, A., 1998. Fluid flow pathways in actively deforming sediments: the role of pore fluid pressures and volume change. Mar. Petroleum Geol. 15 (4), 281–297. http://dx.doi.org/10.1015/S0264-8172(98)00025-7.

Bolton, A.J., Clennell, M., Maltman, A., 1999. Nonlinear stress dependence of permeability: a mechanism for episodic fluid flow in accretionary wedges. Geology 27 (3), 239–242. http://dx.doi.org/10.1130/0091-7613.

Briggs, S.E., Davies, R.J., Cartwright, J.A., Morgan, R., 2006. Multiple detachment levels and their control on fold styles in the compressional domain of the deepwater west Niger Delta. Basin Res. 18, 435–450.

Brown Jr., L.F., Benson, J.M., Brink, G.J., Doherty, S., Jollands, E.H., Jungslagger, A., Keenen, A., Muntingh, A., van Wyk, N.J.S., 1995. Sequence stratigraphy in offshore South african divergent basins. Atlas Explor. Cretac. Lowstand Traps Soekor (Pty) Ltd AAPG Stud. Geol. 41, 184.

Butler, R.W.H., Paton, D.A., 2010. Evaluating lateral compaction in deepwater fold and thrust belts: how much are we missing from “nature's sandbox”? GSA Today 20 (3), 4–10.

Corredor, F., Shaw, J.H., Bilotti, F., 2005. Structural styles in the deep-water fold and thrust belts of the Niger Delta. AAPG Bull. 89, 735–780.

Dahlen, F.A., Suppe, J., Davis, D., 1984. Mechanics of fold-and-thrust belts and accretionary wedges: cohesive Coulomb Theory. J. Geophys. Res. 89 (B12), 10087–10101. http://dx.doi.org/10.1029/JB089iB12p10087.

Dakin, N., Pickering, K.T., Mohrig, D., Baylis, N.J., 2012. Channel-like features created by erosive submarine debris flows from the Middle Eocene Ainsa Basin. Mar. Petroleum Geol. 41, 62–71. http://dx.doi.org/10.1016/j.marpetgeo.2012.07.007.

Dalton, T.J.S., Paton, D.A., Needham, D.T., 2016. The influence of mechanical stratigraphy on multi-layer gravity collapse structures: insights from the Orange Basin, South Africa, in review. In: Sabato, Ceraldi, T., Hodgkinson, R.A., Backe, G. (Eds.), Petroleum Geoscience of the West Africa Margin. Geological Society, London. Special Publications, 438. First published online January 19, 2016. http://doi.org/10.1144/SP438.4.

Dalton, T.J.S., Paton, D.A., Needham, D.T., Hodgson, N., 2015. Temporal and spatial evolution of deepwater fold and thrust belts: implications for quantifying strain imbalance. Interpretation 3 (No. 4). http://dx.doi.org/10.1190/INT-2015-0034.1.

Davis, D., Suppe, J., Dahlen, F.A., 1983. Mechanics of fold-and-thrust belts and accretionary wedges. J. Geophys. Res. Solid Earth 88 (B2), 1153–1172.

Deville, E., Mascle, A., Callec, Y., Huyghe, P., Lallemant, S., Lerat, O., Mathieu, X., Padron de Carillo, C., Patriat, M., Pichot, T., Loubrieux, B., Granjeon, D., 2015. Tectonics and sedimentation interactions in the east Caribbean subduction zone: an overview from the Orinoco delta and the Barbados accretionary prism. Mar. Petroleum Geol. 64 (2015), 76–103.

de Vera, J., Granado, P., McClay, K., 2010. Structural evolution of the Orange basin gravity-driven system, offshore Namibia. Mar. Petrol. Geol. 27, 233–237.

Dreyer, T., Corregidor, J., Arbues, P., Puigdefabregas, C., 1999. Architecture of the tectonically influenced Sobrarbe deltaic complex in the Ainsa Basin, northern Spain. Sediment. Geol. 127, 127–169.

Fillon, C., Huismans, R.S., van der Beek, P., 2013. Syntectonic Sedimentation Effects on the Growth of Fold-and-thrust Belts Geology, January 2013, vol. 41, pp. 83–86. http://dx.doi.org/10.1130/G33531.1 first published on October 15, 2012.

Franke, D., Barckhausen, U., Heyde, I., Tingay, M., Ramli, N., 2008. Seismic images of a collision zone offshore NW Sabah/Borneo. Mar. Petroleum Geol. 25 (7), 606–624.

Futalan, K., Mitchell, A., Amos, K., Backe, G., 2012. Seismic facies analysis and structural interpretaion of the Sandakan sub-basin, Sulu sea, Philippines. article #30254 Search Discov.

Gerrard, T., Smith, G.C., 1982. Post-Palaeozoic succession and structure of the southwestern African continental margin: studies in continental margin geology. AAPG Mem. 34, 49–74.

Hesse, S., Back, S., Franke, D., 2010. The structural evolution of folds in a deepwater fold and thrust belt—a case study from the Sabah continental margin offshore NW Borneo, SE Asia. Mar. Petroleum Geol. 27 (2), 442–454.

Klaucke, I., Berndt, C., Crutchley, G., Chi, W.C., Lin, S., Muff, S., 2016. Fluid venting and seepage at accretionary ridges: the four Way Closure Ridge offshore SW Taiwan. Geo-Marine Lett. 36 (16), 165–174. http://dx.doi.org/10.1007/s00367-015-0431-5.

King, R.C., Backe, G., Morley, C.K., Hillis, R.R., Tingay, M.R.P., 2010. Balancing deformation in NW Borneo: quantifying plate-scale vs. gravitational tectonics in a delta and deepwater fold-thrust belt system. Mar. Petroleum Geol. 27 (1), 238–246.

Krueger, A., Gilbert, E., 2009. Deepwater fold-thrust belts: not all the beasts are equal. Article 30085 AAPG Search Discov.

Lopez-Mir, B., Muñoz, J.A., García-Senz, J., 2014. Restoration of basins driven by extension and salt tectonics: example from the Cotiella Basin in the central Pyrenees. J. Struct. Geol. 69, 147–162.

Lopez-Mir, B., Muñoz, J.A., García-Senz, J., 2015. Extensional salt tectonics in the partially inverted Cotiella post-rift basin (south-central Pyrenees): structure and evolution. Int. J. Earth Sci. Geol. Rundsch) 104, 419–434. http://dx.doi.org/10.1007/s00531-014-1091-9.

Maltman, A.J., 1998. Deformation structures from the toes of active accretionary prisms. J. Geol. Soc. Lond. 155, 639–650. http://dx.doi.org/10.1144/gsjgs.155.4.0639.

Maltman, A.J., Labaume, P., Housen, B., 1997. Structural geology of the décollement at the toe of the Barbados accretionary prism. In: Shipley, T.H., Ogawa, Y., Blum, P., Bahr, J.M. (Eds.), Proceedings of the Ocean Drilling Program, Scientific Results, 156. In: http://dx.doi.org/102973/odp.proc.sr.156.037.1997.

McClay, K., Muñoz, J.A., García-Senz, J., 2004. Extensional salt tectonics in a contractional orogen: a newly identified tectonic event in the Spanish Pyrenees. Geology 32 (9), 737–740. http://dx.doi.org/10.1130/G20565.1.

McGilvery, T. A., Cook, D. L., (2003). The influence of local gradients on accommodation space and linked depositional elements across a stepped slope profile, Offshore Brunei. Shelf margin deltas and linked down slope petroleum systems: global significance and future exploration potential, In: GCSSEMP Foundation 23rd Annual Bob F. Perkins Research Conference, pp. 387–419.

Mohammed, M., Paton, D.A., Collier, R.E.L.I., Hodgson, N., 2015. U. Utjavari, Interaction of Crustal Heterogeneity and Lithospheric Process in Determining Passive Margin Architecture on the Southern Namibian Margin. Geological Society Special Publication, p. 438. http://dx.doi.org/10.1016/S0264-8172 (03)00045.

Moore, J.C., Vrolijk, P., 1992. Fluids in accretionary prisms. Rev. Geophys. 30 (2), 113–135.

Morley, C.K., 2007. Interaction between critical wedge geometry and sediment supply in a deep-water fold belt. Geology 35 (2), 139–142.

Morley, C.K., 2009. Geometry of an oblique thrust fault zone in a deepwater fold belt from 3D seismic data. J. Struct. Geol. 31 (12), 1540–1555.

Morley, C.K., King, R., Hillis, R., Tingay, M., Backe, G., 2011. Deepwater fold and thrust belt classification, tectonics, structure and hydrocarbon prospectivity: a review. Earth Sci. Rev. 104, 41–91.

Muñoz, J.A., Beamud, E., Fernández, O., Arbués, P., Dinarès-Turell, J., Poblet, J., 2013. The Ainsa Fold and thrust oblique zone of the Central Pyrenees: kinematics of a curved contractional system from paleomagnetic and structural data. Tectonics 32 (5), 1142–1175. http://dx.doi.org/10.1002/tect.20070.

Muntingh, A., Brown, L.F.J., 1993. Sequence Stratigraphy of Petroleum Plays, Post-rift Cretaceous Rocks (Lower Aptian to Upper Maastrichtian), Orange Basin, South Africa, Siliciclastic Sequence Stratigraphy. Recent Developments and Applications. American Association of Petroleum Geologists, Tulsa, Oklahoma, pp. 71–98.

Ortiz-Karpf, A., Hodgson, D.M., McCaffrey, W.D., 2015. The role of mass-transport complexes in controlling channel avulsion and the subsequent sediment dispersal patterns on an active margin: the Magdalena Fan, offshore Colombia.

Mar. Petroleum Geol. 64 (2015), 58–75.
Paton, D.A., Carr, M., Trudgill, B., Ortner, H., Medewedeff, D.A., 2007. Alpine-scale 3D geospatial modeling: applying new techniques to old problems. Geosphere 3 (6), 527–549.
Paton, D.A., van der Spuy, D., di Primio, R., Horsfield, B., 2008. Tectonically induced adjustment of passive-margin accommodation space; influence on hydrocarbon potential of the Orange Basin, South Africa. AAPG Bull. 92, 589–609.
Peel, F.J., 2014. The engines of gravity-driven movement on passive margins: quantifying the relative contribution of spreading vs. gravity sliding mechanisms. Tectonophysics 633, 126–142.
Pickering, K.T., Bayliss, N.J., 2009. Deconvolving tectono-climatic signals in deep-marine siliciclastics, Eocene Ainsa basin, Spanish Pyrenees. seesaw Tect. versus eustasy Geol. 37 (2009), 203–206. http://dx.doi.org/10.1130/G25261A1.
Pickering, K.T., Corregidor, J., 2005. Mass transport complex and tectonics control on confined basin-floor submarine fans, Middle Eocene, south Spanish Pyrenees. In: Hodgson, D.M., Flint, S.S. (Eds.), Submarine Slope Systems: Process and Products, vol. 244. Geological Society Special Publication, pp. 51–74.
Price, R.A., 1981. The Cordilleran foreland thrust and fold belt in the southern Canadian Rocky Mountains. In: McClay, K.R., Price, N.J. (Eds.), Thrust and Nappe Tectonics, vol. 9. London Geological Society Special Publication, pp. 427–448.
Robertson, P., Burke, K., 1989. Evolution of southern Caribbean plate boundary, vicinity of Trinidad and Tobago. AAPG Bull. 73 (4), 490–509.
Robson, A.G., King, R.C., Holford, S.P., 2016. 3D seismic analysis of gravity driven and basement influenced normal fault growth in the deepwater Otway Basin, Australia. J. Struct. Geol. 89, 74–87.
Roe, G.H., Stolar, D.B., Willett, S.D., 2006. Response of a steady-state critical wedge orogen to changes in climate and tectonic forcing. Geol. Soc. Am. Special Pap. 398 (2006), 227–239.
Rowan, M.G., Peel, F.J., Vendeville, B.C., 2004. Gravity Driven fold belts on passive margins: thrust tectonics and hydrocarbon systems. AAPG Mem. 82, 157–182.
Saffer, D.M., Bekins, B.A., 1998. Episodic fluid flow in the Nankai accretionary complex: timescale, geochemistry, flow rates, and fluid budget. J. Geophys. Res. Solid Earth 103 (B12), 30351–30370.
Saffer, D.M., Bekins, B.A., 2001. Hydrologic controls on the morphology and mechanics of accretionary wedges. March, 2002 Geology 30, 271–274. http://dx.doi.org/10.1130/00917613.
Simpson, G.D.H., 2010. Formation of accretionary prisms influenced by sediment subduction and supplied by sediments from adjacent continents. Geology 38 (2), 131–134.
Spikings, A.L., Hodgson, D.M., Paton, D.A., Spychala, Y.T., 2015. Palinspastic restoration of an exhumed deepwater system: a workflow to improve paleogeographic reconstructions. Interpretation-A J. Subsurf. Charact. 3, SAA71–SAA87. http://dx.doi.org/10.1190/INT-2015-0015.1.
Stolar, D.B., Roe, G.H., Willett, S.D., 2006. Controls on the patterns of topography and erosion rate in a critical orogen. J. Geophy. Res. 112 http://dx.doi.org/10.1029/2006JF000713.
Tavani, S., Lopez-Mir, B., Muñoz, J.A., 2015. Extensional fold-related fracturing in the Armeña rollover (Cotiella Massif, southern Pyreneed). Italian J. Geoscience 134. http://dx.doi.org/10.3301/IJG.2014.17.
Toto, E., Kellogg, J.N., 1992. Structure of the Sinu-San Jacinto fold belt—an active accretionary prism in northern Colombia. J. S. Am. Earth Sci. 5 (2), 211–222.
Totterdell, J.M., Krassay, A.A., 2003. The role of shale deformation and growth faulting in the Late Cretaceous evolution of the Bight Basin, offshore southern Australia. In: Van Rensbergen, P., Hillis, R.R., Maltman, A.J., Morley, C.K. (Eds.), Subsurface Sediment Mobilization. Geological Society, London. Special Publications, 216, 429–442. http://doi.org/10.1144/GSL.SP.2003.216.01.28.
Vergés, J., Fernàndez, M., Martínez, A., 2002. The Pyrenean orogen: pre-, syn-, and post-collisional evolution. In: Rosenbaum, G., Lister, G.S. (Eds.), Reconstruction of the Evolution of the Alpine-Himalayan Orogen. Journal of the Virtual Explorer, pp. 5–7.
Vinnels, J.S., Butler, R.W.H., McCaffrey, W.D., Paton, D.A., 2010. Depositional processes across the Sinu accretionary prism, offshore Colombia. Mar. Petroleum Geol. 27 (4), 794–809.
von Hagke, C., Oncken, O., Evseev, S., 2014. Critical taper analysis reveals lithological control of variations in detachment strength: an analysis of the Alpine basal detachment (Swiss Alps). Geochem. Geophys. Geosystems 15 (1), 176–191.
Willett, S.D., Fisher, D., Fuller, C., En-Chao, Y., Chia-Yu, L., 2003. Erosion rates and orogenic-wedge kinematics in Taiwan inferred from fission-track thermochronometry. Geology 31 (11), 945–948.
Wood, A.M., Paton, D.A., Collier, R.E.L., 2015a. The Missing Complexity in Seismically Imaged Normal Faults: what Are the Implications for Geometry and Production Response? Geological Society, London. Special Publications, 421, 213–230. http://doi.org/10.1144/SP421.12.
Wood, A.M., Paton, D.A., Collier, R.E.L., 2015b. Understanding regional-scale structural uncertainty: the onshore Gulf of Corinth rift as a hydrocarbon exploration analogue. Interpretation 3 (4). http://library.seg.org/doi/abs/10.1190/INT-2015-0046.1.

Part B –

I: Larger versions of Sections within the thesis

Figure 1.2

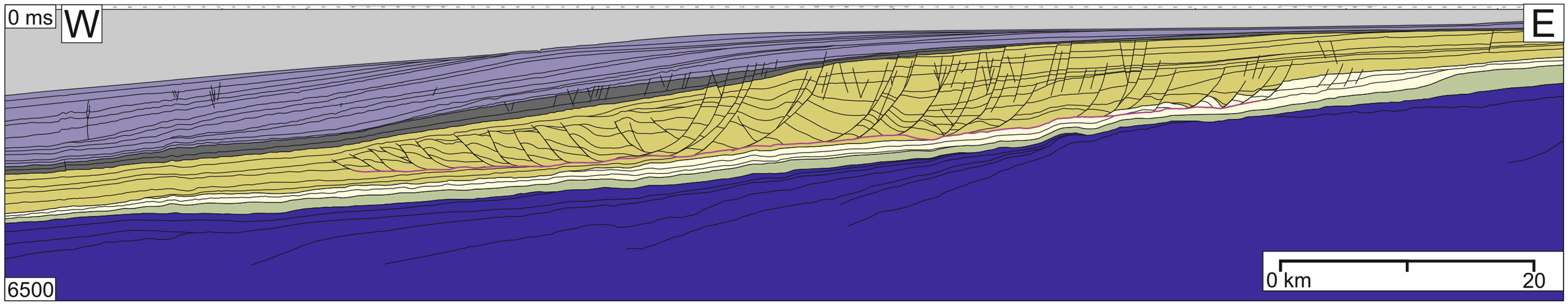

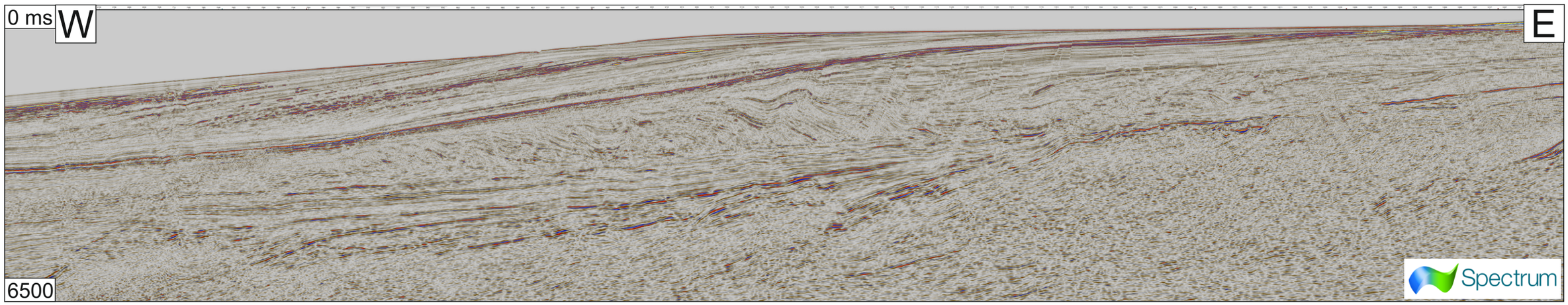

Figure 2.1

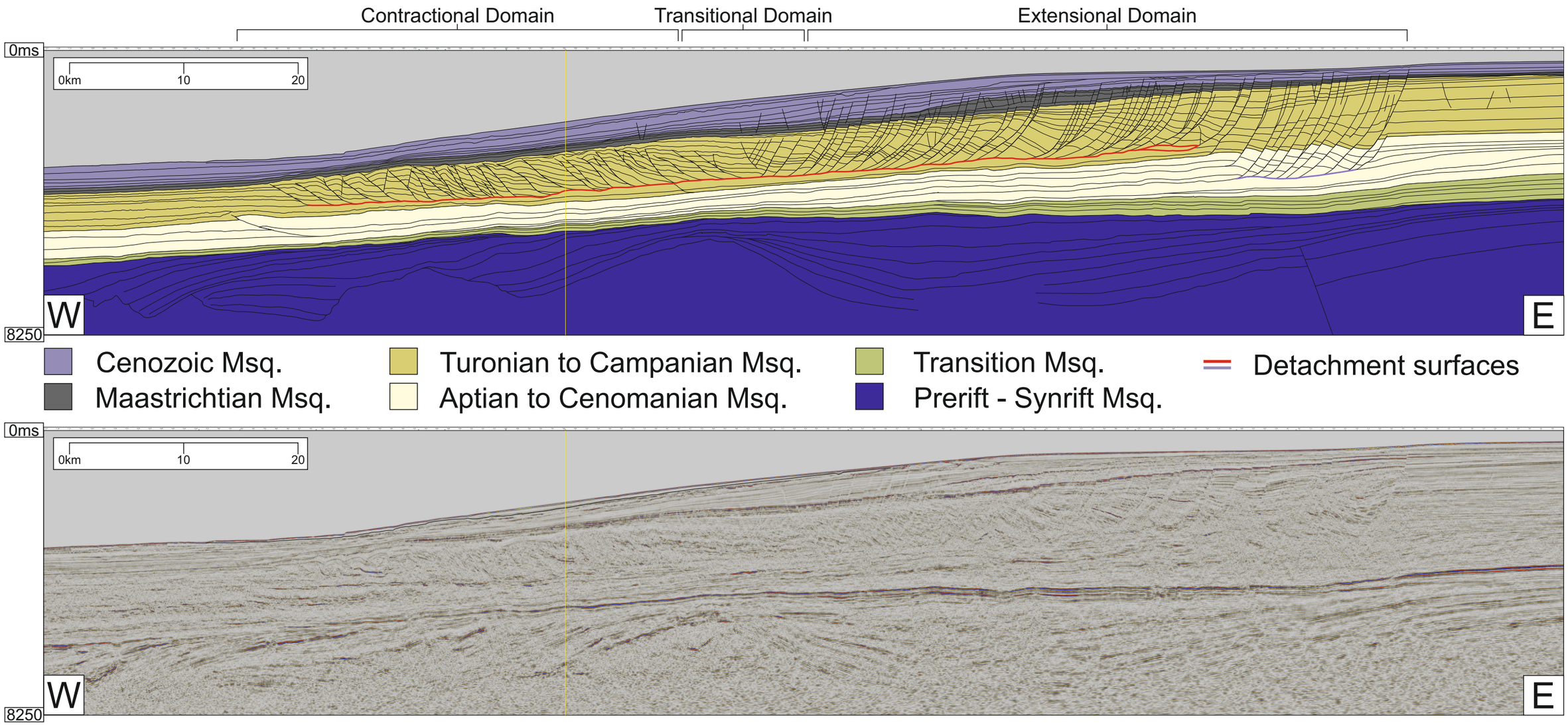
Contractional Domain
Transitional Domain
Extensional Domain
0ms
0km
10
20
W
E
8250
Cenozoic Msq.
Turonian to Campanian Msq.
Transition Msq.
Detachment surfaces
Maastrichtian Msq.
Aptian to Cenomanian Msq.
Prerift - Synrift Msq.
0ms
0km
10
20
W
E
8250

Figure 3.5

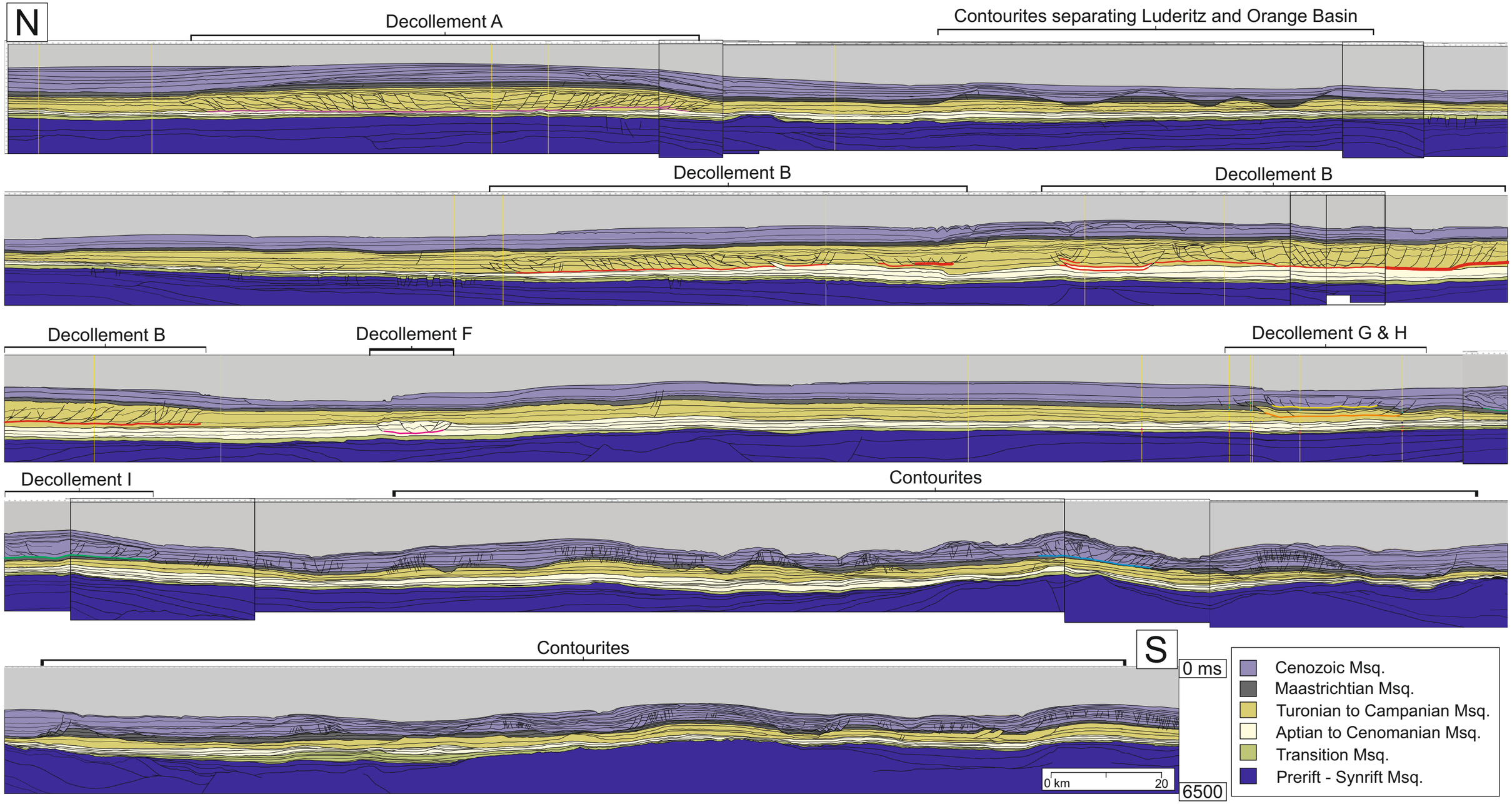
N
Decollement A
Contourites separating Luderitz and Orange Basin
Decollement B
Decollement B
Decollement B
Decollement F
Decollement G & H
Decollement I
Contourites
Contourites
S
0 ms
6500
0 km
20
Cenozoic Msq.
Maastrichtian Msq.
Turonian to Campanian Msq.
Aptian to Cenomanian Msq.
Transition Msq.
Prerift - Synrift Msq.

Figure 3.6

W

E

0 10 20 30 km

a)

0 ms

5800

a)

0 ms

5800

b)

0 ms

6000

b)

0 ms

6000

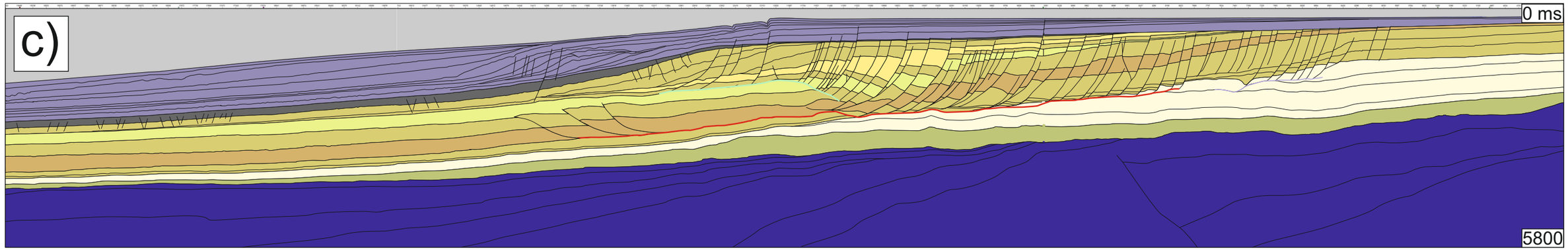

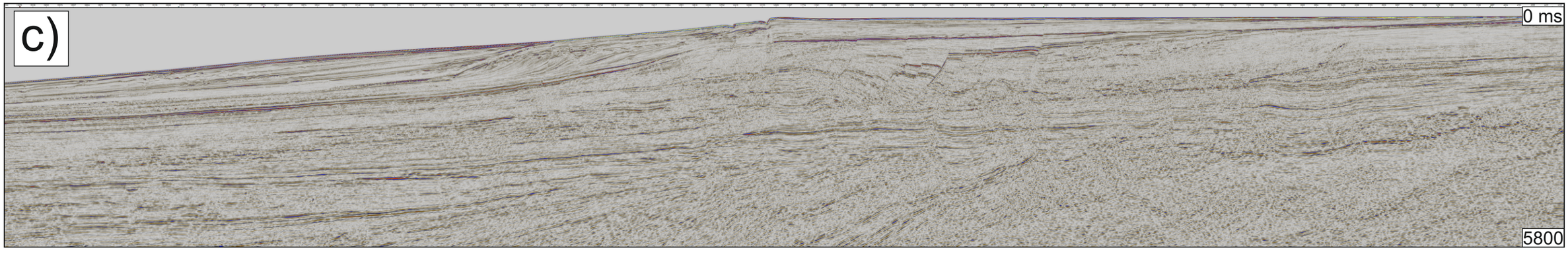

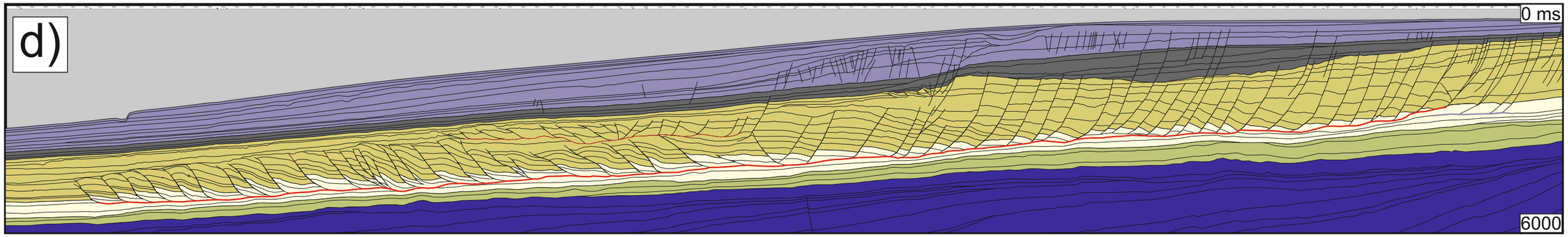

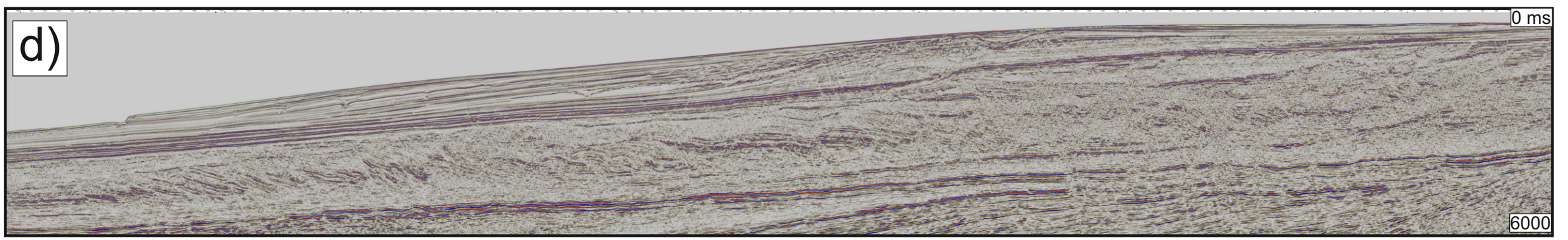

W

0 10 20 30 km

Figure 3.6

E

W

0 10 20 30 km

Figure 3.6

E

e)

0 ms

6500

e)

0 ms

6500

f)

0 m

6500

f)

0 m

6500

W

0 10 20 30 km

E

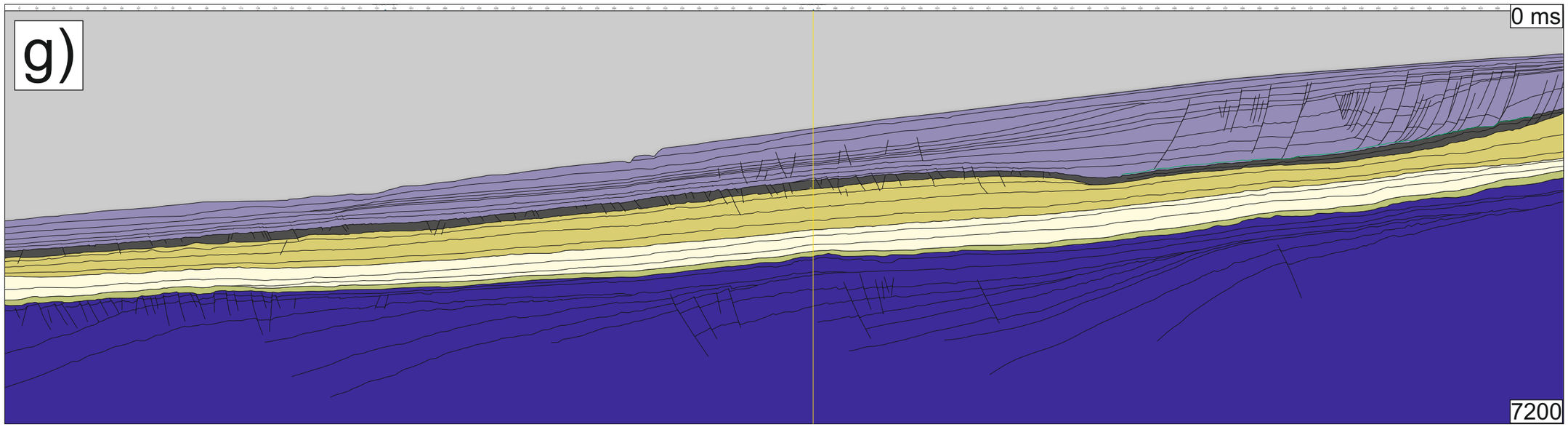

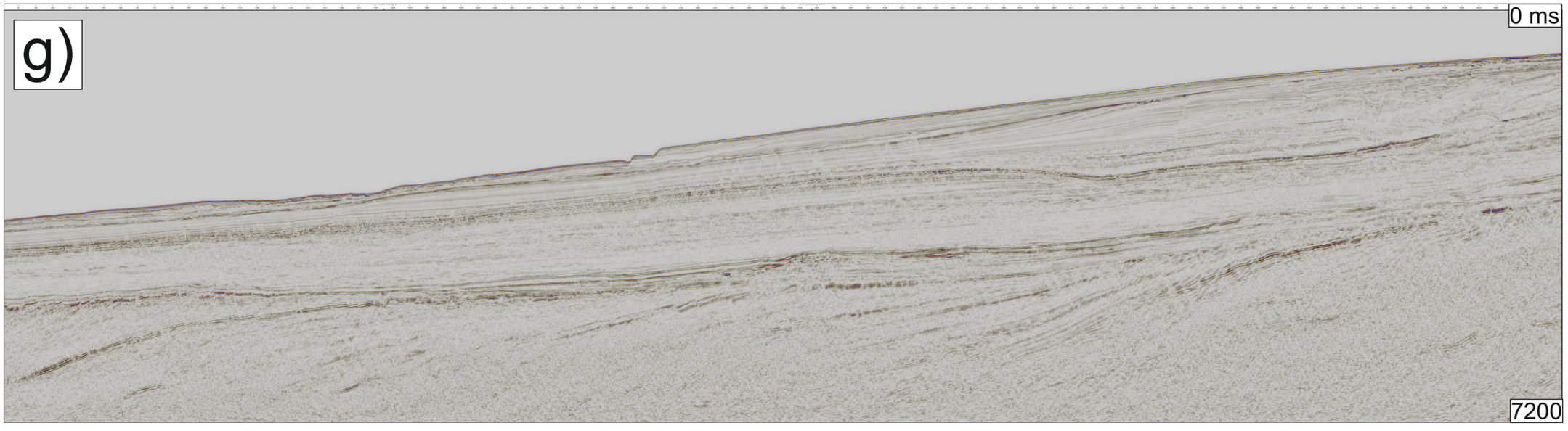

Maastrichtian Msq.
Tu. to Ca. Msq.
Ap-Ce Msq.
Transition Msq.
Pre- Synrift Msq.
Figure 3.5

Figure 3.6

Figure 3.16

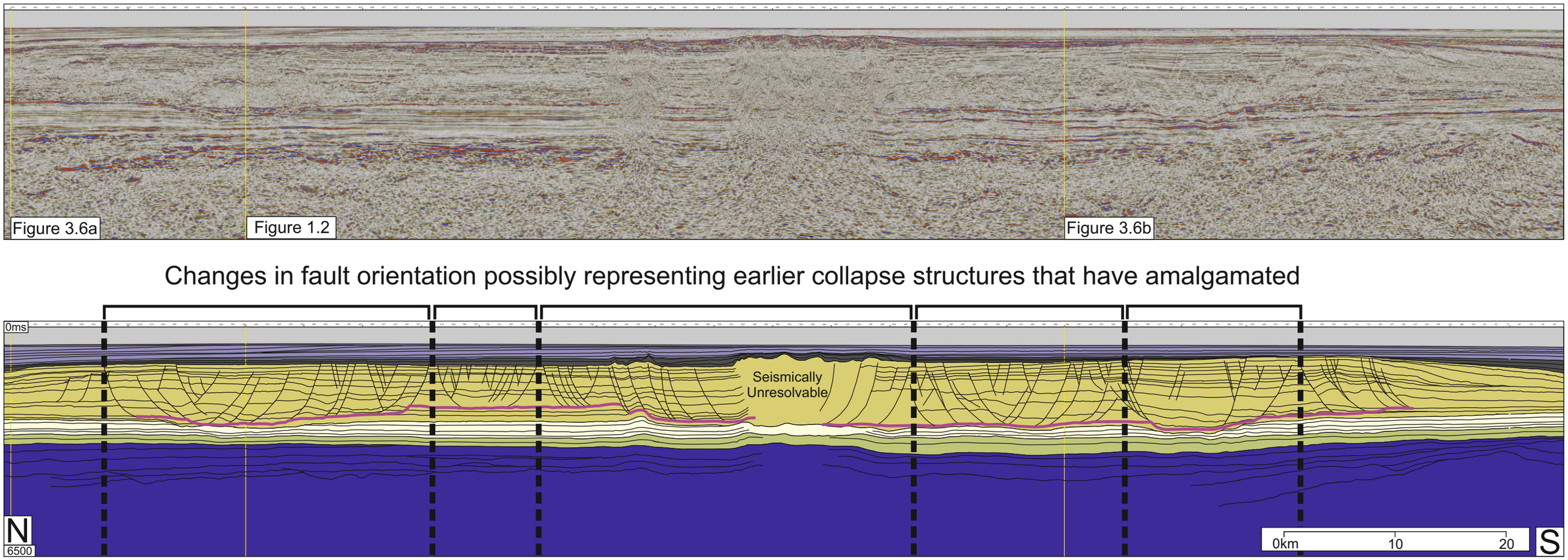
Figure 3.6a
Figure 1.2
Figure 3.6b
Changes in fault orientation possibly representing earlier collapse structures that have amalgamated
0ms
Seismically
Unresolvable
N
6500
0km
10
20
S

Figure 4.4

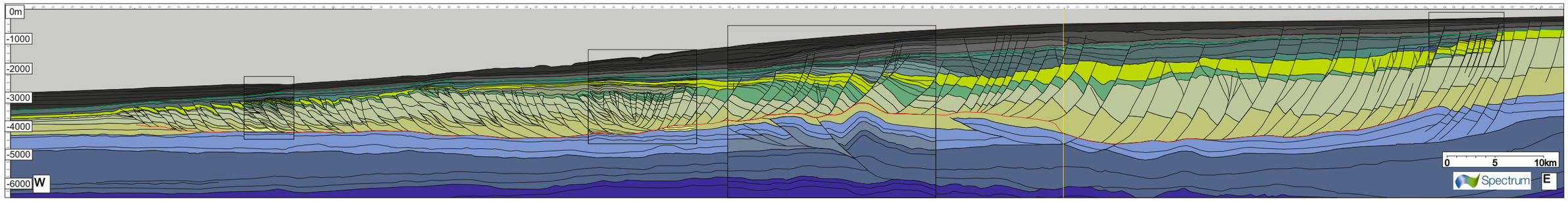
0m
-1000
-2000
-3000
-4000
-5000
-6000
W
0
5
10km
Spectrum
E

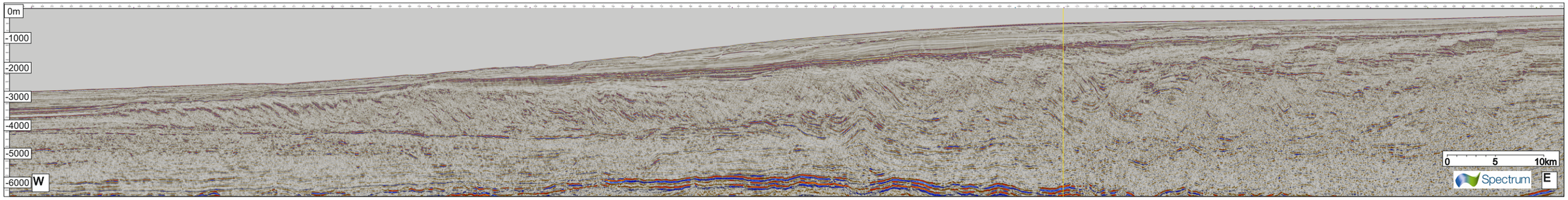
0m
-1000
-2000
-3000
-4000
-5000
-6000
W
0
5
10km
Spectrum
E

Figure 6.9

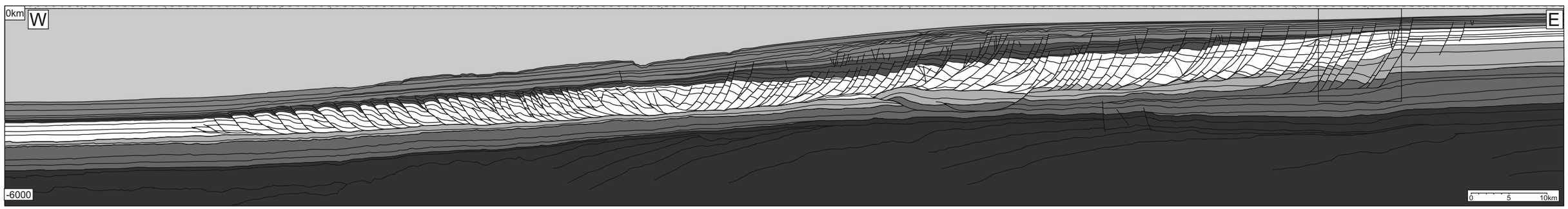

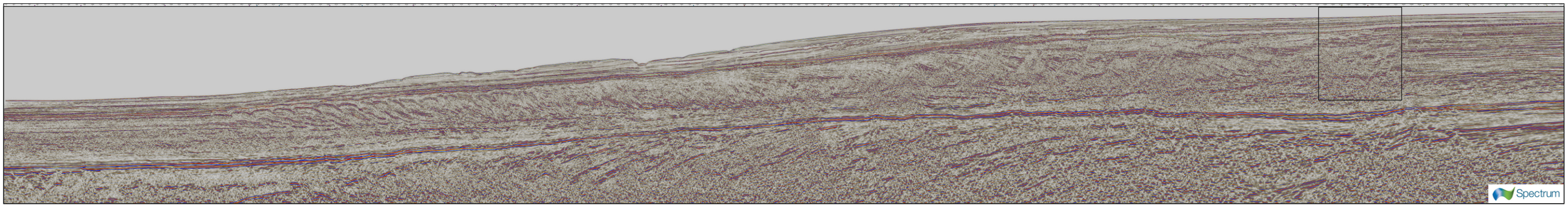

Zoomed in crossline of Figure 7.3

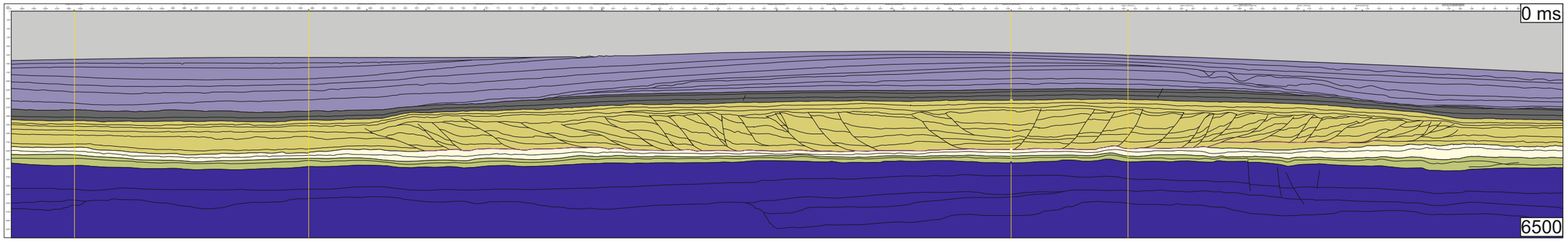

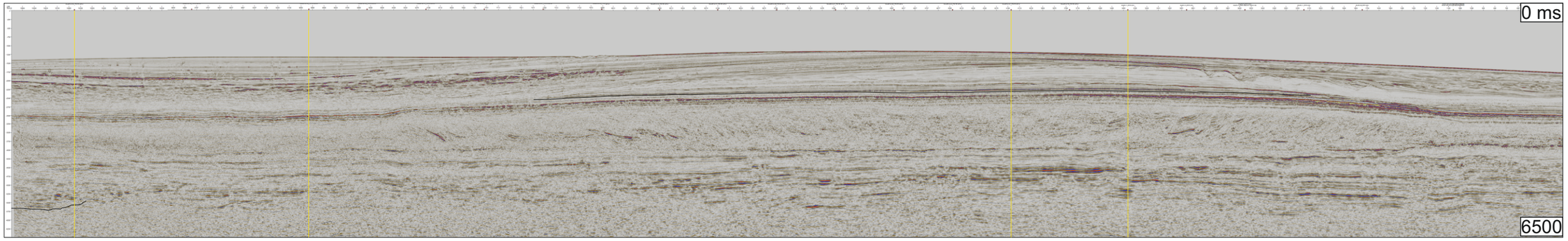

Part B –

II: Additional seismic sections

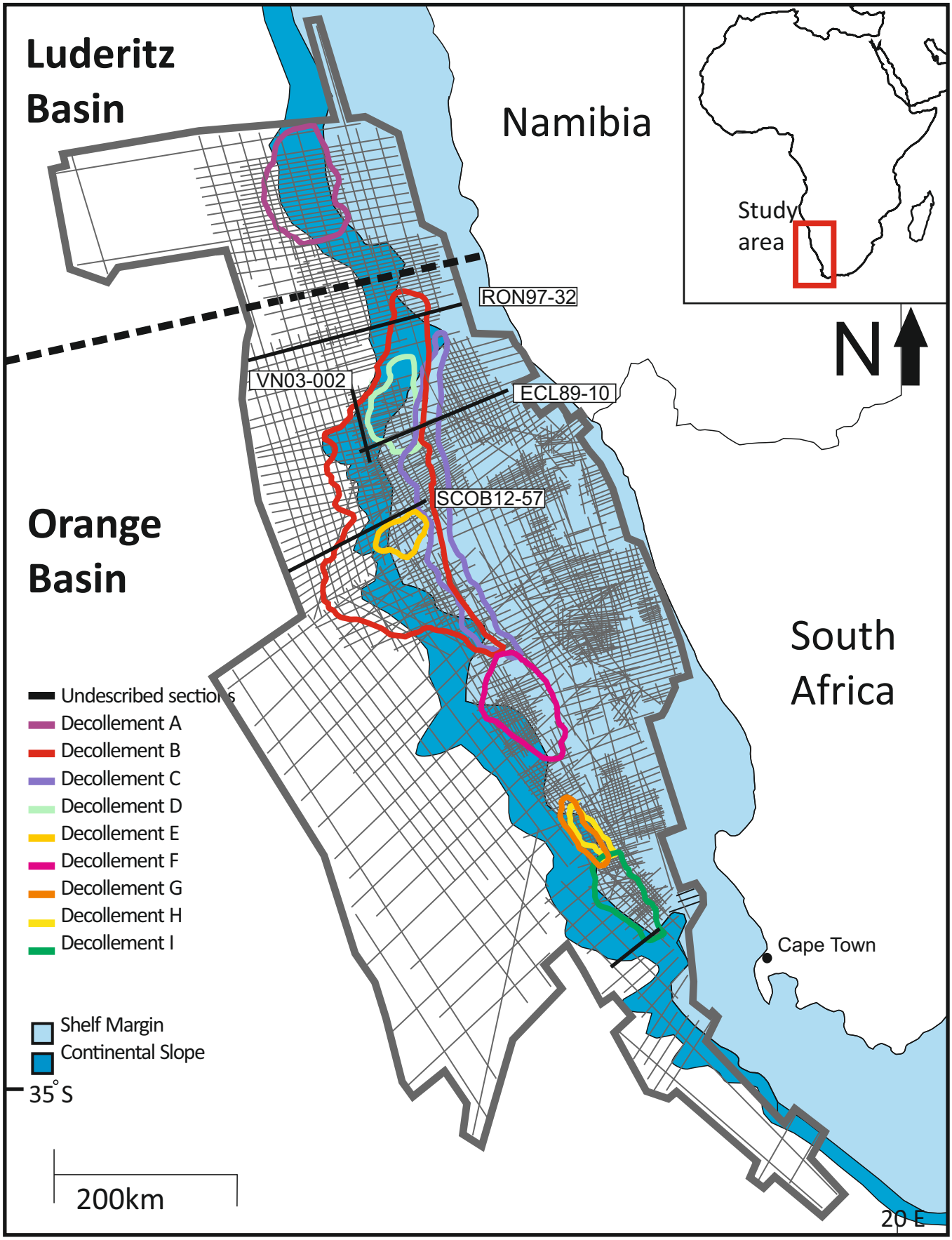
Luderitz Basin
Namibia
Study area
RON97-32
VN03-002
ECL89-10
SCOB12-57
N
Orange Basin
South Africa
Undescribed sections
Decollement A
Decollement B
Decollement C
Decollement D
Decollement E
Decollement F
Decollement G
Decollement H
Decollement I
Cape Town
Shelf Margin
Continental Slope
35° S
200km
20 E

W

E

VN03-002

ECL89-10

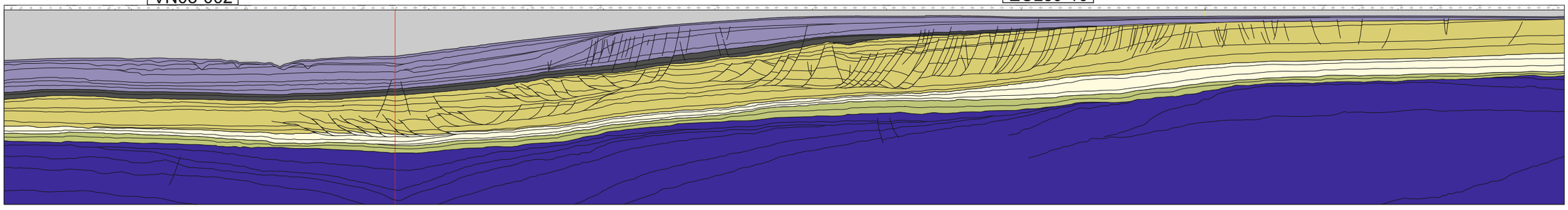

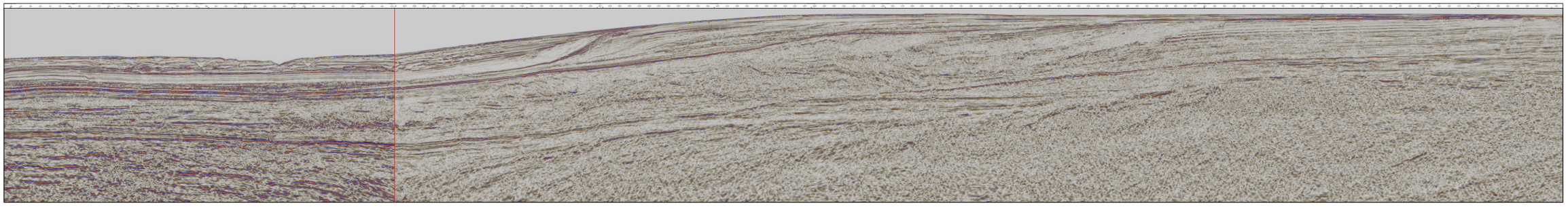

WC2002-20

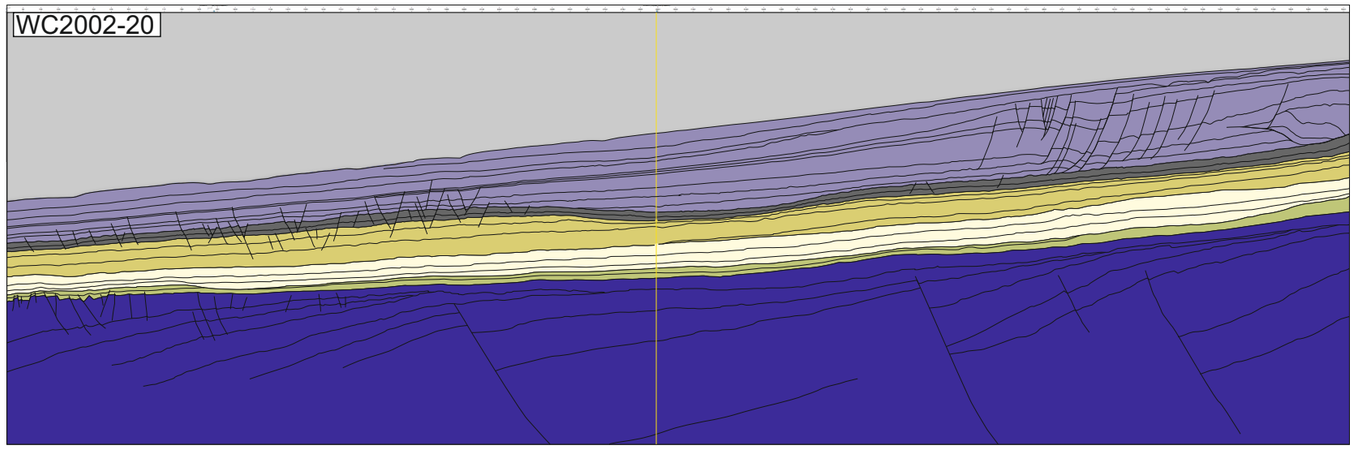

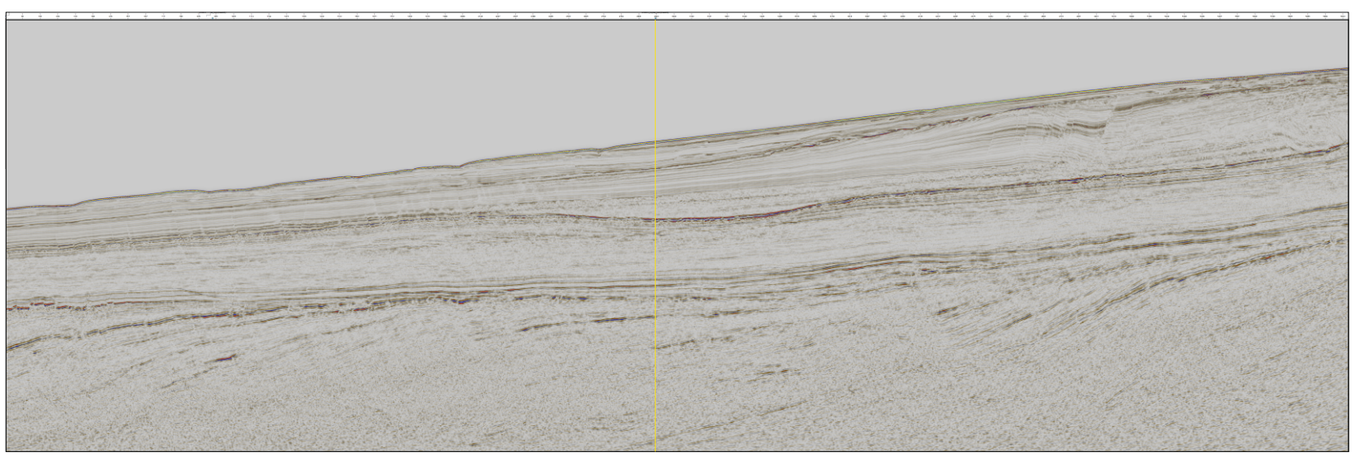

W

E

SCOBIZ-57

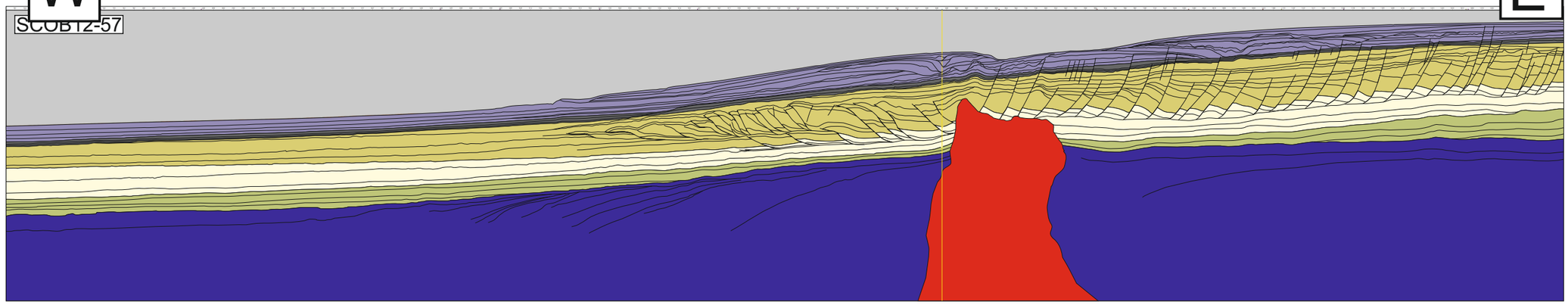

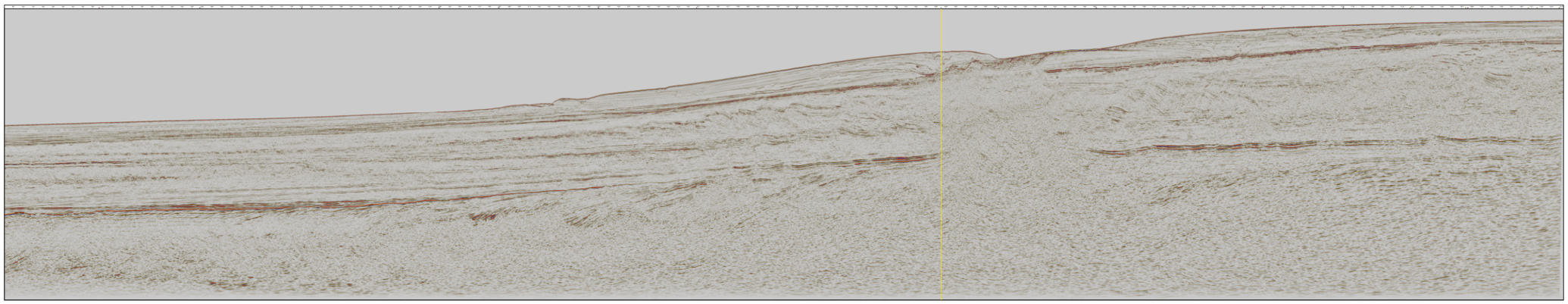

RON97-32

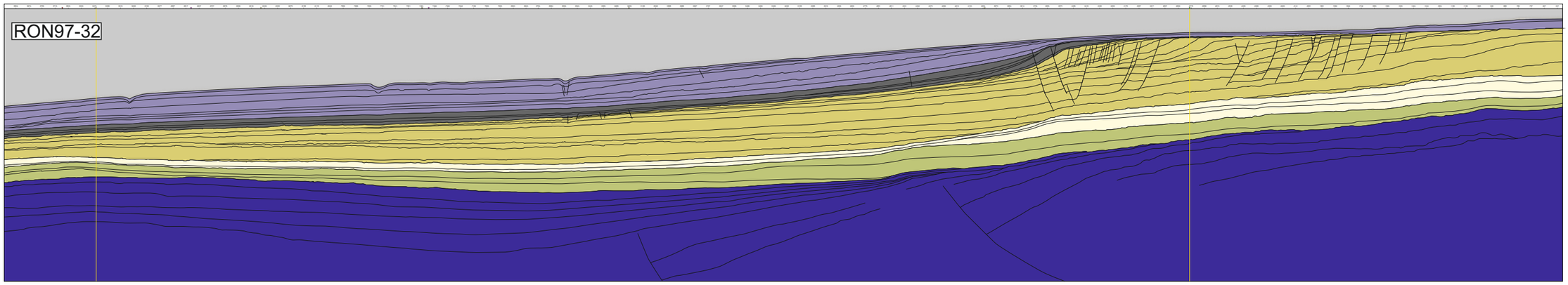

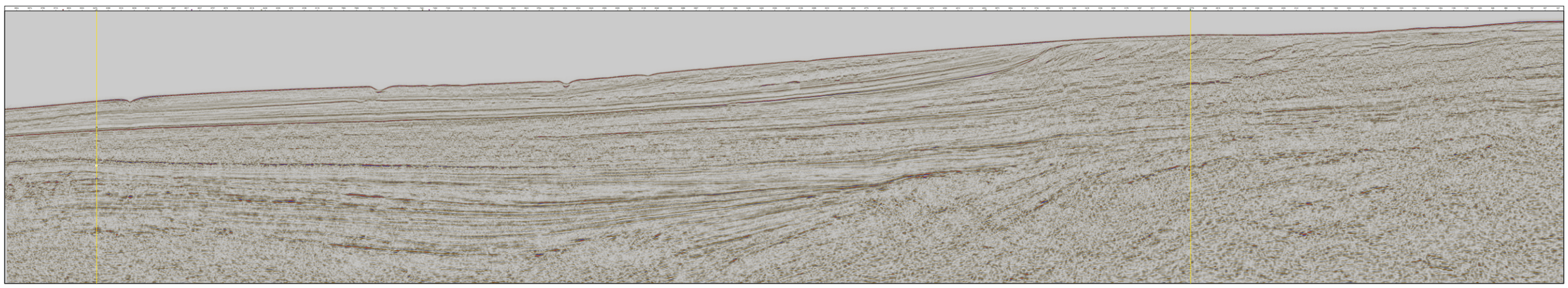

Part B –

III: Décollement maps

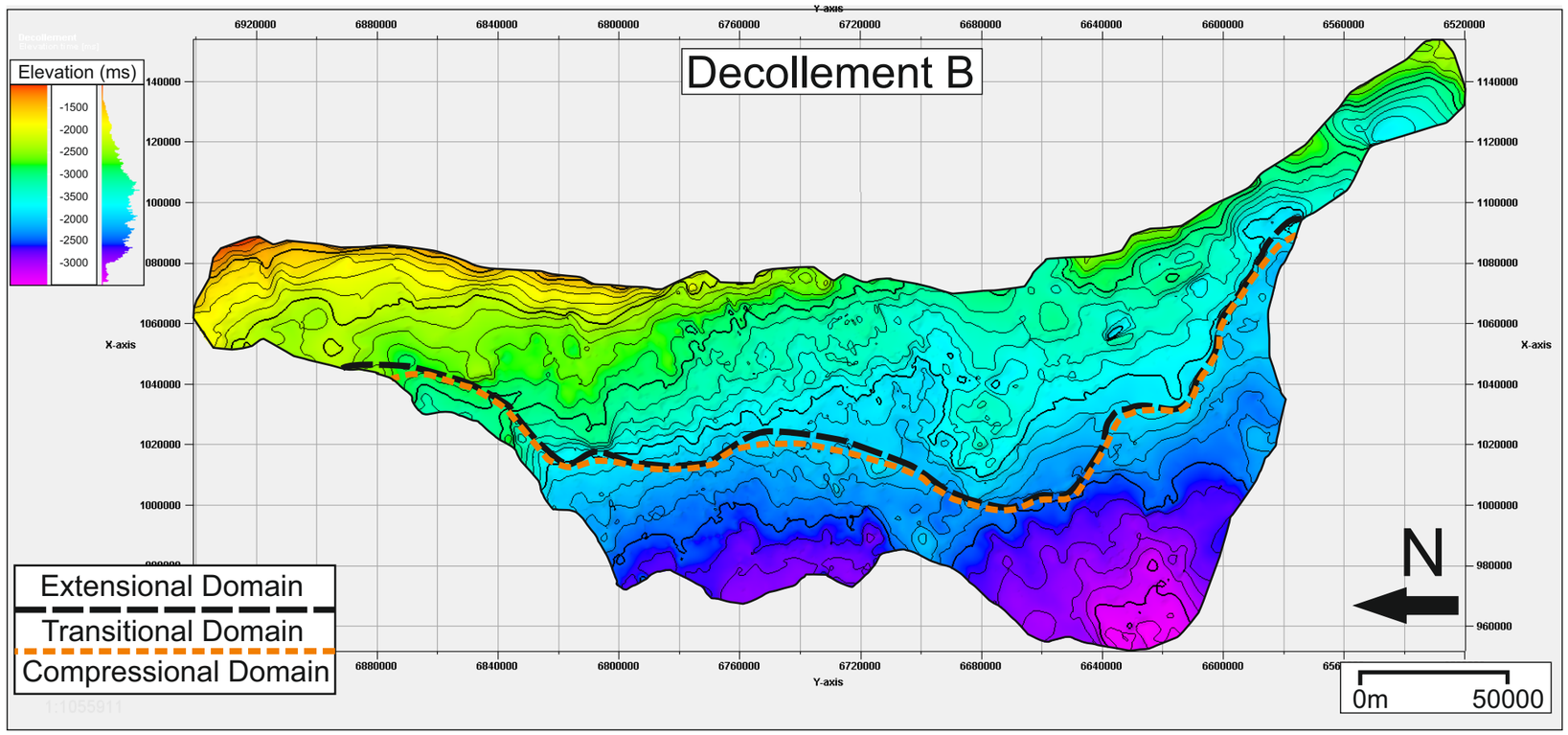
Decollement B
Elevation (ms)
-1500
-2000
-2500
-3000
-3500
-2000
-2500
-3000
Extensional Domain
Transitional Domain
Compressional Domain
X-axis
Y-axis
N
0m
50000

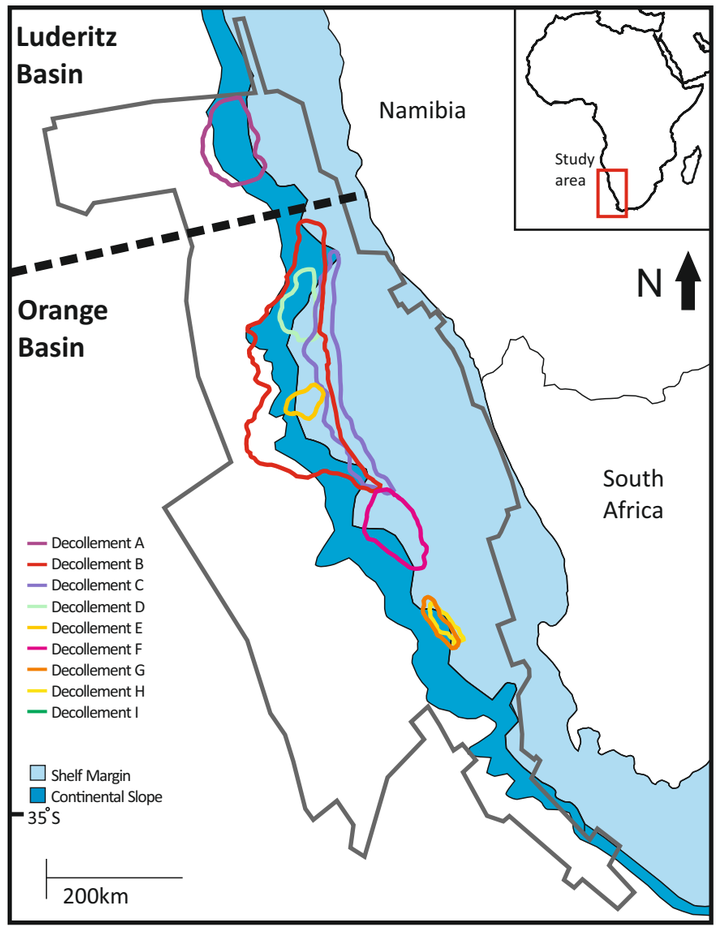
Luderitz Basin
Orange Basin
Namibia
South Africa
Study area
N
Decollement A
Decollement B
Decollement C
Decollement D
Decollement E
Decollement F
Decollement G
Decollement H
Decollement I
Shelf Margin
Continental Slope
35°S
200km

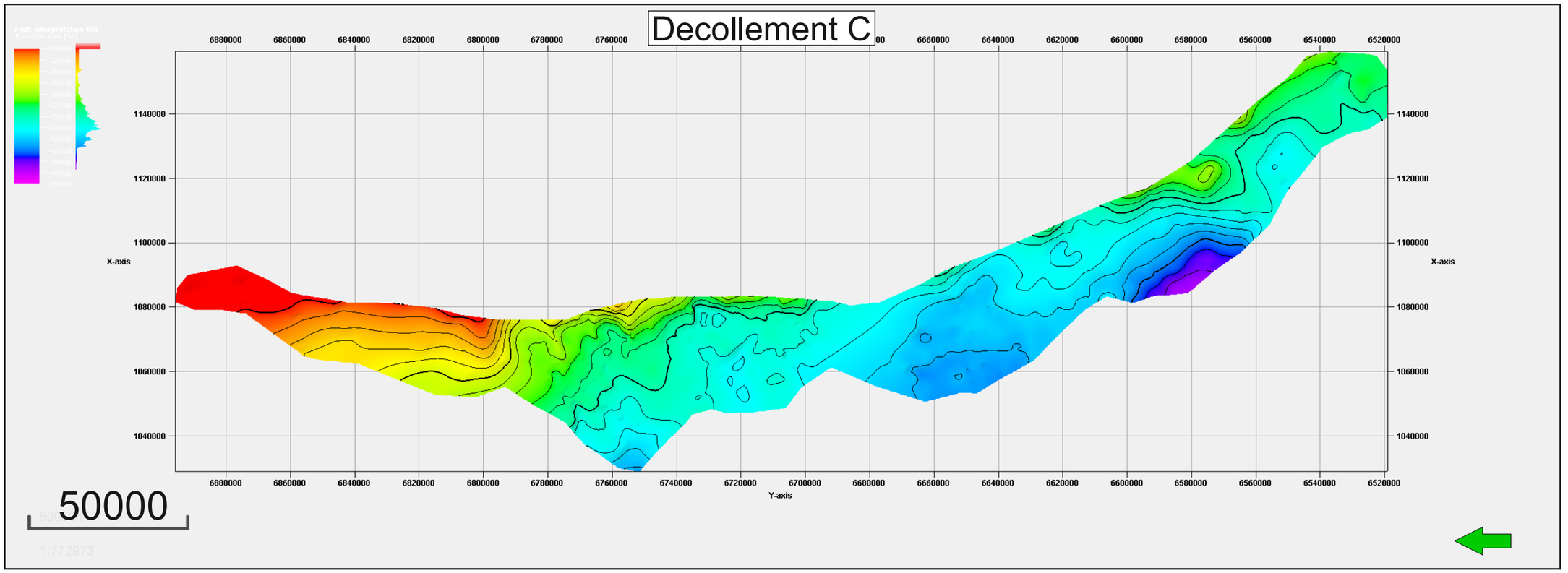
Decollement C
X-axis
Y-axis
50000

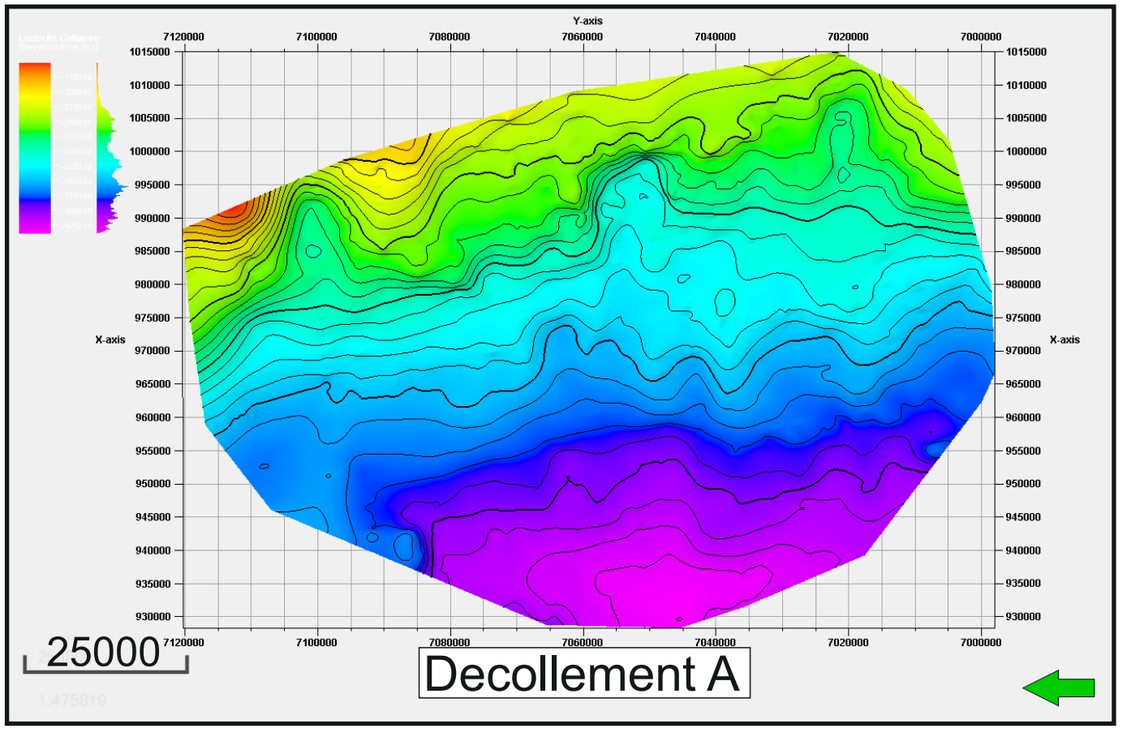
Y-axis
7120000
7100000
7080000
7060000
7040000
7020000
7000000
X-axis
1015000
1010000
1005000
1000000
995000
990000
985000
980000
975000
970000
965000
960000
955000
950000
945000
940000
935000
930000
25000
1:475819
Decollement A

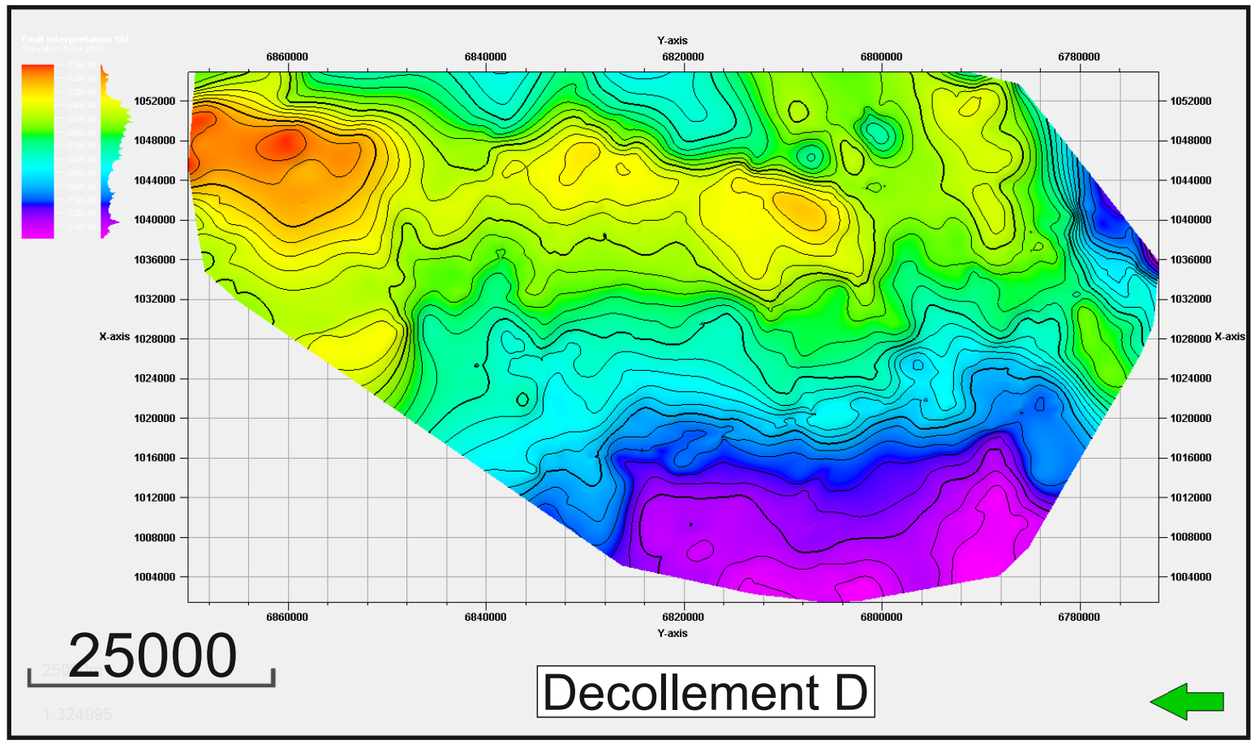
Y-axis
6860000
6840000
6820000
6800000
6780000
X-axis
1052000
1048000
1044000
1040000
1036000
1032000
1028000
1024000
1020000
1016000
1012000
1008000
1004000
25000
1:324995
Decollement D

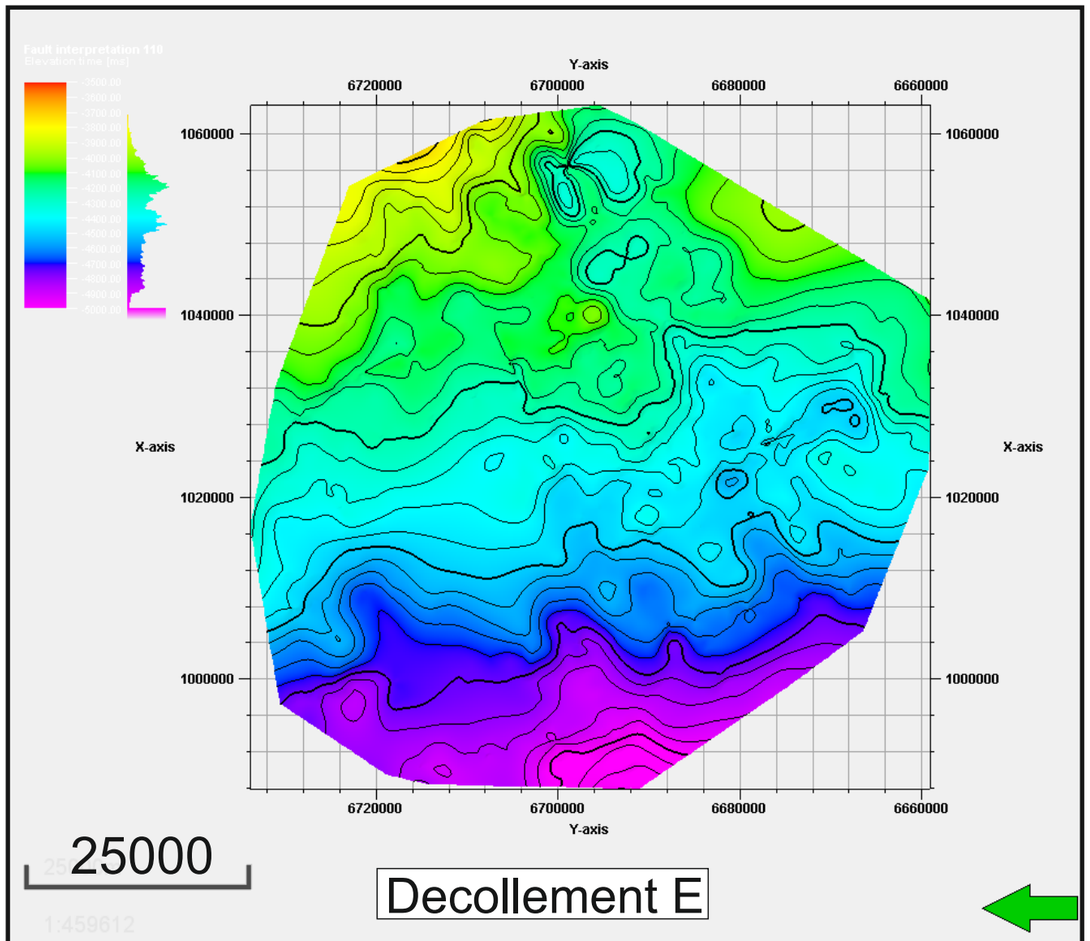
Fault interpretation 110
Elevation time [ms]
Y-axis
6720000
6700000
6680000
6660000
X-axis
1060000
1040000
1020000
1000000
25000
1:459612
Decollement E

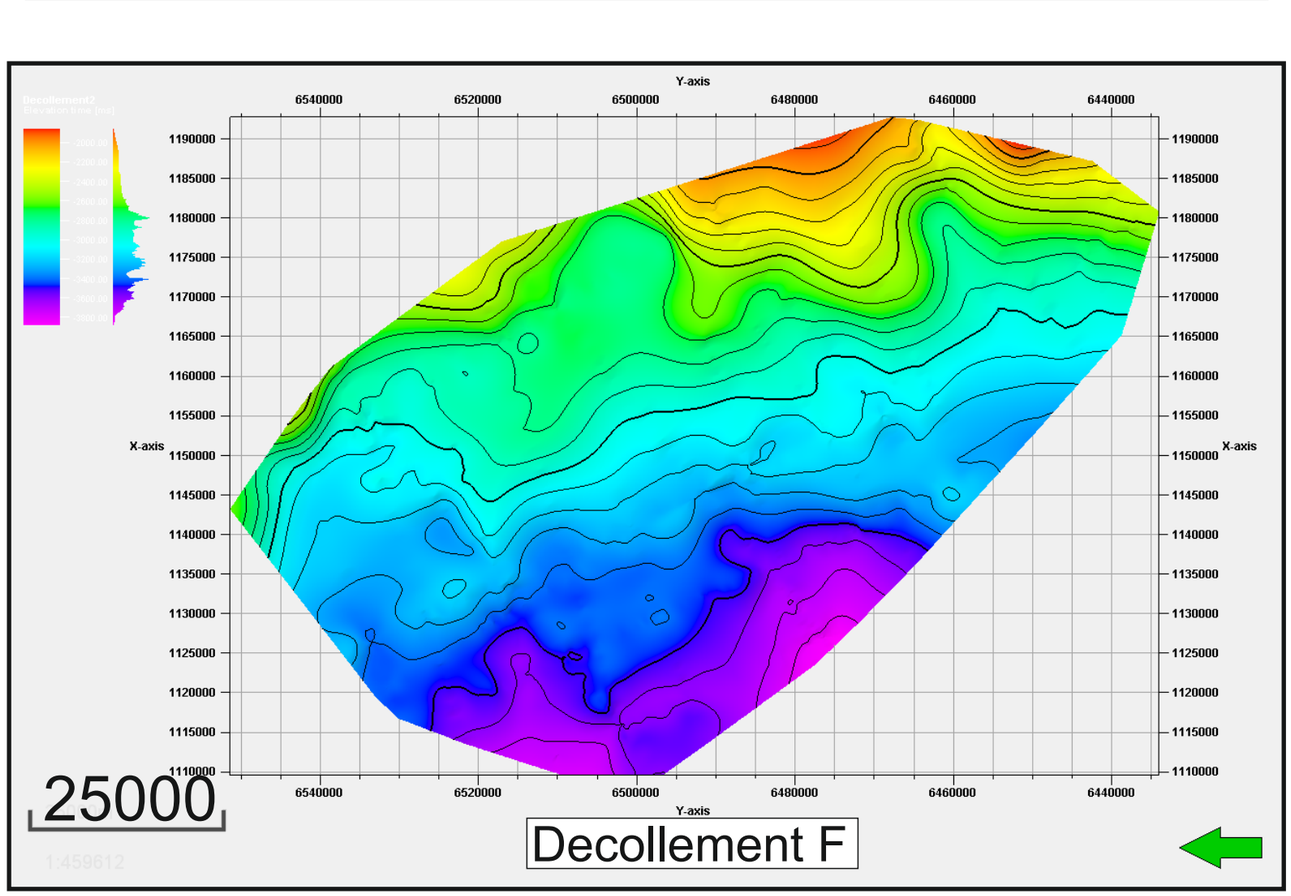
Decollement2
Elevation time [ms]
Y-axis
6540000
6520000
6500000
6480000
6460000
6440000
X-axis
1190000
1185000
1180000
1175000
1170000
1165000
1160000
1155000
1150000
1145000
1140000
1135000
1130000
1125000
1120000
1115000
1110000
25000
1:459612
Decollement F

Decollement G

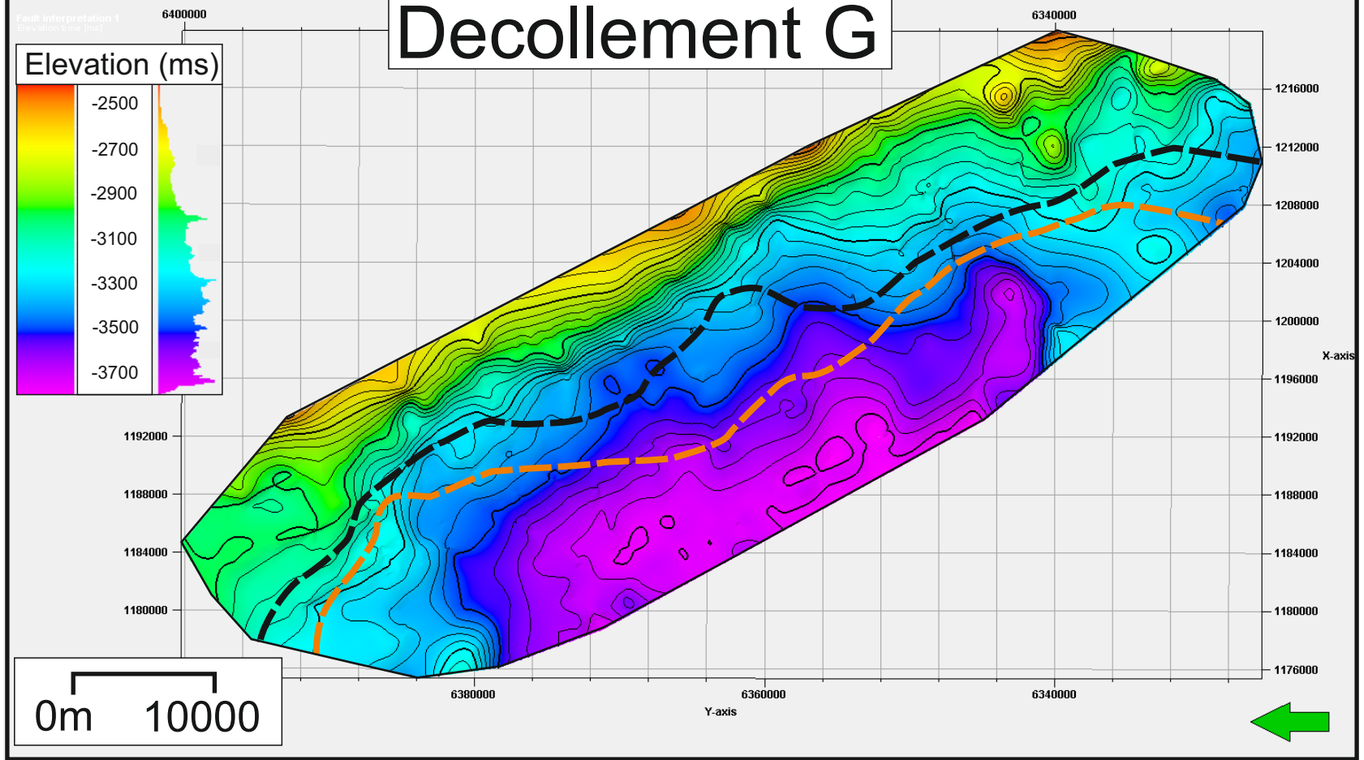

Decollement H

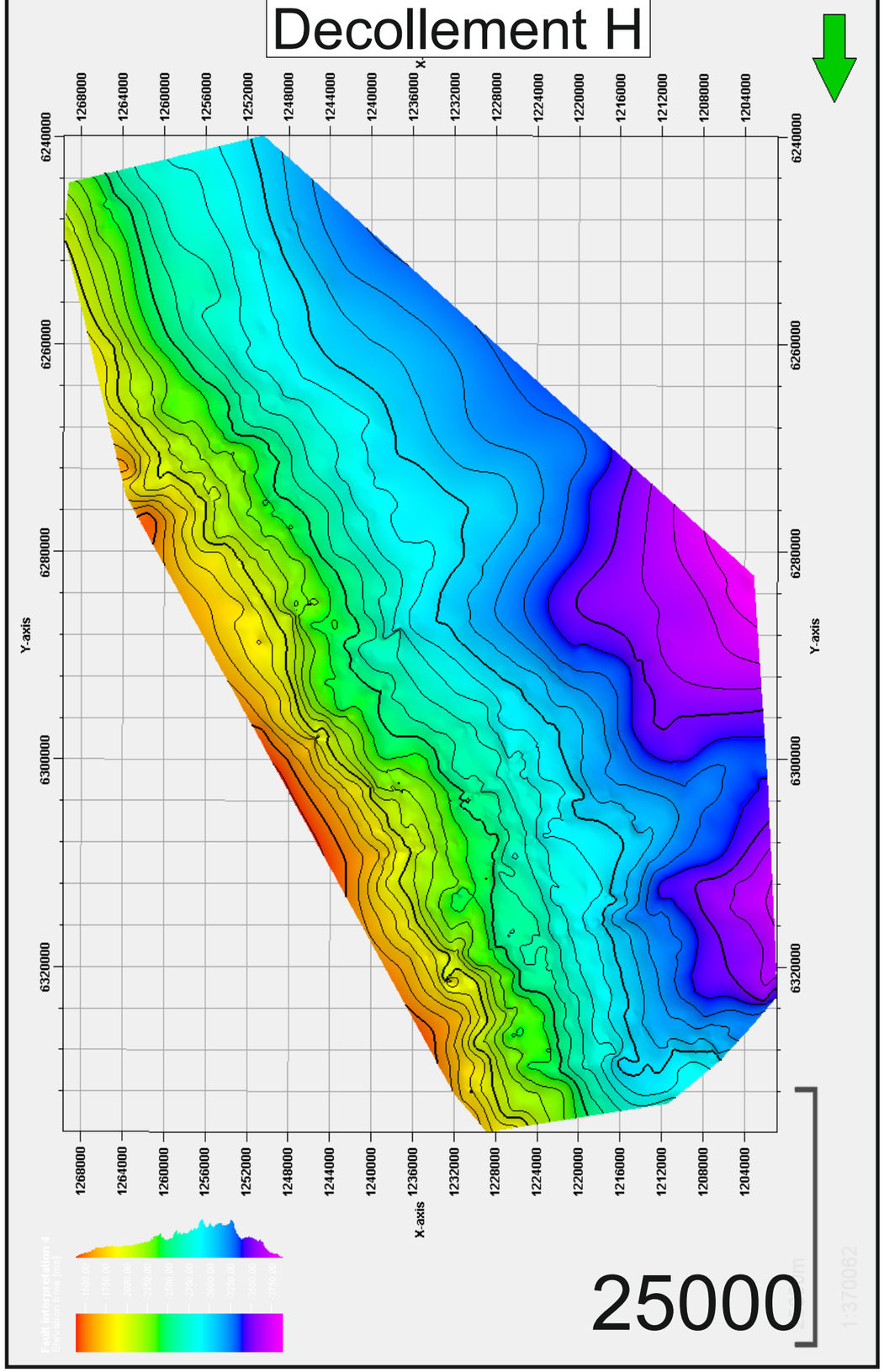

Decollement I

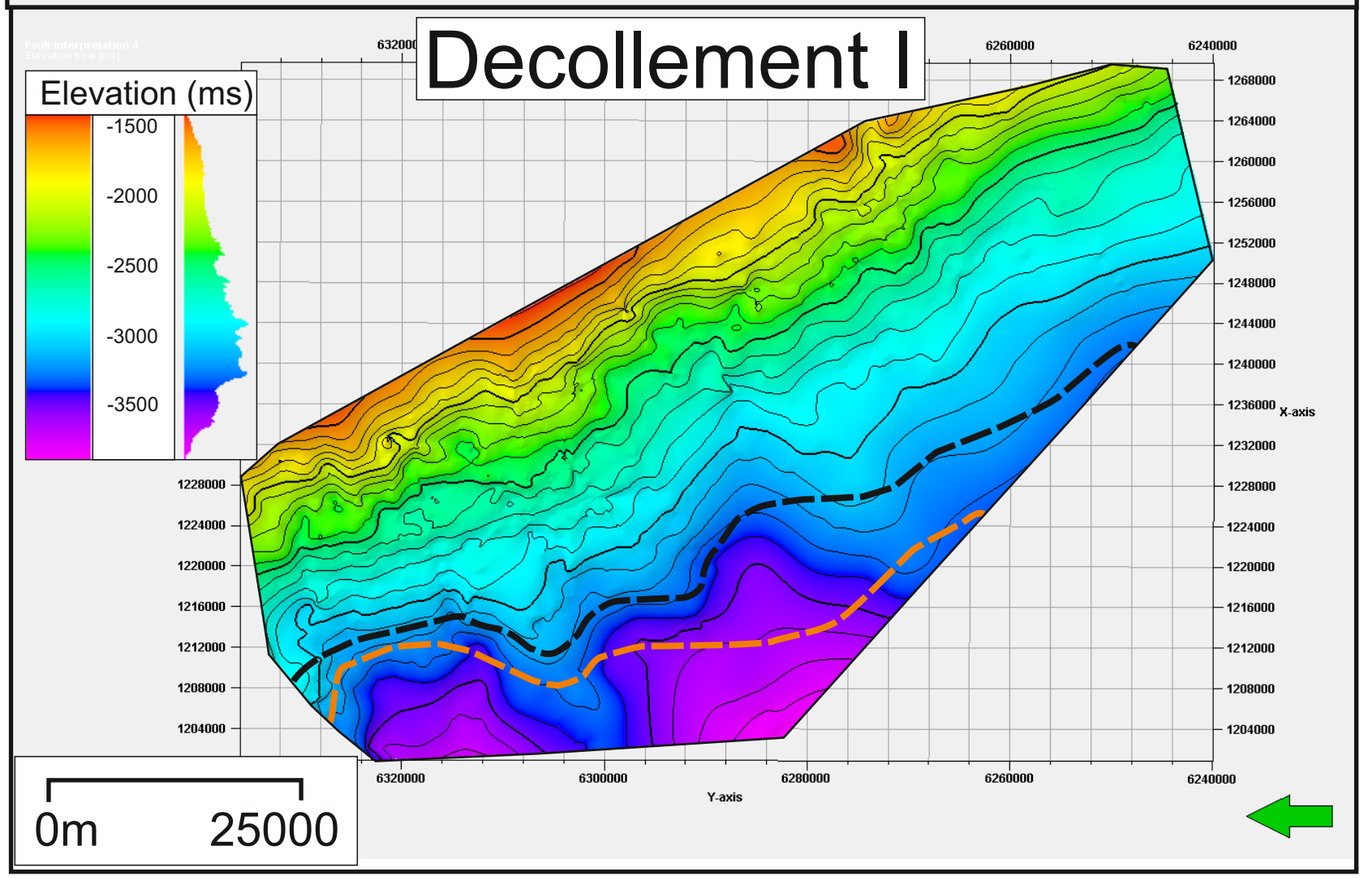

Part C –

I: Depth Conversions

Depth Conversions

In order to produce reliable cross-sections it is necessary to depth convert the PSTM seismic profiles. In the absence of well data a simple depth conversion was achieved using Schlumberger's Petrel software. Significant reflections (Seabed, Tertiary unconformity and Post-rift Unconformity) identifiable in all relevant seismic profiles were picked and surfaces were created, making four packages. Seismic velocities for the top and base of each package were selected based upon their lithology as discussed in the literature. At which point a simple depth conversion was undertaken, these profiles were compared to PSDM data provided by Spectrum to assess there viability. Whilst it is clear this is not the ideal method the lack of raw seismic and appropriate well data prevent a more thorough depth conversion, however a reasonable match is achieved relative to the PSDM data. These Depth conversions were used to produce restorations undertaken in Chapter 5 and mentioned in Chapter 3.

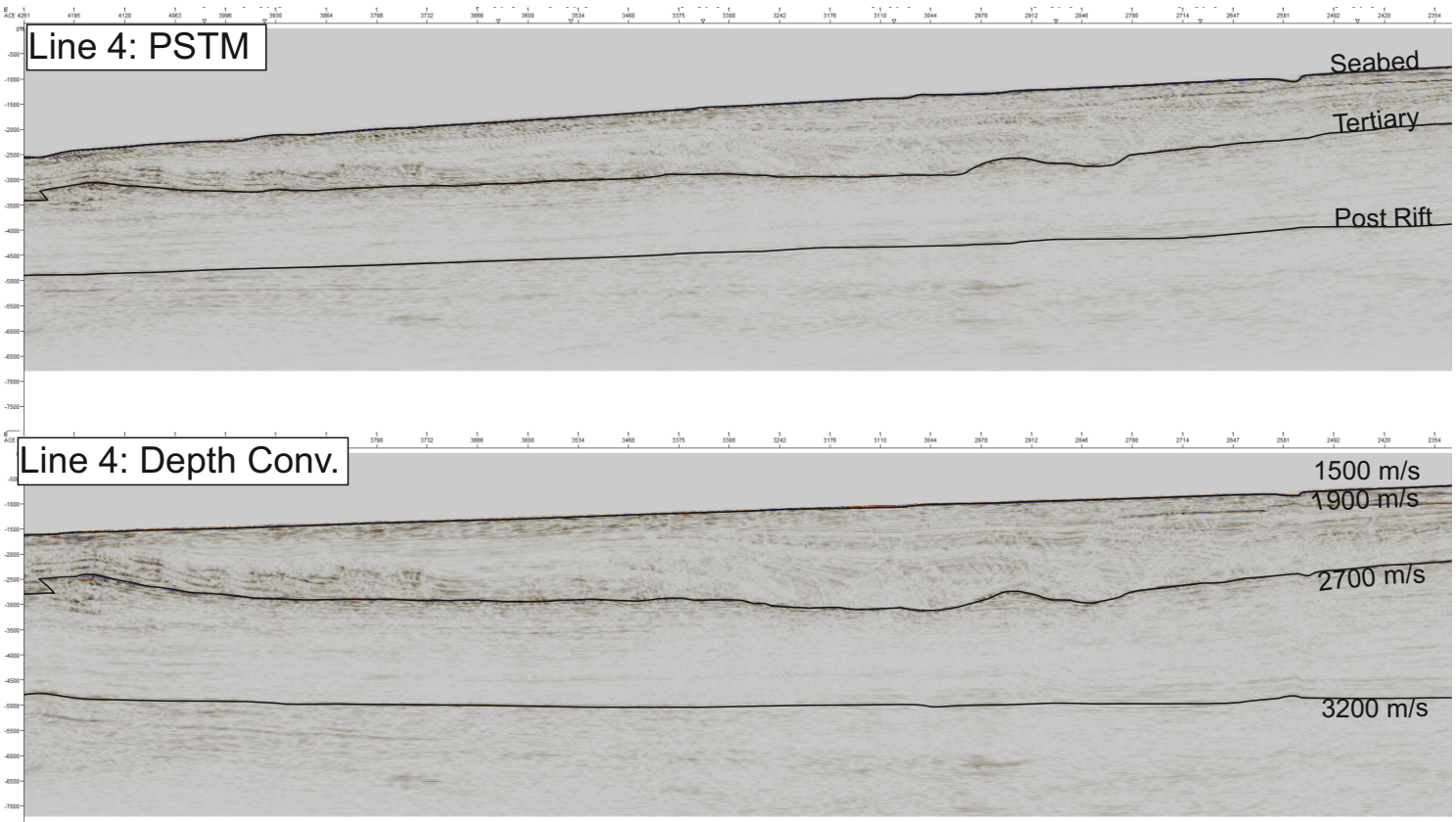

Seismic profiles are projected 1:1. The depth conversion produces a reasonable projection of depths especially for the upper part of the section and is highly comparable with Line 5 below, which used well ties and velocity analysis. Lateral variations in velocities below the post rift unconformity due to volcanics produces an unreliable depth conversion below this horizon using this simplistic analysis.

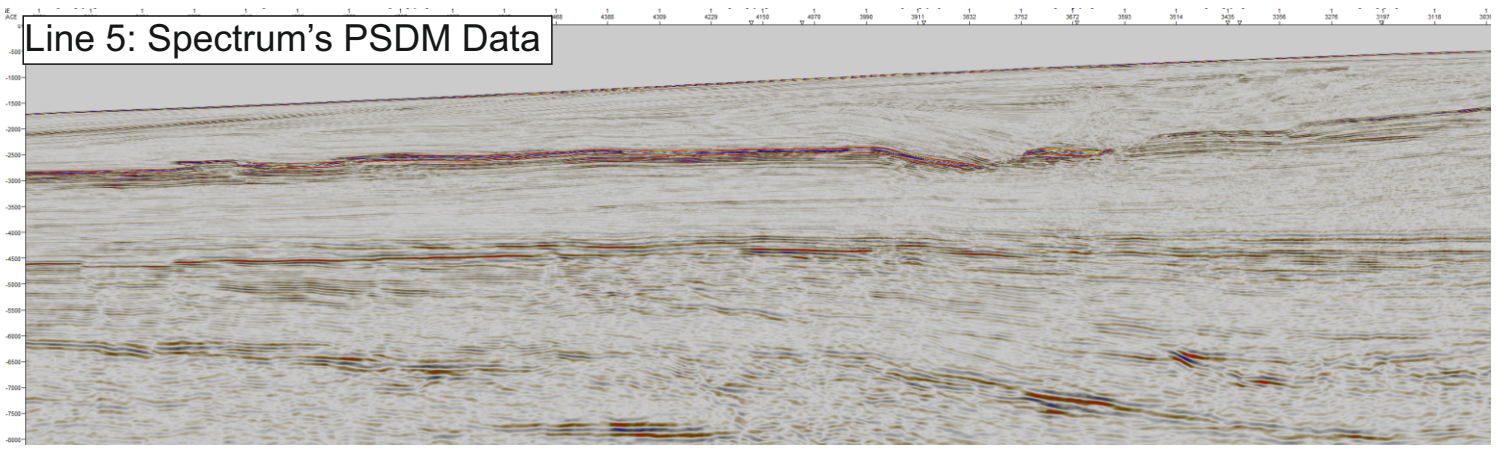

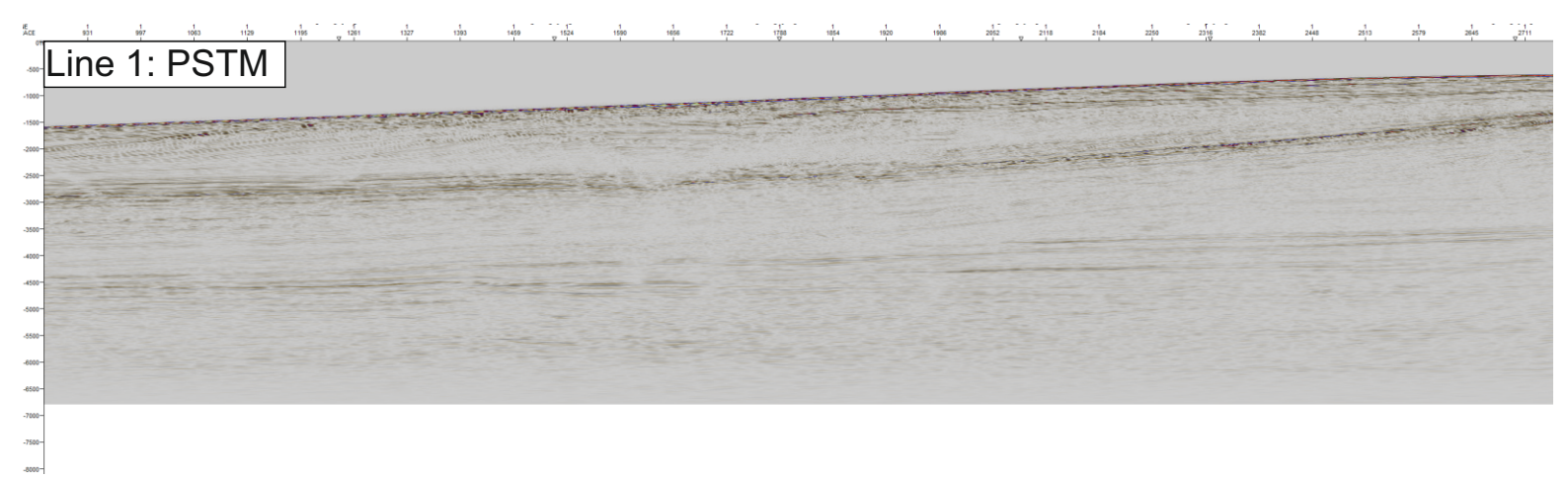
Line 1: PSTM

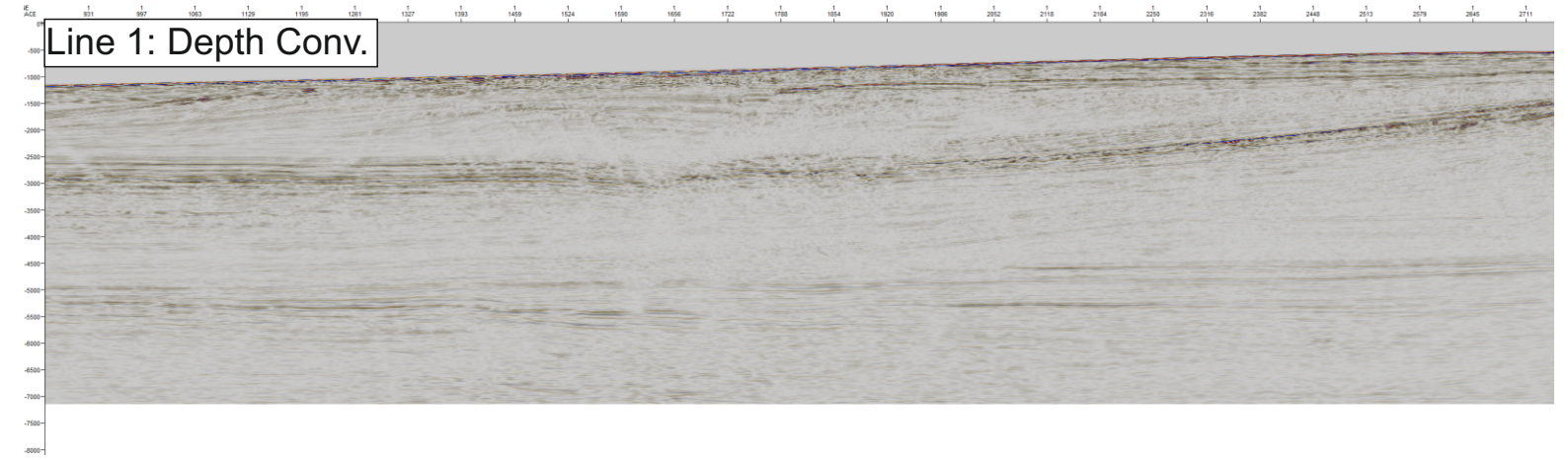
Line 1: Depth Conv.

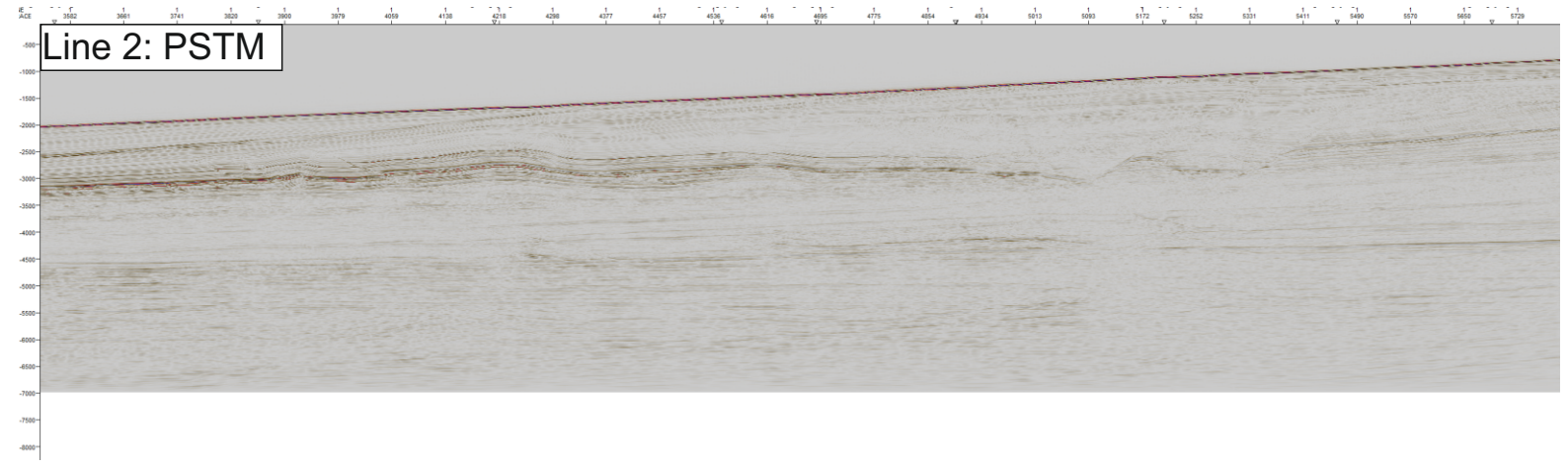
Line 2: PSTM

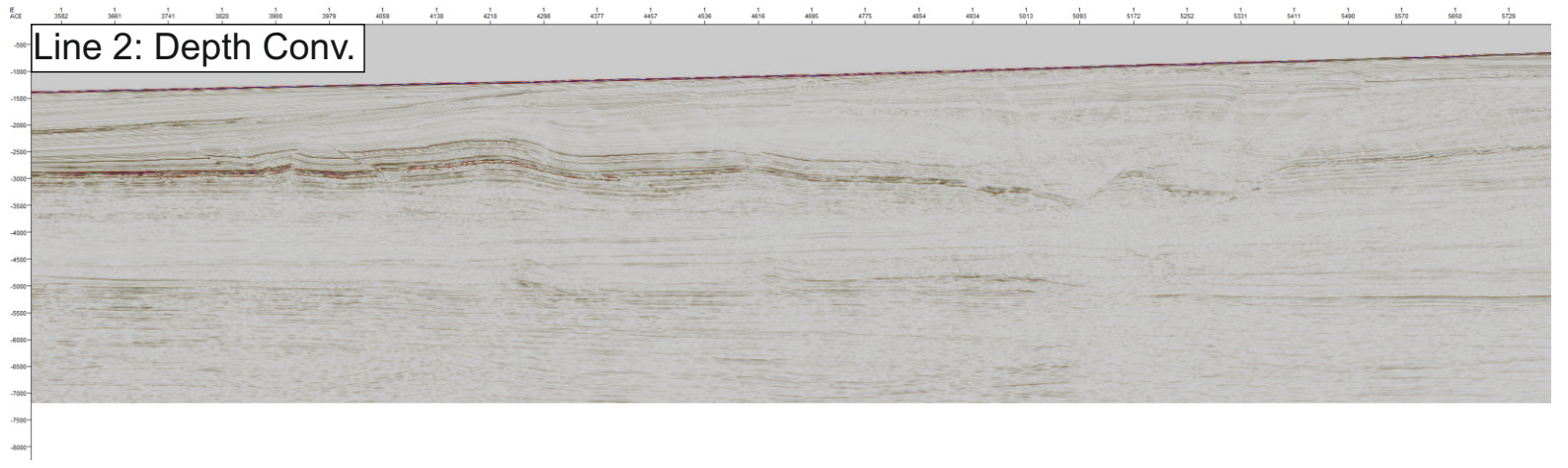
Line 2: Depth Conv.


Line 3: PSTM

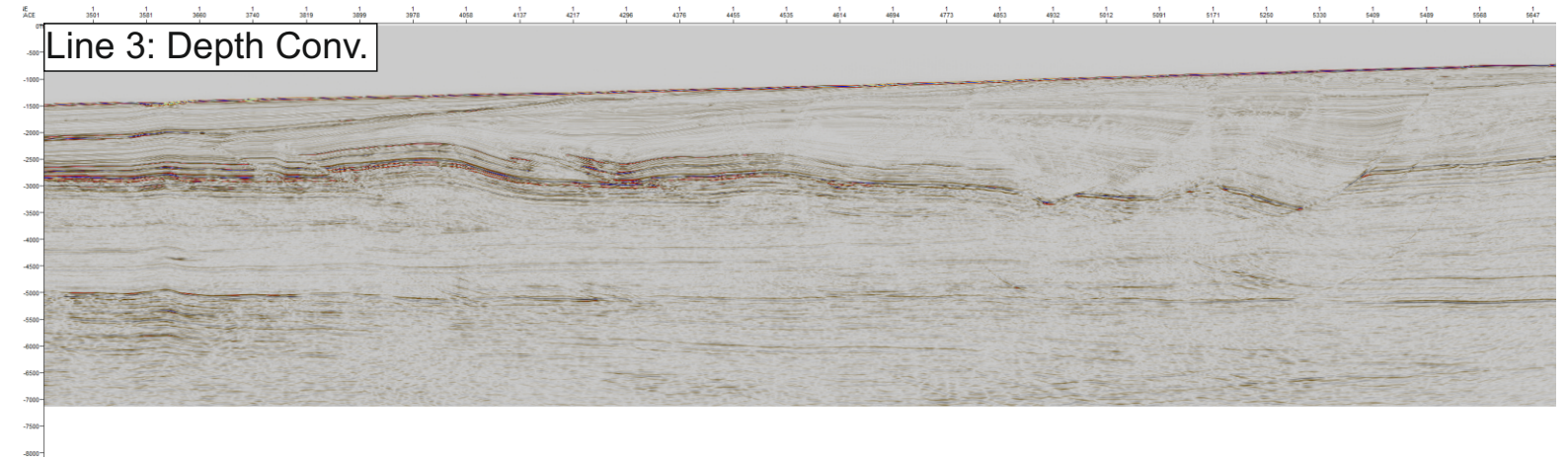
Line 3: Depth Conv.

Part C –

II: Restorations

Restoration of Line 1

This section shows the restorations undertaken in Chapter 5 for Lines 1,2,4 and 5. The methodology and the restoration for Line 3 is included in Chapter 3, Section 3.2.4.

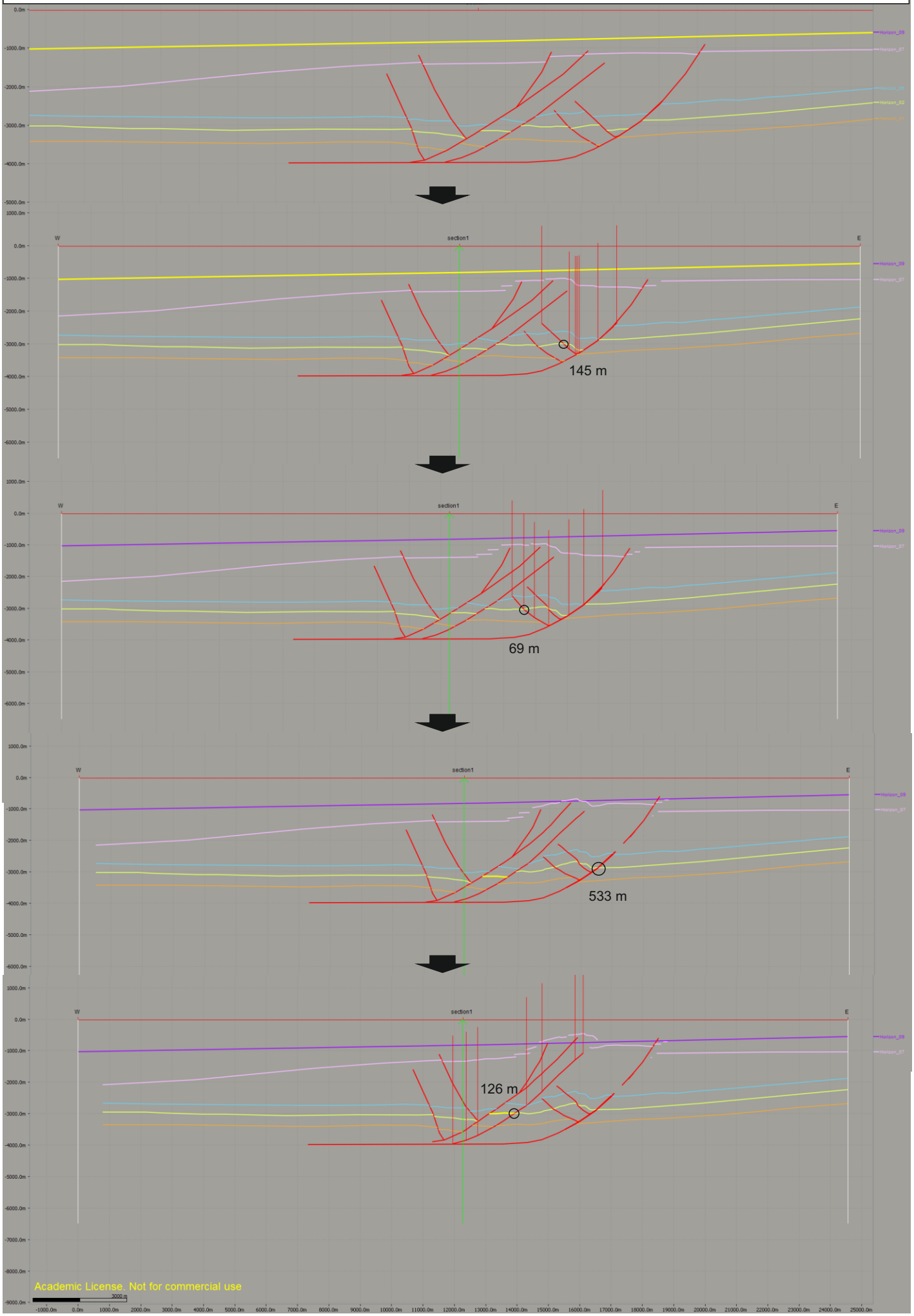

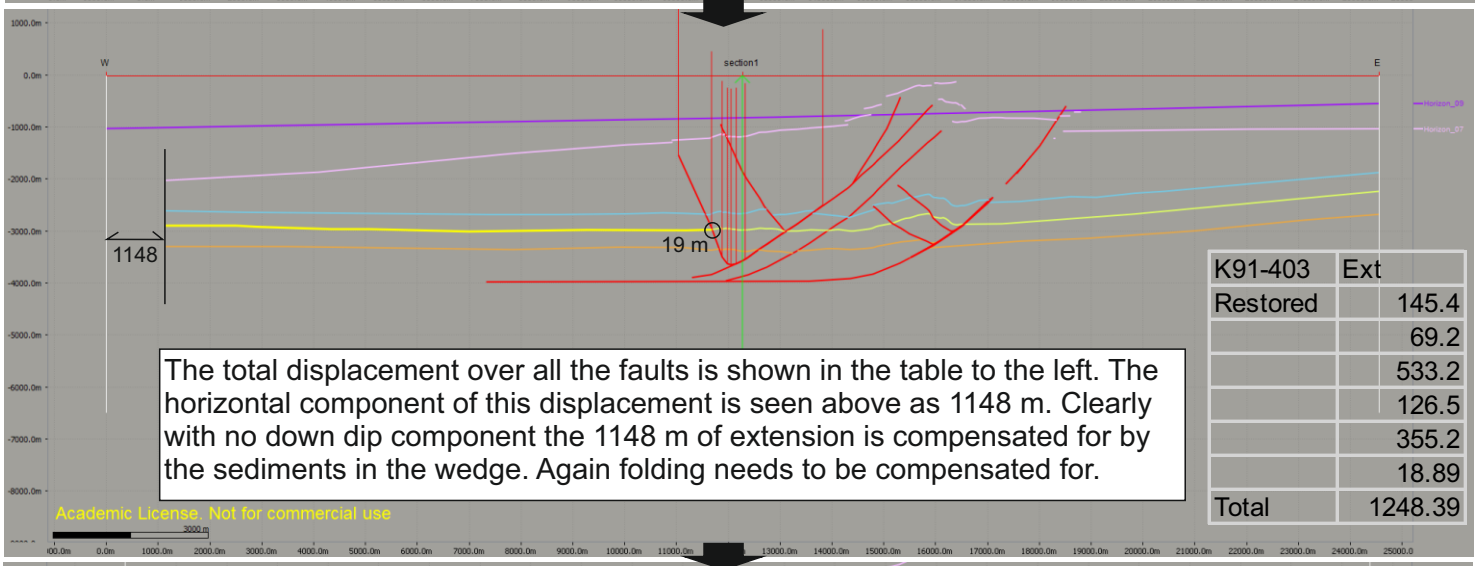

K91-403	Ext
Restored	145.4
	69.2
	533.2
	126.5
	355.2
	18.89
Total	1248.39

The total displacement over all the faults is shown in the table to the left. The horizontal component of this displacement is seen above as 1148 m. Clearly with no down dip component the 1148 m of extension is compensated for by the sediments in the wedge. Again folding needs to be compensated for.

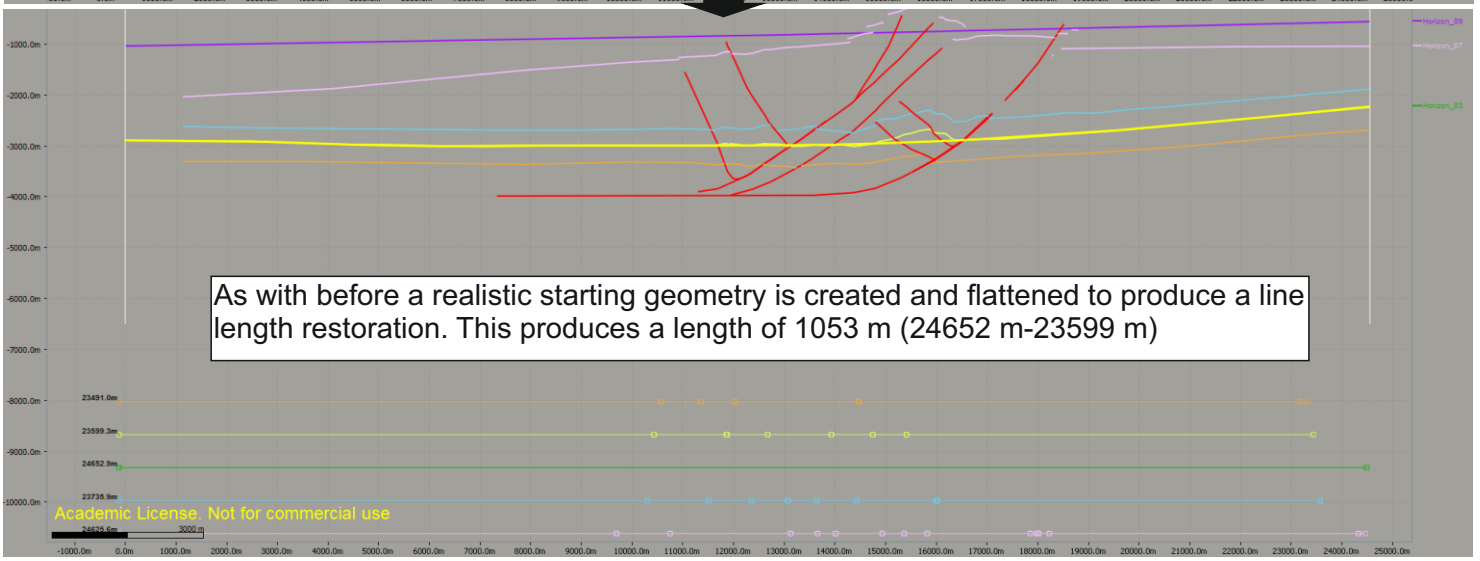

As with before a realistic starting geometry is created and flattened to produce a line length restoration. This produces a length of 1053 m (24652 m-23599 m)

Again a line length restoration without systematic restoration give us a similar figure of 1126 m (24614-23487 m).

Restoration of Line 2

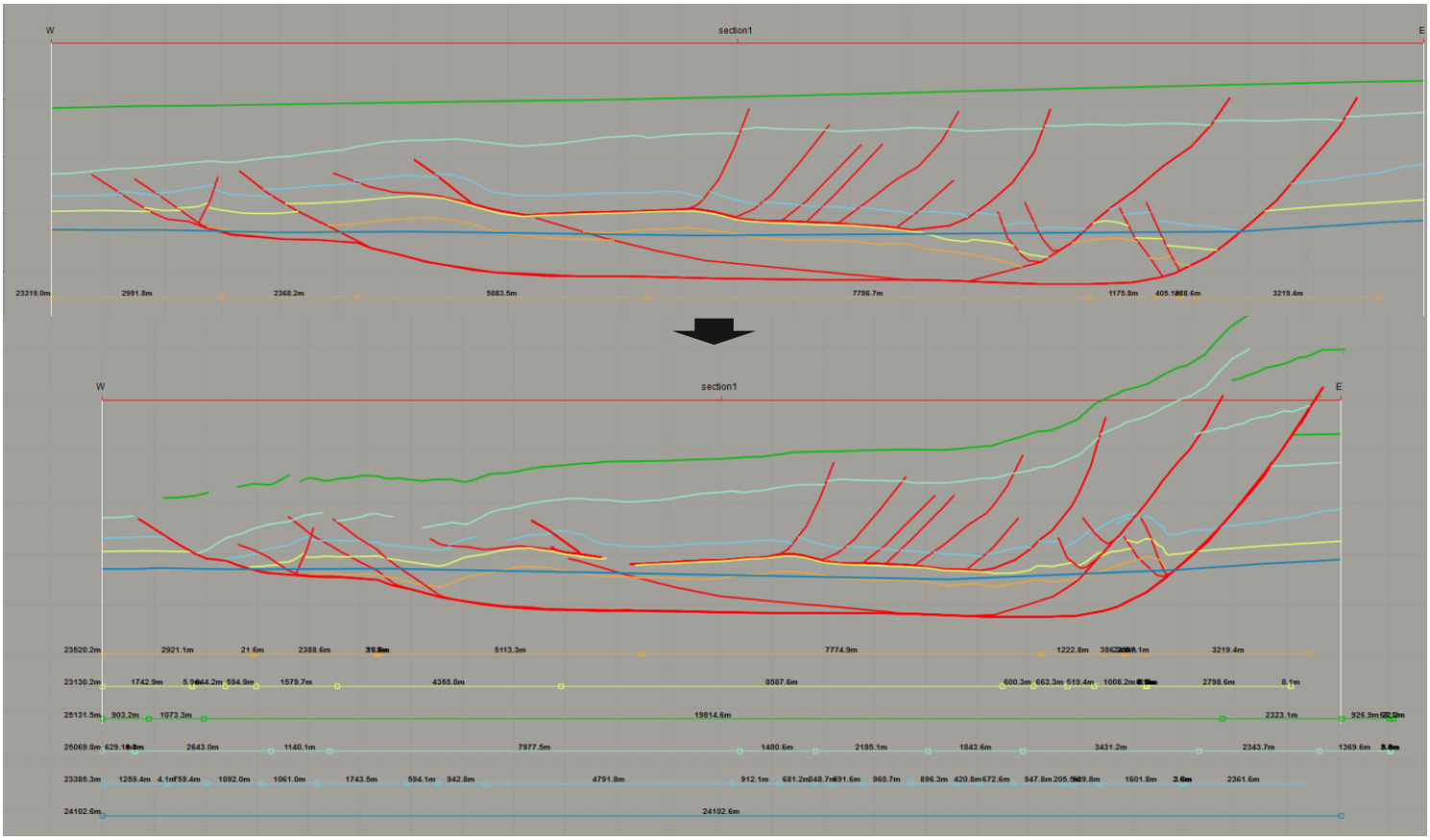

Restoration of Line 4

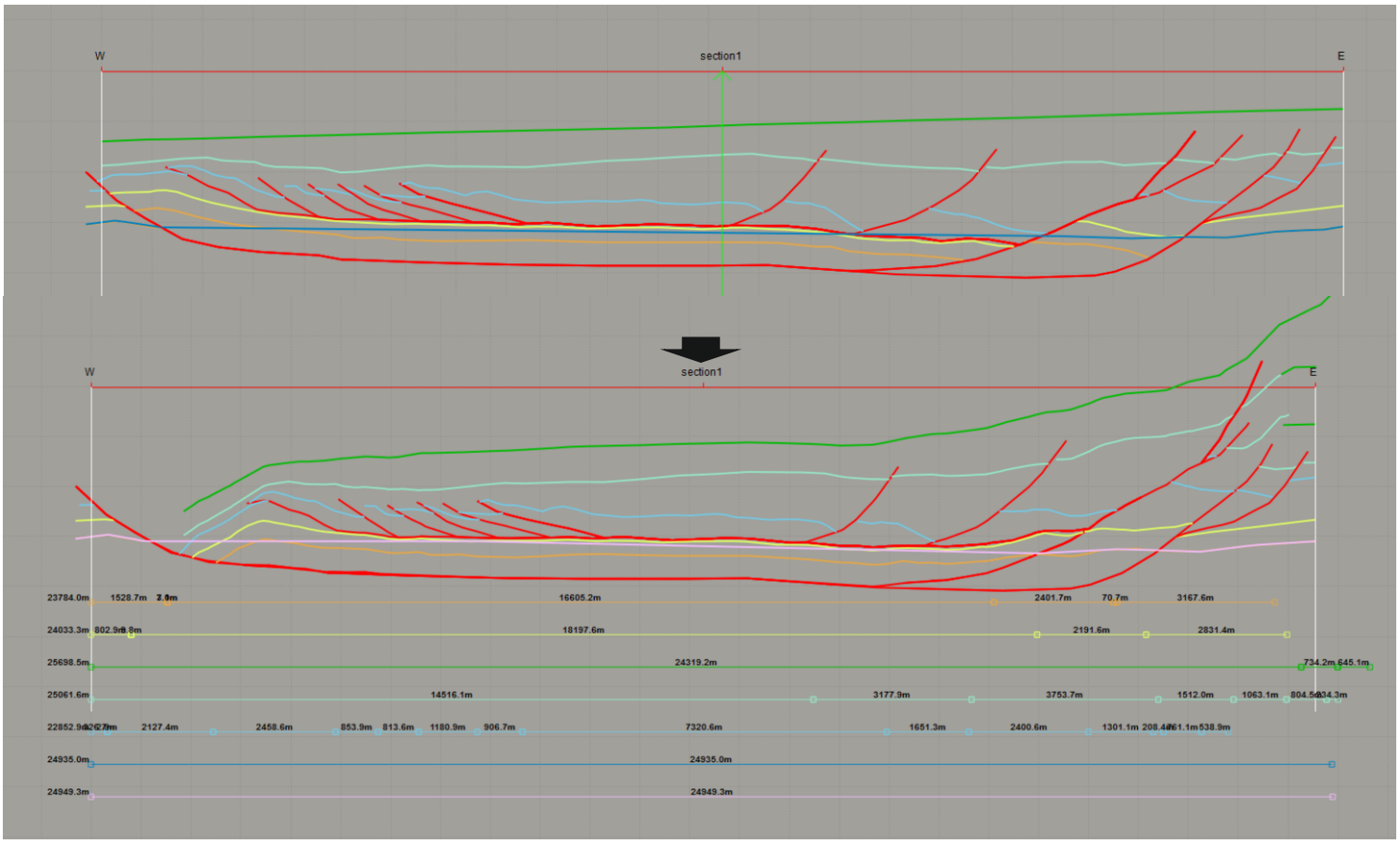

Restoration of Line 5

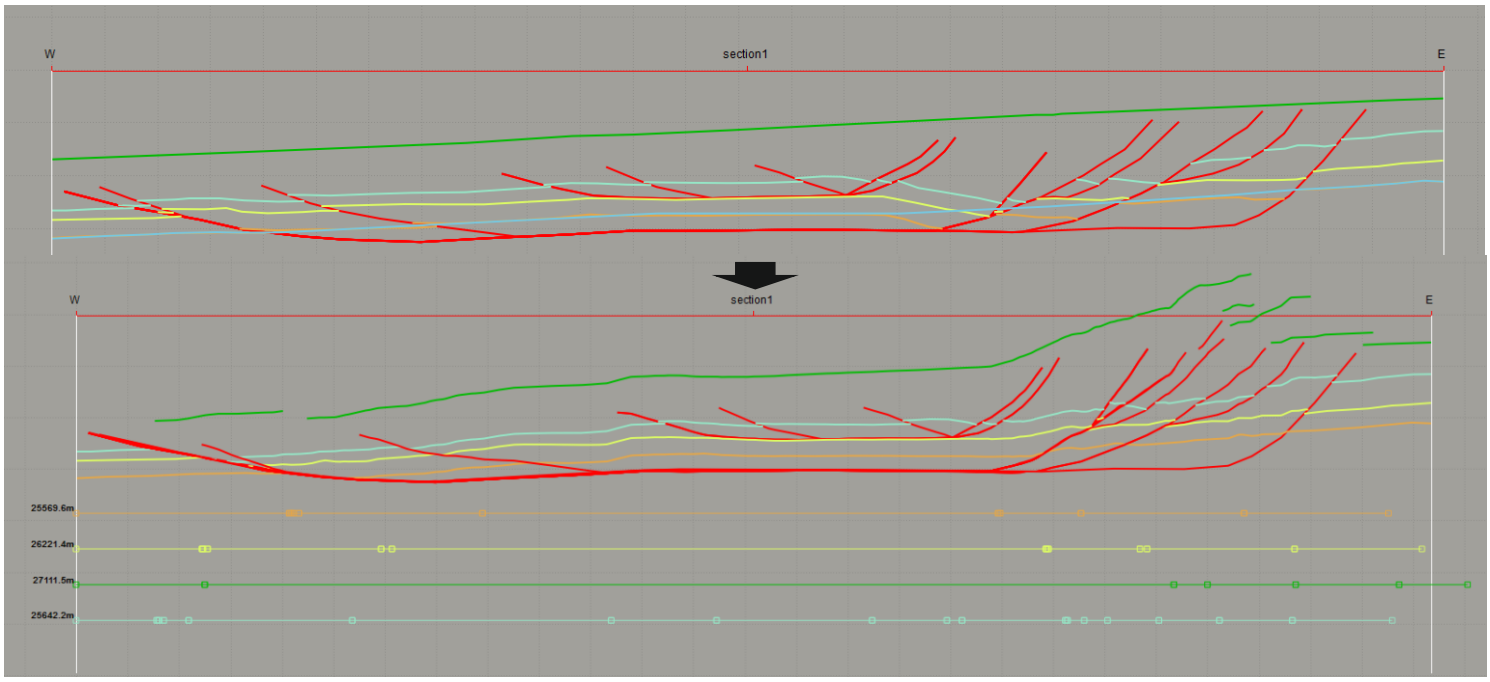

	Compression (m)	Extension (m)	Net (m)	DWFTB length	Missing Strain
Line 1	0	1008	1008	5917	100.0%
Line 2	943	2033	1090	19589	5.6%
Line 3	1043	2166	1123	21985	5.1%
Line 4	577	1673	1096	21767	5.0%
Line 5	818	1836	1018	20847	4.9%
de Vera et al	16000	24000	8000	145000	5.5%
Butler & Paton	25000	44000	19000	150000	12.7%